MINERALOGICAL AND GEOCHEMICAL ASSESSMENT OF PARTICULATE MATTER (PM_{10}) IN IBADAN METROPOLIS, NIGERIA

By

TESLEEM KOLAWOLE
B. Sc. (Hons) Geology 1998, M. Sc. Mineral Exploration (Geochemistry Option) 2003.

A Thesis in the Department of Geology
Submitted to the Faculty of Science
In partial fulfillment of the requirement for the Degree of

DOCTOR OF PHILOSOPHY
of the
UNIVERSITY OF IBADAN
NIGERIA

MARCH, 2015

ABSTRACT

Particulate Matter (PM) are suspended solid and liquid particles in the atmosphere, classified into coarse (PM_{10}, 2.5 to 10µm) and fine ($PM_{2.5}$ <2.5µm) particles. Particulate Matter has been reported to have negative impact on the climate, human health and ecosystems. Previous works in Ibadan had focussed on occurrences and concentrations of PM_{10} without adequate attention to mineralogical and elemental composition. This study was designed to investigate the mineralogical and elemental composition of PM_{10} in Ibadan metropolis in order to ascertain their sources and potential hazards to human health.

Two hundred and five suspended PM_{10} samples were purposively collected from Traffic Area (TA) (40), Industrial Areas (IA) (40), Dumpsite/Incinerator (DI) (40) and Residential Area (RA) (85) using high volume air sampler with cellulose filter. The samples were collected in both dry and rainy seasons from February to December, 2011. Rocks (12), soils (25) and deposited dusts (30) within the metropolis were also sampled. The morphology and mineralogy of the PM_{10}, rocks and soils were determined using Scanning Electron Microscopy/Energy Dispersive Spectroscopy and X-ray Diffractometry while the elemental compositions were determined using inductively coupled plasma optical emission spectrometry. The results of PM_{10} concentration were compared with World Health Organization (WHO), United State Environmental Protection Agency (USEPA) and National Environmental Standards and Regulation Enforcement Agency (NESREA) standards. Data were analysed using descriptive statistic and Principal Component Analysis (PCA).

Minimum (32.2 µg/m^3) and maximum (627.6 µg/m^3) concentrations of PM_{10} were observed at the peak of the rainy and dry seasons respectively; with daily average concentration of 652.1µg/m^3, 377.5 µg/m^3, 285.7 µg/m^3 and 214.8 µg/m^3 for IA, TA, DI and RA respectively. All daily average concentrations exceeded WHO, USEPA and NESREA standards. The morphology of the individual PM_{10} particle are mostly coarse (>2.5 µm) and irregular in shape with very few being regular and fine (<2.5 µm); an indication of the localised nature of the PM_{10} particles. The minerals in the PM_{10} particles are mostly chlorite, illite, kaolinite, smectite, quartz, feldspar, mica and amphibole. Quartz, feldspar, mica and amphibole were the dominant minerals in the rock units while kaolinite and illite were dominant in the soils. The elemental concentrations in the PM_{10}, soils and deposited dusts

follow the order Ca>Fe>Al>Na>Mg>Si>Zn>Cu>Mo>Mn>Ba>Ti>Pb>Ni>La. The IA showed highest average concentration of all elements in the PM_{10} except Ba, which was highest in TA. The elemental composition agreed with the mineralogical data as revealed by the PCA. Factor 1 was loaded with Al, Si, Ca, Fe and Mg while Factor 2 was Ca, Mg, and Na, indicating crustal source for these elements. Factor 3 was loaded with Pb, Zn, indicating industrial emission source while Factors 4 (Cu, La, Mo) and 5 (Ba, Mn) indicated traffic related contribution.

The mineralogy and elemental composition in the Particulate Matter (PM_{10}) were derived mainly from crustal sources with subordinate contributions from anthropogenic sources. The presence of Pb, Cu, Zn and Si in the coarse particulate matter could pose serious health hazard to the human population.

Keywords: Particulate matter, Crustal sources, Principal component analysis, Anthropogenic sources

Word count: 492

ACKNOWLEDGEMENT

Principal on the list of those who contributed directly or indirectly to the success of this work is my former supervisor Late Prof. Akinlolu F. Abimbola, without whose patience and constructive criticisms, this endeavour would not have been successful. Critical review from my supervisor in the person of Dr. Akinade S. Olatunji, greatly improved the quality of this work. Prof. Adreas Taubert from the Institute of Chemistry, University of Potsdam, Germany, sponsored the entire analyses in this work and was also helpful with part of the thesis review. Dr. Christina Günter from the Institute of Earth and Environmental Science, University of Potsdam, Germany, assisted in carrying out the analyses such as X-ray Diffractometery, Scanning Electron Microscopy/Energy Dispersive Spectroscopy and Inductively Coupled Plasma/Optical Emission Spectroscopy (ICP/OES) and thin section and was assisted by Miss G. Anja in ICP/OES analysis, she also helped with part of the thesis review.

The guidance given by the Head of Department Prof. Moshood N. Tijani is appreciated. I wish to thank all the lecturers in the Department Prof. Azubuike A. Eleueze, Prof. Idowu A. Olayinka, Prof. Gabriel O. Adeyemi and other Academic Staff in the Department. I thank Dr. Olubunmi C. Adeigbe for his assistance and constant advice on this work, may Almighty Allah bless him in many folds. I also appreciate the effort of Dr. Olumuyiwa M. Ajibade for being supportive throughout my Ph.D work. My special thanks goes to Dr Ibraheem Oyediran and Mr. Mutiu Adeleye for their support and word of encouragement towards the success of my programme.

My field work was assisted by Messrs Femi Okunola, Ibraheem Adisa, Tolu Odeshi and Mustapha T. Jimoh, may Almighty Allah reward them abundantly. Drs. Iyayi Onuabonah and Austin Ofomaja's contributions to this work are highly treasured.

The immense contribution of the entire Geochemical Group is highly acknowledge. The Advice given to me by Dr. O. O. Ocan was appreciated. Colleagues at the Department of Geological Sciences, Osun State University, Osogbo Campus Dr. Akwinga Asaah, Messrs Olarinre Salako, Olugbenga A. Fajemila, Olawale K. Aromolaran, Charlse A. Oyelami, Olabanji A. Ojo and Mrs Grace Oluwadebi, were a great source of encouragement. I thank the entire staff of chemistry

laboratory, Department of Chemical Sciences, Osun State University for the assistance rendered during filter measurements.

Worthy of note is the academic guidance received from Prof. Adebisi C. Ajibade which helped shape my thinking. The advice and support given by Dr. Matthew Nton will be remembered forever, the Merciful God will forever rewards him abundantly.

My profound gratitude goes to Prof. Siyan Oyeweso whose support can never be quantified and I will always appreciate him for his drive and courage to conclude this work. I Thank Alhaji Akeem Adewolu for his assistance during this programme.

My profound gratitude goes to my late father Mr. Olayemi Kolawole (May his gentle soul rest in peace), my mother Alhaja Osenatu Kolawole and my siblings Mr. Taofeek Kolawole, Mrs Shakirat Kolawole Oyetunji, Miss Tawakalitu Kolawole, Miss Bashirat Kolawole, Alhaji Rauf Kolawole and Alhaja Barakat Kolawole and the entire Kolawole family for their support during this program.

The love and support of my wife Mrs Marufat Adekilekun Kolawole and my children Aishat, Ibraheem, Mustapha and Murtala sustained me in good as well as in difficult times will always be remembered.

The prayer and morale support given me by Sheiks Lukman Adisa Moshood, Bashiru Opeloyeru Kahafi and Dr. Murtala Ghazal is highly appreciated. I also wish to thank everybody in THE HOUSE.

This work benefited from financial support from the Tertiary Education Trust Fund (TETFund) Scholarship under Academic Staff Training and Development Programme of Osun State University, Osogbo to carry out part of my Ph.D work in the Institute of Chemistry and Earth and Environmental Science, University of Potsdam, Germany. At this junction I would like to thank Prof. Oguntola J. Alamu for facilitating my visit to Germany.

To the above-mentioned individuals and corporate bodies, as well as to my many friends especially Alhaji Nasiru Akewusola, Mr. Surajudeen Oyetune, Mr. Rasheed Amototo, Alhaji Bolakale Aliu and relatives, who supported me one way or the other through these years, but whose names have been unavoidably omitted, I say THANK YOU!

Finally, I thank Almighty Allah for the gift of life, and for His constant blessings and love bestowed on me and my family to see through everything in life.

CERTIFICATION

I certify that this work was carried out in the Department of Geology, University of Ibadan by Kolawole Tesleem.

_____

Supervisor

Dr. Akinade S. Olatunji

B. Sc. (Ilorin), Ph.D (Ibadan)

Department of Geology,

University of Ibadan

Dedication

This Ph. D. thesis is dedicated to my late father Mr. Mustapha O. Kolawole, my late wife Mrs. Jelilat O. Sanusi-Kolawole and my late supervisor in the person of Prof. A. F. Abimbola. May Almighty Allah bless them with Aljanat Fridaus (Amin).

TABLE OF CONTENTS

LIST OF TABLES

LIST OF FIGURES

CHAPTER ONE
INTRODUCTION

1.1 General Statement

Particulate Matter (PM) is a complex mixture of substances suspended into the atmosphere in solid or liquid state; basically formed from two sources- anthropogenic and geogenic. The effect of airborne particles in atmospheric processes strongly depends on a variety of physico-chemical parameters such as size distribution, sources, atmospheric lifetime and mixing processes in the atmosphere (Rosenfeld *et al.*, 2008; Sokolik and Toon, 1999).

Mineral dust sourced from natural (geogenic) sources is one of the most abundant aerosol species in the atmosphere in terms of emitted mass (Chou et al. 2008). Atmospheric mineral dust is produced by weathering of rocks and soils at the surface of the earth. They undergo mobilization into the atmosphere by winds and are then carried over long distances (Kalderon-Asael *et al*., 2009). The distance between the source and deposited region influences particles size distribution and composition hence they often reflect the composition of the material available from this provenance (Rashki et al. 2013). Where topsoil is not covered by vegetation, its finer fractions can be easily released to the atmosphere and may contribute to re-suspended PM (Alfaro-Moreno *et al.,* 2007). This is particularly expected in case of soil dryness and wind erosion conditions.

The chemical composition of PM may vary widely owing to the mixture of substances, a function of emission sources and the subsequent chemical reactions which take place in the atmosphere (Engelbrecht *et al*., 2009; Mishra *et al.*, 2008). This necessitates the knowledge of the chemical composition of airborne dust, in order to clarify the likely source regions as well as to undertake quantitative climate modeling, in understanding possible effects on human health, precipitation, ocean biogeochemistry and weathering phenomena (Goudie and Midelton, 2006).

PM have been identified as an important atmospheric pollutant in the world because they cause a range of environmental problems, such as having a positive association with wide range of illnesses including pulmonary and cardiovascular disorders, material damage (Chapman *et al.*,

1997; Donaldson *et al.*, 2001; Li *et al.,* , 1997; Pope III *et al.,* 2004; Richards, 2003) and affecting the Earth's radiative forces by directly absorbing or scattering incoming solar radiation (Buseck, and Posfai, 1999).

PM contaminants affect human health when they are transported over densely populated areas (Larney *et al.,* 1999), retained in residences and other occupied structures (Lioy *et al.,* 2002); impact the nutrient loading of waters flowing from adjacent watersheds (Wood and Sanford, 1995) and terminal bodies of water by direct and indirect deposition (Ganor *et al.,* 2003; Lawrence and Neff, 2009).

There is considerable gap between developed and developing countries of the world in terms of air quality and pollution monitoring. In the former their environmental protection agencies ensure that emission facilities such as industries install and maintain pollution abatement technologies, so as to reduce concentrations of the pollutants and to conform to stiff guidelines. However, in the latter, environmental protection agencies are hardly effective, in that, very little efforts are geared towards pollution control devices, if they exist at all. The consequence of this ineffectiveness is that emission of pollutants into the workplace and neighborhood environments are common practices. Emission sources are sometimes located in residential and commercial areas due to lack of proper enforcement of urban planning laws. The populace in the vicinity of such facilities are exposed to the pollutants as they spend large fraction of their lives within the polluted environment (Akeredolu *et al.,* 2006).

In Nigeria, dust (mineral dust) re-suspension, traffic and industrial emission are major sources of particulate matter in the atmosphere (Abdulkarim *et al.,* 2007; Dimari *et al.,* 2008).

It is more difficult to analyze the mineral composition of PM than to analyze the chemical composition due to the size of retrievable samples. For this reason various studies undertaken in Nigeria focused on evaluating the mass concentrations as well as the elemental composition of airborne particle only (Oluyemi and Asubiojo, 2001; Okuo and Ndiokwere, 2006; Olatunji *et al.,* 2010; Owoade *et al.*, 2009) rather than mineral composition. But elsewhere in the world especially Europe and Asia both chemical and mineralogical composition of PM have been reported (Abu-Allaban *et al.*, 2006; Krueger *et al.,* 2004; Lu *et al.*, 2007; Xie *et al*., 2005; Xie *et al*., 2009) with emphasis on single particle analysis.

The geology of Ibadan is comprised of extensive Basement Complex rocks with dominant minerals found in the rocks to include quartz, feldspars of various types, biotite, and hornblende

while the dominant rock types are generally gneissic – granitic in character (Okunlola *et al.*, 2009; Olayinka *et al.*, 1999). Studies have also shown that soil of the study area were formed as a result of in situ weathering of the most common rock types the aforementioned minerals in the rocks are released by weak to moderate degree of chemical weathering and hence incipient pedogenetic influence on the bedrock unit (Odewande and Abimbola, 2008; Okunlola *et al.*, 2009; Tijani *et al*., 2006).

There are currently no published work on single particle mineralogical analysis of dust in Nigeria as a whole and only a few work on the geochemical studies and potential impact of airborne dust on human health in Ibadan have been published (Ana *et al.*, 2012; Olatunji *et al.*, 2010; Oluwole *et al*., 2012; Onianwa, 2001).

It is against this background that this research work was undertaken. Understanding the influence of PM on the atmospheric environment can only be achieved by investigating size distribution, mineralogical and geochemical composition of particulate matter in the atmosphere.

1.2 Objectives of Study

The objectives of this research are to

1. Assess the mass load of Particulate Matter (PM) in the atmosphere within Ibadan metropolis.
2. Determine the constituent major/trace elements of the PM and evaluate the degree of enrichment of these elements in them and
3. Identify the constituents morphology and minerals of the PM

1.3 Problems and Justification

Ibadan is one of the largest cities in Nigeria in terms of land mass with total area of 300Km^2 and population of about 3.57 million people, according to the Nigerian population Census of 2006. Within the city, several human activities that could cause air pollution in the environment are prominent. Such activities include mineral dust re-suspension by wind, vehicular movement and quarry activities, industrial emission, indiscriminate burning of domestic waste in illegal dumps

and traffic congestion and vehicular emission. This is further aggravated by limited street space, poorly maintained vehicles and roads, lack of emission control and management programs.

One of the most serious consequences of this pollution is exposure of large part of the population to different doses of air pollution on daily basis. The exposure has been linked to various diseases and mortality in humans as a result of the proximity of residence to the aforementioned emission sources (Ana *et al*., 2012; Olatunji and Akinsoji, 2013; Oluwole *et al.*, 2012).

Although, much work have been done on the environmental pollution of Ibadan in respect to water, stream sediments and soil (Adeyemo *et al*., 2008; Ikotun, *et al.*, 2012; Odewande & Abimbola, 2008; Osibanjo *et al*., 2011; Taylor *et al*., 2009; Tijani *et al*., 2006). Only a limited number of such studies have been conducted on atmospheric quality (Ana *et al.,* 2012; Olatunji and Akinsoji, 2013; Olatunji *et al*., 2010; Oluwole *et al.*, 2012; Onianwa, 2001).

Such studies have been limited to chemical characterization and to some extent mass of airborne particles. This is the common type of study in relation to air pollution in Nigeria (Oluyemi and Asubiojo, 2001, Akeredolu *et al.*, 2006; Owoade *et al*., 2009). However, these works do not include determination of the mineralogical constituents of dust. The little known about mineralogical constituent of dusts in Nigeria (Wilke *et al.*, 1984; Adedokun *et al.*, 2000) were mainly focused on bulk sample analyses using major elemental study and XRD, rather than single particle analysis.

Single particle analysis have known to be an effective tool in deciphering the sources of pollutant (Reid, 2003; Reid, 2003; Xie *et al*., 2009). It is therefore possible to reveal whether a mineral occurs as a major component in a small fraction of the particles or as a minor component in many particles. In bulk sample analysis, these characteristics are largely masked. It is generally necessary to analyse a large number of bulk samples in order to deduce the pollution sources by multivariate techniques, while by individual particle analysis, a limited number of representative samples are usually enough to extract a fairly well resolved source profile and therefore revealing the different types of mineral component in the atmosphere.

This research work involved the analysis of a large number of bulk samples and individual particles in order to reveal definitive information about elemental association and detailed variation of composition with particle size. This will help to decipher the relationship among other geological media used in the assessment of pollution status of the environment.

Therefore, the aim of this research is to characterize the particulate matter mass load, mineralogical and chemical composition of aerosol dust in order to unravel the different contributory sources from the study area.

1.4 Location of the Study Area

Ibadan is located in the southwestern part of Nigeria, about 143 km northeast of Lagos. The city is on the railroad line linking Lagos with the northern part of the country and is well connected by road to other cities in the region. The study is limited to latitudes 7º15' and 7º30'N and longitudes 3º44' and 4º00E (Figure 1.1). The population of Ibadan, which was estimated to be 175, 000 in 1911, has increased tremendously to about 2 million as at 1991 Census figure (NPC, 1991) and had risen to about 4million according to the 2006 Census. The growth of Ibadan can, according to Ayeni, 1994 , be attributed to its location and accessibility in relation to the older Yoruba cities of Abeokuta, Oyo, Ijebu-Ode and Ile-Ife, as well as a point for bulk-trading of most of the agricultural produce from the other south-western and virtually all the northern States of the country. Access within the metropolis is by network of major and minor roads and this made the field-work easily achievable.

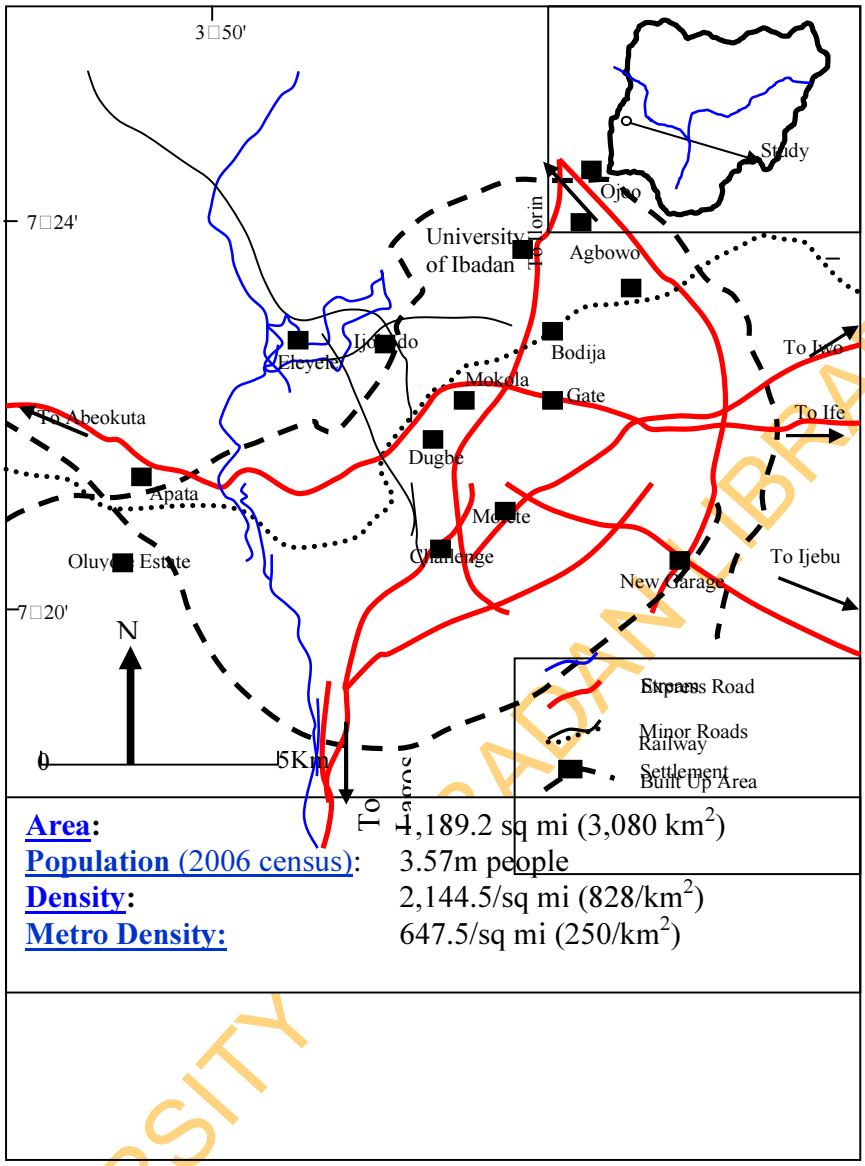

Area:	1,189.2 sq mi (3,080 km^2)
Population (2006 census):	3.57m people
Density:	2,144.5/sq mi (828/km^2)
Metro Density:	647.5/sq mi (250/km^2)

1.5 Climate and Geomorphology

Ibadan is located within the forest grassland of South-western Nigeria and lies in the transition zone between the humid and the sub-humid tropical climates. The climate is characterised by well-defined rainy (wet) and dry seasons. In Ibadan, two pronounced rainy seasons exist, one in April-June and the other in September-November (Table 1.1 and Figure 1.2). The minor dry season is between July till August; this lull divides the wet season into two. The major dry season is from December-February, when the northeasterly wind known as the Harmattan wind blows from the Sahara region.

Dust is transported from the Sahara to the Gulf of Guinea by the north-easterly trade winds in a south-westerly direction. This occur in Nigeria, Benin, Togo, Ghana and the Côte d'Ivoire (Sunnu *et al.,* 2008). The dry, dusty wind is one of the predominant atmospheric phenomena in West Africa and it is known as the Harmattan. It lasts from late November to March in the sub-region (Afeti & Resch 2000). According to D'Almeida, 1986, overall 60% of the total particles from the Sahara Desert are transported to the Gulf of Guinea. The number of particles, mass distribution, dust flows, the deposition rate and the mean size of the particles have been estimated in several countries, especially in Ghana (Afeti & Resch, 2000; Afeti 2000; Breuning-Madsen , 2005; Resch *et al,* 2007) Mali (McTainsh *et al.,* 1997) and Nigeria (McTainsh, 1980). These studies show that the dust quantity (which varies from year to year) is greater in the northern parts of these countries and that the dust particles become finer in size as they move further south.

The mean annual rainfall ranges from 788mm – 1844m with a mean temperature of 26^0C (Table 1.1 and Figure 1.1). The northeast trade wind keeps the humidity extremely low, but occasionally there are sporadic showers of rain. The monthly mean temperature is between 25°C and 30°C throughout the year.

The topography of the area is characterised by a rugged and rolling topography made up of hills, plains and river valleys with the hills being the most striking features making up to 5% of the total area. Studies have shown that in Ibadan, areas of high relief coincide with the regions of quartzite ridge especially in the southern part of the metropolis (Olayinka *et al,* 1999).

Table 1.1: Average Climatic Conditions in Ibadan (*Source: BBC Weather*, 2011)

Month	*Average Sunlight (hours*	*Temperature*				*Discomfort from heat and humidity*	*Relative humidity*		*Average Precipitation (mm)*	*Wet Days (+0.25 mm)*
		Average		*Record*						
		Min	*Max*	*Min*	*Max*		*am*	*pm*		
Jan	6	21	33	10	37	High	94	51	8	1
Feb	7	22	34	12	39	High	92	49	23	2
March	6	23	34	18	38	High	95	54	76	5
April	6	23	33	18	38	High	95	60	125	9
May	6	22	32	18	35	High	96	67	145	11
June	5	22	29	18	33	High	97	74	163	12
July	3	21	28	16	31	Medium	97	78	132	12
Aug	2	21	27	16	31	Medium	97	78	74	10
Sept	3	22	29	17	36	High	97	75	170	15
Oct	5	22	30	18	33	High	98	70	152	12
Nov	7	22	32	14	34	High	97	63	43	4
Dec	7	21	33	14	35	High	96	56	10	1

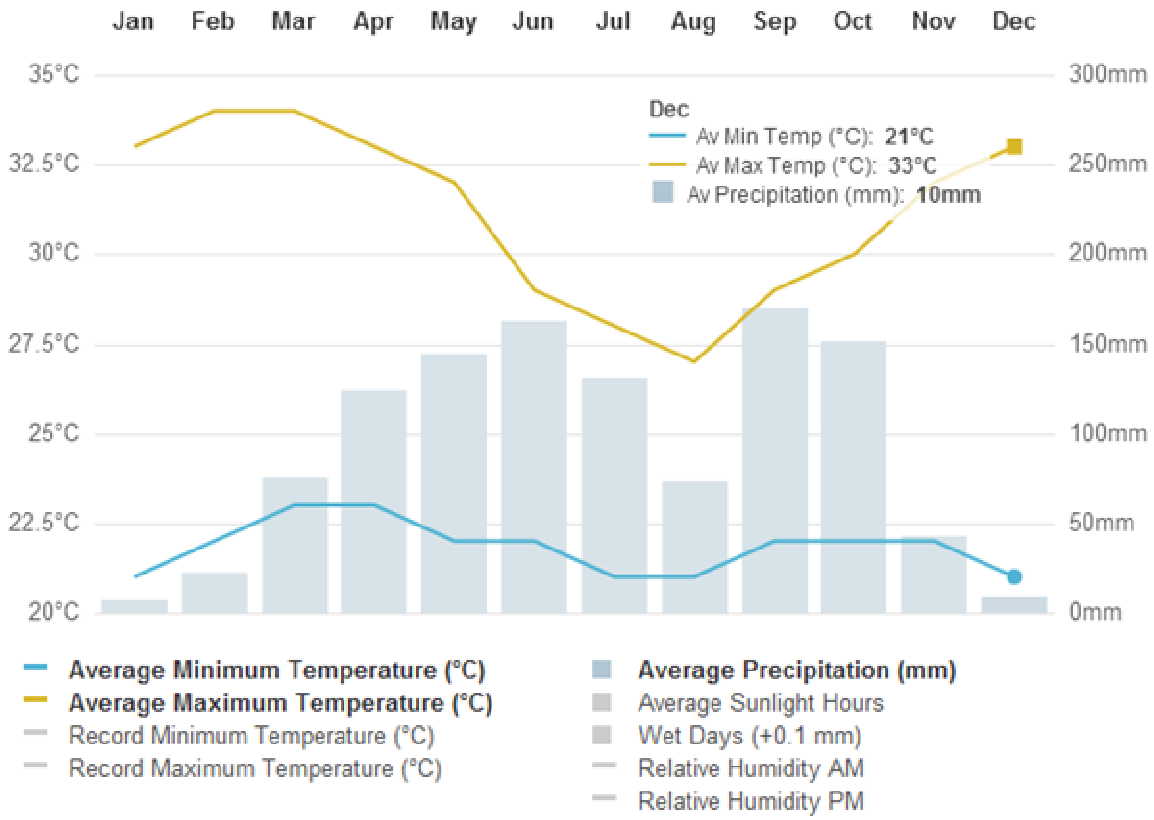

Figure 1.2: The bar chart for **Ibadan, Nigeria** shows the yearly average weather condition readings covering rain, average maximum daily temperature and average minimum temperature (*Source: BBC Weather*, 2011).

1.6 Soil

The soil of Ibadan was formed as a result of weathering of the Basement Complex rocks (Tijani *et al* 2006) under moist semi-deciduous forest cover (Hopkins 1965) and belonged to the major soil group known as ferruginous tropical soils (D' Hoore 1964). Smyth and Montgomerry, 1962 classified them into four groups based on soil association and series, namely: Iwo, Okemesi, Egbeda and Mamu (Figure 1.3). The classification was based on soil parental materials (Aweto 1994), and were formed from coarse grained granite gneisses, quartz-schists/quartzite, fine grained biotite gneisses and pegmatites respectively. Because quartzite are resistant to weathering, Okemesi group are usually shallower with thickness of weathered profile generally less than 1m. While soils of Iwo and Mamu group are fairly clay due to their parent materials (granite gneisses and pegmatite respectively (Tijani *et al*., 2006).

1.7 Site Description

Four zones based on the land use patterns (environmental units) within Ibadan were identified and selected for sampling purposes. The identified land use zones were commercial zone with mixed residential areas (RA), industrial areas (IA), dumpsites area (DA), and traffic areas (TA). Descriptions of the Sampling points are presented in Table 1.2. PM were collected at these selected zones at a height of 1.8 m for 11 months between February and December in 2011

Ibadan roads are of various categories such as Major Express-way (main), Sub-major and minor roads. Most of these roads are poorly maintained and in several cases un-paved.

Increase in vehicle traffic as a result of increase in vehicle ownership consequently causes traffic congestion. These factors combine to create air pollution hotspots near roads (Figure 1.4 a, b, e, f). In order to make up for current trend in the traffic density of the roads in the study area, effort was made to classify the roads based on Onianwa, (2001), who categorized the traffic density in Ibadan into three classes, high (>1000 vehicles per hour), medium (250-1000 vehicles per hour) and low (<250 vehicles per hour). Traffic counts were used to know the numbers of each category of vehicles per hour (e.g buses, cars, trucks and motorcycle). Hence, the average traffic count per hour was estimated (Table 1.2).

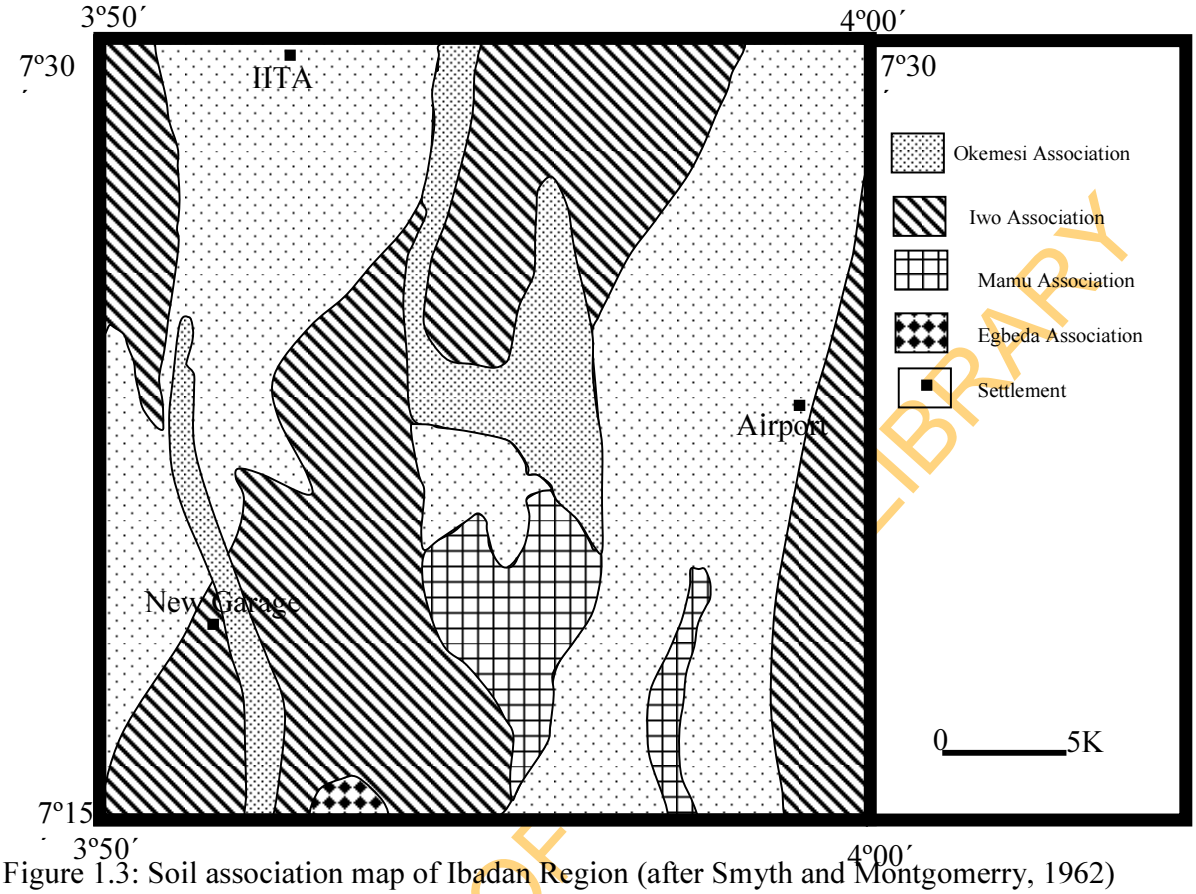

Figure 1.3: Soil association map of Ibadan Region (after Smyth and Montgomerry, 1962)

Table 1.2: Description of the activities in the study area

	Zone	Classification	Area	Grades	Activities/ Possible sources of Pollutants	Average Traffic Density (counts/hour)*	No of sample
1	Traffic	High	Iwo Road intersection[a], Beere, Ojo intersection[a], Agbowo, Sango, Dugbe, Challenge, Apata	Express Roads/Main Road	Traffic congestion, Vehicular emission (Heavy Duty/light duty Exhaust), resuspension of road dust, fugitive dust from road construction, incineration,	1800-2500	
		Medium	Bodija Market Road, Agodi Gate (Minor road), Sabo, Abadina Quarters, Apete	Branch/Sub-main Roads	wood burning	600-1000	
		Low	U.I Senior Staff Quarters (Imo Road), New Bodija	Minor Roads		<200	40
2	Industrial	High	Oluyole Industrial Estate	Point Source	Oluyole Industrial Estate consists of different industries which include food and beverage and confectioneries processing, organic chemicals manufacturing, basic steel production, agricultural produce processing and production, auto repair workshops, concrete production, pharmaceuticals, agro-allied chemicals and manufacturing.	20 companies	40
3	Dumpsite		Awotan (Odo-Ona Elewe) dumpsites		Off-loading and compaction of domestic and industrial waste, wind scouring of waste surfaces, Vehicles driven on the facility can cause resuspension of deposited particulates on roadways; transport of larger particles on vehicle bodies and generation of particulates by vehicular exhaust fumes.		40
4	Residential/ Commercial	Commercial zone with mixed density residential areas	Bodija market and its environs, Beere, UI staff Quarters and Apete		Biomass burning, incineration, mechanic workshops, exhaust from power generating sets		85

Figure 1.4: Traffic and Industrial activities (a) Traffic Congestion in the Study area, (b) traffic emission (c) Industrial facility (d) Industrial emission (e) Poor and untarred road (f) Vehicular Dust Resuspension and Deposition in the Zone.

Despite the fact that for over two decades, Ibadan city has been gradually developing into an important industrial city in Nigeria; the rate of industrialization has not been matched with proper planning to prevent or mitigate environmental pollution problems that are usually associated with such development. Most of the industries are concentrated in the southwestern part of the city (Oluyole Industrial Estate) while other small scale industries are in different areas

generally outside the Oluyole Industrial Estate and are located very close to residential areas. This research monitors airborne particulate matter in Oluyole Industrial area which accommodates various industries ranging from small scale to large scale.

Among these were 7Up bottling company, Procter and Gamble, cookies and confectionary (manufacturer of Biscuit and sweet e.g Yale Biscuit), glass Industry and iron and steel company, they all generate airborne particles that could have health impact (Figure 1.4 c, d). Meanwhile, other minor activities are evident in the area are imprint of traffic from haulage vehicles and indiscriminate wood burning utilised by informal restaurants for cooking in the area.

There are four accredited land fill dumpsites regionally located in Ibadan (Northeast; Aba-Eku, Northwest; Awotan, Southeast; Akanran and Southwest; Ajakanga). These dumpsites are associated with activities common with any waste facilities elsewhere. However unlike the practice in well-developed dumpsite, the dumping of refuse is usually done indiscriminately without any prior sorting. (For example plastic, garbage scrap metal wastes were dumped together in the same place). Some of the activities that generate particulate matter and disperse it in air around and within the waste facilities include movement of waste to and from the facility; off-loading and compaction of waste, incineration of waste and wind scouring of waste surfaces. Vehicles driven on the facility can also have a significant impact through the: resuspension of deposited particulates on roadways and hard-standing; transport of larger particles on vehicle bodies; generation of particulates by vehicular exhaust fumes.

Apart from the effect of these three regions on the residential area, there are other household activities such as cooking with both kerosene stove and in many cases with wood and charcoal burning (biomass burning) and the use of power generating sets, which could cause pollution of the environment (Figure 1.5). Also, most of the people living in the residential areas often

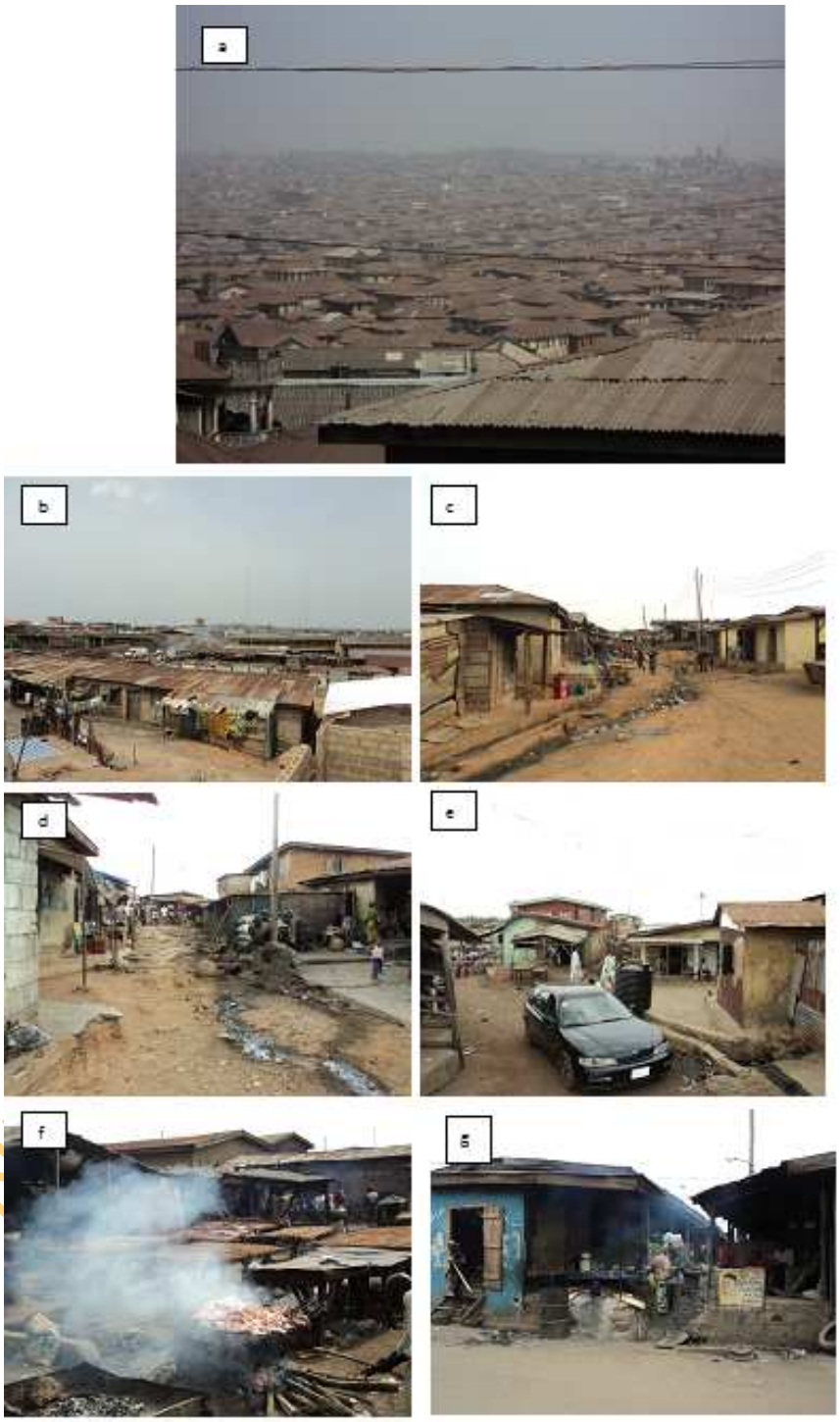

Figure 1.5: Residential Area with mixed Commercial Area. Overview of the Area and Different Activities in the

engage in different commercial activities (market, mechanic workshops etc) within their neighborhood as means of sustenance.

This study also monitors the residential area close to one of the biggest commercial center/market (Bodija market). This market has been studied by some workers for its various level of pollution. The market has different sections ranging from abattoir (generate big heaps of waste, incineration and biomass burning is common), planks/saw mills (the use of generator with diesel and a very big saw dust burning points) and auto-mobile village.

CHAPTER TWO
LITERATURE REVIEW

2.1 Particulate Matter

Particulate matter consists of solid or liquid aerosol particles suspended in the air and has diverse mineralogical and chemical composition related to its sources. Particulate matter includes mineral dust, soot, smoke, and liquid droplets emitted into the air by different sources such as factories, power plants, vehicles, construction activities, fires, and wind-blown soil dust (Abu-allaban *et al.*, 2003).

Mineral dust plays an important role in the optical, physical and chemical processes in the atmosphere (Xi and Sokolik, 2012), while dust deposition adds exogenous mineral and organic material to terrestrial surfaces, having a significant impact on the Earth's ecosystems and biogeochemical cycles (Jickells *et al.*, 2005; Lawrence and Neff, 2009).

Mineral dust particles are fine airborne soil and/or weathered or transported rock particles removed from the Earth's surface as a result of wind erosion under certain climatic, meteorological and soil conditions.

The Earth's surface is composed of a large number of minerals, which occur in heterogeneous mixtures within rocks. It is estimated that 1000–3000Tg of mineral aerosols are emitted annually into the atmosphere over the globe (D'Almeida, 1987; Jones *et al.,* 1995), which can be transported over long distances (e.g. Prospero, 1999).

On the other hand, dust deposition may influence biogeochemical cycling in terrestrial ecosystems, while dust accumulation in soils can influence texture, element composition and acid-neutralising capacity (Larssen and Carmichael, 2000; Muhs and Benedict, 2008). Furthermore, the chemical and mineralogical composition of soil dust provides useful

information about its provenance (Yang *et al.,* 2007), radiative forcing implications (Sokolik and Toon, 1999) and human health effects (Erel *et al.,* 2006).

PM can be classified based on its properties, but the most important are sizes, morphology (shape or phase) and chemical species (both organic and inorganic for example Polycyclic Aromatic Hydrocarbons (PAHs) and heavy metals respectively).

The sizes are generally categorized as fine and coarse mode; with the fine particles (those with <2.5 µm aerodynamic diameter) produced by combustion sources such as fossil fuel and biomass burning, while many of the coarse particles between 2.5 and 10 µm are fugitive dust derived from re-suspension of soil-dust from roadways, construction sites, mechanical wear of rock and minerals (Godish 1991; Whitby 1978).

The size of the particle is a main determinant of where in the respiratory tract the particle will come to rest when inhaled. Larger particles are generally filtered in the nose and throat and do not necessarily cause problems. But particulate matter smaller than 10 micrometers (µm), referred to as PM_{10}, can settle in the bronchi and lungs and cause health problems. Seinfeld, and Pandis, (2006) stated that the 10 micrometer (µm) particle size does not represent a strict boundary between respirable and non-respirable particles, but has been agreed upon for monitoring of airborne particulate matter by most regulatory agencies. Similarly, particles smaller than 2.5 micrometers, $PM_{2.5}$, tend to penetrate into the gas-exchange regions of the lung, and very small particles (< 100 nanometres) may pass through the lungs to affect other organs. A study by Fubini and Arean, (1999) indicated that $PM_{2.5}$ led to high plaque deposits in arteries, causing vascular inflammation and atherosclerosis- a hardening of the arteries that reduces elasticity, which can lead to heart attacks and other cardiovascular problems.

Particulate matter, along with ozone, carbon monoxide, nitrogen dioxide, sulfur dioxide, and lead are the six "criteria pollutants" that are regulated by the United States Environmental Protection Agency (EPA) under the Clean Air Act. These "criteria pollutants" are widespread in ambient air and are potentially harmful to human health. Therefore, maximum concentrations for the six "criteria pollutants" have been established, according to the National Ambient Air Quality Standards (NAAQS) to protect human health.

The NAAQS criteria are 15μg/m^3 (annual arithmetic mean) and 65 μg/m^3 (24-hour average) for $PM_{2.5}$ as well as 50 μg/m^3 (annual arithmetic mean) and 150 μg/m^3 (24-hour average) for PM_{10} (Massey *et al.*, 2013). When an area does not meet the air quality standards for any "criteria pollutant", it may be designated as "non-attainment". These "non-attainment" areas are required to develop air pollution control strategies to decrease the emissions of criteria pollutants in order to meet the standards (Sharma *et al.,* 2013).

The Polycyclic Aromatic Hydrocarbons (PAHs) and heavy metals present in the $PM_{2.5}$ and PM_{10} samples have been studied extensively with regard to their roles in inducing toxicity effects (Kim *et al.*, 2013).

Various classifications of $PM_{2.5}$ and PM_{10} constituent according to their chemical composition have been reported (Kalderon-Asael *et al.*, 2009; Liu *et al.*, 2005; Lu *et al.*, 2007; Rizzo and Scheff, 2007; Wang *et al.*, 2006 Chow *et al.*, 2003) such as metal oxide, sulfates and nitrate, sodium chloride, sodium nitrate, particulate organic carbon and PAHs.

The metal oxide of Al, Si, Al, Mg, Ca, Na, K, Ti, Fe are usually generated by geological materials in the form of suspended soil-dusts, the atmosphere in the coastal area are usually enriched in sodium chloride and sodium nitrate- indicative of reaction of nitric acid with sea salt, and are also classified as a geological materials with coarse particle (PM_{10}).

Sulfur is present as ammonium sulfate, ammonium bisulfate, and sulfuric acid. These compounds are water soluble and exist almost exclusively in the $PM_{2.5}$ size fraction. Nitrogen occur as ammonium nitrate being the most abundant nitrate compound and are generated by different anthropogenic sources such as vehicular and industrial emission.

The concentrations and properties of airborne particles in a given location is dependent on a variety of factors such as road indigenous geological materials carried away due to wind weathering, construction activity and other industrial activities.

The $PM_{2.5}$ fraction is comprised of mostly primary and secondary anthropogenic combustion products (Wang *et al.*, 2012) originating mainly from traffic and energy production. Due to their origins in the combustion of hydrocarbon fuels, fine particles are usually more carbonaceous in nature than coarse particles and tend to contain both organic and elemental carbon.

2.2 Exposure impacts

2.2.1 The source–pathway–receptor chain

Particulate matter is a global phenomenon in that they can be transported from a short or long distance from where they are originated depending on their sizes, release and transport mechanism. For this reason, monitoring of air quality around different sources form part of the management of environmental risk (EPA, 2004). Therefore, Source-Pathway-Receptor (S-P-R) relationship needs not to be underestimated.

Three components need to be present before an exposure risk exists, a source (primary and secondary) where the emission takes place, a pathway which is made up of a release mechanisms and a transport mechanism (e.g. dispersion of the aerosol in ambient air) and a receptor (e.g. a neighboring resident) located at an exposure point (e.g. a nearby residential dwelling), who experiences exposure via an exposure route (e.g. inhalation of the aerosol). This chain of events, shown diagrammatically in Figure 2.1, is termed an exposure pathway and is the complete environmental route by which particulates from the source can reach receptors. If any parts of the source-pathway-receptor chain are missing, then there is no risk of exposure (EPA, 2004).

2.2.1.1 Sources

There are two main sources – the primary and the secondary. The primary sources include geologic or crustal material, sea salt, elemental carbon, organic carbon and biogenic aerosol while the secondary sources include the nitrate, sulphate and carbonate. Lack, (2003) reported on PM sources ranging from natural and anthropogenic sources on the basis of their estimated contribution and their relative sizes distribution.

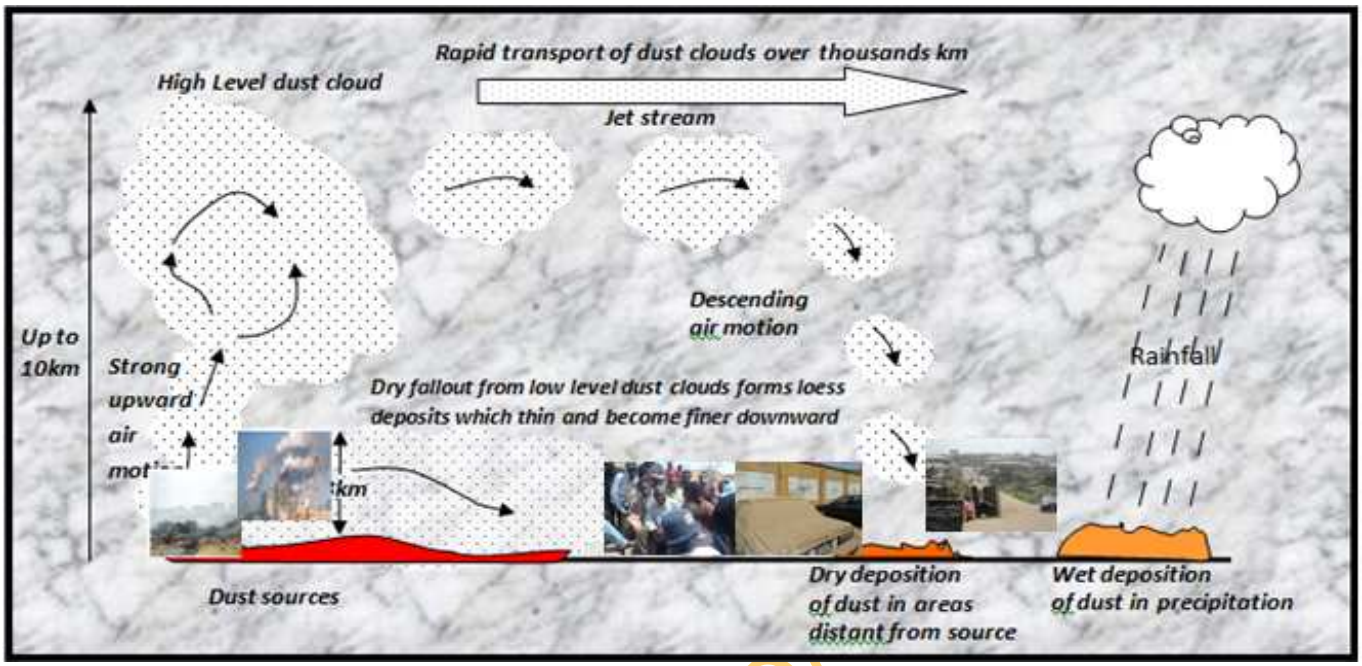

Figure 2.1: Principal atmosphere pathways between dust sources and dust sinks, involving both dry and wet deposition modes (modified after Pye, 1987)

The crustal materials mobilized into the atmosphere are estimated to contribute up to 2250 Tg/yr to the atmospheric load and they have diameter ranging from 1-10 µm which make them efficient scatters of solar radiation and absorbers of infra-red radiation (Wolf and Hidy, 1997). The formation of crustal aerosol is a natural occurrence from farming, construction land clearing practices and vehicular dust re-suspension all of which increase the mobility and availability of crustal material into the atmosphere.

Sea salt aerosol is said to contribute about 3340Tg/yr to the atmospheric aerosol this is dependent on wind speed, as salt spray is formed from turbulent mixing on the ocean surface. The sea salt formation mechanism can produce particles ranging in diameter from 0.02-10µm with a size dependency on wind speed.

Elemental carbon (EC) aerosols are composed mainly of elemental carbon produced from combustion of fossil fuels, biomass and other combustion processes. Direct emission of EC aerosol from combustion produces very small particles of mass media diameter of 0.1µm. EC aerosol from fossil fuels combustion is essential and contributes 11-17 Tg/yr to aerosol load. This is an efficient absorber of solar radiation due to its colour, contributing to atmospheric warming estimated to be $+0.2Wm^{-2}$ (Wolf and Hidy, 1997). The result of this absorption within combustion processes is the production of fine particles of large surface area with high concentrations of atmospheric pollutants which can contribute significantly to adverse effects of human health. In addition to elemental carbon, combustion processes produce large quantities of organic carbon (OC) aerosol.

Primary OC aerosol is the product of incomplete combustion and is comprised of high molecular weight, usually PAHs. Like EC aerosol, OC aerosol commonly have diameter less than 1µm (Wolf and Hidy, 1997), with ranges between 0.1 and 0.4µm for OC aerosol reported for fossil fuel combustion and biomass burning source (Pandis *et al.*, 1992). Optical properties of OC aerosol, and hence the effect on the radiation balance, can be variable due to their variable composition.

Biogenic aerosol refer to that fraction of OC aerosol that is comprised of plant and organism materials such as leaf fragments, pollen, waxes, bacteria, fungi, viruses, algae or spores. The contribution to the atmospheric aerosol load for OC aerosol is estimated to be about 56Tg/yr.

Biological aerosol particles (BAP) describes the airborne solid particles (dead or alive) derived from living organisms, including microorganism and fragments of all varieties of living things. BAP includes viruses ($0.005<r<0.25\mu m$), bacteria ($r \geq 0.2\ \mu m$), fungi ($r \geq 0.5\mu m$), pollen ($r \geq 5\mu m$), algae, spores of lichen mosses, ferns, plant debris like leaf litters, part of insect, human and animal epithelia cells (usually $r \geq 1\mu m$) (Mathias-Maser 1998).

Secondary aerosols are those atmospheric aerosols that are not emitted directly into the atmosphere, rather were produced from gas-atmospheric species via chemical reaction. They include sulfate, nitrate, ozone and organics.

Secondary sulphate aerosol is a common component of the atmospheric load that is formed through photochemical production of sulphuric acid from sulphur dioxide (SO_2). Production can be in the gaseous or aqueous phase. The precursor to sulphate aerosol, SO_2 can be emitted directly from volcanoes or fossil fuel combustion or can be formed from sulphur containing species such as hydrogen sulphide or dimethyl sulphide. Direct sulphate emission can also contribute to sulphuric acid particles formation. SO_2 emissions in the atmosphere are generally of natural sources, while concentrated NO_x emissions are most commonly associated with anthropogenic processes.

In areas where emission of NO_x and NH_3 occur together, ammonium nitrate (NH_4NO_3) can form aerosol (Seinfeld and Pandis, 1998). If the ammonia is in the presence of sulphuric acid, it will act to neutralise the sulphuric acid aerosol-forming sulphate forming ammonia based salt. Particulate are generally formed as a result of atmospheric reaction of NO/NO_2 involving gas-to-particle conversion. In addition to ambient temperature, ammonia concentration influences the nitrate aerosol formation (Sonibare and Jimoda, 2009).

2.2.2.2 Pathway

Aerosol particles are characterized by long residence time in the atmosphere and thus undergo transport and dynamic processes. Aerosol transport and dynamics denote the physical and chemical changes they undergo from a certain state to a more stable state.

Particulate matter rise up in the atmosphere due to buoyancy effect, advect downwind, and disperse horizontally and vertically due to the turbulent field and prevailing meteorological patterns. The lifetime of particulate matter in the atmosphere ranges from a few days to a few weeks. These relatively long residence time result in long range transport of aerosol particles from urban to non-urban or remote area. The transport of particulate matters in the atmosphere is similar to those gaseous pollutants for the fine particles fraction but deviate at larger sizes due to deposition process. Therefore, long range transport of particulate mass contributes significantly in the background particles mass and number size distribution. Aerosol particles were found in the atmosphere to undergo changes in their chemical composition and size. This is due to variety of physical and chemical processes such as nucleation (new particles formation), condensation, evaporation, coagulation, deposition (dry and wet), action due to water and other gaseous species and aqueous phase reactions (Seinfeld and Pandis, 1998).

Particle size is regarded as the most important physical characteristic of air borne particulate matter, which control the residence time of particle in ambient air. The emitted particles have certain falling velocity (depending on size of the particle) due to downward force of gravity, which is opposed by aerodynamic drag of atmosphere. The balance between these forces is readily attained and the particle remains suspended in air for long time. The size of particulate matter can vary from 0.002 μm to 500 μm and particles larger than 50 μm can be seen with unaided eyes. The particles in the 0.005 – 0.05 μm range are produced either by high temperature combustion or by chemical process or by condensation of vapor. Particles in 0.005 – 2.0 μm range are usually formed by coagulation of smaller particles or from particles through vapor condensation. Coarse particles are formed due to mechanical process, such a grinding, wind action, soil erosion and also agglomeration of smaller particles. The particles having falling speed less than about $3x10^{-3}$ m/s, which is equivalent to that of about 7μm diameter easily penetrate into human respiratory system, while the particles with aerodynamic diameter above 10

μm do not usually penetrate beyond the nasal passage, while particles above 50 μm could not be breathed with low suction pressure generated at mouth and nose during action of breathing, therefore do not pose much health hazard and also settles faster in the form of dry deposited matter or dust (Connan et al. 2013)

Large particles (>30 μm) responsible for most dust annoyance mostly deposit within 100 m of the source. Intermediate-sized particles (10–30 μm) are likely to travel up to 200–500 m. Smaller particles (<10 μm) can travel up to 1 km from the source, although very small particles can travel much further (DETR, 2000a). The solubility of particulate matter in aqueous media or in lipids is of great biological significance because it influences the rate of depositing in the body. The chemical composition of particulate matter has direct bearing on the resulting health effect and is generally related with the process from which it is derived.

2.2.2.3 Deposition

Pollutants are released into the atmosphere from variety of activities, including emission of mobile (automobile) and stationary sources which include factories and power plants (Goforth and Christoforou, 2006). Once in the atmosphere, they may undergo changes, be transported over short or long distances depending on particle sizes and ultimately scavenged and delivered to the earth surface, either by wet deposition (during rainy weather, snow or fog condition) or dry deposition (during dry weather by gravitation settling), the major pathways for the transport of particulate pollutant from air to land and water is dry deposition (Zufall and Davidson, 1997).

The concept of deposition velocity is often used to parameterise the deposition process. Seinfeld and Pandis (1998) defined deposition velocity as the ratio of the deposition flux of the specified pollutant to the pollutant concentration. There are two general approaches to determine the dry deposition velocity. In the first method, available experimental data for different aerosol and gaseous species are used while the second method is based on the transfer of material from the atmosphere to the earth's surface through different resistance mechanism, the aerodynamic resistance, the surface resistance and the transfer resistance (Slinn and Slinn, 1981).
The particle deposition varies with particle size and can be expressed as

$$V_d = \frac{1}{r_a + r_d + r_a r_d V_g^i} + V_g^i$$

V_d is the deposition velocity (m/s) of particles in the size bin I, r_a is the aerodynamic resistance (s/m), r_d is the deposition layer resistance (s/m) of particles in the size bin I, V_g^i is the gravitational settling velocity (m/s) of particles in the size bin i.

2.3 Effect of PM

2.3.1 Effect on Human Health

Particulate matter (PM) had recently become issue of increasing importance in pollution sources due to its noticeable effect on human health. Various studies on air pollution effect on health indicated a strong positive correlation between air pollution concentration and observed health effect. World Health Organization (WHO) estimates that almost 800,000 people die prematurely every year due to air pollution (WHO, 2002). Samet *et al*., (2000) found that PM influences the rate of mortality from cardiovascular and respiratory diseases. In addition, if the concentration of PM_{10} is increased, each additional 10 mg/m^3 raises the overall mortality by 0.51% and raises mortality from cardiovascular and respiratory disease by 0.68%.

Harvard Six-Cities study by Harvard School of Public Health and a cohort study by the American Cancer Society have shown that the life expectancy of long-term residents of areas with high particle concentrations is 2-3 years shorter than that of people living in areas with lower particle concentrations (Dockery *et al*., 1993).

Epidemiological studies reveal an association between exposure to crystalline silica dust and an increased probability of developing lung cancer. Administration of crystalline silica to rats by inhalation or intra-tracheal instillation also led to the development of lung tumours. Therefore, crystalline silica is classified by International Agency for Research on Cancer (IARC) as a Group 1 carcinogen to humans. The epidemiological studies show that the incidence of lung cancer is increased especially in workers with silicosis. The first step in reducing the cancer risk, therefore, must be the prevention of silicosis (Ehrlich *et al.,* 2013; IARC, 1997).There is strong evidence that fine particles (<2.5µm) play an important role in the observed health effect (Stern *et al.*, 1984). Coarse particles ($PM_{2.5\text{-}10}$) are effectively removed in the upper part of respiratory track while fine

particles are deposited on the bronchi walls (Akeredolu, 1996). Particles smaller than 0.1 µm experience Brownian motion as a result of which they get deposited in the bronchi. However, particles between 0.1 and 1 µm are too large for Brownian motion and too small to be trapped in upper part of the trachea. Particle behaviors in the long are dependent on the aerodynamic characteristics of particles in flow streams. The aerodynamic properties of particles are related to their size, shape and density. The nasal opening permit very large dust particle to enter the nasal region, along with much finer airborne particulate.

Long term exposure to air polluted with Particulate Matter (PM) increases the risk of lung cancer, respiratory diseases and arteriosclerosis, whereas short-term exposure can exacerbate several forms of respiratory diseases, including bronchitis and asthma, as well as changes in heart rate variability (Dominici *et al*., 2007; Peacock *et al.*, 2011; Pope *et al.*, 2009; Raaschou-Nielsen *et al.*, 2011; Rusconi *et al*., 2011).

During the last decades, much effort has gone into discerning physicochemical characteristics and adverse health effects of air pollution (Elliott *et al*., 2007; Hales and Howden-Chapman, 2007; Pope *et al*., 2009). In developed countries, the level of air pollution by PM is generally decreasing; in contrast, in most of the developing countries, it is dramatically rising (Dieme et al., 2012). A critical situation could also be expected in Sub-Saharan Africa countries, where the urban population has grown faster than in any other world region during the last decades (WHO, 2002).

At present, it is well-known that, depending upon its natural and/or anthropogenic emission sources, air pollution PM is generally a complex mixture of metals (e.g. Fe, Al, Pb, Mn, Zn), organic chemicals (e.g. Volatile Organic Compounds, VOCs; Polycyclic Aromatic Hydrocarbons, PAHs; paraffins), and biological materials, coated onto carbonaceous cores (Alfaro-Moreno, et al., 2007; Baulig *et al*., 2004; Billet *et al.*, 2007; Gualtieri *et al.*, 2010; Osornio-Vargas *et al*., 2011; Quintana, *et al*., 2011). However, epidemiological evidence indicated that the greatest health risks correlate with the smallest PM, which has the capacity to reach the distal regions of the lung, and is often associated with the most significant human health effects (Pope *et al*., 2009).

The mechanisms for PM induced human health effects are still not totally clear, but oxidative stress and inflammatory reaction seem to be of fundamental importance (Baulig *et al.,* 2009; Garc-on *et al*., 2006; Lodovici and Bigagli, 2011; Lonkar and Dedon, 2011). Experimental and epidemiological data indicate that lung disorders are often associated with pro-oxidant/antioxidant imbalance and

inflammatory reaction, and there is increasing evidence that air pollution by PM induces acute responses as well as exacerbate existing inflammatory diseases in the lung (Peacock *et al*., 2011; Raaschou-Nielsen *et al.,* 2011; Rusconi *et al*., 2011).

Under physiological conditions, the normal production of Reactive Oxygen Species (ROS) is counteracted by antioxidant scavengers and enzymes, which includes enzymes and non-enzymatic scavengers (i.e. glutathione) (de Kok *et al*., 2005; Garc-on *et al*., 2006). However, under abnormal conditions, excessive levels of ROS exceed the detoxification capacity of antioxidant defenses, thereby causing a change in the redox status of the cell (Jomova and Valko, 2011; Lonkar and Dedon, 2011; Ziech *et al* , 2011). Oxidative stress thereafter triggers a cascade of events closely associated with inflammation, which is believed to play a key role in the air pollution PM induced development and/or exacerbation of acute and/or chronic lung diseases (Garc-on etal., 2006; Lodovici and Bigagli, 2011).

2.3.2 Visibility reduction

Visibility degradation is one of the most readily perceived impacts of fine particulate matter. Fine particles absorb and scatter light and therefore reduce visibility (Seinfeld and Pandis, 1998). Fine particles with diameter between 0.3-1.0µm make the major contribution to visibility reduction (EPA 1996). The most immediate and obvious impact of urban pollution is its impairment of visibility. Most cities of the world like Lagos are experiencing visibility degradation due to high emission intensity and adverse meteorology (Oluyemi and Asubiojo, 2001). This high emission intensity is as a result of fine particles that interact more strongly with visible radiation due to their diameter being similar to that of wavelength of light.

In most urban atmosphere, visual degradation is largely associated with presence of aerosol particles. This is because aerosol interacts with visible light in different manner. Hence, aerosol appears bright against a blue sky when observer is looking towards the sun and dark when the sun is behind the observer. Hanel, 1976 observed that the relative humidity has considerable effect on the extinction properties of the aerosol as a result of absorption and water uptake capacities of the various mineral aerosol properties. One of the primary reasons for the persistence of visibility problem is lack of methods that can be quantitatively used to show how different sources contribute to visibility

impairment. Previous studies have shown that secondary particulate that are formed in the atmosphere from the reaction of precursor gases contribute significantly to visibility impairment in pollution areas. In polluted area, anthropogenic pollutants significantly reduce the visual range.

2.3.3 Soiling and Damage to Materials

An important part of particulate matter pollution is the soiling of man-made surfaces. Hence, the process of cleaning and repairing exposed surfaces become an economic burden. Acid particles can severely deteriorate art works and historic monuments (cultural heritage) and result to the loss of their aesthetic appearance and shorten their life span (Hamilton and Mansfield, 1993; Nazaroff and Cass, 1991).

Chemical degradation of materials due to deposition of atmospheric acid particles is an important of material damage (Butlin *et al.*, 1992). PM_{10} and $PM_{2.5}$ differ not only on sizes but also in sources, chemical composition, physical properties and formation process. PM tend to soil cities surfaces due to the reciprocal attempt to dust or clean in different manners by humans, which in an effect distort the surfaces. Also, the dust which is alkaline, damages painted surfaces such as wall, doors and automobile. The soiling of exterior building materials was investigated by Watt et al., 2008 to be dependent on type of paints. For white paints, the soiling was found to be directly proportional to the square of the particle dose of the particulate matter. The degree of soiling is influenced by the optical and chemical compositions of airborne PM. Butlin *et al.*, 1992 observed that diesel particulate is about 3.5 times more in the average urban particulate. Hence, diesel smoke tends to stick to surfaces more than average particulates. He argued that only 1/3 to ¼ of the mass of diesel soot compared with other urban particulates was required to achieve a stain of equivalent darkness. Hence, diesel soot is expected to have a greater affinity to surface than generated atmospheric particulates. The liquid components of diesel particulates allow it to adhere to a surface more readily than dry average particulates. Diesel soot has a greater propensity to smear and is more difficult to remove than dry particulate due to its liquid components.

2.3.4 Earth Radiative Forcing

Particulate matter influences the climate directly (through scattering and absorption of the solar radiation) and indirectly through the formation of cloud condensation nuclei (CCN). The direct aerosol contribute to radiative forcing is due to sulphate aerosols, fossil fuel soot and biomass burning (Buseck and Posfai, 1999; Penner *et al.*, 1993). The radiative forcing due to sulphate aerosol is estimated to be $-0.4Wm^{-2}$ with a factor of two uncertainties. The effect of soot aerosol is $+0.1Wm^{-2}$ with a factor of three uncertainties and the contribution from biomass burning is estimated to be $-0.2Wm^{-2}$ with a factor of three uncertainties. Therefore, the total direct forcing is estimated to be $-0.5Wm^{-2}$ with a factor of three uncertainties.

Climate forcing is defined as the change imposed by certain forcing agent which include greenhouse gases and aerosol particles in the energy balance of the earth (in units of W m^{-2}) that eventually alters global temperature (Haywood and Boucher, 2000). However, the definition is only useful under the assumption that there exists a general relationship between global mean equilibrum surface temperature response that is similar for all the different types of forcing. Aerosol can interact both directly with solar radiation and terrestrially re-emitted infrared radiation, and directly alter the planetary albedo (reflected sun light) by modifying the properties of cloud. The first of these mechanism is known as the direct radiative forcing effect of particles (Charlson *et al.*, 1992), whereas the latter is referred to as the indirect radiative forcing effect of particles. Size distribution, complex refractive index (chemical composition and state of mixing), solubility and change in size with relative humidity influence the magnitude of these effect.

2.4 PM Standards

The Clean Air Act requires EPA in the United States of America to set National Ambient Air Quality Standards (NAAQS) for six criteria pollutants and particle pollution (also known as particulate matter) is one of these.

The Clean Air Act established two types of national air quality standards for particle pollution. **Primary standards** set limits to protect public health, including the health of "sensitive" populations such as asthmatics, children, and the elderly. **Secondary standards** set limits to protect public welfare, including protection against visibility impairment, damage to animals, crops, vegetation, and buildings.

The EPA revised the air quality standards for particle pollution in 2006 and tighten the 24-hour fine particle standard from the current level of 65 micrograms per cubic meter ($\mu g/m^3$) to 35 $\mu g/m^3$, and retain the current annual fine particle standard at 15 $\mu g/m^3$. The Agency decided to retain the existing 24-hour PM_{10} standard of 150 $\mu g/m^3$. The Agency revoked the annual PM_{10} standard, because available evidence does not suggest a link between long-term exposure to PM_{10} and health problems.

The Clean Air Act requires EPA to review the latest scientific information and standards every five years. Before new standards are established, policy decisions undergo rigorous review by the scientific community, industry, public interest groups, the general public and the Clean Air Scientific Advisory Committee (CASAC).

2.5 Previous Work

The results of pollution indicator parameters investigated, that is, particulate matter deposition rate, sulphate and heavy metal concentration from harmattan dust in Maiduguri Metropolis, show significant level of increase which is indicative of an aggravation of atmospheric air pollutants during the Harmattan seasons which portend consequential implication for human health and Environment (Dimari *et al*., 2008).

Oluyemi and Asubiojo, 2001 subjected elemental concentration of ambient air particulate matter in Lagos, Nigeria to factor analysis and chemical mass balance in order to identify their sources and source apportionment respectively. It was deduced from the factor analysis that four sources were prominent in their contributions to air particulate loading and the sources include soil, marine, automobile traffic and incineration.

The spatial distribution of particulate air pollution in the Warri metropolis was studied by Efe and Efe, 2008. This study was done in order to ascertain the differences between the distribution of particulate matter (PM_{10}) in the urban and the surrounding rural areas. The major findings of the study was that Warri metropolitan area was polluted with PM_{10} levels of over 126 $\mu g/m^3$, which is

81% over the 70 µg/m^3 threshold of the World Health Organization. However the built-up area of the Warri metropolis is 150% more polluted with PM_{10} particulates than the surrounding rural areas.

Owoade *et al*., 2009, sampled particulate matter ($PM_{2.5}$ and PM_{10}) from various sections of the industry in Lagos, Nigeria. The sampling locations were selected to reflect locations where workers in the industry spend most of their working hours, and the samples were collected at a height of about 1.6m above the floor and the sampling was carried every month for 1 year covering both wet and dry seasons. He observed that the mass concentration of PM_{10} levels ranged from 86 to 8765 µg/m^3 while $PM_{2.5}$ ranged from 10 to 462 µg/m^3. The elements Cr, Mn, Fe, Cu, Zn and Pb measured in PM_{10} and $PM_{2.5}$ fractions of the particulate matter were found to be high in the electric furnace section as result of the scrap and additives used in the process and the rate of the emission is relatively high when compared with other production sections within the industry. It was also observed that there is no significant difference in seasonal variation.

Air particulate matter collected by gravimetric method at five locations where industrial activities are concentrated in Warri, was analysed for 14 elements by Atomic Absorption Spectrometric Method (Okuo. and Ndiokwere, 2006). It was observed that the particulate mass concentration ranged between 922-2333 µg/m^3 and the highest elemental concentrations measured in the samples were for As, Se, V, Na and Ca. The results that As, Cd, Se, V and Pb are derived from combustion and industrial activities and are highly enriched while the elements Na, Ca and Al which are soil derived are moderately enriched.

Ideriah *et al*., (2001) determined the concentration of indoor and outdoor of suspended particulate matter in south-eastern Nigeria. The findings of this study agree with the statement that in many rural areas and in most cities, people in developing countries are exposed to a range of local, but strong, sources of SPM. The results of the rural communities in the study area are more polluted than the urban community in both indoor and outdoor SPM.

The concentration of gaseous pollutant such as CO and CO_2 with suspended particulate matter at Benue Cement Company and Tse-Kucha community was investigated by Abdulkarim et al., (2007). Result obtained, showed concentration of carbon dioxide of 34.40, 39.50, 48.50, 78.55, 65.25, 26.80 and 29.5ppm for quarry, raw mill, kiln packing house, limestone stockpile and Tse-Kucha community

respectively all of which were below detection the maximum standard natural concentration of CO_2 in Atmosphere of 600ppm while concentration of CO (1.25-4.00ppm) measured in all the sample station were below the Nigeria Ambient Air Quality Standard (NAAQS) and WHO maximum limit of 10-20ppm. The concentration of suspended particulate matter of 375 and 290µg/m^3 at the cement mill, packing house and raw mill respectively were also above the world Health Organization Guidelines and Standards for Ambient Air Quality which stipulates a range of 150 to 230µg/m^3.

2.6 Regional Geological Settings

The study area, Ibadan, lies within the Precambrian Basement Complex of South-western Nigeria, which is part of the Proterozoic mobile belts located between the West African and Congo Cratons (Figure 2.2). It lies within the region which have been subjected only to a thermo tectonic event (Grant 1970). It has been established that the Precambrian Basement Complex of Nigeria including Southwestern Nigeria is polycyclic in nature, (Ajibade and Fitches 1988). The southwestern Nigerian Basement Complex had undergone four major orogeny:

- Liberian 2800 ± 200my
- Eburnean 2100 ± 200my
- Kibarian 1100 ± 250my
- Pan-Africa 600 ± 150my

The Eburnean and the Pan-African are major events which modified the Precambrian Geology of Nigeria including the Southwestern Nigerian basement complex. The Eburnean event is marked by the emplacement of the Ibadan granite gneiss in Southwestern Nigeria which has been dated 2100 ± 200my (Rahaman, 1988) and a pink granite gneiss at Ile-Ife Southwestern Nigeria dated 1875Ma using U-Pb on Zircon. The Liberian, Eburbian and Kiberian were characterized by intense deformation and isoclinals folding accompanied by regional metamorphism, which was followed by extensive migmatization (Obaje, 2009). The Pan African deformation was accompanied by regional metamorphism, migmatisation and granitisation. The end of the orogeny was marked by faulting and fracturing (Olayinka, 1992). However, based on the

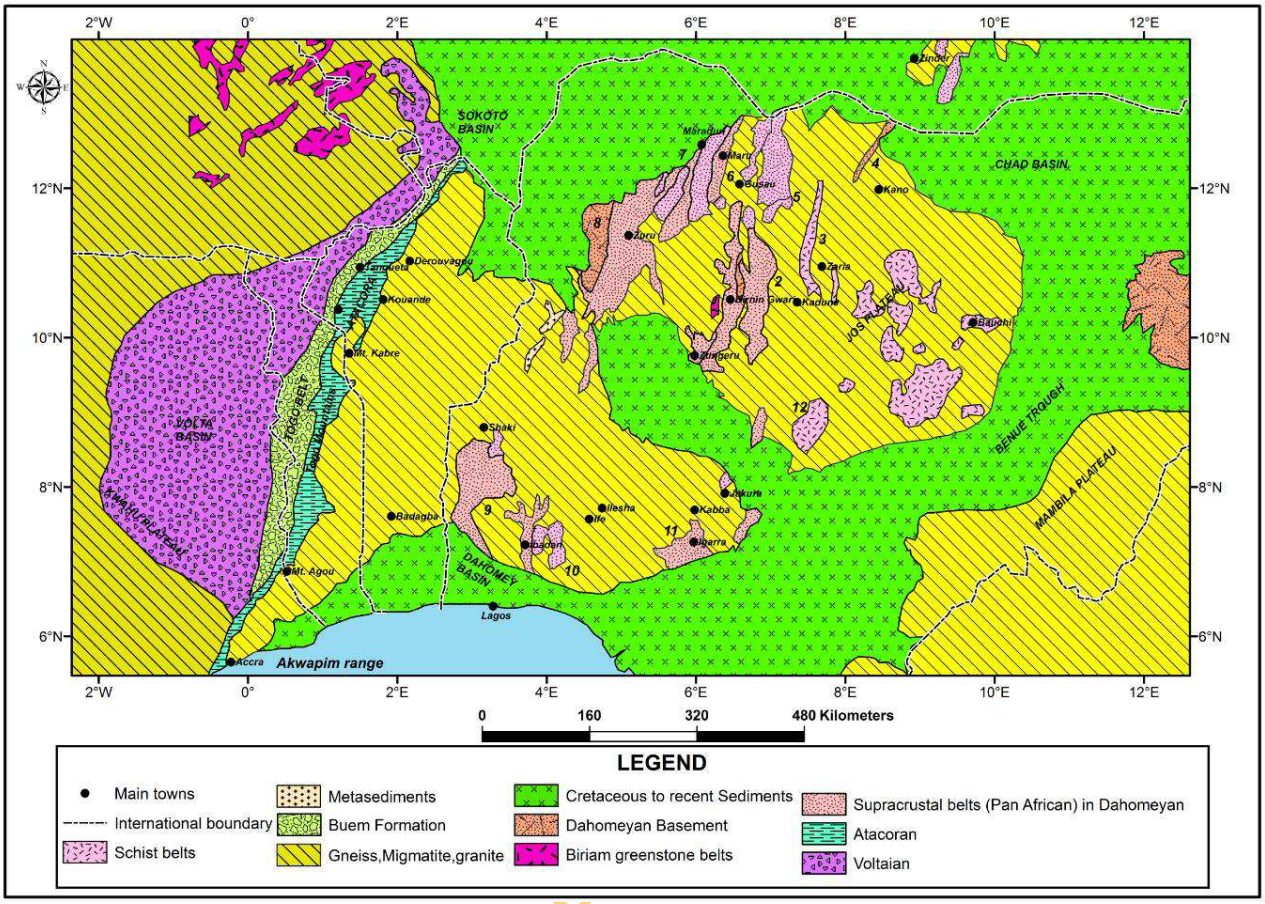

Figure 2.2: Basement Complex of Nigeria within the frame work of the geology of West Africa (adapted from Wright, 1985).

classification scheme developed for the Basement Complex by Falconer, (1911), Jones and Hockey, (1964) and Rahaman, (1976) the following rock suites were classified:

- Migmatite - Gneiss Quartzite Complex Suite
- Slightly migmatised to unmigmatised metasedimentary and meta-igneous rock
- Charnokitic rocks suite
- Older granite suite etc.

2.6.1 The Migmatite-Gneiss Complex

The Migmatite-Gneiss Complex also termed as migmatite-gneiss-quartzite complex make up about 60% of the surface area of the Nigerian Basement (Rahaman and Ocan, 1978). These rocks record three major geologic events (Rahaman and Lancelot, 1984); the earliest, at 2,500Ma, involved initiation of crust forming processes (e.g the Ibadan banded and grey gneiss of mantle origin) and of crustal growth by sedimentation and orogeny; subsequently followed by the Eburnean marked by the Ibadan type granite gneisses; this was followed by ages in the range of 900-450 Ma which represent the imprint of the Pan-African event. Most authors on the Nigerian Basement Complex subscribe to the view that the rocks of these suites comprise largely a metasedimentary series with associated minor igneous rocks which has been variably altered by metamorphic, migmatic and granitic processes (Okunlola *et al.,* 2009; Oyawoye, 1972; Rahaman, 1988). The migmatites gneiss complex comprises gneisses, quartzite and calc-silicate rocks; the gneisses include banded, granite and augen gneisses. They are presumably the oldest because it bears imprints of Liberian and Eburnean events (Oversby 1975). The Migmatite-gneisses complex is dominated by quartzo-feldspathic, biotite-hornblende bearing gneisses, schist and Migmatite in which minerals such as garnet silimannite, kyanite and staurolite suggest high amphibolite facies metamorphism.

2.6.2 The Schist Belt

The schist belt mostly comprise of low-medium grade metasediments belt trending N-S, which are well developed in the western part of the country. These belts are considered to be Upper Proterozoic supercrustal rocks which have been infolded into the migmatite-gneiss-quartzite complex. The lithological variations of the schist belts include coarse to fine grained clastics, pelitic schists, phyllites, banded iron formation, carbonate rocks and mafic metavolcanics

(amphibolites). The contact relationships of the schist belt rocks with the gneiss-migmatite complex are frequently oriented to regional north-south tectonic elements (Olade and Elueze, 1979). Rahaman, (1988) concluded from a review of various metamorphic studies that metamorphism in all the Nigerian Schist belts ranges from green schist to lower amphibolite metamorphic facies. The common rocks of the schist belt include biotite, biotite-garnet and biotite-garnet-staurolite schists, amphibolite talc-tremolite-chlorite schist, marbles, calc-silicates, gneiss quartz schist. Schist belt have been mapped in the southwestern Nigeria in Iseyin-Oyan, Ilesha and Igarra. The Iseyin-Oyan Schist Belt extends to Ibadan, which composed mainly of mica schist. Banded amphibolite schists are common and have been interpreted as metamorphosed calcareous sediments; more massive amphibolites may represent mafic igneous rocks (Jones and Hockey, 1964). Metamorphism is higher in grade than in most northern schist belt, with politic rocks containing biotite, garnet, staurolite and sillimanite (Rahaman, 1976).

2.6.3 Pan African Granitoids

The Older Granites are believed to be syn-to-post tectonic granite rocks which cut across both the Migmatite-gnesis-qurtzite complex and the schist belts in Nigeria. These granitoids include Charnokite, gabbros, dolerites and Older granites, which are Pan-African in age. They range in age (750-450 Ma) and composition. They represent a varied and long lasting magmatic cycle associated with the Pan-African orogeny. The rocks of this suite in composition from tonalite and diorite through granodiorites to true granites and syenites. They generally outcrop as smooth rounded boulders, dyke-like bodies within the Older granite and migmatites complex. The charnokitic rocks are believe to be either derivatives of partial melting of Older granites and or gneisses during magma emplacement or intrusive bodies emplaced during a granulite facies metamorphism (Hubbard, 1975). The Older Granites are mainly brought about by the Pan-African orogeny. Dada, (2006) was of the opinion that the Older Granite should be termed Pan-African Granite not only on the basis of the time of emplacement but because they are also important petrographic group formed at the same time. The granitoids which outcrop with the schist belts in both north-western and south-western Nigeria include biotite muscovite granite, syenites, and charnockites.

2.6.4 Structural Geology

It was observed by several workers that in the basement complex area of Nigeria, metamorphism is commonly associated with deformation. (Annor, 1983) with the aid of a suite of minor

metamorphosed intermediate dykes, distinguished three successive episodes of ductile deformation in the evolution of the Basement Complex of Nigeria as exposed around Okene. According to him, the first episode is the high-grade gneisses, which predate the dyke. The second episode is distinguished by a syn-dyke planar metamorphic structure developed in metasediments and some meta-intrusive rocks. The last episode is distinguished by major fold structure defined by the proceeding planar fabric and also by syn-fold minor shear zones and axial plane foliation in zone of high strain.

In Nigeria three phases of metamorphism (M_1, M2, and M3) and two phases of deformational episodes (D1 and D2) have also been recognized. The dominant N-S structural trend associated with fold of steep axial planes generally regarded as Pan-African Imprint is common within the Nigerian Basement Complex (Annor, 1986).

CHAPTER THREE

RESEARCH METHODOLOGY

3.1 Sample Collection

Five (5) major monitoring stations and several sub-stations within the study area were used throughout the sampling campaign (Figure 3.1). They represented the afore-mentioned zones, that is, one station each, except for the traffic section that has two (2) stations (Ojoo and Iwo Road).

Samples for IA were collected during the dry season (February-March) with total of 40 samples. Forty (40) samples were also collected in DA spanning between dry and wet season (March to June) and the sampling was done in order to reflect the effect in the vicinity (i.e. 500-1500m away from the dumpsite). The traffic sections were also monitored and total number of 40 samples was taken in areas with busy traffics (Ojoo and Iwo Road) areas and less busy area. Considerable attention were given to Residential area where monitoring of PM was undertaken throughout the year except January during weekends and few cases in midweek and a total number of 85 samples were collected within 4 and 6 hrs.

In order to assess the sources of mineral dust in the study area, rocks and soils of this region were also sampled along with PM samples. The rocks samples collected were migmatite gneiss, granite gneiss, quartz-schist and granite and pegmatite, since they occupy more than 80% of the rocks in the study area.

Soils developed on these lithologies were sampled up to depth of 5cm with plastic scoop and packed with polythene bags. They were subsequently air dried and sieved through <65µm before analyses.

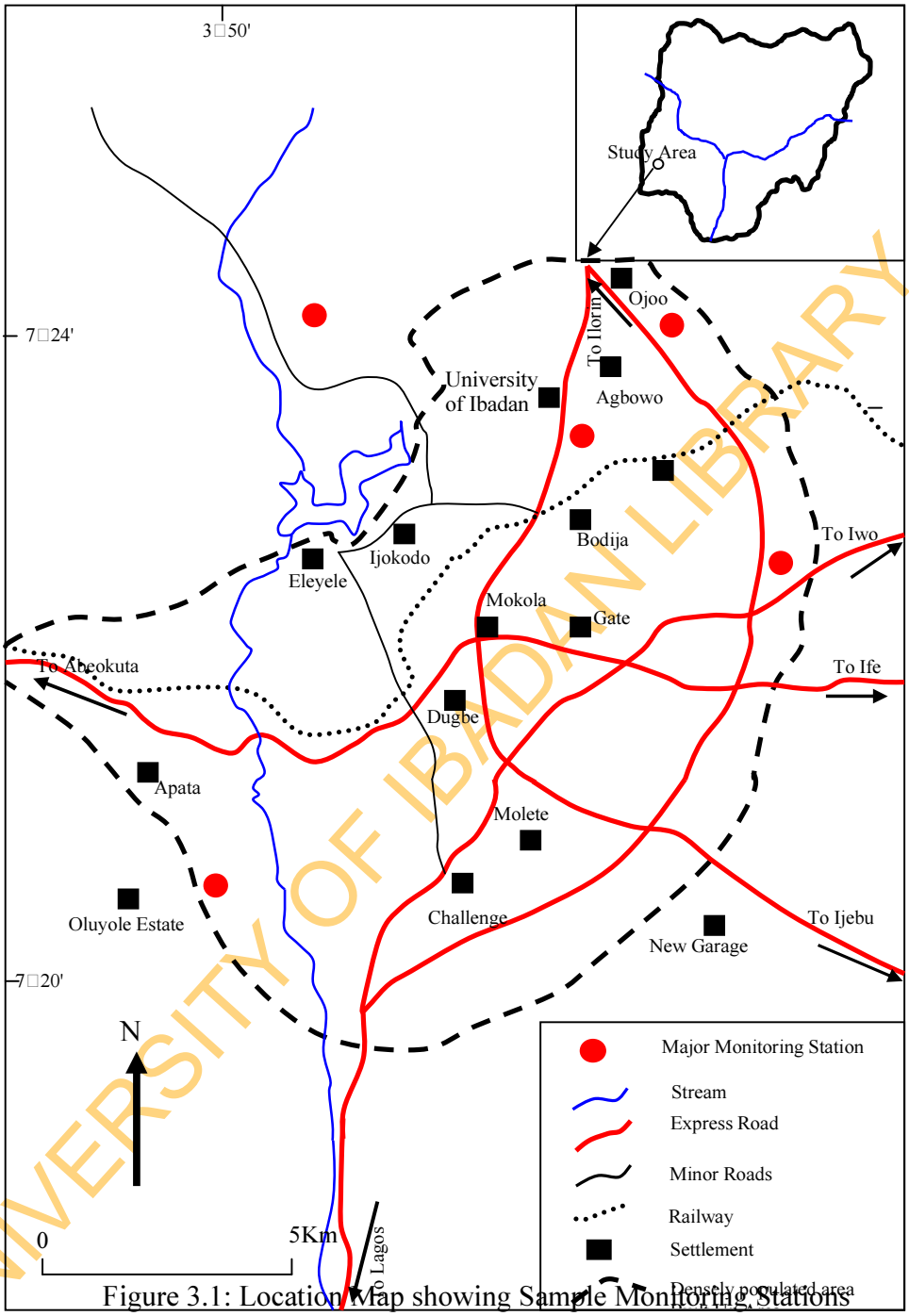

Figure 3.1: Location Map showing Sample Monitoring Stations

In order to have enough dust particles for XRD analysis which is difficult in the case of suspended particles using filter, deposited dust were collected with Petri-dish mounted on top of multiple floor buildings in different locations.

3.2 Sample Measurement

The High-Volume Air Sampler (HVAS) model #15000 manufactured by science resource with cut-point of 10µm, was used for the collection of PM samples in the study area (Figure 3.2). The HVAS is a device for sampling large volumes of atmosphere and collecting the contained particulate matter by filtration. It is a compact unit consisting of a protective housing; an electric motor driven; a high-speed, high-volume blower; a filter holder and a manometer for controlling the air-flow rate through the instrument at the recommended flow rate of 630 l/min. It also required a desiccator and analytical balance to measure the net gain of the filter to the nearest milligram. In operation, this sampler draws air into the sampler through the air inlet gap between the cover and the sampler housing walls. The weather cap design for the sampler allows the sampled air to be evenly distributed over the surface of filter and protect larger particles from falling on the filter during operation.

The type of filter media is important both for the efficiency of sampling as well as the selected analysis method. Filter media are judged for specific applications according to Chow, (2003) based on their mechanical stability, chemical stability, particle or gas sampling efficiency, flow resistance, loading capacity, blank values, artifact formation, and compatibility with analysis methods, cost, and availability. The most commonly used filter media for atmospheric particle and gas sampling are Teflon membrane, quartz fiber, nylon membrane, cellulose fiber, Teflon-coated glass fiber, etched polycarbonate membrane, and glass fiber. For this study cellulose filter was used throughout the operations, with surface area of about 120mm$^{2.}$ The Filters were prescreened to exclude particles up to a given size, the filter was placed in such a way that the rougher surface was placed upward. The sampler was then calibrated using manometer attached to the HVAS.

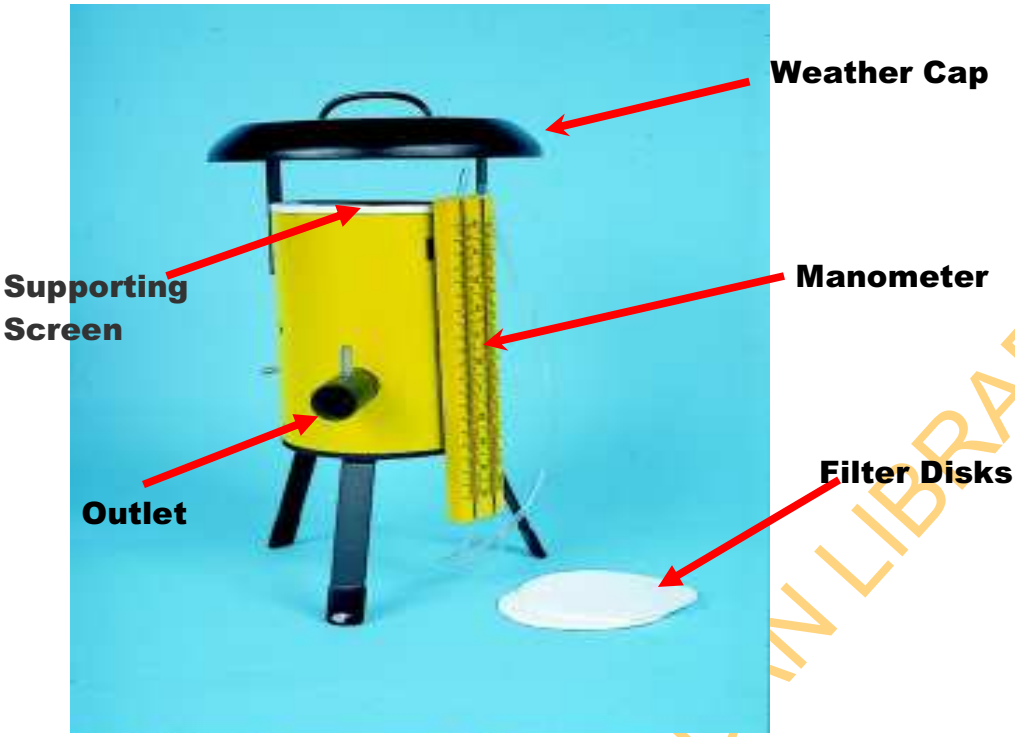

Figure 3.2: Photograph of High Volume Air Sampler

The pre-weighed filter sheet was mounted in the filter holder or filter cover in order not to lose any fiber; this was clamped in place by means provided. It sealed into place easier by facing the smooth side into the housing if there was a difference in texture. The filter holder was then mounted on the intake port of the sampler, making sure that it was tight.

The sampler was placed 20-50m away from the scene so as to avoid localize effect and this is in accordance to the standard set by National Ambient Air Quality Standard (NAAQS). The sampler motor was then started and the time and date were recorded, a stopwatch was used to measure all time required so also to detect any loss of test time due to power interruption. The flow rate was read from the flow-rate indicator and the corresponding flow rate was read from the calibration. The barometric pressure differences were noticed and measured. A continuous record of the sampling flow rate and sampling time was obtained by the use of a continuous pressure (or flow rate) recorder. The sample was run for maximum of four hours as specified by the manufacturer. During this period several readings of flow rate was taken. A final set of reading was taken at the end of the test period.

At the end of the sampling period, all the final readings were recorded. The filter was then removed from the mount very carefully so as not to lose any of the fiber material or collected particulate matter. This was folded in half upon itself with the collected material enclosed within. The folded filter was placed in a clean tight envelope and marked for identification to prevent any loss or damage to the filter.

In the laboratory the filter was removed from its container. The container was then tapped so as to knock any loose fiber or particulate matter onto the inside surface of the folded filter and accidental objects such as insects were removed. The calculation of the mass load is given as (EPA, 1999a)

$$SPM = \frac{(Wf * Wi) * 10^6}{V_{std}} \quad \text{.....equation 1}$$

where: SPM = mass concentration of suspended particulate matter (TSP or PM_{10}), µg/std m^3.

W_i = initial weight of clean filter, g.

W_f = final weight of exposed filter, g.

V_{std} = air volume sampled, converted to standard conditions (25EC and 760 mm Hg), std m^3.

10^6 = conversion of g to µg.

3.3 Sample Preparation and Analysis

3.3.1 Sample Preparation for Chemical Analysis

Elemental analysis of the sample in the filters involved hot acid extraction as proposed by EPA, 1999. The processes was done by adding 5 ml of nitric acid (Merck Suprapur 65%), 2 ml of hydrochloric acid (Merck Suprapur 36%) and 10 ml of ultra-pure water (18 MΩ cm−1 of specific resistivity) in a Pyrex tube and sat still for 2 h at 95°C in a heating plate (Fernández et al., 2000). The extracted solution was filtered, using a Whatman n° 41 (WH1441-110) filter, completed to 50 ml with ultra-pure water and kept in pre-cleaned polyethylene bottles in the refrigerator until analysed (Beceiro-González *et al*., 1997; Serrano *et al*., 1996).

Filter and reagent blanks were processed following the same treatment. The metal content of the blanks for Ca, Mg, K, Na, Mo, Mn, Fe, Zn, Cu, Co, Ni, Al and Pb were less than 8% of samples average content. Metals were determined by inductively coupled plasma optical emission spectroscopy (ICP-OES) (Figure 3.3) following (EPA, 1999b). Both, detection limits and accuracy for the method were also determined following (EPA, 1999b). The obtained results were in an acceptable agreement with the certificate of analysis, with a difference lower than 8%.

3.3.2 X-Ray Diffractometry (XRD) Analysis

Few tenths of a gram of the rock and soil samples obtained were ground to a fine powder to achieve 200-mesh fraction. They were subsequently placed into a sample holder and pressed in order to have a smooth surface and uniform smear on the plastic slide (the substrate was usually amorphous to avoid interference). Care was taken to create a flat upper surface and to achieve a random distribution of lattice orientations.

Figure 3.3: Photograph of Inductively Coupled Plasma with Optical Emission Spectrometer Machine at the Institute of Earth and Environmental Sciences, University of Potsdam, Germany.

The powdered samples were subjected to X-ray diffractometer (XRD) analysis. The XRD analysis was on a Brauker (Siemens) AXS 5005 diffractometer with Cu-Kα radiation at 40 kV and 125 Ma. Scans were performed from 3° to 70°, at a rate of 3° (2θ)/min, and the sampling distance was 0.01° (2θ).

The samples were put in a small cuboid aluminum trough for XRD analysis. The intensity of diffracted X-rays was continuously recorded as the sample and detector rotate through their respective angles. A peak in intensity occurs when the mineral contains lattice planes with d-spacing appropriate to diffracted X-rays at that value of θ. Although each peak consists of two separate reflections at small values of 2θ the peak locations overlap with $K\alpha_2$ appearing as a hump on the side of $K\alpha_1$. Greater separation occurs at higher values of θ. Typically these combined peaks are treated as one. The 2λ position of the diffraction peak was typically measured as the center of the peak at 80% peak height.

The d-spacing of each peak was then obtained by solution of the Bragg equation for the appropriate value of λ. Once all d-spacing have been determined, automated search/match routines compare the *d*s of the unknown to those of known materials. Because each mineral has a unique set of d-spacing, matching these d-spacing provides an identification of the unknown sample. A systematic procedure was used by ordering the d-spacing in terms of their intensity beginning with the most intense peak. Files of d-spacing for hundreds of thousands of inorganic compounds were available from the International Centre for Diffraction Data as the Powder Diffraction File (PDF). Many other sites contain d-spacing of minerals such as the American Mineralogist Crystal Structure Database. Commonly this information was an integral portion of the software (PDF-Data Base Sets, 1996 Version) that comes with the instrumentation.

3.4.3 Scanning Electron Microscope/ Energy Dispersive X-ray-Spectroscopy (SEM/EDX)

Individual particle of suspended dust particles were analysed at the Institute of Earth and Environmental Science, University of Potsdam, Germany using a JEOL (JSM 6510) scanning electron microscope (SEM) (Figure 3.4). The instrument was equipped with an Oxford 6853 energy dispersive spectroscopic detector, and was automated by Oxford Instruments INCA Energy and Feature software, which was used to collect the X-ray spectra. The samples were

Figure 3.4: Photograph of Scanning Electron Microscope coupled with Energy Dispersive Spectrometer Machine at the Institute of Earth and Environmental Sciences, University of Potsdam, Germany.

mounted on aluminum stub after cutting a portion of the filter in each case. The mounted stubs were then carbon coated with 30 nm of carbon.

The microscope operated at 15 keV spot 5 in the EDS imaging mode with a beam size of 5 nm and a beam current of 2.39 nA and the X-ray spectrum was accumulated for 30s as described by Reid et al., 2003. An analysis grid ranging from 10 X 10 to 20 X 20 was set up for each sample to ensure that at least a specific number of separate fields would be analyzed and imaged in backscatter mode at 2300X magnification during automated analysis.

The EDAX EDS software used gray scale thresholding of the backscatter image to identify particles. Once identified, each particle was characterized by longest axis, diameter. EDAX Remote Particle/Phase Analysis software was used to fit reference elemental spectra to the particle spectra. The peak to background counts ratio threshold was set to 0.4 for peak identification.

Spectral peak values were corrected using the ZAF matrix correction to generate weight percents of the elements for each analyzed particle (Reid et al., 2003; Xie et al., 2005). From the weight percent, mole fractions of elements were calculated and subsequently there formula.

From the EDX analysis, about 3500 particles and 13 elements were obtained and such a relatively large data set of the particles needed to be reduced and characterised into their corresponding mineral groups. For this to be realized data reduction techniques such as hierarchical cluster analysis were employed in order to identify particles according to their chemical similarity. This technique has been very useful and effective (Liu *et al.*, 2005; Reid *et al*., 2003; Xie *et al*., 2009) for the purpose of sorting particles into different groups depending on the degree of association (strong or weak) between member of the same clusters. Also from the result generated from the Automated SEM/EDX analysis were subjected to size distribution analysis. In this study longest axis of the individual particles were measured and were related to their corresponding chemistry in order to depict the sources of the individual particles. For example Xie *et al*. 2009 reported that coarse particles that contain compound of major element

are likely to be sourced from wind-blown soil, but finer particles containing elemental and organic carbon are likely to come from combustion sources.

3.4 Data analysis

Series of statistical techniques have been employed by different workers (Fang *et al*., 2012; Xie *et al*., 2009) to assess the complexity of the data generated from monitoring PM in the atmosphere. These analyses include descriptive statistical analysis such as mean, median, mode, standard deviation with their accompanying charts in order to show the similarity with the group of the data generated. These were successfully used to identify area of high pollution caused by PM in some urban cities such as UK, Beijing, Hong Kong, Ibadan and Warri (Davis & Jixiang, 2000; Olatunji *et al*., 2010; Owoade *et al*., 2009). Reports have shown the significance of correlation coefficient and multivariate analysis (such as Principal component analysis and cluster analysis) in source identification. Principal component analysis is widely accepted for apportioning and identifying pollution sources and is used as a tool in source-receptor modeling. This study therefore adopted the aforementioned statistical techniques for the assessment of geochemical data acquired in the study area.

CHAPTER FOUR

RESULTS AND DISCUSSION

4.1 Mass Load of PM

The average concentration for the PM collected were 652.05 µg/m^3 (Industrial), 377.51 µg/m^3 (Traffic), 285.67 µg/m^3 (Dumpsite) and 214.79 µg/m^3 (Residential). Their values ranged from 48.28 - 1094.30 µg/m^3 (Traffic), 48.28-756.35 µg/m^3 (Dumpsite), 337.94 - 949.46 µg/m^3 (Industrial) and 32.19-466.69 µg/m^3 (Residential) (Table 4.1, Figures 4.1 and 4.2). The highest value was observed in the traffic area (Ojoo), where traffic density was high. The lowest values were observed in residential area around Odo-Ona Elewe (Ajakanga) where population density was low.

PM concentration from Traffic Area (TA) revealed a strong relationship between traffic density and the quantity of PM introduced into the environment (Figure 4.3). Ojoo, with the highest average of PM_{10} (681.25 µg/m^3) has a corresponding 25,000 vehicles/day with 38% of the vehicles being heavy duty trucks, while vehicles such as buses, cars and Lorries makes up the remaining 68%. This was further observed in samples from areas with relatively low traffic density as the PM mass load for those areas were much lower in concentrations (Fig 4.3).

The mean concentration of PM within the Dumpsite area is 330.36µg/m^3. Decrease in the concentration was observed at locations sited at about 500m and 1000m away from the dumpsite, with average concentrations of 128.74 µg/m^3 and 112.74 µg/m^3 respectively (Figure 4.4). It can thus be affirmed that the localized effects around and within the dumpsite facilities was responsible for the poor air quality around the dumpsites.

A similar trend of PM concentrations were observed in the industrial area, with locations close to the industries recording relatively high concentrations of PM with considerable decrease as

Table 4.1: Statistical Summary of Mass Load of Particulate Matter (PM) in the Four Environmental Units of the Study Area and their respective Standard.

	Traffic (n=40)	Dumpsite (n=40)	Industrial (n= 40)	Residential (n=85)
Mean (µg/m^3)	377.51	285.67	652.05	214.79
Median (µg/m^3)	337.94	241.39	659.80	185.06
Std. Deviation (µg/m^3)	231.69	194.23	146.36	92.34
Range (µg/m^3)	48.28 - 1094.30	32.19 -756.35	337.94 - 949.46	48.28 - 466.69
WHO (µg/m^3)	50			
USEPA (µg/m^3)	150			
UKEPA (µg/m^3)	150			
FEPA (µg/m^3)	250			

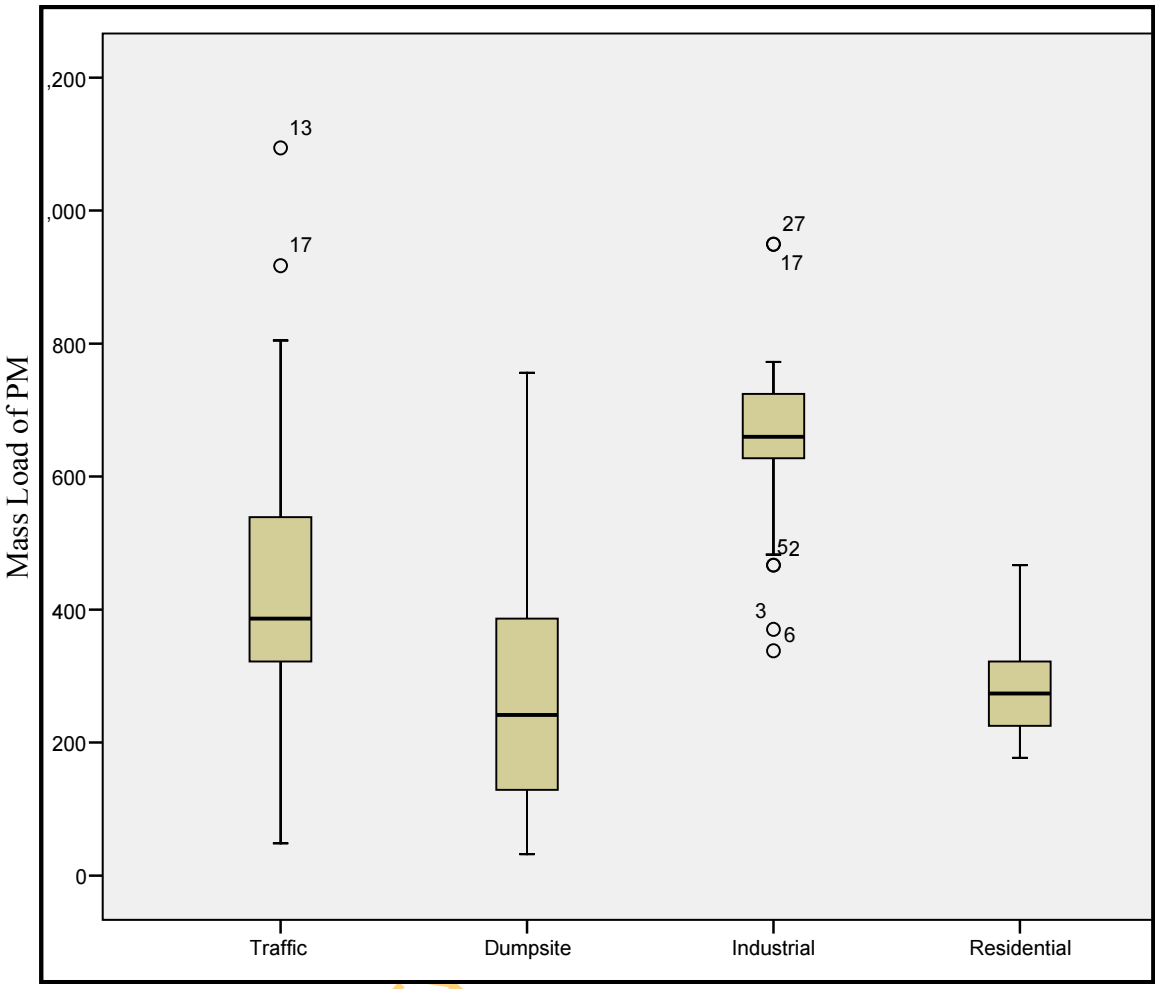

Figure 4.1: Statistical Summary of the Mass Load of PM in the Environmental Units.

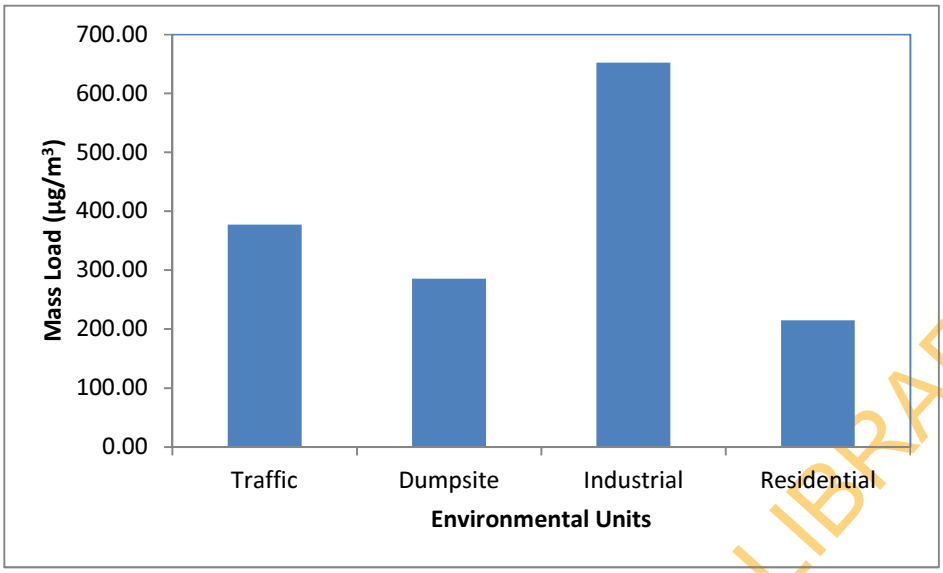

Figure 4.2: Average Mass Load in the Environmental Units of the Study Area

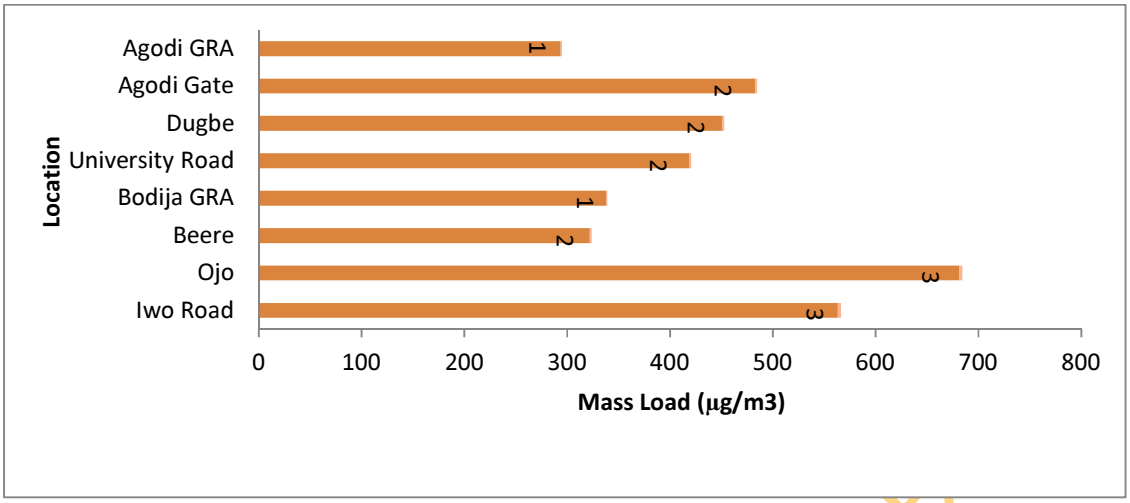

Figure 4.3: Average Mass Load of Traffic Area based on Traffic Density and Road Grade

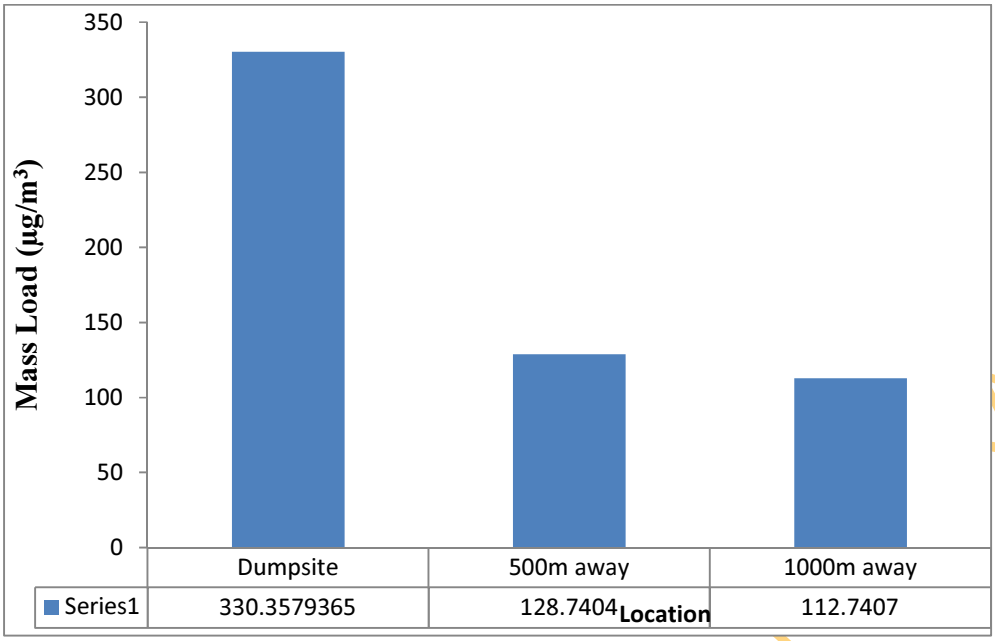

Figure 4.4: Average Value of Mass Load around Dumpsite Area

sampling locations moved away from the industries (Figure 4.5). The high mean concentration of PM observed in the Industrial Area (IA) may also have been affected by the conditions of the industrial estates where most of the roads are unpaved and contributions from the heavy duty vehicles that service the industries.

The mean PM concentration in the residential/commercial area (Figure 4.6) revealed that the planks market contributed the highest level of PM (402.30µg/m^3) while the lowest value was observed in mechanic workshop (168.97µg/m^3) and a mean concentration of 252.00µg/m^3 was observed for locations within residential areas.

The PM samples were collected in both seasons (wet and dry) in order to evaluate the effects of the seasons on the concentration and type of the PM. Results obtained in the dry season (February to December, 2011) were compared with metrological data such as wind direction and speed, temperature and precipitation (Table 4.2 and Figure 4.7). The range of mass load in dry season was 198.22-488.14 µg/m^3 while the wet season value ranged from 159.04-296.94 µg/m^3. The maximum concentration (627.61 µg/m^3) of PM was observed at the peak of the dry season while the lowest concentration (32.19 µg/m^3) was obtained in the wet season. The very high values recorded for the dry season confirmed that the PM concentrations are influenced greatly by seasons.

There was negative correlation between precipitation and concentration of PM_{10} (Figure 4.7), while the average Monthly precipitation was inversely proportional to the corresponding concentration of PM. This could be attributed to wet deposition of the particulate matter, thereby causing the air in the environment relatively cleaner. Unlike the precipitation, the wind speed and average monthly temperature are positively correlated with concentration of the PM_{10}, except for July where the mass load increase with decrease in temperature (Figure 4.8).

Comparing the Result of mass load of PM_{10} with established standards such as World Health Organization (WHO), United State Environmental Protection Agency (USEPA), United Kingdom Environmental Protection Agency (UKEPA) and National Environmental Standards and Regulation Enforcement Agency (NESREA) for both 24-Hour and annual levels of PM_{10}

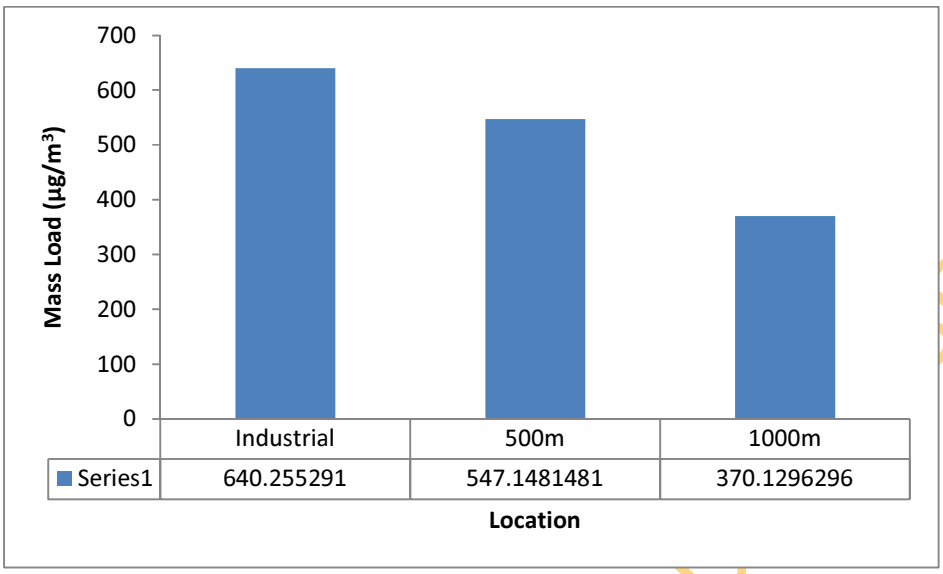

Figure 4.5: Average Value of Mass Load around Industrial Area

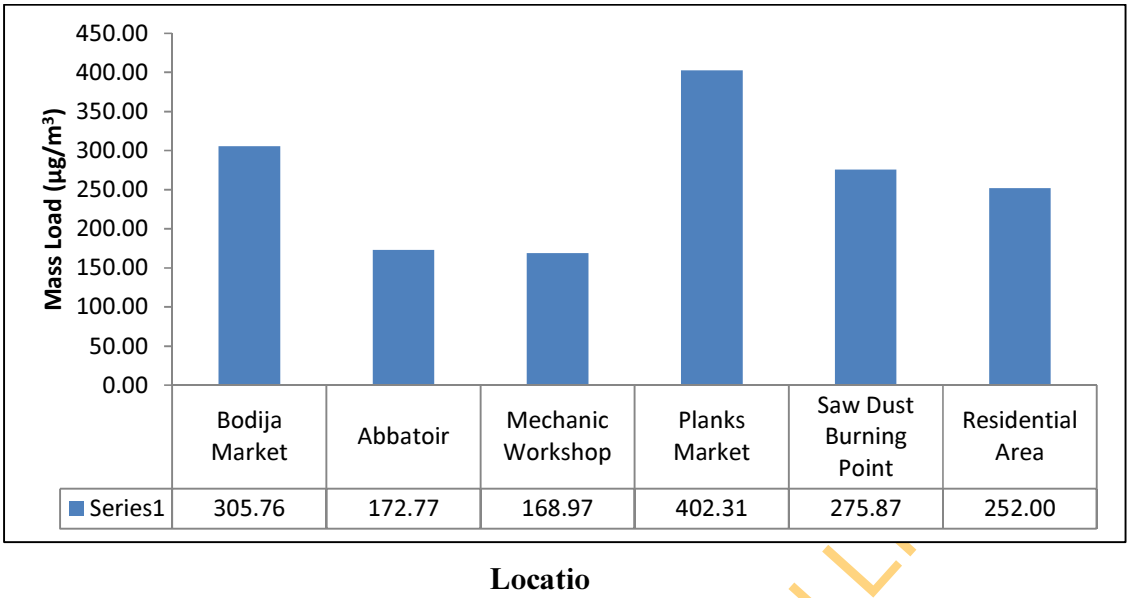

Figure 4.6: Average Value of Mass Load around Residential/Commercial Area

Table 4.2: Statistical Summary of Seasonal Variation of Mass Load

	Mean	Std. Dev.	Range
February	436.00	157.32	80.46- 466.69
March	488.14	130.07	370.13-627.61
April	399.10	73.22	321.85-482.78
May	296.94	79.12	225.15-381.78
June	174.60	64.38	32.19-225.30
July	272.63	44.61	193.11-354.04
August	166.67	13.71	152.88-185.06
September	159.05	10.23	144.83-177.02
October	174.67	4.06	169.98-177.02
November	198.22	39.18	160.93-263.11
December	348.33	39.46	299.89-413.64

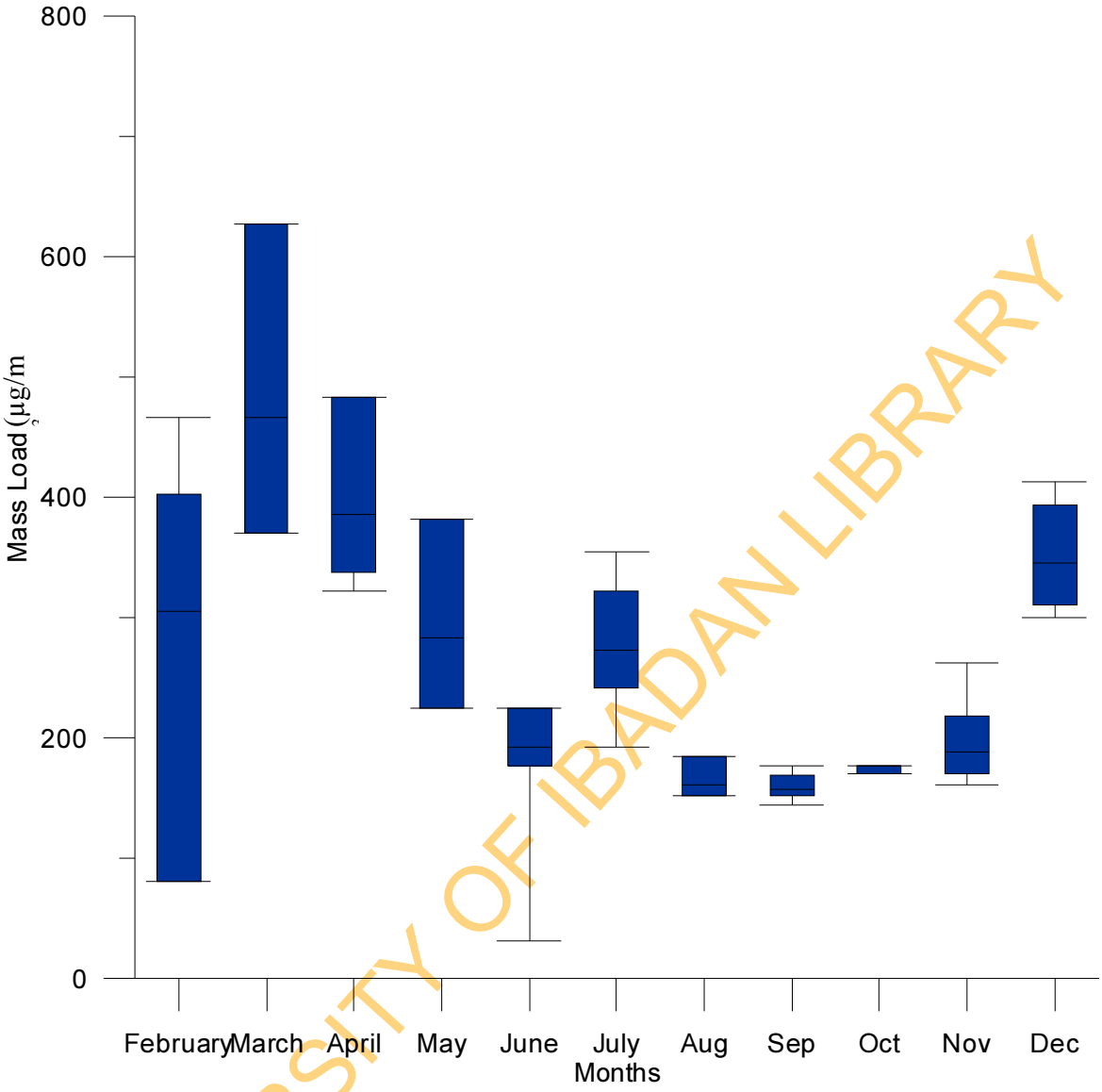

Figure 4.7: Seasonal Variation of PM in the study area

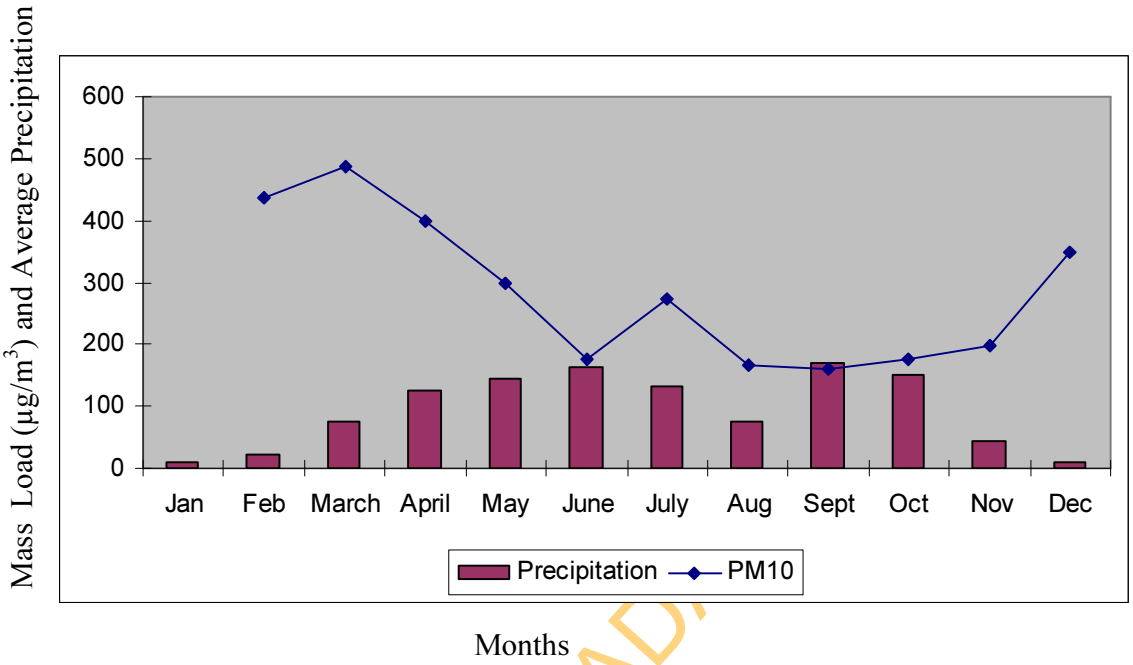

Figure 4.8: Seasonal variation of PM against Precipitation

revealed that less than 20% of the samples fall within any of the standards. These samples were found in the sub-urban environment (Ajakanga) where activity is minimal. 80% of the locations have higher values than the respective standards and could be described as not having attained the prescribed levels of air quality.

Air Quality Index (AQI) was determined from the results of concentration of the PM_{10}; this was with the intention of measuring the air quality with respect to its effects on the human health. This is a daily quality index which was proposed by Environmental Protection Agency (EPA, 1999). It was defined with respect to the five main criteria pollutants: carbon monoxide (CO), nitrogen dioxide (NO_2), ozone (O_3), particulate matter (PM_{10}) and sulphur dioxide (SO_2). Pollutants concentrations are converted into a numerical index (AQI) which assumes values in the range 0–500. The overall range was then subdivided into six ranges to which six categories of air quality correspond (Table 4.3). Comparison of data with AQI is basically dependent on break point concentration defined by EPA on the basis of NAAQS, and on the results of epidemiological studies of the effect of single pollutant on human health. Different breakpoint concentration values and air quality standard have been reported (WHO 2000; EC 2000; EC 2002).

Evaluating the results of the concentration of the PM from the study area using the AQI as proposed by EPA (Table 4.3) gave the results reported in Table 4.4. The interpreted data revealed that the air quality in the study area had deteriorated considerably. The air quality in the Traffic (TA), Dumpsite (DA), Industrial (IA) and Residential (RA) areas can generally be classified as very poor and tends to be more hazardous in description using the AQI index. The air quality in the residential area (RA) is better but must also be noted that few of the locations within the RA also have very low air quality conditions that tends to the hazardous class (Table 4.4 and Fig 4.9).

Table 4.3: Breaking points for the AQI of EPA

AQI Category	Index Value	PM_{10} (24h) ($\mu g/m^3$)
Good	0-50	0-50
Moderate	51-100	51-143
Unhealthy for sensitive group	101-150	144-237
Unhealthy	151-200	238-330
Very unhealthy	201-300	331-395
Hazardous	301-500	396-563

Table 4.4: Application of EPA AQI to Data Measured in the Study Area

Category	Number of Samples (%)			
	Traffic (n=40)	**Dumpsite (n=40)**	**Industrial (n=40)**	**Residential (n=85)**
Good	3	0	0	6
Moderate	18	21	0	15
Unhealthy for sensitive group	13	14	0	51
Unhealthy	18	30	0	21
Very unhealthy	12	21	12	3
Hazardous	36	14	88	4

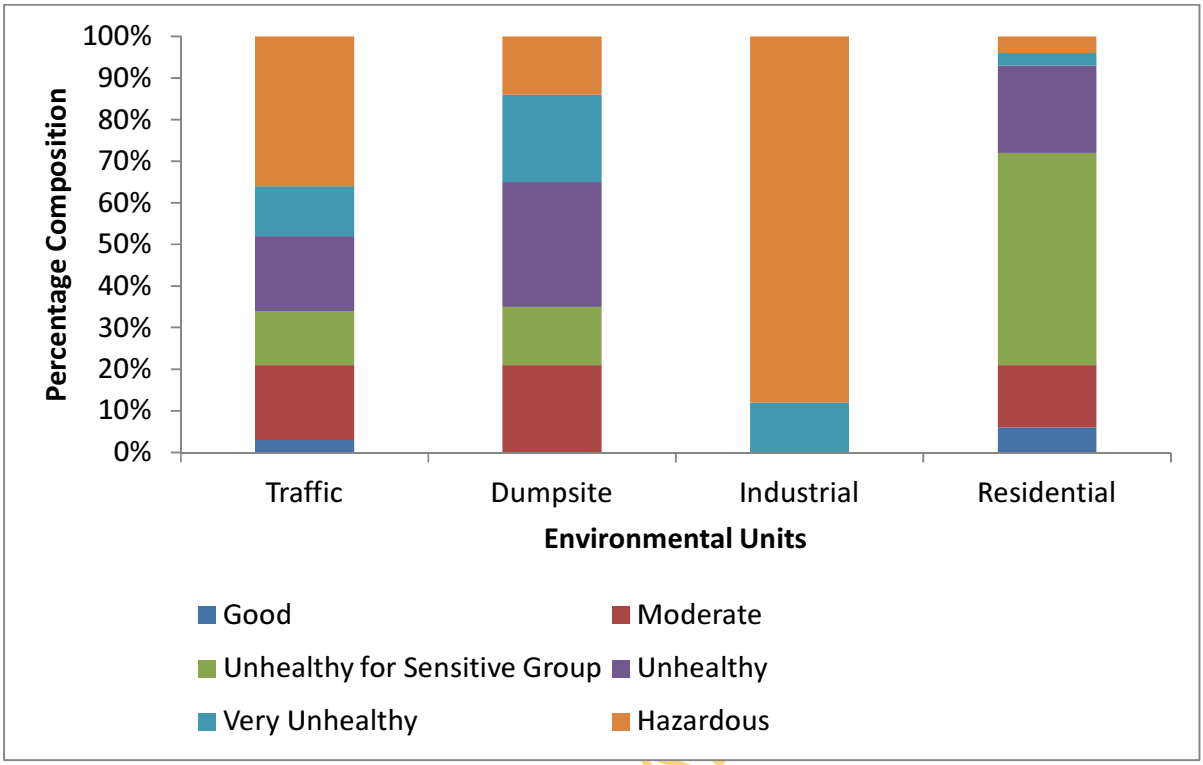

Figure 4.9: Air Quality Index of the study area.

4.2 Geology of the study area

The study area is underlain by rocks of both igneous and metamorphic origins. Most authors agreed (Okunlola *et al*., 2009; Olayinka *et al*., 1999; Tijani *et al*., 2006) that the dominant rock types are quartzites of the metasedimentary series and the migmatite complex comprising banded gneisses, augen gneisses and migmatites (Figure 4.10). These rocks are intruded by pegmatite, quartz vein, aplite and dioritic dykes. Minor rocks of substantial coverage include the

amphibolites and pegmatites. In lots of places the rocks are overlain by thick weathered regolith and outcrops are correspondingly few.

4.2.1 Migmatite-Gneisses Complex

Gneisses are dominant in Ibadan occurring as different types such as banded gneisses, augen gneisses and granite gneisses. The dominant rock types are quartzites of the metasedimentary series and the migmatite complex comprising banded gneisses, augen gneisses and migmatites.

Banded Gneisses

Banded gneiss is a dominant rock and constituted 75% of rocks in and around Ibadan (Olayinka *et al*., 1999). The outcrops of the banded gneiss occur as a continuous body from south to north and mostly occur as low lying outcrop (Figure 4.10). The texture of the banded gneiss varies from medium to coarse grained. The banded gneiss is foliated and folded in places with prominent synforms and antiforms, especially around Ojoo area. Millimetre to centimetre sized quartz veins is common and some of these barren quartz veins are folded. They have alternating bands of mafic and felsic minerals which are medium to coarse grained.

Petrographically, the rock is composed mainly of plagioclase, biotite, hornblende and quartz in variable proportions. The mafic bands contain hornblende and minor biotite while the felsic bands consist of plagioclase, microcline, and quartz. Microcline occurs as medium to coarse grained crystals. Quartz occurs as fine- to coarse-grained xenomorphic grains with irregular grain boundaries, and exhibits undulatory extinction (Figure 4.11 and Table 4.5). Fine-grained

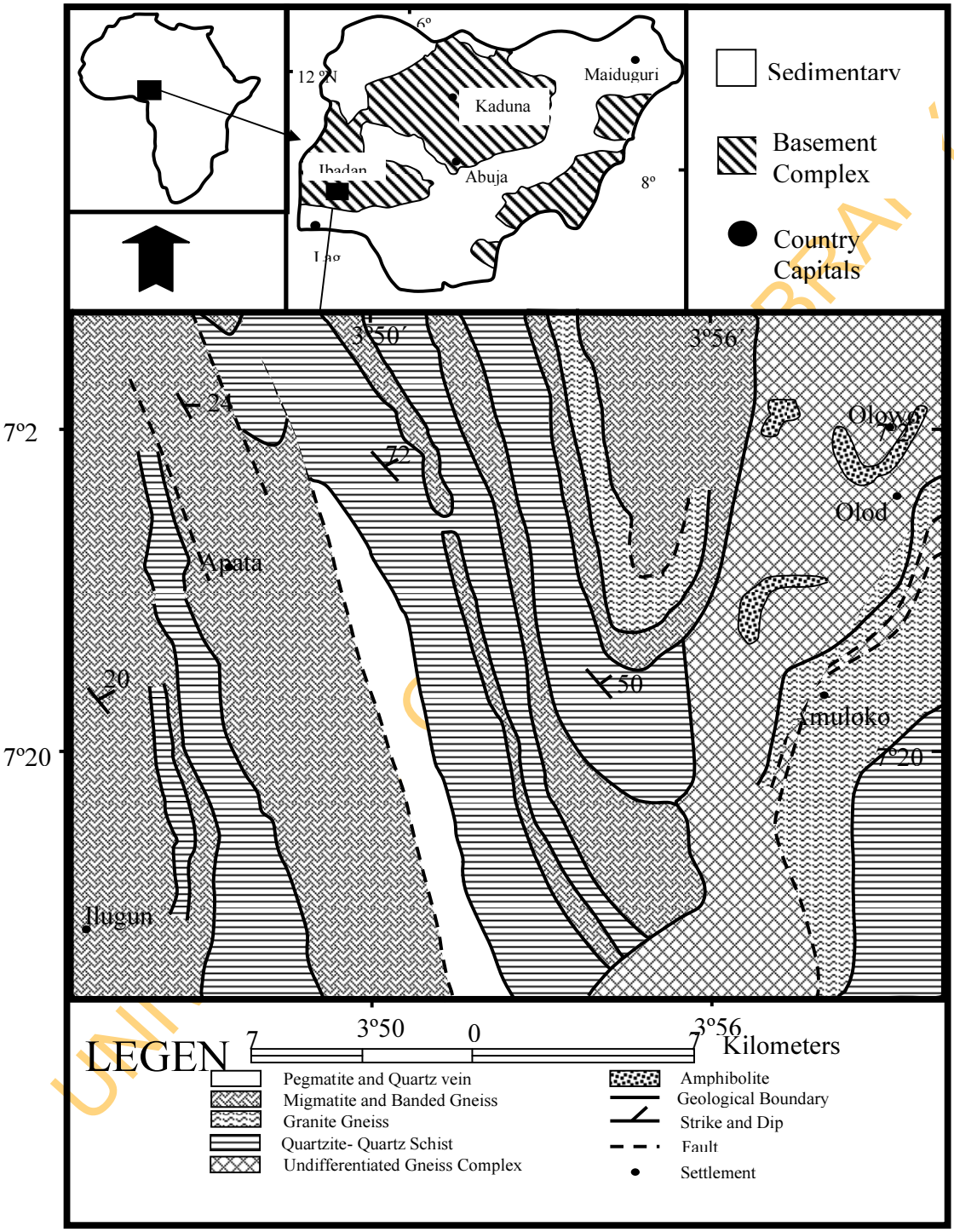

Figure 4.10: Geological Map of the Study Area (after Okunlola *et al*., 2009)

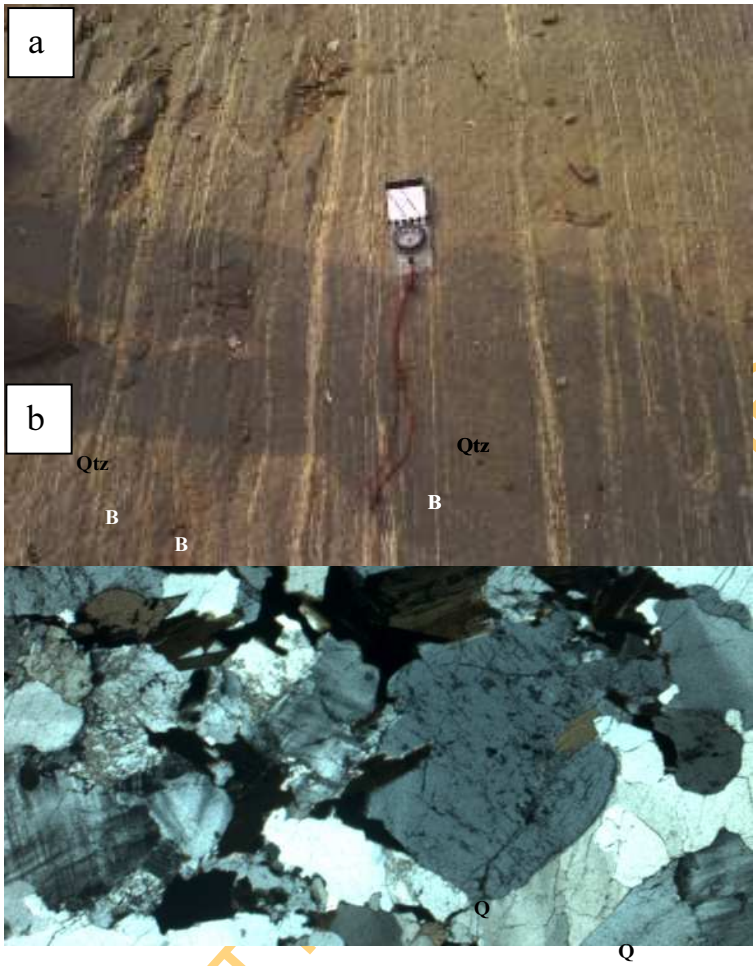

Figure 4.11: (a) Banded gneiss outcrop from Ojoo (b) Photomicrograph (crossed nicol) of one the samples. H= hornblende, B= Biotite, Qtz= Quartz, Plg= Plagioclase, M= Muscovite

Table 4.5: Modal composition of Banded Gneiss

Minerals	Sample 1	Sample 2	Sample 3
Quartz	60	54	53
Microcline	25	24	22
Plagioclase	1	2	6
Hornblende	2	3	18
Muscovite	1	2	trace
Biotite	11	15	10
Zircon	Trace	Trace	Trace

recrystallised quartz grains adorn the margins of coarser quartz. Accessory minerals include zircon, apatite, ilmenite, magnetite and muscovite. Banded gneiss outcrop along Ife Road, Lagos-Ibadan Express Way, Agbowo, Ojoo, and University of Ibadan (U.I) (Tijani *et al*., 2006).

Augen Gneisses

This rock occurs mostly in the northern part of Ibadan metropolis such as U.I (Abadina). Medium-gray to spotted, fine to medium-grained, porphyritic, foliated and lineated granitic gneiss, composed of microcline (largely as megacrysts or augen up to 10 cm long), quartz, plagioclase, biotite and minor hornblende. The eye-like structures (augen) are defined by flowage of micaceous minerals around less developed quartz and feldspar. They are coarse grained, angular to sub-angular in shape and composed minerals such as quartz, feldspar (plagioclase), biotite and garnet. The rock is segmented into large boulders by a well-developed joint system. The general strike is NNW-SSE direction.

Granite Gneisses

The outcrop of the granite gneiss occurs as continuous body from south to north in the eastern section of the study area. The texture of the granite gneiss varies from medium-grained to very coarse grained.. The granite gneiss is foliated and it is defined by mafic (biotite) and felsic (quartz and feldspar) mineral bands. Within the granite gneiss there are small scale pegmatites rich in K-feldspars and biotite. In some outcrop, the granite gneiss is composed of biotite, K-feldspars, quartz and garnet. In thin section the biotite flakes are aligned. The K-feldspars are mostly microcline and are porphyroblastic. Well formed zircon crystals occur in association with some of the microcline grains. Apatite, monazite, magnetite, ilmenite and sphene are other accessory minerals. Large phenocrysts of K-feldspars, porphyroblasts of hornblende and biotite flakes are the prominent mineral components of the granite gneiss (Figure 4.12 and Table 4.6). The texture of this rock varies from medium-grained in the middle section to very coarse almost becoming pegmatitic. In thin section, foliation is defined by elongate hornblende, biotite and drawn-out K-feldspar phenocrysts.. They outcrop at U.I, and Ife Road, they are fine to coarse grained, but very rich in minerals like feldspar, quartz, biotite and less amount of garnet.

Figure 4.12: (a) Granite gneiss samples (b) Photomicrograph (crossed nicol) of one the samples. H= hornblende, B= Biotite, Qtz= Quartz, Plg= Plagioclase, M= Muscovite

Table 4.6: Modal composition of Granite Gneiss

Minerals	Sample 1	Sample 2	Sample 3
Microcline	60	58	62
Quartz	20	25	20
Biotite	12	10	10
Plagioclase	5	4	6
Hornblende	2	1	1
Muscovite	1	Trace	1
Zircon	Trace	Trace	Trace

Quartzite

Quartzite in the study area is believed to be metasedimentary series, and forms a barren chain of low ridges running N-S (Figure 4.10). They are dominantly made of tightly interlocking grains of quartz of medium grain sizes. These units were later intruded by Pan-African granitic rocks of adammellitic and pegmatitic varieties (Okunlola *et al*, 2009).

The grains are mostly granoblastic in texture. Although pure quartzite are often whitish to greyish, but more commonly in the study area, they exhibit brownish to reddish colour as a result of weathering of the outcrops and subsequently stained by varying amount of iron oxides (Fe_2O_3). In most cases they are observed as Quartz-schist (Tijani *et al.,* 2006), this are foliated metamorphic rock dominated by quartz (90 vol%) and muscovite (10%) with minor accessories (Figure 4.13).

Quartz are found as granular (<0.4 mm), with a grain-flattening fabric, and as lenticular polycrystalline bodies up to 3 mm in width. In these lenticular regions quartz exhibits undulose extinction and has indent boundaries with neighbouring phases. Muscovite occurs as platy crystals in finer-grained regions and is orientated parallel to the grain-flattening fabric of quartz (Figure 4.13 and Table 4.7). The Quartz-Schist occurs as elongated ridges striking NW-SE. They are mostly massive, dominantly made up of quartz, outcropping along Total–Garden–Gate, State Secretariat, Oke Itunu and Oje-Bere neighborhoods of Ibadan metropolis. The quartz schist form prominent features especially west of Ajibode and Sango area and their outcrop pattern indicate possibly a refolded fold (Okunlola, *et al.,* 2009). They are usually fine grained and form extensive north-south trending bodies. In places, they are characterized by preponderance of quartz rubbles and usually whitish grey in color. In these locations outcrops of quartz-schist are well fractured and generally concordant to the bedding of the rocks, and in some cases discordant. Quatrz-Schist sampled are made up of quartz and muscovite with accessory opaque minerals. Field studies show that schist-quartzite constitutes over 10% of the rocks in and around Ibadan metropolis (Oyawoye, 1972).

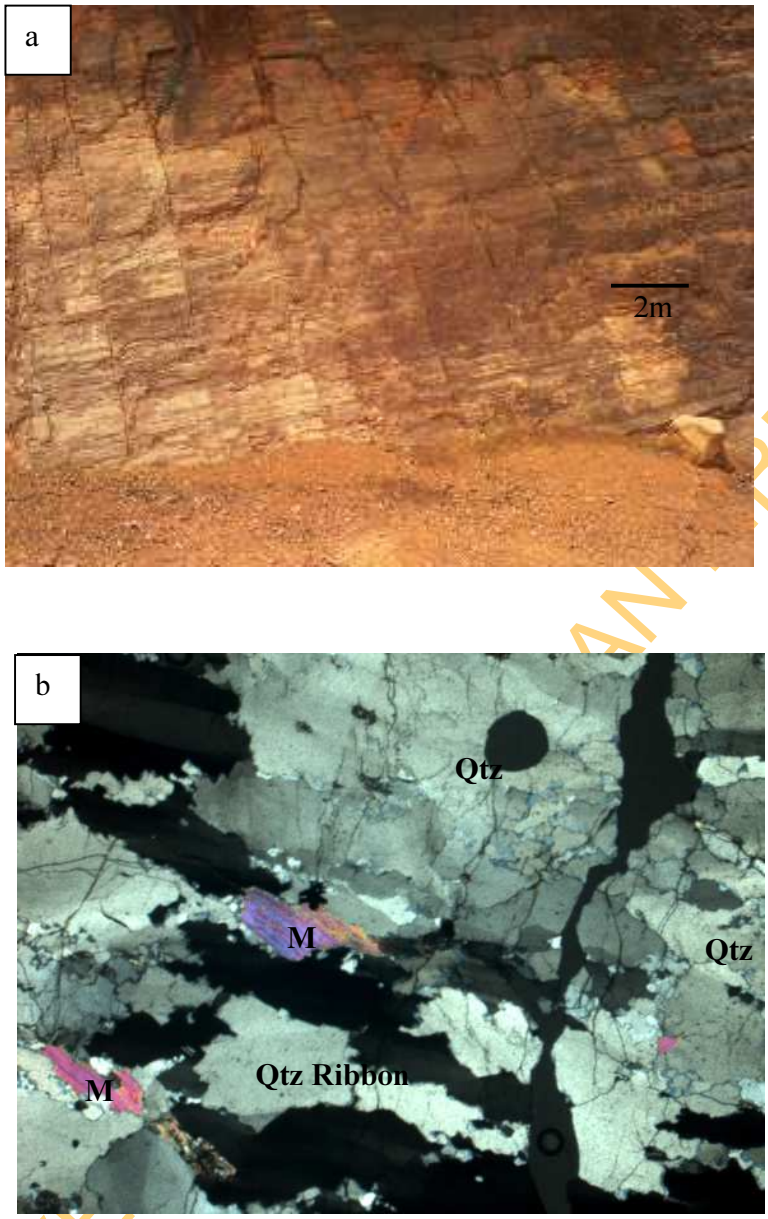

Figure 4.13: (a) Quartzite outcrop from Mokola Area (b) Photomicrograph (crossed nicol) of one the samples. H= hornblende, B= Biotite, Qtz= Quartz, Plg= Plagioclase, M= Muscovite

Table 4.7: Modal Composition of Quartzite

Minerals	Sample 1	Sample 2	Sample 3
Quartz (%)	95	97	98
Muscovite (%)	4	2	2
Zircon (%)	Trace	Trace	Trace
Rutile (%)	Trace	Trace	Trace
Magnetite	Trace	Trace	Trace

Quartzite form a prominent topography feature in the study area especially around Oke-Aremo, Oke-Tunu, Premier Hill, Mokola,-Oremeji Ridge. This rock represents a quartz-rich zone within a mass of gneissose rock. It consists essentially of interlocking mass of medium to coarse grained anhedral quartz grain which show parallel elongation. Scattered within the mass of quartz are occasional subhedral laths of muscovite, which exhibit strong birefringence.

The petrographic studies of major rock types in the study area were carried out in order to have better understanding of the influence of local geology on the mineralogical components of PM collected. These rocks revealed the abundance of quartz, feldspar, amphibole and mica.

Quartz is present in all the rocks and occurs as anhedral grain with undulose extinction. In quartzite and foliated granite, the quartz has been drawn into ribbon-like structure and the long axes are aligned in the direction of foliation. Plagioclase and microcline are the common feldspar, with their characteristic twinning.

The rocks outcropping in the study area show a wide range of mafic mineral composition with biotite and hornblende contents of the rock varying from almost being absent in felsic alkali granite/ quartzite to being abundant in Amphibolite and biotite granite gneiss/migmatite gneiss.

In some cases the biotite minerals form parallel alignment with specific orientation which is a characteristic of gneissic rocks. Amphibole minerals are revealed under the microscope as hornblende and tremolite. Hornblende occurs as xenoblastic crystal, greenish in colour while tremolite grains are long, prismatic and pleochroic from pale green to dark green.

4.3 Mineralogy of the bulk samples using X-ray Diffraction

The analysis of the bulk samples of rocks, soils and deposited airborne particles by X-ray diffraction gave an impression of the mineralogical composition in study area (Figures 4.14, 4.15 and Appendix I).

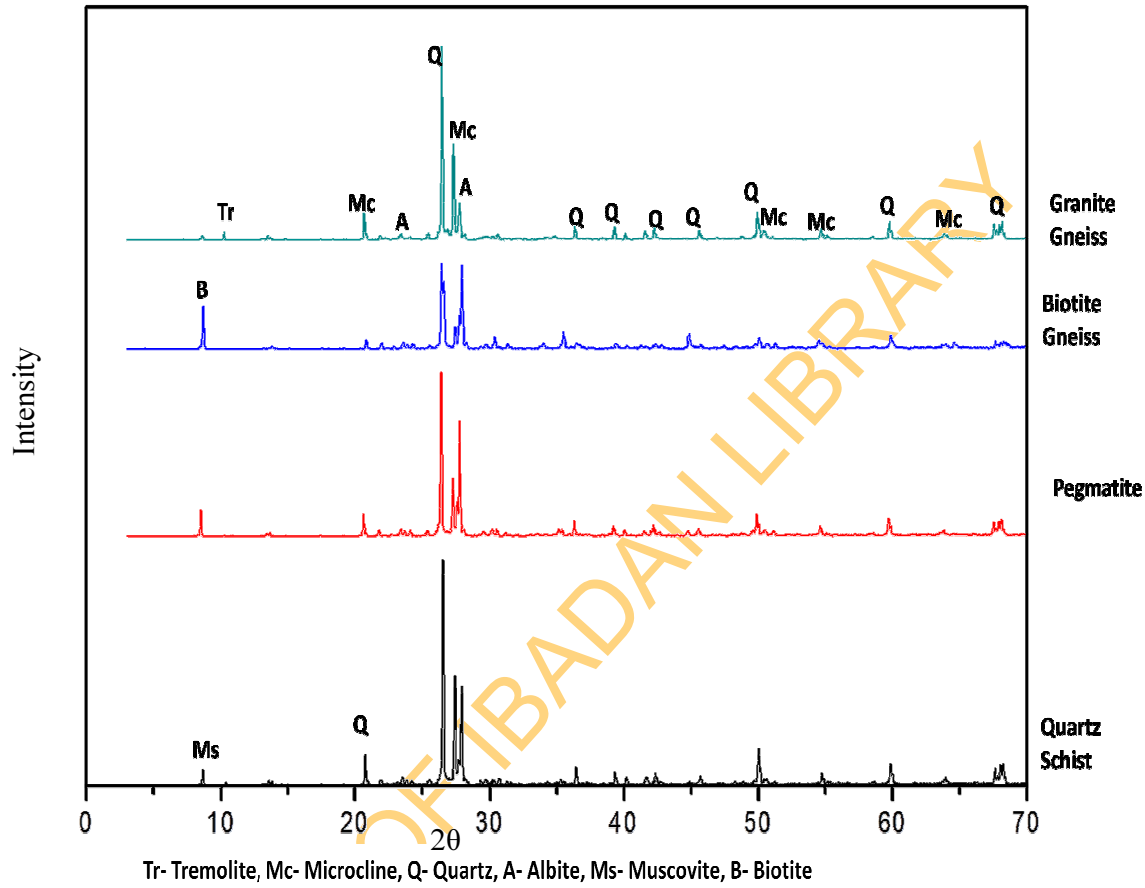

Figure 4.14: XRD diffractogram of selected rock samples

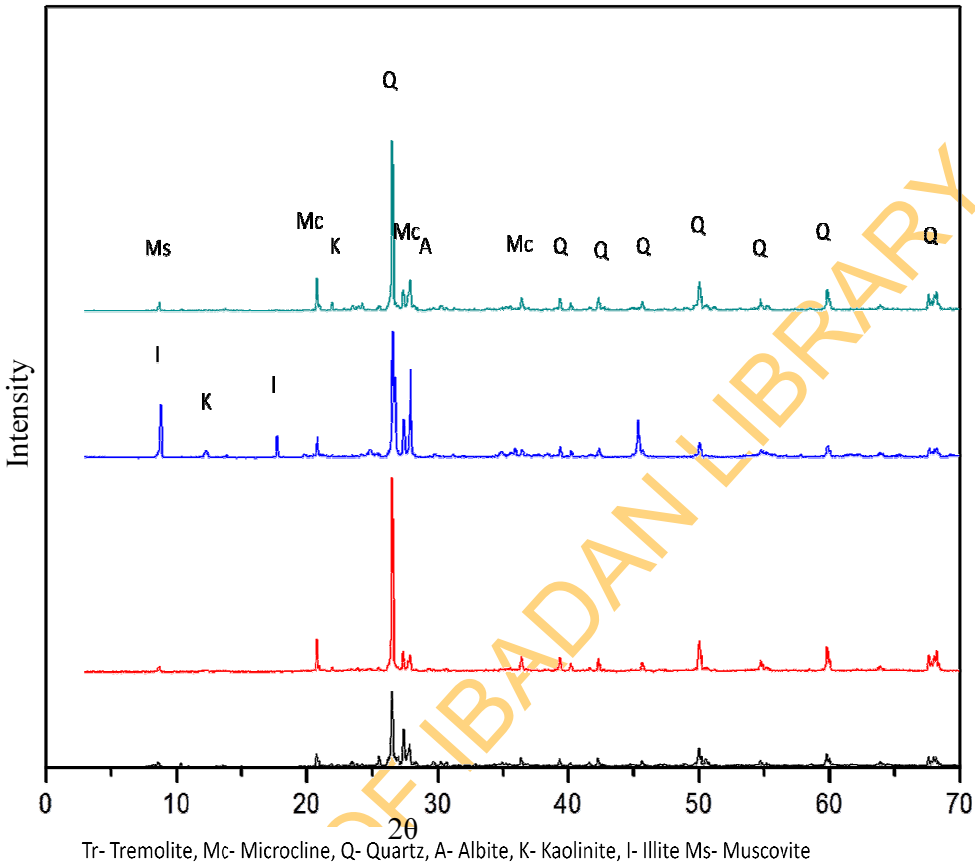

Figure 4.15: XRD Diffractogram of selected soil samples

The semi-quantitative mineral (Table 4.8) identification of these rocks shows that quartz is the predominant mineral, while feldspar, mica and amphibole are also present in various amounts. The feldspars are basically plagioclase (Albite) and K- feldspar (microcline). This was consistent with the result of the petrographic studies. The XRD also revealed that hornblende and tremolite were the amphibole mineral present in the rocks while micas were revealed to be biotite and muscovite.

The results of XRD for the soil mineralogy revealed quartz as clearly dominant mineral with fractions up to 50% , but with samples taken at distances from the dust source, feldspars (plagioclase, microcline) and phyllosilicate minerals (illite and kaolinite) become more prominent in the mineralogical composition.. The low mica contents of the soil samples (Figure 4.15) could be attributed to chemical weathering of rocks which had altered to clay minerals such as illite and chlorite. This is in agreement with Odewande and Abimbola, (2008).

A complex mineral assemblage was observed for deposited dust, with the dominant minerals being quartz, kaolin, illite, plagioclase, microcline and in few cases mica. These minerals in the deposited dust are as a result of weathering of the underlying bedrocks. A comparison of the results showed that the mineralogy of the soil and the deposited dust samples have common origin.

4.4 Suspended Mineral Dust

4.4.1 Particles Morphology

About 2500 individual particles were investigated using SEM/EDX. The relatively large number of data was reduced by the application of hierarchical cluster analysis. Subsequently, they were sorted by comparing their oxides and subsequently classified after the classification of Rosler and Lange, 1976. This method has been used successfully by mineralogists and other related specialists in the field of geology to identify minerals. This was also recently adopted for the investigation of mineral aerosol particles (Abdul-Wahab *et al*, 2005; Gao, 2001; Jibiri and Bankole, 2006; Lu *et al*., 2007; Rashki *et al*., 2013).

Table 4.8: XRD quantitative mineralogical abundance

Minerals	Soil (%)	Deposited Dust	Rocks (%)
Quartz	55-72	50-63	43-53
Biotite	0-3	0-5	3-16
Muscovite	0-7	0-7	2-5
K-feldspar	5-22	2-20	6-18
Plagioclase feldspar	4-10	3-15	3-27
Amphibole	<1	0-1	1-8
Kaolinite /Chlorite	0-5	5-25	-
Illite	0-1	1-10	-
Smectite	<1	0-1	-
Unidentified Minerals	-	6	-

Figure 4.16 showed the sizes and shapes (morphology) of the various aerosol particles observed from secondary electron micrographs. The Number percentages and number-size distributions of the particles were calculated from the image analysis, the identified characteristics shapes were spherical, irregular, long and prismatic; with most of the particles in the coarse fraction of the samples resembling fragments of freshly crushed rocks (Figure 4.16e and f). Spherical and irregular particles <5 µm were mainly particles aggregates (clay aggregate), whereas large crystals of 8– 20µm were mica (Figure 4.16 f). In some cases, the regular particles of 5–10 µm in PM_{10} samples were mainly sharp in edges or irregular in shapes (Figure 4.16 d). Most of the particles were observed as single particles or included in some form of aggregate. Although most of the particles were irregular in shape and are often coarse in nature, a few fine fraction identified were spherical or close to spherical. This could be as a result of long transport or particle ageing in the immediate environment as a result of particle re-suspension.

Some of the spherical particles observed were probably carbonaceous materials (soot aggregate) generated as a result of fossil fuel combustion which is attributed to vehicular, industrial emission, fugitive fly ash from incineration or from road construction materials. These were more prominent in samples from Traffic Areas where there are active and dense vehicular activities. Irregular or flaky particles are found in areas where there are active road construction or area with freshly constructed roads where use of crushed rocks are common.

The most abundant particle size were the coarse mode fraction (>2.5µm) and they are made up of ~86% by number of the total particles collected. 64% of the total fine particles occur as irregular particles (<2.5 µm) which reflect the contribution from the soil in the region. This was the prevailing mode in all the environmental units except at Bodija Market (residential/commercial area) where more than 45% of the particles were fine mode. This could be as a result of incineration of different material ranging from animal bones to saw dust.

The size distributions were often uni-modal (Figure 4.17) and mostly peaked between 3.0 and 4.5 µm. For example, in the Traffic Area where there are suspension and re-suspension of dust particles, the

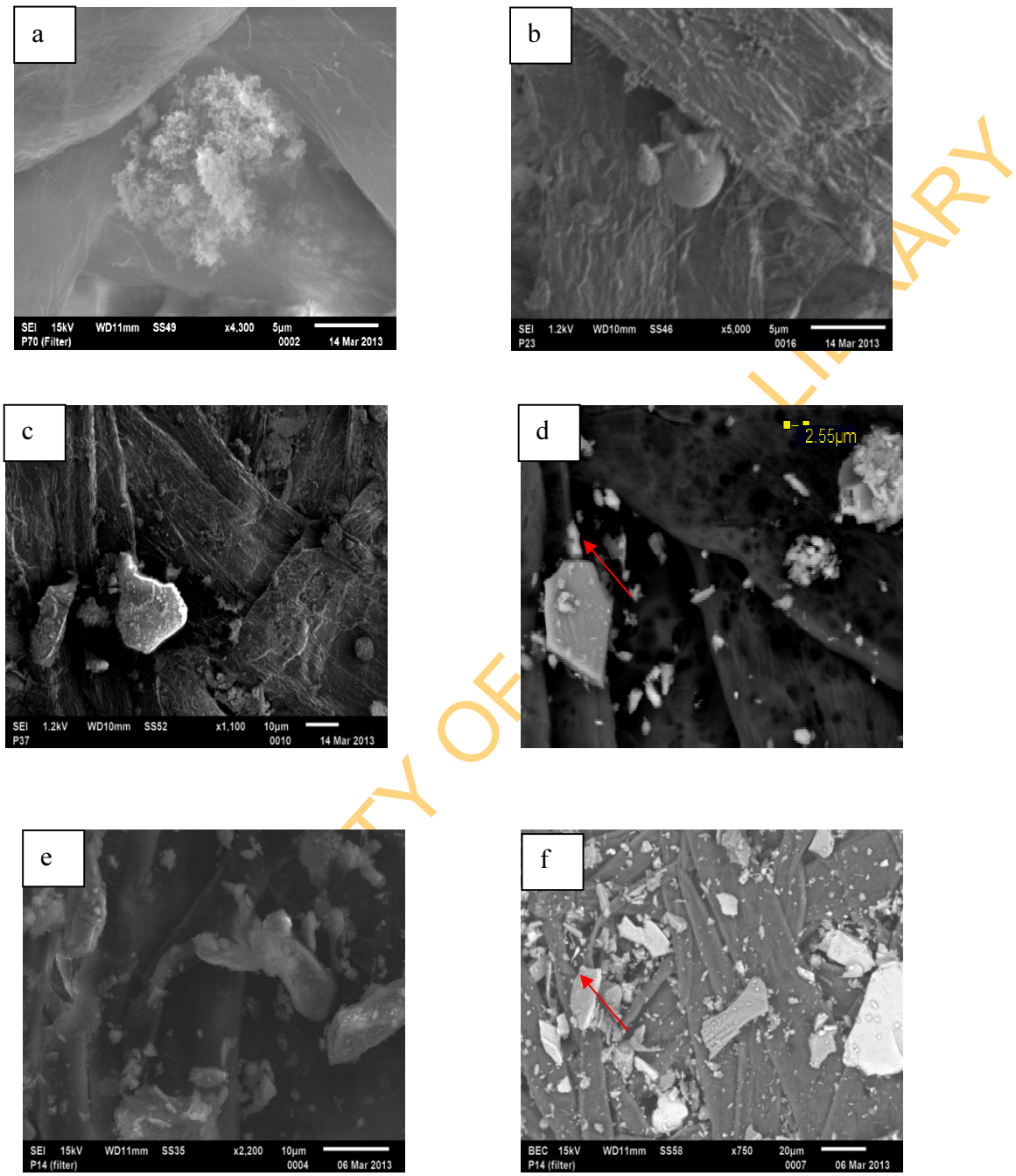

Figure 4.16: SEM photomicrograph of airborne particles collected in the study area showing particle size and shapes (morphology).

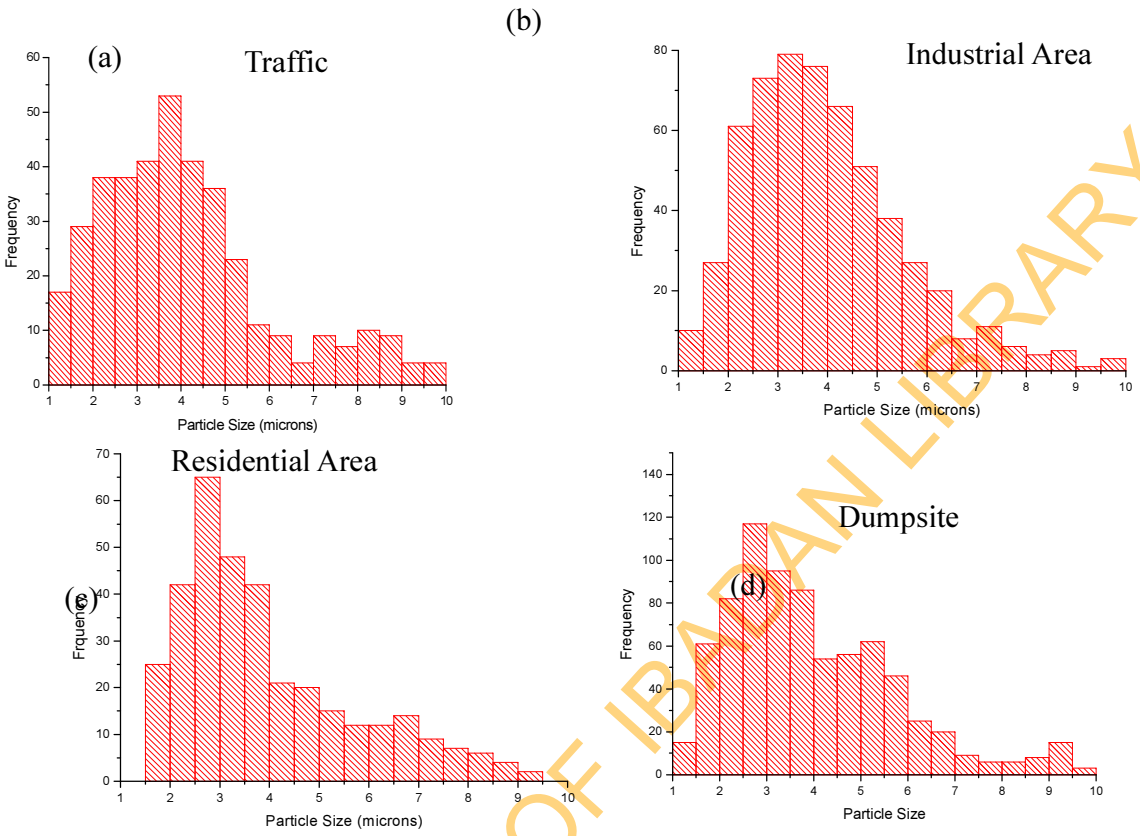

Figure 4.17: Size Distributions of Aerosol Particles Collected at (a) Traffic Area (b) Industrial Area (c) Residential/Commercial Area, (d) Dumpsite Area.

modal frequency was between 4 and 4.5 and their maximum value can reach 20 µm, especially where there is active road construction.

4.4.2 Mineralogical Characterization of PM

The results of mineralogical composition of individual particles are presented in Table 4.9. Qualitative EDX analysis showed that the major elements in the particles analyzed are Si, O, Al and with significant amount of Ca and Fe. Other major elements include, Mg, K, Na and to some extent Ti. Mineral formulae was automatically calculated by EDX software by normalizing element concentrations to 12 O atoms per formula unit, assuming 4 tetrahedral crystallographic positions (occupied by all Si and part of the Al), with the remainder of the Al and all Mg, Fe, and Ti assigned to the octahedral positions. K, Ca and Na were assumed to occur in the interlayer positions, as was typical for these minerals, according to Posfai *et al*., 2013. Carbon was excluded in the analyses because of the introduction of carbon during the preparation of the samples for EDX analysis and also the filter is mainly composed of carbon. However, important particle types such as soot, organic carbon and particles of biological origin could not be identified. Therefore, the nature and origin of other particles were adequately addressed.

The dominant particles are alumino-silicates and mostly as clay minerals. In addition to clay minerals, rock forming minerals such as Feldspar, Mica, quartz, amphibole and pyroxene were also identified. Particles rich in Ca, Fe and Ti were also somewhat common while some clay minerals were associated with sulphate particles.

Aluminosilicate Particles

Clay Minerals

It was obvious that the dominant particles in the study area are aluminosilicate in nature. This dominance was shown by elemental mapping of selected elements (Figure 4.18), which showed

Table 4.9: Mineralogical composition results of individual particles derived from SEM/EDS analysis of PM_{10} in the study area

S/N	Minerals	SiO_2	Al_2O_3	MgO	CaO	Na_2O	K_2O	TiO_2	FeO	MnO	ZnO	SO_2	BaO	P_2O_5	% Abundance
1	Quartz	92.2	4.32	0.19	1.10	0.08	0.37	0.04	1.47	0.00	0.00	0.00	0.00	0.00	11
2	Mica	44.03	19.25	4.95	2.51	0.29	5.74	2.43	20.73	0.00	0.00	0.00	0.00	0.00	3
3	Amphibole	44.89	18.16	6.76	7.06	0.43	2.48	2.00	17.99	0.00	0.00	0.00	0.00	0.00	1
4	Illite	54.22	25.21	3.01	2.01	2.2	9.80	0.97	2.1	0.00	0.00	0.00	0.00	0.00	13
5	Smectite (Montmorillonite)	56.43	25.12	4.10	2.79	0.19	2.60	0.70	7.49	0.00	0.00	0.00	0.00	0.00	7
6	K-feldspar	65.16	19.57	0.00	0.62	1.12	11.63	0.05	1.77	0.00	0.00	0.00	0.00	0.00	2
7	Plagioclase Feldspar	60.73	22.16	0.19	8.75	4.26	1.0	0.06	2.50	0.00	0.00	0.00	0.00	0.00	2
8	Ca-rich particles	16.12	7.23	3.20	**68.66**	1.90	0.76	0.02	2.07	0.18	0.18	1.01	0.01	0.13	11
9	Ti-rich particles	26.07	11.75	0.64	11.30	2.08	0.72	**34.27**	14.54	0.48	0.00	0.42	0.00	0.87	2
10	Kaolinite	47.75	46.09	0.09	0.70	0.00	0.06	0.40	3.98	0.00	0.00	0.00	0.00	0.00	7
11	Fe –rich particles	23.58	18.87	0.08	1.35	0.33	0.06	4.26	**48.22**	0.00	0.11	0.58	0	0.17	4
12	Clay Minerals + Sulfate	42.25	18.22	9.31	3.90	0.75	3.8	0.71	12.26	0.00	0.00	**9.20**	0.00	0.01	16
13	Chlorite	32.12	25.33	2.20	1.1	0.10	1.00	1.10	35.20	0.00	0.00	**1.20**	0.00	0.00	21
14	Sulphur-rich particles	12.33	5.31	0.33	33.41	1.23	3.14	0.00	4.91	0.12	0.00	**39.23**	0.00	0.00	0.9

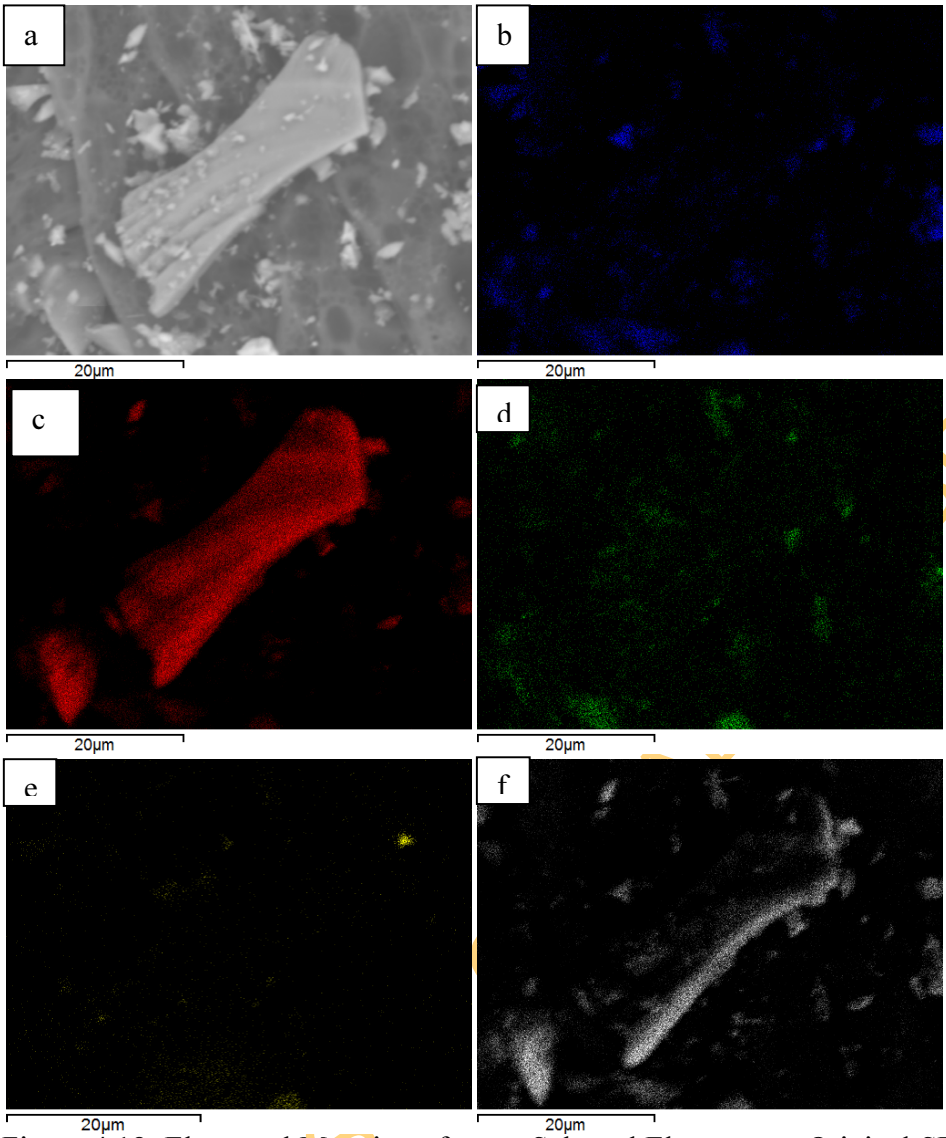

Figure 4.18: Elemental Mapping of some Selected Element: a= Original SEM Photomicrograph, b= Al, c= Si, d=Fe, e=Ca, f=O

correlation among Si, Al, O and to some extent Fe. They comprised roughly 43-66% of the particle number, where the lowest contribution was from residential area and the highest contribution was samples from dumpsite area (Figure 4.19). About 84% of these particles were in the coarse mode (particles >2.5µm).

The alumino-silicate particles include chlorite, illite, kaolinite and smectite (montmorillonite) and these accounted for about 47% of the total particles analysed. In addition to mixed layers such as Chlorite/Smectite (C/S) and Illite/Smectite that were also present. The Silica (SiO_2) and Alumina (Al_2O_3) contents ranged from 37.5-57.6% and 15.89-39.80% for Illite; 48.52-59.79 and 15.67-26.71% for smectite (montmorillonite); 42.39-49.65 and 20.67-40.19 for Kaolinite respectively. They comprise Fe in varying amounts and can reach 34% especially in chlorite. There is also significant contribution from other major element such as Na, Mg. Stoichiometrically, ratio 2:1 of Si/Al is consistent with montmorillonite and illite while Si/Al ratio in kaolinite is 1:1 as revealed by molar percentages. It was however revealed that, chlorite was the most abundant clay minerals amounting to 21% by particle number and approximately 78% of these particles are mostly in coarse mode fraction with average particle size of 3.48µm. The second most abundant clay mineral is illite contributing 13% of the total particles analyzed. Their average size fraction is 3.18µm, indicating coarse mode While smectite (montmorillonite) and kaolinite contributed 6 and 7% respectively, with the same average size fraction (3.7µm).

Feldspars

Feldspars were observed in the study area, mainly as K-feldspar and plagioclase feldspar (Figure 4.18). Their sizes ranged from 2.3-10.4 and averaged 6.0µm in diameter. They are angular to irregular in shapes. They were identified by their chemical composition with K-feldspar ranging from17.11-23.57 (Al_2O_3), 60.38-68.28 (SiO_2) 9.99-15.58 (K_2O) with traces of Na_2O, CaO and Fe oxides while plagioclase feldspar chemistry was in the range of Al_2O_3 (16.07-27.6), SiO_2 (55.79-68.52), Na_2O (2.83-10.56), CaO (1.11- 4.36) and traces of K_2O and Fe oxides (Table 4.20). Both Accounted for 4% of the particle number. They are more in samples from Traffic area (12% of total particles collected in the area) as a result of mechanical crushing and grinding of rocks for road construction works.

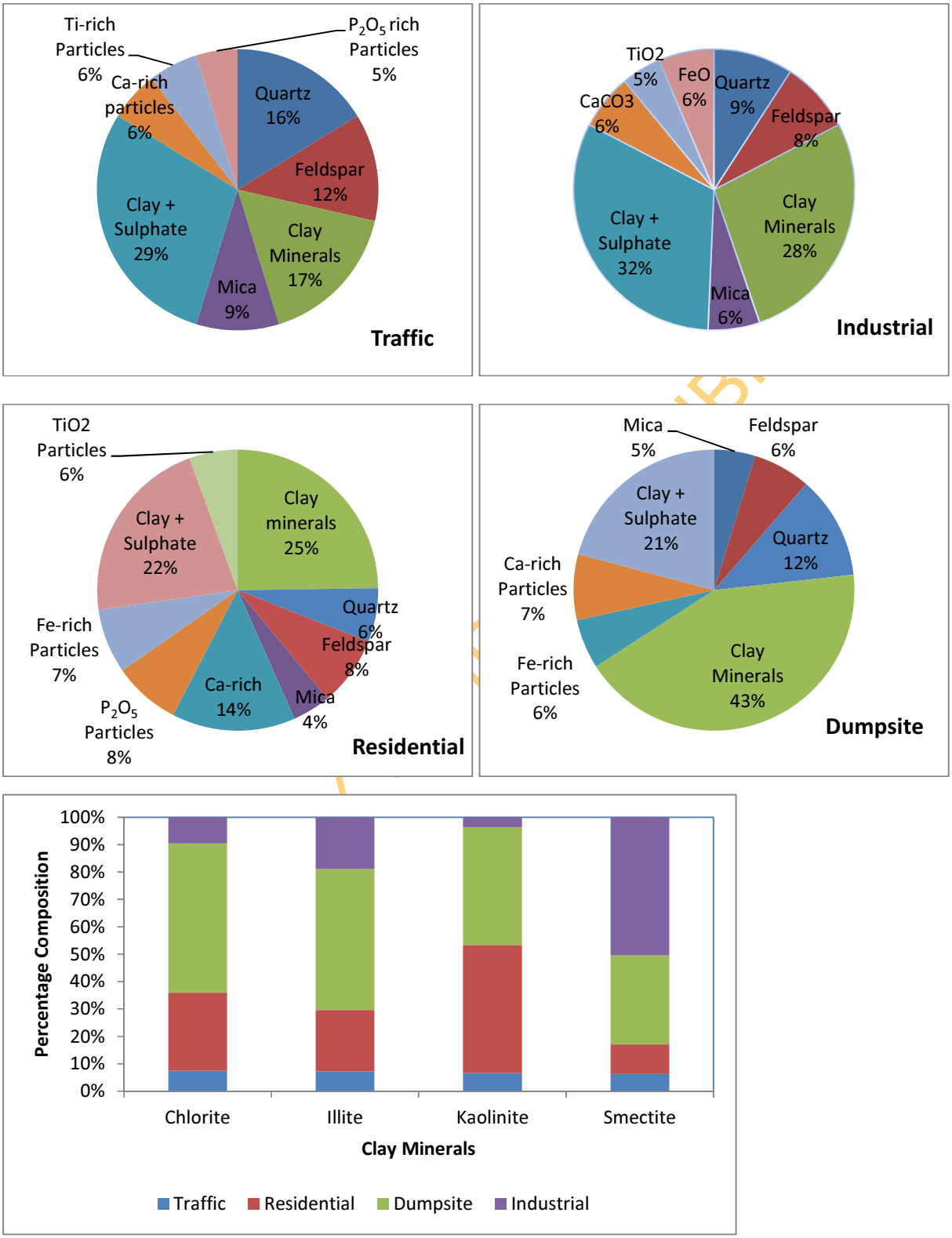

Figure 4.19: Composition of Airborne Particles in the Environmental Units

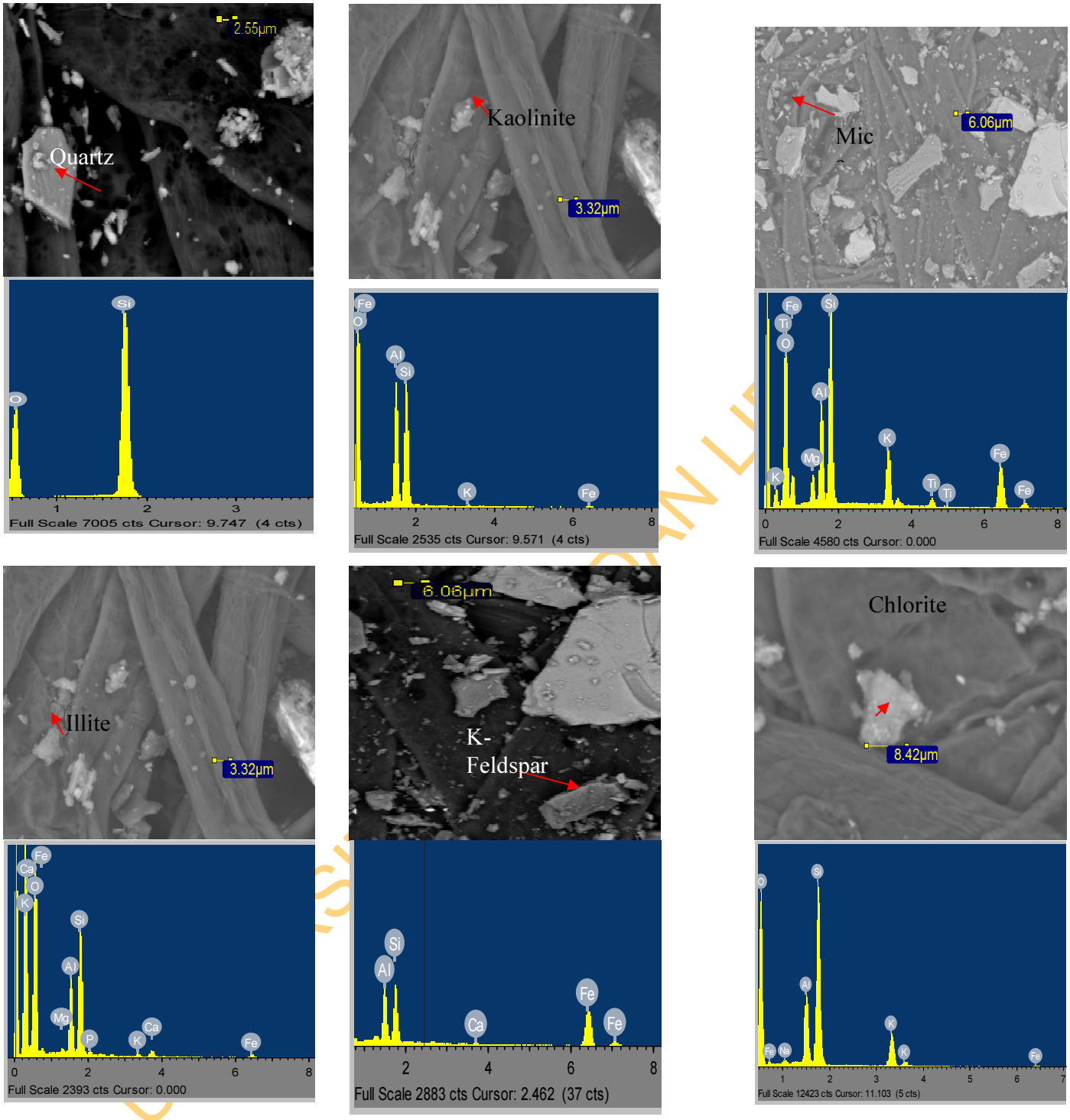

Figure 4.20: Back scattered images of PM_{10} and their corresponding Spectra

Micas

Micas are sheet silicate ferromagnesian minerals with specific composition of SiO_2 (34.68-59.25%), Al_2O_3 (12.1-31.28%), FeO (15.42-34.45%) and MgO (2.69-11.92%) and TiO_2 reaching 11.38% in few cases. They have similar chemistry with clay minerals and contributed 3% of the particle number. Most of these were contributed from Traffic Area where there are active road construction activities especially around Ojoo. The particles show distinguishing flaky features, which made visual examination adequate for their identification, especially in their coarse mode (often >15µm) without EDX spectrum (Figure 4.20). They were mostly represented in the samples by Biotite and muscovite and their sizes commonly ranged between 3.3 and 20 µm in diameter.

Ferromagnesian minerals

Although, amphibole (mainly hornblende) and pyroxene are usually very rare minerals species in the PM in analyzed, they amounted to around 1% of the particle number with all falling under the coarse mode fraction (4.4-9.2µm). These minerals have their chemical composition ranging as of SiO_2 (39.17-49.66), Al_2O_3 (12.76-28.36), FeO (10.78-23.45), MgO (5.18-9.56), CaO (4.53-10.17) with all values expressed in %.

Quartz

Quartz was the second most abundant individual minerals identified (6-12%) of the particle analyzed as observed in the study area. They were found in the coarse mode with average size of 3.9 µm and range from 2.1-6.7µm and they are sharp, angular fragments, chips and flaky in shape (Figure 4.18). The SiO_2 content usually range from 79 to 100% with average composition reaching 92.22%. Those particles that are characterized by fine mode fractions contained other elements such as Al, Ca, Fe and in some cases they were found in association with S. Highest contribution of quartz was observed in dumpsites samples (32%) with low contributions coming samples from traffic area (16%)

Summarily, it was observed that the mineralogy if the PM from all the zones were dominated by clay minerals (14–43%). Quartz particles, mainly consisting of SiO_2, were the second dominant mineralogical component (11%). This was followed by Feldspar (plagioclase-albite and K-

feldspar-microcline) about 9% and Micas (biotite and muscovite) about 6%. The remaining components of rock forming minerals contribute little to the mineral dust mass. The mineralogical analysis for the four zones (Figure 4.17) showed more or less similar results. However stations, located closer to the DA, the source of dust exposures exhibits higher percentages of clay, while TA exhibits highest concentrations of quartz, Mica and feldspar. While most of the minerals (quartz, feldspars and muscovite) can easily be tied to basement-type lithology of generally gneissic–granitic character, others (chlorite, pyroxenes and hornblende) rather suggest mafic parent rocks.

Sulfur Containing Particles

It was observed from the single particle elemental analysis that the amount of major crustal element such as Al and Si found in the samples were less compared to their respective crustal abundance. This could be attributed to their association with other materials such as Sulphur generated by anthropogenic activities in the form of emission of biomass burning and fossil fuel combustion (Ma et al., 2012). Studies have shown that there is very low reactivity between sulphate and alumino-silicate minerals and therefore sulfate tends to coat the surface of alumino-silicate minerals (Ma *et al.*, 2012; Rashki *et al*., 2013; Reid *et al*., 2003).

High SO_2 emission have been reported in the study area especially areas with high traffic and industrial emission (Ana et al. 2012; Oluwole et al. 2012). However in this study 21-32% of clay minerals contain sulfur at various levels (Figure 4.19 and Figure 4.21). These particles are mostly coarse with size range of 1.8-8.5µm and averaged 4.4µm, which are more abundant in the industrial area, contributing 32% (Figure 4.17).

Figure 4.21 showed the relationship between the predominant minerals (clay minerals) with other mineral species such as sulphate and Fe. The most striking population is the cluster of particles in the Al/Si corner, often with low level of S and indicating coarse fraction. While the second population clustered along Al+Si-Fe line. The few clusters at S corner are often fine fraction especially in industrial area. The important clusters could be as a result of external mixture of clay with sulfate particles, this was in agreement with the findings of

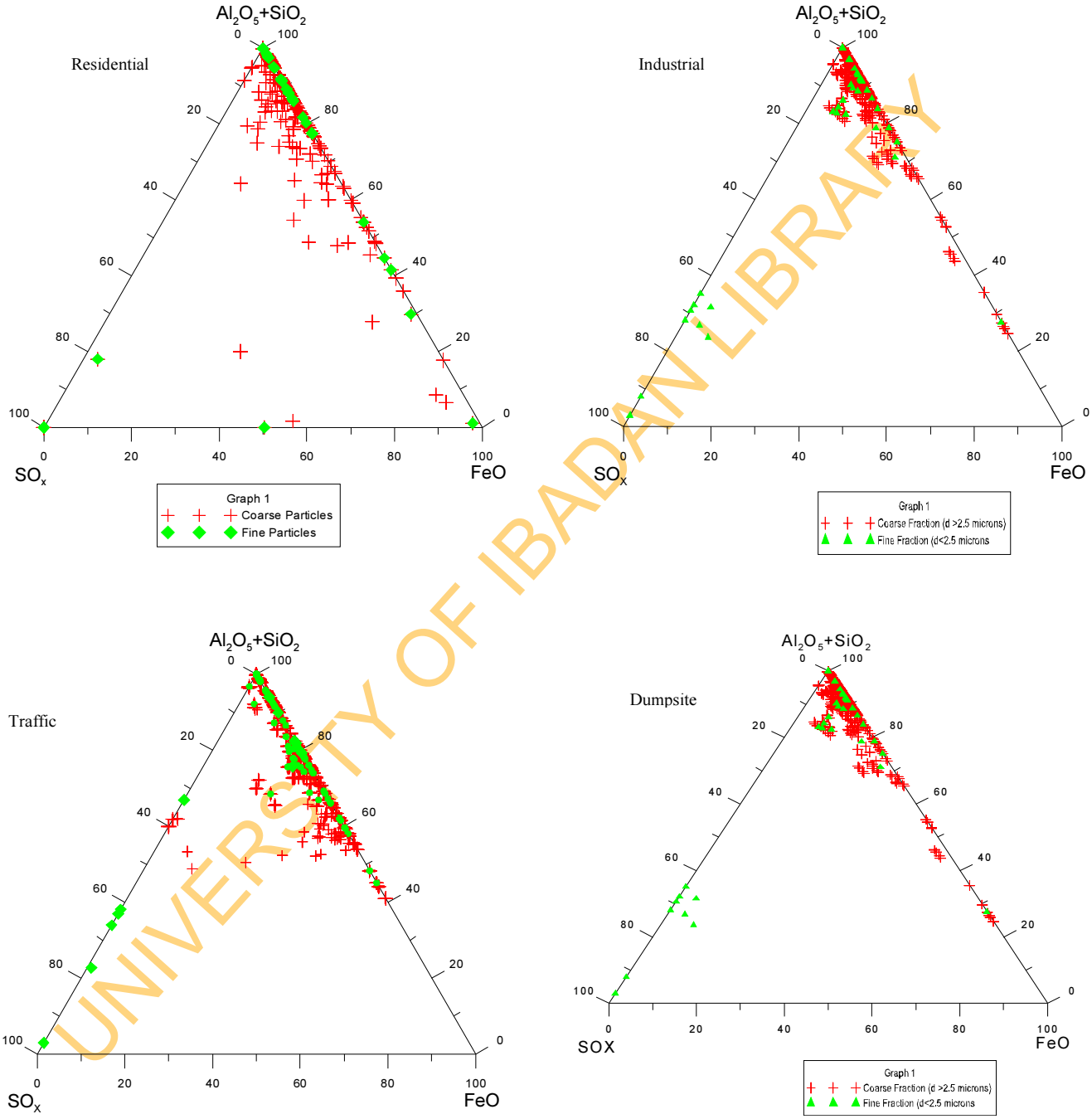

Figure 4.21: Ternary compositional plots that show the proportions of Al+Si/S/Fe within individual mineral particles in the different environmental units, as obtained from EDS spectra.

Calcium-rich Particles

Pósfai *et al.,* (2013) and Chou *et al.*, (2008) who argued that both external and internal mixture do occur among sulfate and mineral particles, but external mixture is most common with insoluble minerals such as alumino-silicate especially in their coarse mode while internal mixing was only significant in their fine mode. Therefore, as particle age in the air they can be coated with these substances, and once coated they are potentially even more of health concern.

Fe-rich Particles

Fe-rich were also identified and their sizes ranged from 1.4-3.1µm with average size of 2.2µm. 41% of these particles were found in coarse mode fraction. They were characterized by defined shapes mostly close to spherical. In some cases they are irregular especially in the coarse mode. The chemical composition ranged as FeO (58.07-79.81%), SiO_2 (4.01-34.36%), Al_2O_3 (1.67-31.38%) with traces of Ti, Mn, S and P (Table 4.9). They accounted for approximately 7% of the total particles analyzed and have considerable contribution from Residential/Commercial (50%). Figure 5.7 showed the importance of Fe in the particles analysed and it was known to be significant component in its oxidized form because it was considered the most dominant light absorbing species (Sokolik and Toon, 1999). In the plot, there was a strong relationship between Al/Si and Fe in virtually every particle analysed. The vast majority of the particles have less than 40% Fe which is normal mineralogy for alumino-silicate minerals. The fine mode, iron-rich

particles are characterized by nearly balanced Al and Si molar percentages, supporting a kaolinite mineralogy and often times they tend to aggregate or coat the surface of the minerals (Figure 4.22).

Particles with higher percentages of Fe are Iron-rich particles and ranged from 60 to as high of 90% Fe, but were less compared to the one associated with clay minerals. The highest relative proportion of Fe to Al/Si particles is seen in are mostly coarse which is suggestive of close range source. These minerals reflect iron contamination of kaolinitic minerals or may simply indicate aggregation of fine Fe rich kaolinite particles (Figure 4.22) as well as lateritisation processes.

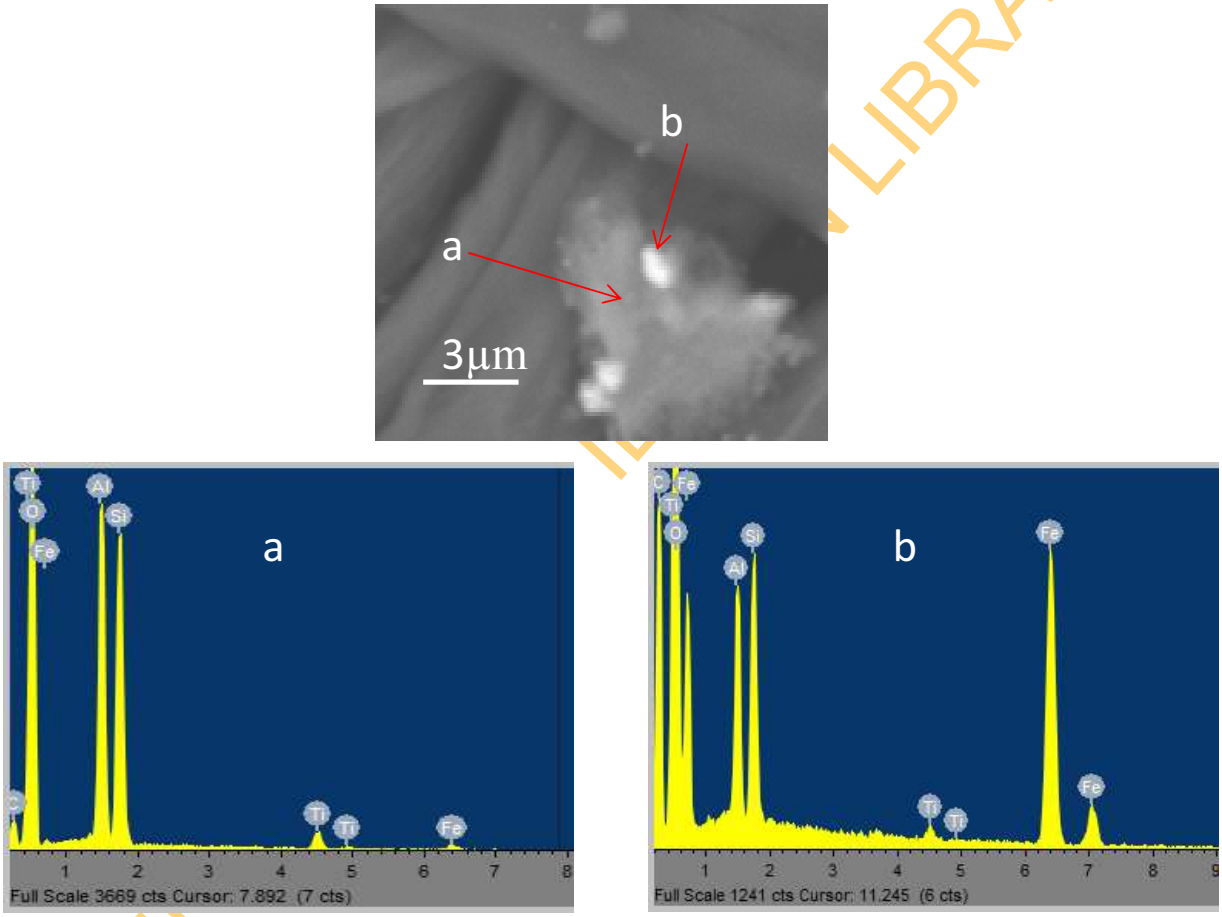

Figure 4.22: Back scattered images of PM_{10} and their corresponding Spectra showing Iron contamination in Kaolinite

Calcium-rich particles were observed in the atmosphere of the study area with varying sizes ranging from 1.2-9.9µm with average of 3.4µm with shapes that were close to rounded. CaO range between 52.9% and 94.9% with an average of 68.7% with the average of other components such as Al, Si, and S and P ranging between 1.01 and 16.12µm. About 8% of these particles was accounted for from the total particles analyzed with 64% falling within coarse mode while 33% were in fine mode (63%).

Their presence was mainly observed as Ca-Al/Si, but in some cases they were associated with P and S (Figure 4.23 and 4.24). Their association with P and S are mostly observed in residential/commercial area (especially in Bodija Market area), which showed the highest contribution of Ca-rich particles, accounting for 14% of the total particle analyzed in this area.

Because of the absence of calcite in the soil and rock of the study area, its presence in the atmosphere suggests varied sources including fugitive dusts from construction materials (especially Portland cements) and combustion of burning of animal bones at abattoirs.

In Figure 4.22 calcium containing alumino-silicate (Ca-Al-Si) was the most striking population confirming their possible association with Portland cement sources

Calcium-rich Particles

Calcium-rich particles were observed in the atmosphere of the study area with varying sizes ranging from 1.2-9.9µm with average of 3.4µm with shapes that were close to rounded. CaO range between 52.9% and 94.9% with an average of 68.7% with the average of other components such as Al, Si, and S and P ranging between 1.01 and 16.12µm. About 8% of these particles was accounted for from the total particles analyzed with 64% falling within coarse mode while 33% were in fine mode (63%).

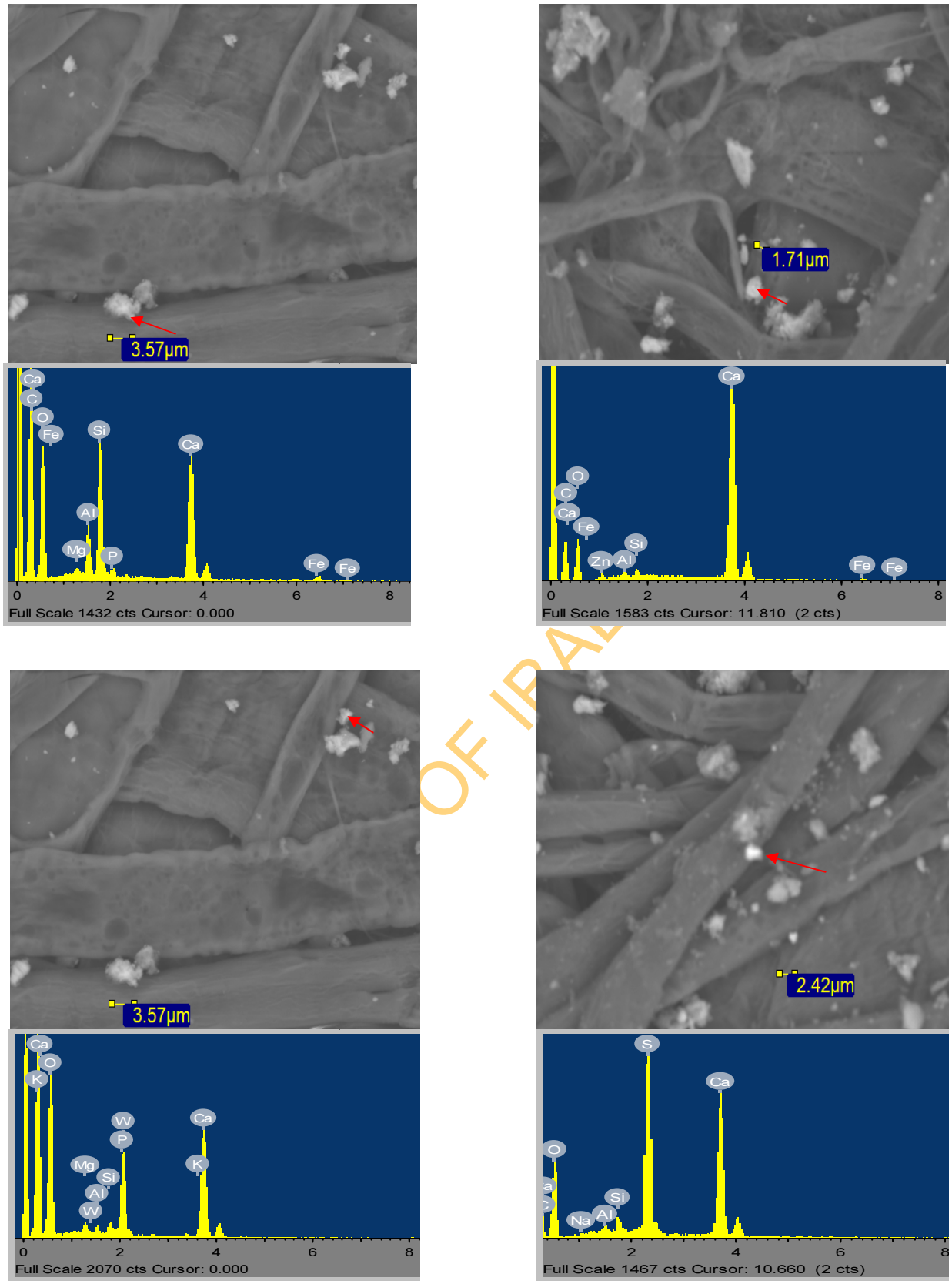

Figure 4.23: Back scattered images of PM_{10} and their corresponding Spectra Ca-rich particles

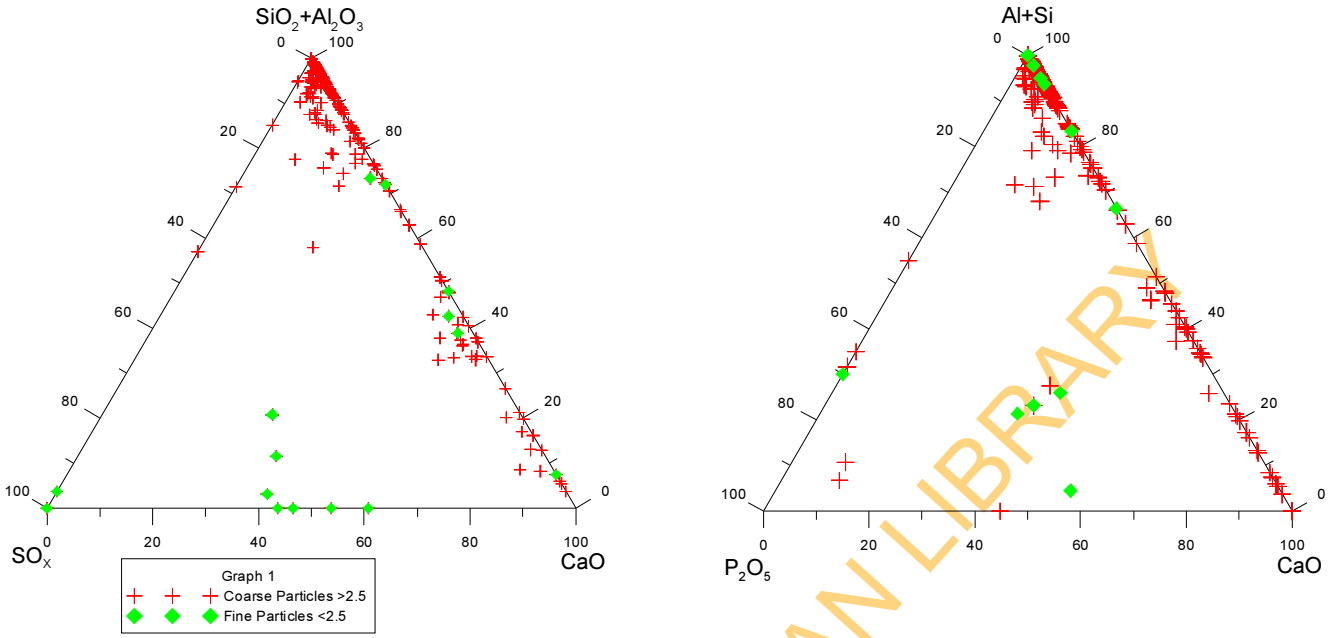

Figure 4.24: Ternary compositional plots that show the proportions of Al+Si/S/Ca within individual mineral particles in the different environmental units, as obtained from EDS spectra.

Ti-rich Particles

Ti-rich particles were observed in the study area as TiO_2 (titanium dioxide) and they were mostly rounded in shape. Ti made up 2% of the analyzed particles, and contains particles having >20%. Ti ranged from 24.7-90.94% and averaged 34.27% with other oxides such as Si, Al, Ca and Fe reaching 26, 12, 11 and 15% respectively. These particles were rare and showed two separate mineralogy. These were those associated with alumino-silicate in their high concentration and those that associated with Fe. The latter were mostly fine while those that were associated with alumino-silicate were in coarse mode. The presence of Ti in the PM could be related to both weathering of the parent rock and contribution from anthropogenic sources

4.5 Geochemistry of the Particulate Matter

4.5.1 Elemental Distribution in the PM samples

Elemental analysis of PM provides valuable information about potentially harmful elements such as lead, and other heavy metals (Co, Cr, Cu, Ni,); while the major-element analyses provide estimates of mineral components, overabundance of which may also be hazardous to human health and ecosystems. The elemental analysis of PM samples was performed using ICP-OES. The summary of the elemental data of PM from the different environmental units is presented in Table 4.10 and Figure 4.25. A comparison of mean elemental composition in Traffic, Residential, Dumpsite and Industrial areas is shown in Figure 4.26.

The major elements showed high concentration when compared to the trace element in all the units. Ca was highest in concentration with no significant differences in the mean concentration in all the units except industrial area, where t it was almost two folds more than the other major elements. Ca values ranged from 65.2-1700µg/m^3.

The mean concentration of the major elements are in the order Ca>K>Fe>Al>Na>Mg>Si. Al and Mg were more than Fe in residential and dumpsite area respectively (Table 4.10).

Table 4.10: Statistical Summary of Geochemical Result of the Study Area

Elements	Traffic		Residential		Dumpsite		Industrial		Study Area	
	Mean±SD	Range	Mean±SD	Range	Mean±SD	Range	Mean±SD	Range	Mean±SD	Range
Al (µg/m^3)	104.3±49.6	62.3-284.04	109.7±34.54	56.7-184.59	79.3±29.52	59.8-152.13	146.1±42.56	95.5-268.78	109.6±42.30	56.8-284.04
Ba (µg/m^3)	1.7±1.4	nd-8.0	1.66±.8	0.5-2.7	0.53±.15	0.41-.7	1.3±.4	0.8-2.3	1.6±1.1	nd-8.0
Ca (µg/m^3)	260.3±67.3	133.6-416.3	242.4±193.4	65.2-1700.0	260.2±58.0	131.4-319.8	414.6±330.4	135.3-1250.8	269.9±190.7	65.2-1700.0
Cu (µg/m^3)	2.9±3.2	nd-11.3	2.1±1.8	nd-10.1	2.1±1.0	nd-3.8	3.5±2.8	0.7-10.4	2.5±2.3	nd-11.3
Fe (µg/m^3)	189.0±123.2	72.2-447.1	96.2±32.5	58.7-243.3	85.7±18.4	61.0-116.2	161.2±46.0	92.8-265.3	126.4±79.8	58.7-447.1
La (µg/m^3)	0.5±0.6	nd-2.0	0.2±.3	nd-1.49	0.1±0.1	nd-0.3	1.1±1.2	0.3-4.7	0.4±.7	nd-4.7
K (µg/m^3)	863.9±400.9	31.0-1550.1	311.7±113.5	170.1-537.1	317.8±68.2	177.1-388.1	329.1±90.1	158.3-505.2	469.1±365.3	158.1-1550.1
Mg (µg/m^3)	95.5±14.7	78.8-155.3	87.8±10.3	63.7-106.4	90.2±7.5	71.3-99.4	145.4±89.2	85.1-358.8	97.0±37.1	63.7-358.8
Mn (µg/m^3)	2.2±1.4	nd-5.7	1.5±1.0	0.1-4.9	1.1±0.7	nd-2.0	2.9±1.4	nd-4.8	1.8±1.3	nd-5.7
Mo (µg/m^3)	3.8±2.9	nd-8.6	1.3±2.2	nd-9.0	0.2±0.6	nd-2.1	2.8±2.2	0.7-9.4	2.2±2.7	nd-9.4
Na (µg/m^3)	131.8±44.8	59.7-198.1	88.0±84.5	53.9-505.9	78.9±39.5	54.7-189.9	145.2±62.6	55.6-266.5	105.1±73.4	53.9-505.9
Ni (µg/m^3)	0.4±0.7	nd-2.5	0.6±1.9	nd-15.4	0.1±0.2	nd-0.6	1.7±2.7	0.4-11.7	0.7±1.8	nd-15.4
Pb (µg/m^3)	1.0±2.4	nd-10.4	0.51±1.2	nd-6.5	0.6±1.6	nd-4.9	2.8±3.2	0.4-13.2	0.9±2.0	nd-13.2
Si (µg/m^3)	89.8±26.3	60.1-54.8	78.0±13.2	50.0-136.7	73.5±13.6	56.7-107.5	123.1±21.3	80.1-154.7	86.0±23.6	50.0-154.8
Ti (µg/m^3)	1.6±2.4	nd-12.8	0.5±0.6	nd-3.1	0.5±.4	nd-1.1	2.6±2.2	nd-5.8	1.0±1.7	nd-12.8
Zn (µg/m^3)	4.1±9.0	nd-54.0	2.6±1.6	nd-5.7	2.1±1.4	nd-4.8	4.1±2.5	1.4-12.0	3.1±4.8	nd-54.0
PM (µg/m^3)	**378.6±235.0**	**48.3-1094.3**	**215.90±85.0**	**48.3-466.7**	**270.1±193.1**	**32.4-756.4**	**613.4±158.7**	**337.9-949.5**	**311.3±203.3**	**32.4-1094.3**

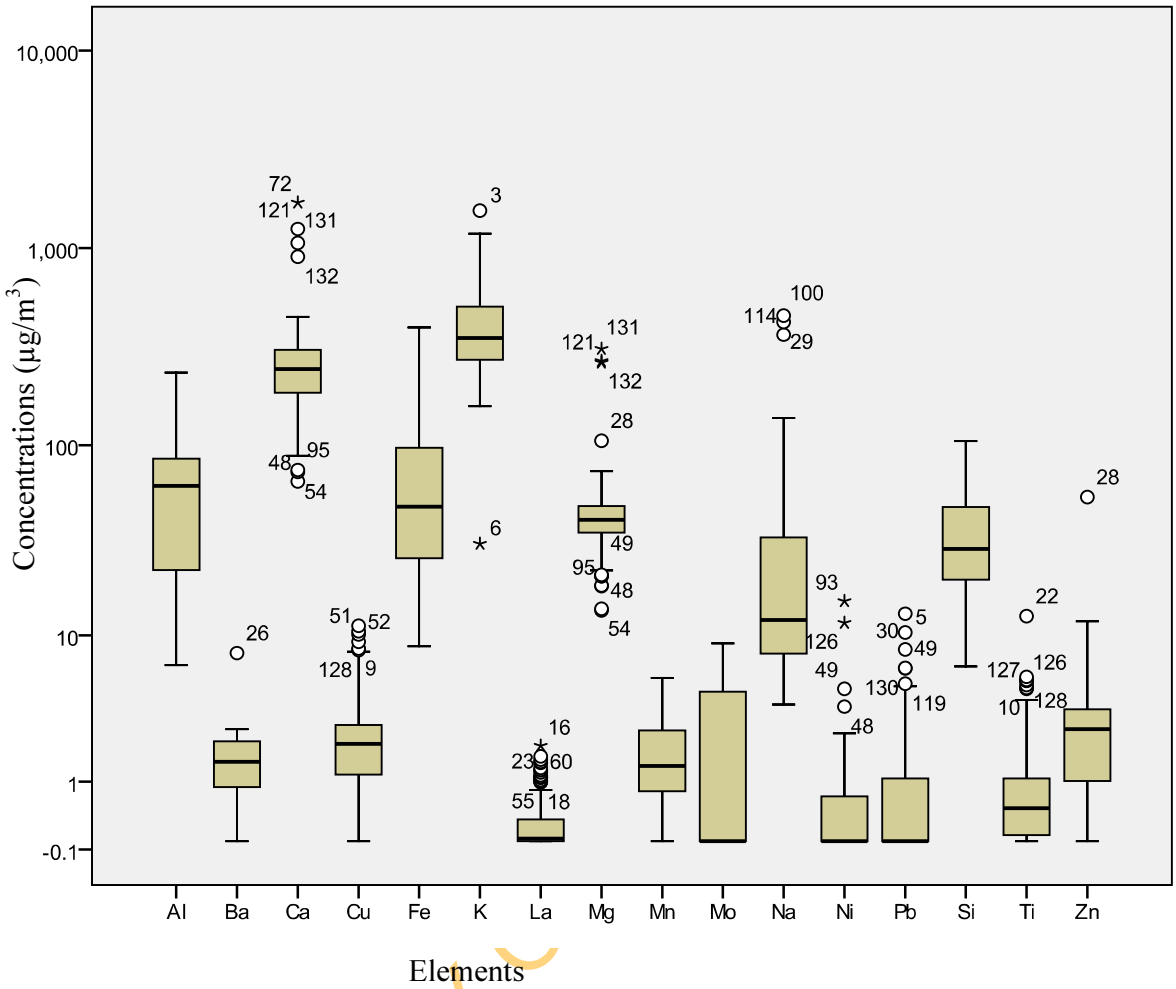

Figure 4.25: Geochemical Summary of the Elements of the PM

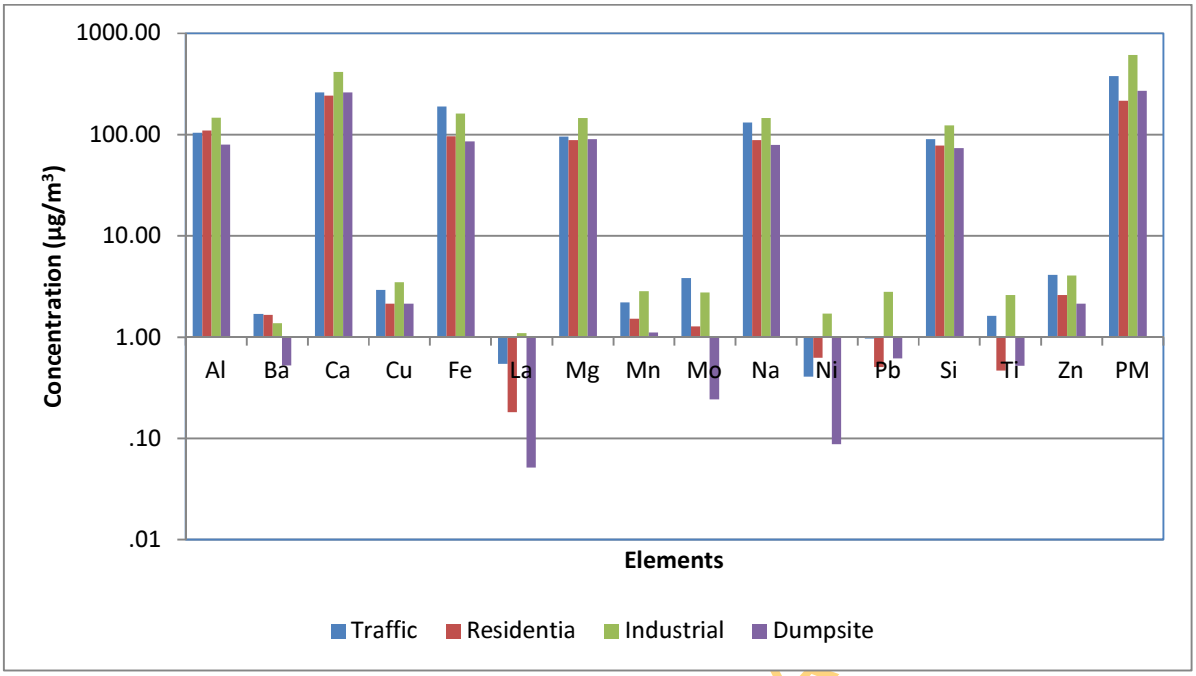

Figure 4.26: Average Composition of Elements in the Study Area

PM samples from industrial area have the highest concentration of most metals except for Fe, which had highest concentration in PM samples from traffic area.

The average ratios of Mg/Al (0.91±0.37-RA and 1.23±0.31-DA), Ca/Al (2.63±1.16 and 3.59±1.28 DA) and Fe/Al (0.97±0.43-RA and 1.73±0.69-TA) at the stations suggested contributions of clays and Ca-rich particles to the chemical compositions of the PM. It should be noted that this ratio remains nearly invariant (Table 4.11 and Figure 4.27) for all the collected PM samples at all the zones and can be a good reflection of the source region. In contrast, the Ca/Al ratio exhibited the highest variations from sample to sample (2.63-3.59), since it was influenced by particle size. All the ratio values and the low standard deviations suggest similarity in geochemical characteristics over the study area and a uniform source for the PM.

Heavy metals such as Ba, Cu, La, Mn, Mo, Ni, Pb, Ti, Zn were found above detection limit from for more than 95% of the samples (except Pb-65% and Ba-75. As and Cd were also observed especially in industrial and traffic areas but the data population was not statistically significant hence were screened out.

The summary of the heavy metal concentration is in Table 4.10. The mean concentration are in the order Zn> Cu> Mo>Mn>Ba>Ti>Pb>Ni>La.

Zn, Cu and La were consistent in their concentrations levels in all the sampled areas. Industrial area showed the highest average concentration of all these metals except Ba, which was highest in samples from traffic area (Figure 4.25). The outliers such as Ba, Ni and Pb identified within the hotspots suggested the intensity of the metal generating activities in the zone.

4.5.2 Elemental Association in the PM

The relationship among the various elements in the PM of the study was better explained by using Pearson correlation analysis. The correlation coefficient matrix is given in Table 4.12.

Table 4.11: Average Ratio of major element with Al

	Si/Al	Mg/Al	Ca/Al	Fe/Al
Industrial Area	0.91±0.20	1.1±0.44	3.14±2.18	1.14±0.32
Dumpsite Area	0.97±0.14	1.23±0.31	3.59±1.28	1.14±0.26
Traffic Area	0.92±0.16	1.03±0.27	2.82±0.85	1.73±0.69
Residential Area	0.76±0.19	0.91±0.37	2.63±1.16	0.97±0.43

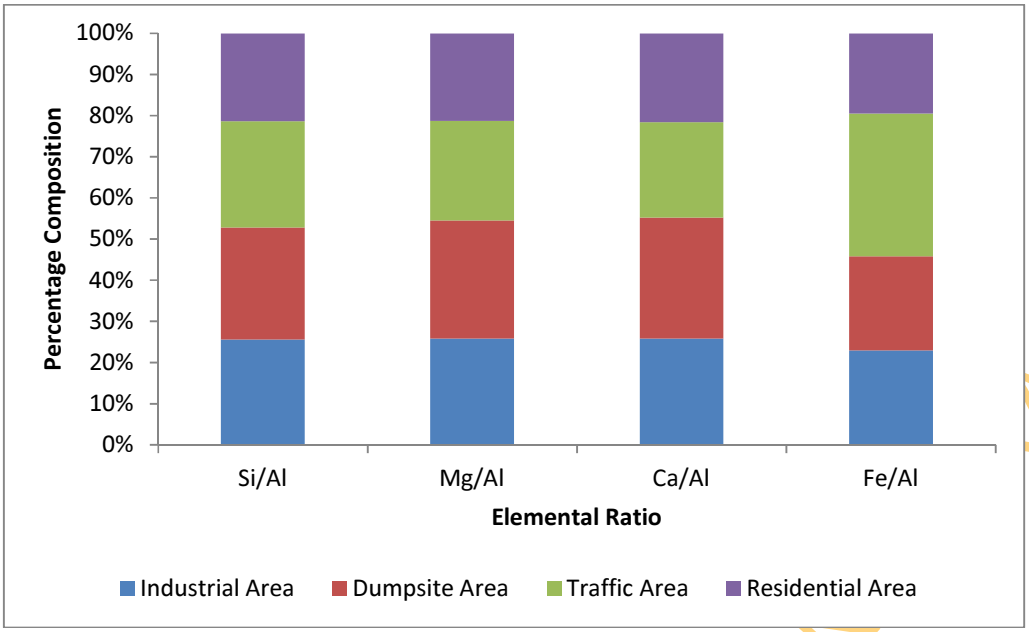

Figure: 4.27: Average Ratio of major element with Al

Table 4.12: Correlation Coefficient of Elements in the Study Area

	Al	Ba	Ca	Cu	Fe	La	Mg	Mn	Mo	Na	Ni	Pb	Si	Ti	Zn	PM
Al	1.00															
Ba	.38	1.00														
Ca	.10	-.07	1.00													
Cu	-.04	-.18	.13	1.00												
Fe	**.56**	.32	.21	.03	1.00											
La	.18	.26	.13	.28	.11	1.00										
Mg	.34	.04	**.95**	.11	.26	.16	1.00									
Mn	.25	**.60**	.27	.11	.39	.25	.28	1.00								
Mo	-.26	.10	.02	**.53**	-.13	.51	-.04	.25	1.00							
Na	.01	-.10	.46	.27	.36	-.04	.35	.21	-.04	1.00						
Ni	.12	-.13	.06	.30	.00	.34	.07	.07	.11	.19	1.00					
Pb	.26	-.04	.03	.04	.20	-.09	.09	.04	-.16	.16	.07	1.00				
Si	**.62**	.21	.14	.24	**.70**	.34	.25	.28	-.06	.39	.33	.33	1.00			
Ti	.27	-.12	.12	**.53**	.45	.19	.16	.19	.13	.34	.26	.17	**.68**	1.00		
Zn	.24	-.07	.27	.10	.26	-.01	.34	.17	-.06	.30	.11	.10	.14	.09	1.00	
PM	**.51**	.18	.25	.17	.48	.30	.31	.38	-.07	.27	.16	.15	**.65**	**.60**	.08	1.00

Table 4.13 shows the summary of elemental association in each zone (the entire matrix is given in Appendix II).

Three significant elemental associations were observed in the study area. They include Al-Si-Fe-Ti (0.5-0.85), Ca-Mg (0.95) and Cu-Mo-La (0.51-0.53). This indicated a common source for these groups of metal.

The first elemental association affirmed association with geogenic material in the PM, which has a greater influence on mass load of PM as indicated by the positive correlation (Table 4.12). Similar elemental association was observed in dumpsite, traffic and industrial area. However, Mn, Zn and Ba were the additional trace metals introduced by dumpsite and industrial area in such corresponding association.

The second elemental association which was also common to all the zones was the Ca-Mg relationship, which showed significant positive correlation (0.95) with each other and explained the source to be as a result of domestic wood burning; an assertion also supported by the work of (Saud et al. 2013). This was further confirmed by the high negative correlation with PM mass load in dumpsite/incineration zone (Figure 4.28).

The third elemental association was Cu-Mo-La which possibly signified traffic and industrial elemental contributory fingerprint.

4.5.3 Principal Component Analysis

Principal component analysis (PCA) is the most common multivariate statistical methods used in environmental studies (Juneng *et al*., 2009; Zhang *et al*., 2011). Factor Analysis (FA) can be applied on explanatory or confirmatory basis. In the explanatory application to airborne particulate study, it was used to uncover the underlying structure of elemental compositions with the assumption that any indicators (element) could be associated with any factor. Such factor loading was used to infer the source/source type.

Table 4.13: Summary of Correlation Coefficient of the four Environmental Units.

	Association 1	Association 2	Association 3	Association 4
Dumpsite	Al, Fe, Si, Ti, Zn, Mn	Cu, La	PM, (Mg, Ca)	
Traffic	Al, Si, Fe, Ti, PM	Ca, Mg, Zn	Cu, Ni	
Residential	Ba, La, Mn, Mo, Cu	Ca, Mg, PM	Ti, Zn	Al, Si, Pb
Industrial	Ba, Fe, Mn, Na, Si, Ti, PM	Cu, La, Mo, Zn	Ca, Mg	
Study area	Al, Fe, Si, Ti, PM	Ca, Mg	Cu, Mo, Ti	

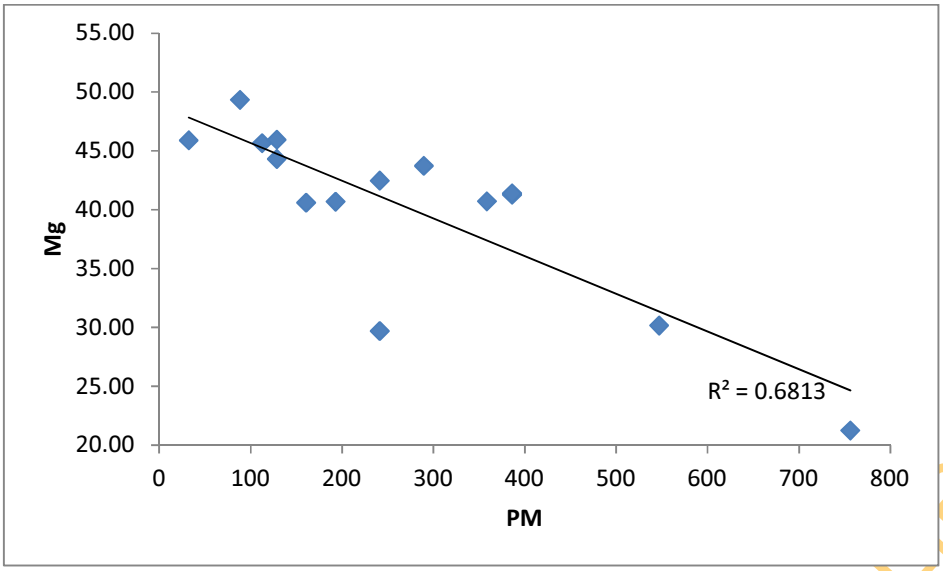

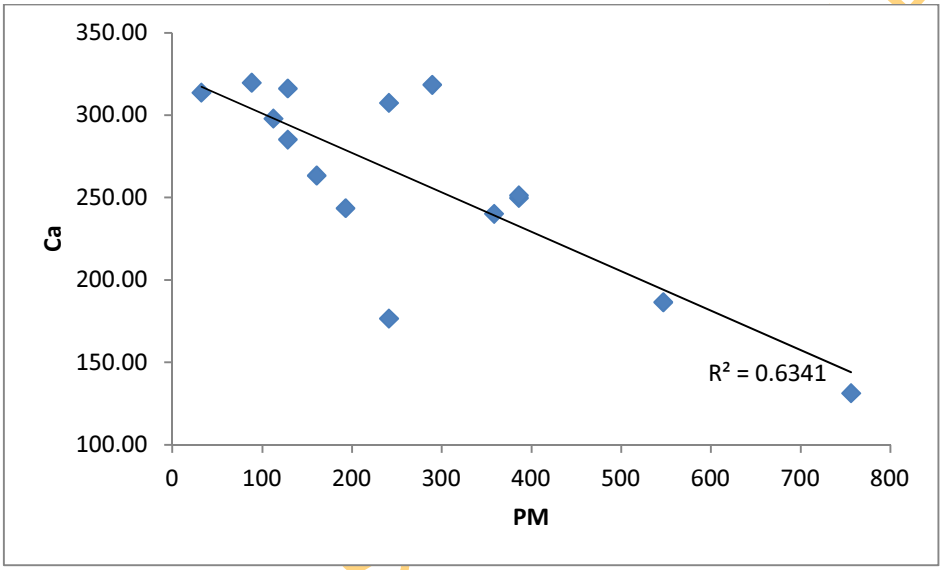

Figure 4.28: Selected Scatter plots PM and some Elements

PCA is widely used to reduce data (Toledo, 2008; Smyth et al., 2013) and to extract a small number of latent factors (principal components, PCs) for analysing relationships among the observed variables. If large differences exist in the standard deviations of variables, PCA results will vary considerably depending on whether the covariance or correlation matrix was used. The concentrations of the heavy metals evaluated in this study vary by different orders of magnitude. PCA was therefore applied to the correlation matrix for this study, and each variable was normalized to unit variance. To make the results more easily interpretable, the PCA with VARIMAX normalized rotation was also applied, which can maximize the variances of the factor loadings across variables for each factor. Factor loadings N 0.71 are typically regarded as excellent and b 0.32 very poor. In this study, all principal factors extracted from the variables were retained with eigenvalues >1.0, as suggested by the Kaiser criterion. When PCA with VARIMAX normalized rotation was performed, each PC score contains information on all of the metal elements combined into a single number, while the loadings indicate the relative contribution each element makes to that score.

Tables 4.14 and 4.15 presents the factor loadings of the principal component analysis and those with loading values >0.50 are marked bold. Five (5) factors were obtained with total data variability of 97.48% while factors 1 and 2 constituted 52.76% of total variability. Although, the impact of other factors such as factors 3-5 were also considered against factor 1 in order to illustrate the similarity or dissimilarity of individual zone.

For better understanding of the sources identification of pollutants each environmental unit was considered separately. It was observed that the first factor describes 34.89% of the common variance and was loaded with **Al, Si, Fe and PM,** ranging from 0.86-0.93 and to some extent with **Mg and Ca (0.55)**, suggesting similar behavior within the group and that they were basically elemental signature of topsoil/ lithogenic materials. Although the nature of the sampling site differs from one to another, the association of Al, Si, and Fe are relatively comparable among these locations. The soil is the dominant source for these elements. This grouping was also evident in the other zones, except for Ba in Industrial and Mo in dumpsite areas.

Table 4.14: Factor Analysis of Elements of the Study Area

Elements	Factor 1	Factor 2	Factor 3	Factor 4	Factor 5	Communalities
Al	**0.92**	-0.20	0.23	-0.16	0.06	**0.96**
Ba	0.37	-0.23	-0.06	0.10	**0.83**	**0.90**
Ca	**0.55**	**0.93**	0.21	-0.13	-0.15	**0.94**
Cu	0.10	0.00	0.14	**0.70**	-0.43	**0.70**
Fe	**0.90**	0.33	0.05	0.08	-0.02	**0.92**
La	0.26	-0.13	-0.22	**0.86**	0.04	**0.87**
Mg	**0.55**	**0.62**	0.46	-0.20	0.06	**0.94**
Mn	-0.09	-0.03	0.21	-0.05	**0.81**	**0.71**
Mo	-0.40	-0.29	-0.02	**0.79**	0.11	**0.89**
Na	0.04	**0.89**	0.14	-0.11	0.03	**0.83**
Pb	0.00	0.15	**0.94**	0.10	0.11	**0.93**
Si	**0.95**	0.07	-0.07	0.15	-0.06	**0.94**
Ti	0.48	-0.25	0.06	0.24	**-0.68**	**0.81**
Zn	0.16	0.28	**0.87**	-0.20	0.00	**0.90**
PM10	**.75**	-.08	.16	-.12	-.05	**0.93**
eigenvalue	**3.48**	**2.50**	**2.11**	**2.10**	**2.06**	
% Variance	**34.89**	**17.87**	**15.06**	**14.97**	**14.69**	
Cumulative %	**34.89**	**52.76**	**67.82**	**82.79**	**97.48**	

Factor 1: Al, Si, Ca, Fe, Mg, PM10-Soil
Factor 2: Ca, Mg, Na-soil
Factor 3: Zn, Pb-Industrial
Factor: Cu, La, Mo-Traffic
Factor 5: Ba, Mn-Traffic

Table 4.15: Summarized Factors in the Zones

	Factor 1	Factor 2	Factor3	Factor 4	Factor 5
Traffic	Al, Fe, Si, Ti, PM	Ca, Mg, Na, Zn	Cu, Mo, Ni	Ba, Mn	Pb
Industrial	Ba, Fe, Mn, Na, PM	Cu, La, Mo, Ni, Zn	Na, Ti	Ca, Mg	Pb
Residential	Ca, Mg, Na, PM (Al)	Ba, Cu, La, Mn, Mo	Ti, Zn	Fe, Si	Ni, Pb
Dumpsite	Fe, Mo, PM (Ca, Mg)	Al, Si, Zn	Mn, Ti, Zn (Na)	Cu, La	Mn, Ni, Ti
Factor Loading	0.62-0.99	0.61-0.95	0.54-0.91	0.52-0.97	0.61-0.91
% Variance	24.58-28.21	20.44-25.80	13.78-15.98	12.38-14.33	6.64-14.05
Cumulative %	24.58-28.21	45.02-54.01	58.80-69.99	71.18-84.32	77.82-98.37

The elemental associations displayed in factors 2 **(Ca, Mg, Na)** accounting for 17.84% of the total data variability are metals believed to be the product of wood burning, a signature similar to all the environmental units.

The third factor, describing 15.06% of the common variance of the data set, was highly loaded with **Pb (0.94)** and **Zn (0.87)**. This could be product of industrial emission, brake and tyre wears (Abu-allaban et al. 2003). In addition, vehicles exhaust cannot be ruled out in the case of Zn, since it is used widely as catalyst in the cracking of engine oil.

Factor 4 was strongly loaded with **Cu, La and Mo** (0.70-0.86) and constituted 14.97% of total variability of data set and could be sourced from traffic related components in the aerosol.

Factor 5 with high factor scores for **Ba (0.83) and Mn (0.81)** and 14.69% as total variance are also attributed to traffic emission.

A major contributor to the aerosol in this area is vehicular traffic exhausts rich in **Pb, Zn, Ba, Cu, La, Mo** and **Mn** (De Migue *et al*., 1999), the association of Mg with the other element in this group was not unexpected as Mg is widely used as metallic fuels in vehicle as contrary to its geogenic source.

4.5.4 Geo-environmental Assessment of Metals in PM

The calculation of Enrichment Factors (EFs) relative to the Earth's upper crust composition can be used to discriminate between the origins of elements from crustal or non-crustal sources (Zhang et al., 2003). EFs of elements in different particle fractions were determined by comparing the concentration of each element against the concentration of a reference (crustal) element to obtain a preliminary idea about possible origin, i.e. crustal or anthropogenic. Usually Si, Al or Fe is used as the reference element, but there is no universally accepted rule for its choice. For this study Aluminum was chosen as the reference element for the enrichment factor calculations. This research assumed that the dominant fraction of aluminum in the study area is primarily derived from geogenic clay materials. The appropriateness of choosing Al is attributed to its more significant distribution in coarse particles than other elements, with very low contribution from non-crustal inputs.

In general, the enrichment factor for any element X relative to crustal material is defined by

$$EF_{CrustalX} = (X/Y)_{air}/(X/Y)_{crustal}$$ ---------- Equation 2

Where $EF_{crustalX}$ is the enrichment factor of X, Y s a reference element for crustal material, $(X/Y)_{air}$ is the concentration ratio of X to Y in the aerosol sample, and $(X/Y)_{crustal}$ is the average concentration ratio of X to Y in the crust. If EF Crust approaches unity, then crustal soils are most likely the predominant source of element (Gao, 2001). In practical terms, if the EF Crust value is above 10, then the element is considered to be of non-crustal origin, possibly anthropogenic. EF Crust values in the range of 1–5 suggest no significant contribution of anthropogenic sources to the ambient level of these elements. In general, as the EF Crust value increases, the non-crustal source contribution also increases. Estimates of EF aid in (a) differentiating between element concentrations that originate from human activities and those from natural sources and, in (b) assessing degree of anthropogenic influence (Rashki et al., 2013).

It is obvious from this research, that the predominant sources of airborne particles are strongly influenced by soil derived from the region. Thus the actual composition of soil would be more appropriate for calculating EF in this region. Table 4.16 and 4.17 show the results of enrichment factor calculations, based on the bulk concentrations of trace elements obtained through the ICP/OES procedure. Enrichment factors for most elements in the study area are relatively low. This implies that the bulk of the contribution of Ba, Cu, La, Mn, Mo, Ni, Pb, Ti and Zn (60-100%) come from crustal materials (soil).

They are also moderately enriched in all the zones, except Ba which is only moderately enriched in Traffic area. The percentage contribution of moderate enrichment ranged from 4% (Ni, Pb) -64% (Zn) in dumpsite and industrial area respectively. Significant enrichment for Ba, Cu, La, Mo, Mn, Ni and Zn were only common in traffic area (6-17%) and to some extent in residential area (1-5%) (Figures 4.29 to 4.30).

It was believed that the enrichment of these elements in PM in the atmosphere can be attributed to the atmospheric transport of substances primarily derived from soil/crust, since they tends to concentrate on fine particles that have a long resident time in the atmosphere (Gao, 2001). It must however be stated that some were anthropogenically introduced by fossil fuel combustion and wood burning, which were also prevalent in the study area.

Table 4.16: Summary of Enrichment Factor

Elements	Mean ± S. D	Range
Ba	0.84	0.0-8.00
Ca	1.66	0.0-6.00
Cu	1.50	0.0-12.00
Fe	1.16	0.0-3.00
La	1.06	0.0-10.00
Mg	1.41	0.0-7.00
Mn	1.58	0.0-8.00
Mo	1.06	0.0-9.00
Na	1.47	0.00-28.00
Ni	1.88	0.00-15.00
Pb	0.42	0.00-7.00
Si	1.09	0.00-2.00
Ti	0.85	0.00-4.00
Zn	1.32	0.00-6.00
PM_{10}	1.35	0.00-6.00

Table 4.17: Percentage Composition of Trace Elements of Enrichment Factor

Zones	Class	Definition	Ba	Cu	La	Mn	Mo	Ni	Pb	Ti	Zn
	1	EF<2	60	60	75	49	57	84	89	69	54
Traffic	2	EF=2-5	23	26	12	37	20	20	11	31	34
	3	EF=5-20	17	14	13	14	23	6	-	-	8
	1	EF<2	100	33	94	33	94	96	87	60	40
Dumpsite	2	EF=2-5	-	53	6	67	6	4	13	40	60
	3	EF=5-20	-	14	-	-	-	-	-	-	-
	1	EF<2	94	70	90	61	92	88	95	85	67
Residential	2	EF=2-5	6	25	5	36	5	8	4	15	33
	3	EF=5-20	-	5	5	3	3	4	1	-	-
	1	EF<2	100	76	76	67	94	82	65	47	36
Industrial	2	EF=2-5	-	24	24	33	6	12	35	53	64
	3	EF=5-20	-	-	-	-	-	6	-	-	-

1= Deficiency/lithogenic origin, 2= Moderate Enrichment 3=Significant Enrichment

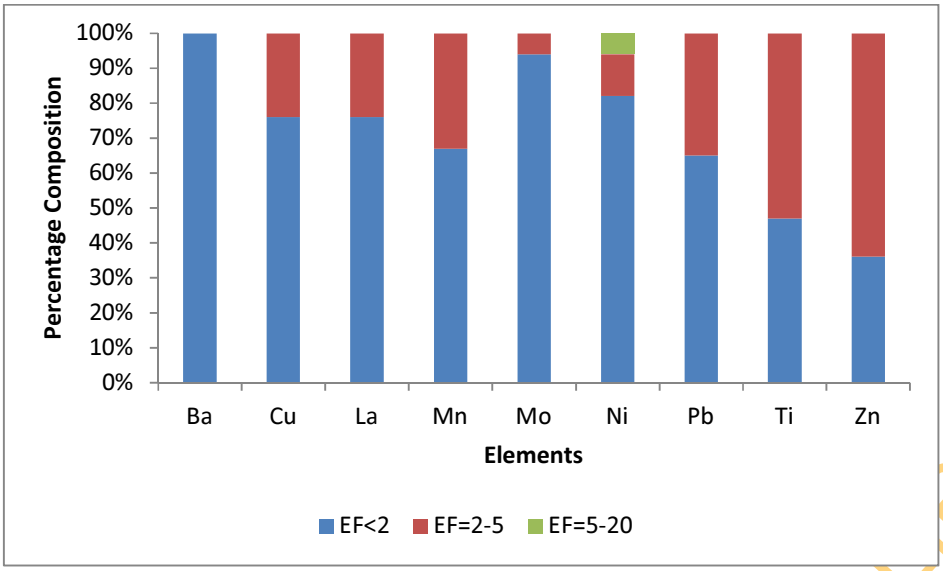

Figure 4.29: Enrichment Factor of Traffic Area

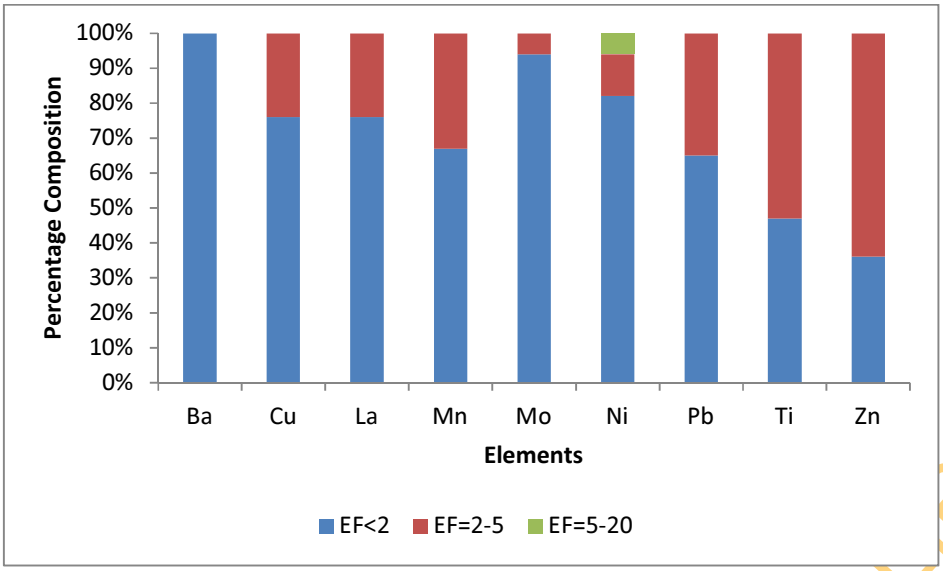

Figure 4.30: Enrichment Factor of Dumpsite Area

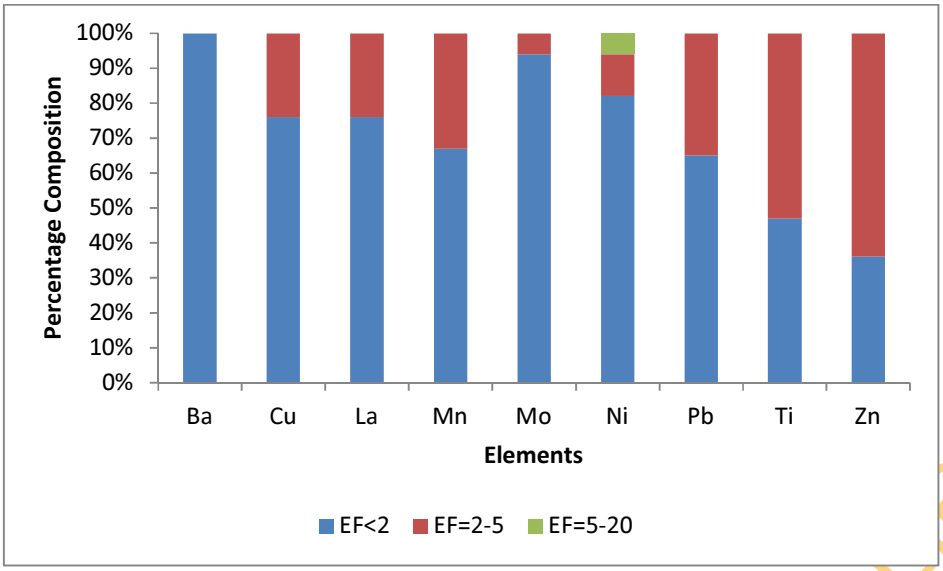

Figure 4.31: Enrichment Factor of Industrial Area

CHAPTER FIVE
SUMMARY, CONCLUSION AND RECOMMENDATION

5.1 Summary

The study of the concentration, morphological/mineralogical and geochemical composition of PM from the different zones of the study area has been undertaken. The characteristics of the PM were observed by SEM/EDS while the PCA was used to constraint the possible sources of the particulate matter.

Scanning Electron Microscopy coupled with Energy Dispersive Spectrometry (SEM/EDS) analysis performed on the PM revealed that mineral dust, that is, soil dust is the most abundant particles in the PM, which occupied about 70% of the entire particles. While the remaining 30% are particles emitted from anthropogenic origin as a direct consequence of traffic and industrial emission. Clay minerals such as chlorite, kaolinite, illite and smectite occupied the larger volume of the minerals dust and constituted 55% of the total mineral dust particles while 15% is shared among the rock forming minerals such as quartz, mica, feldspar and amphibole. There is no much variation in the mineralogy of the PM in both seasons except for the enhanced concentration of calcite minerals in the dry season, which could be as a result of the contribution from the harmattan dust. These types of single inhalable particles from the different sampling sites are mostly from windblown and resuspension of soil dust as well as road construction.

The morphology of the mineral dust is mostly irregular in shape and coarse in size fraction (PM_{10}). This is an indication of local source of mineral dust, which is in agreement with the mineralogy of soil, as revealed by XRD analysis of soil samples. The mineralogy of parent rocks in the study area, as revealed by petrographic study and XRD gave the impression of the same mineral assemblages observed in the soil and eventually in the dust. This is due to the

weathering of the parent rocks within the study area, which is eventually blown into the atmosphere.

The soot aggregation as revealed by particle morphology- mostly from emissions of combustion sources, including vehicle exhaust, and biomass burning. These particles appear as fluffy round aggregations and are often spherical and mostly in fine mode fraction.

The result of the principal component analysis of elements also identified the same pollution source revealed by the SEM/EDS analysis. Among the 14 elements of PM in the study area, the elements that made up the cumulative contribution rate over 52% from the total variability were Al, Si, Ca, Fe, Mg and Na, which is an indication of their crustal sourcing. These elements also have high association with the concentration of PM as revealed by factor loading of F1. The other three factors almost have the same variability of about 15% each and elemental association of Zn, Pb; Cu, La, Mo; Ba, Mn of F3, F4, F5 respectively. The associations of these elements depict an anthropogenic contribution which could be from industrial and traffic emission.

5.2 Conclusion

The concentration of PM is in many folds higher than the recommended standards especially during the dry season. Industrial area is 2-3 folds higher than traffic, dumpsite and residential area in terms of average concentration of PM. Unhealthy situation was observed in all the units, but to lesser extent in residential area that are not close to the activity driven areas. Among the sources that contributed significantly to air pollution problem in Ibadan are soil dust resuspension, fossil fuel combustion, biomass burning.

High concentration of Particulate Matter (PM) was observed in the area especially in the vicinity of driven areas. This high concentration was worsened during the dry season due to low precipitation, relative humidity and consequently high gravitational settling of the PM. The study area did not meet the Clean Air Act and the environment could be denoted as non-attainment as established by NAAQS. This impaired air quality could pose a negative impact on the health of the populace especially to the sensitive group (the young, the unhealthy and the old

people) and the people living very close to source of PM generation. The Traffic and Industrial Area displayed relatively unhealthy and very unhealthy air quality index (AQI) and this of course, could be attributed to traffic and industrial emission plus soil dust resuspension by micro scale event of windblown that is often experienced and to a larger extent from vehicular movement.

SEM/EDX revealed that most of the particles in the PM are mostly coarse and irregular in shape and are dominantly clay minerals and other rock forming minerals. This is an indication that these particles were sourced from the crustal materials. Anthropogenic particles such as soot were also revealed, which are likely sourced from traffic and industrial emissions. The interaction of the clay minerals and the soot particles were also obvious, suggestive by the coating of sulfate particles on the clay minerals.

The major elements showed a correlation that was consistent with the geochemistry of the soil of the study area as revealed by PCA. Their relationships with the major elements indicated that they have dual sources of generation, which are mainly from the soil and anthropogenic input.

5.3 Recommendation

It is recommended that epidemiological study should be undertaken to ascertain the health implication of the consequence of the particulate matter on the populace in the study area.

It is also important to carry out chemical mass balance analysis (CMB) so as to apportion specific sources of the pollutants.

References

Abdulkarim, B. I., Chiroma, T. M. & Joseph, T., 2007. Assessment of CO , CO_2 and Suspended Particulate Matter Emissions. *Leonardo Electronic Journal of Practices and Technologies*, 11, pp.109–116.

Abdul-Wahab, S. A., Worthing, M. A. and Al-Maamari, S., 2005. Mineralogy of atmospheric suspended dust in three indoor and one outdoor location in Oman. *Environmental Monitoring and Assessment*, 107(1-3), pp.313–27.

Abu-allaban, M. Gillies, J. A., Gertler, A. W., Clayton, R. and Proffitt, D. 2003. Tailpipe, resuspended road dust, and brake-wear emission factors from on-road vehicles. *Atmospheric Environment*, 37, pp.5283–5293.

Abu-Allaban, M., Hamasha, S. and Gertler, A., 2006. Road dust resuspension in the vicinity of limestone quarries in Jordan. *Journal of the Air & Waste Management Association*, 56, pp.1440–4.

Adedokun, J. A., Emofurieta, W. O. and Adedeji, O. A., 2000. Theoretical and Applied Climatology Physical , Mineralogical and Chemical Properties of Harmattan Dust at. *Theoretical and Applied Climatology*, 169(1989), pp.161–169.

Adeyemo, O. K., Adedokun, O. A., Yusuf, R. K. and Adeleye, E. A., 2008. Seasona Changes in Physico-chemical Parameters and Nutrient Load of River Sediments in Ibadan City, Nigeria. *Global Nest*, 10(3), pp.326–336.

Afeti, G. M. and Resch, F. J., 2000. Physical characteristics of Saharan dust near the Gulf of Guinea. *Atmospheric Environment*, 34(8), pp.1273–1279.

Ajibade, A. C and Fitches, W. R., 1988. The Nigerian Precambrian and the Pan-African Orogeny. *In: Precambrian Geol Nigeria. Geological Survey of Nigeria (ed)*, pp.45–54.

Akeredolu, F. A., 1996. Environmental Engineering Notebook, Department of Chemical Engineering, Obafemi Awolowo University, Ile Ife.

Akeredolu, F. A., Latinwo, L. and Sonibare, J. A., 2006. Modelling of the Ambient Air Particulate Matter in a Nigeria Steel Industrial Environment Using Multivariate Techniques and Engineering Control Implications. *Ife Journal of Technology*, 15, pp.1–14.

Alfaro-Moreno, E., Ponce-de-Leo´ N, S., Osornio-Vargas, A. R., Garcı´a-Cuellar, C., Martınez, L., Rosas, I., 2007. Potential toxic effects associated to metals and endotoxin present in PM10: an ancillary study using multivariate analysis. *Inhalation Toxicology*, 19(49-53).

Ana, G. Adeniji, B., Ige, O. and Oluwole, O. 2012. Exposure to emissions from firewood cooking stove and the pulmonary health of women in Olorunda community, Ibadan, Nigeria. *Air Quality, Atmosphere & Health*, 6(2), pp.465–471.

Annor, A. E., 1983. Metamorphism of Pelitic Rocks in Relation to deformation episodes around Okene, Nigeria. *Journal of Mining and Geology*, 20, pp.17–25.

Annor, A. E., 1986. Structural Class of the Precambrian Basement Complex of Nigeria. Journal of Pure and Applied Sciences. *Journal of Applied Sciences*, 1, pp.84–89.

Aweto, A. O., 1994. *Soils of Ibadan region* I. Filani, M.O. & C. O. F.O., Areola, eds., Ibadan Region: Rex Charles Publ.

Ayeni, M. O. A., 1994. The metropolitan area of Ibadan: Its growth and structure: In. Filani, M. O. & Areola C. O. F.O., Ibadan Region: Rex Charles.

Baulig, A., Poirault, J. J., Ausset, P., Schins, R., Shi, T., Baralle, D., Dorlhene, P., Meyer, M., Lefevre, R., Baeza-Squiban, A., Marano, F., 2004. Physicochemical characteristics and biological activities of seasonal atmospheric particulate matter sampling in two locations of Paris. *Environmental Science and Technology*, 38, pp.5985–5992.

Baulig, A., Singh, S., Marchand, A., Schins, R., Barouki, R., Garlatti, M., Marano, F., Baeza-Squiban, A., 2009. Role of Paris PM2.5 components in the pro-inflammatory response induced in airway epithelial cells. *Toxicology*, 261, pp.126–135.

Beceiro-González, E., Andrade-Garda, J. M., Serrano-Velasco, E., & Lópes-Mahía, P., 1997. Metals in airborne particulate matter in La Coruña (NW Spain). *Science of the Total Environment*, 196(131–139).

Bergametti, G., Gomes, L., Coudé-Gaussen, G., Rognon, P., Le Coustumer, M. N., 1989. African dust observed over Canary Islands: source-regions identification and transport pattern for some summer situations. *Journal of Geophysical Research*, 94(D12), pp.14855–14864.

Billet, S., Garc-on, G., Dagher, Z., Verdin, A., Ledoux, F., Courcot, D., Aboukais, A., Shirali, P., 2007. physicochemical characterization and metabolic activation of the organic fraction in human lung epithelial cells(A549). *Environmental Research*, 105, pp.212–223.

Breuning-Madsen H and Awadzi, A. T., 2005. Harmattan dust position and particle size in Ghana. *Catena*, 63, pp.23–38.

Buseck, P. R., and Posfai, M., 1999. Airborne minerals and related aerosol particles: Effects on climate and the environment. Proceedings of the National Academy of Sciences of the United States of America. , 96, pp.3372–3379.

Butlin, R. N., Coote, A. T., Devenish, M. I., Hughes, S. C., Hutchens, C. M., Irwin, J. G. Lloyd, G.O., Massey, S. W., Webb, A. H. and Yates, T.J.S., 1992. Preliminary results from the analysis of metal samples from the National Materials Exposure Programme (NMEP). *Atmospheric Environment*, 26, pp.199-200).

Census, 2006. *Legal Notice on Publication of the Details of Breakdown of the National and State, 2006 Census, Federal Republic of Nigeria Official Gazette.*

Chapman, R. S., Watkinson, W. P., Dreher, K. L., & Costa, D.L., 1997. Ambient particulate matter and respiratory and cardiovascular illness in adults: Particle-borne transition metals and the heart–lung axis. *Environmental Toxicology and Pharmacology*, 4, pp. 331–338.

Charlson, R. J., Schwartz, S. E., Hales, J. M., Cess, R. D., Coakley, J. A., Hausen, J. E. and Hofman, D.J., 1992. Climate Forcing by Anthropogenic Aerosol,. *Science*, 255, pp.423–430.

Chen, J., Wang, W., Liu, H. and Ren, L., 2012. Determination of road dust loadings and chemical characteristics using resuspension. *Environmental monitoring and assessment*, 184, 1693–709.

Chou, Chou, C., Formenti, P., Maille, M., Ausset, P., Helas, G., Harrison, M. and Osborne, S., 2008. Size distribution, shape, and composition of mineral dust aerosols collected during the African Monsoon Multidisciplinary Analysis Special Observation Period 0: Dust and Biomass-Burning Experiment field campaign in Niger, January 2006. *Journal of Geophysical Research*, 113, D00C10.

Chow, J. C., Watson, J. G., Ashbaugh, L. L. and Magliano, K. L., 2003. Similarities and differences in PM 10 chemical source profiles for geological dust from the San Joaquin Valley , California. *Atmospheric Environment*, 37, 1317–1340.

Connan, O., Maro, D., Hébert, D., Roupsard, P., Goujon, R., Letellier, B. and Le Cavelier, S., 2013. Wet and dry deposition of particles associated metals (Cd, Pb, Zn, Ni, Hg) in a rural wetland site, Marais Vernier, France. *Atmospheric Environment*, 67, 394–403.

D' Hoore, L.J., 1964. *Soil Map of Africa*, CCTA Publisher Lagos. 214

D'Almeida, G.A., 1986. A model for Saharan dust transport. *Journal of Climatology Applied Meteorology*, 25, 903–16.

D'Almeida, G.A., 1987. On the variability of desert aerosol radiative characteristics. *Geophysical Research*, 92, 3017–3026.

Dada, S.S., 2006. Proterozoic Evolution of Nigeria. In O. O, ed. *The Basement Complex of Nigeria and its Mineral Resources (A Tribute to Prof. M. A. O. Rahaman).* Akin Jinad and Co Ibadan, 29–44.

Davis, B. L. and Jixiang, G., 2000. Airborne particulate study in five cities of China. *Atmospheric Environment*, 34, 2703–2711.

De Migue, E. Llamas, J. F., Chacon, E. and Mazadiego, L. F., 1999. Sources and pathways of trace elements in urban environments : a multi-elemental qualitative approach. , 355–357.

DETR, 2000. Controlling and mitigating the environmental effects of minerals extraction in England. Mineral Planning Guidance Note 11, consultation paper. DETR, London.

Dieme, D., Cabral-Ndior, M., Garçon, G., Verdin, A., Billet, S., Cazier, F., Courcot, D. and Diouf, A. Shirali, P., 2012. Relationship between physicochemical characterization and toxicity of fine particulate matter (PM2.5) collected in Dakar city (Senegal). *Environmental research*, 113, pp.1–13.

Dimari, G. A., Hati, S. S., Waziri, M. and Maitera, O. N., 2008. Pollution Synergy from Particulate Matter Sources : The Harmattan , Fugitive Dust and Combustion Emissions in. *European Journal of Scientific Research*, 23(3), pp.465–473.

Dockery, D., Pope C., XU X., Spengler J., Ware J., Fay M., F.B. and S.F., 1993. An Association between Air Pollution amd Mortality in Six U.S. Cities. *Journal of Medicine*, 329, pp.1753–1759.

Dominici, F., Peng, R.D., Zeger, S. L., White, R. H., Samet, J. M., 2007. Particulate Air Pollution and Mortality in the United States: Did the Risks Change from 1987 to 2000? *American Journal of Epidemiology*, 166, pp.880–888.

Donaldson, K., Stone, V., Seaton, A., & MacNee, W., 2001. Ambient particle inhalation and the cardiovascular system: Potential mechanisms. *Environmental Health Perspective*, 109, pp.523–527.

EC, 2000. Directive 2000/69/EC of the European Parliament and of the Council of 16 November 2000 relating to limit values for benzene and carbon monoxide in ambient air. OfficialJournalL 313, 13/12/ 2000, pp.0012–0021.

EC, 2002. Directive 2002/3/EC of the European Parliament and of the Council of 12 February 2002 relating to ozone in ambient air. Official Journal L 67, 9/3/2002, pp.14–30.

Efe, S. I. and Efe, A.T., 2008. Spatial Distribution of particulate Matter (PM10) in Warri Metropolis, Nigeria. *Journal of Environmental Health and Rsearch,* 7, pp.22-31

Ehrlich, C., Noll, G., Wusterhausen, E., Kalkoff, W., Remus, R. and Lehmann, C., 2013. Respirable Crystalline Silica (RCS) emissions from industrial plants e Results from measurement programmes in Germany. *Atmospheric Environment*, 68, pp.278–285.

Elliott, P., Shaddick, G., Wakefield, J.C., de Hoogh, C., Briggs, D.J., 2007. Long-term associations of outdoor air pollution with mortality in Great Britain. *Thorax*, 62, 1088–1094.

Engelbrecht, J.P., McDonald, E.V., Gillies, J.A., Jayanty, R.K.M., Casuccio, G. & Gertler, A.W., 2009. Characterizing mineral dusts and other aerosols from the Middle East - Part 1: ambient sampling. *Inhal. Toxicol.*, 21, 297–326.

EPA, 1996. *Air Quality Criteria for Particulate Matter. Technical Reports.*, North Carolina, U.S. Environmental Protection Agency (EPA/600/P-95/001aF.

EPA, 1999a. *Compendium of Methods for the Determination of Inorganic Compounds and Determination of Metal in Ambient Particulate Matter Using Inductively Coupled Plasma (ICP)*, Cincinnati, OH. 276

EPA, 1999b. *Compendium of Methods for the Determination of Inorganic Compounds Selection, Preparation and Extraction.*, Cincinnati, OH. 339

EPA, 2004. *Monitoring of particulate matter in ambient air around waste facilities*, Bristol, U.S. Environmental Protection Agency.

Erel, Y., Dayan, U., Rabi, R., Rudich, Y., Stein, M., 2006. Trans boundary transport of pollutants by atmospheric mineral dust. *Environmental Science and Technology*, 40, 2996–3005.

Falconer, J.D., 1911. The Geology and Geography of Northern Nigeria, Macmillian, London. 135.

Fang, G. C., Huang, Y.-L. & Huang, J.-H., 2012. Atmospheric arsenic (As) study at five characteristic sampling sites in Taiwan. *Environmental monitoring and assessment*, 184, 729–40.

Fernández, A. J., Ternero, M., Barragán, F. J., & Jiménez, J.C., 2000. An approach to characterization of sources of urban airborne particles through heavy metal speciation. *Chemosphere*, 2, 123–136.

Fubini, B. & Arean, C.O., 1999. Chemical aspects of the toxicity of inhaled mineral dusts. *Chemical Society Review*, 28, 373–381.

Ganor, E., Foner, H.A., Gravenshorst, G., 2003. The amount and nature of the dust on Lake Kinneret (the Sea of Galilee), Israel: flux and fractionation. *Atmospheric Environment*, 37, 4301–4315.

Gao, Y., 2001. Characteristics of Chinese aerosols determined by individual-particle analysis. *Geophysical Research*, 106, 18,037–18,045.

Garc-on, G., Dagher, Z., Zerimech, F., Ledoux, F., Courcot, D., Aboukais, A., Puskaric, E., Shirali, P., 2006. Dunkerque city air pollution particulate matter-induced cytotoxicity, oxidative stress and inflammation in human epithelial lung cells (L132) in culture. *Toxicology in Vitro*, 20, 519–528.

Godish, T., 1991. Air quality. *Lewis Publishers, Boca Raton, New York.* 301.

Goforth, M. R. and Christoforou, C.S., 2006. Particle size distribution and atmospheric metals measurements in a rural area in the South Eastern USA. *The Science of the total environment*, 356(1-3), 217–27.

Goudie, A. S., Midelton, N.J., 2006. Saharan Dust: sources and trajectories. Trans. Inst. British Geography. 26, 165-181.

Grant, N. K., 1970. Geochemistry of Precambrian Rocks from Ibadan. Southwestern Nigeria. Earth and Planet Science. Lett. , 10, 29–38.

Gualtieri, M., Øvrevik, J., Holme, J. A., Perrone, M. G., Bolzacchini, E., Schwarze, P. E., Camatini, M., 2010. Differences in cytotoxicity versus pro-inflammatory potency of different PM fractions inhuman epithelial lung cells. *Toxicology in Vitro*, 24, 29–39.

Hales, S., Howden-Chapman, P., 2007. Effects of air pollution on health. *British Medical Journal*, 335, 314–315.

Hamilton, R. S. and Mansfield, T. A., 1993. The soiling of materials in the ambient atmosphere. *Atmospheric Environment*, 27, 1369–1374.

Hanel, G., 1976. Atmospheric Suspension and Relative Humidity. *Advance Geophysics*, 19,74–188.

Haywood, J. S. and Boucher, O., 2000. Estimate of the direct and indirect radiative forcing due to Tropospheric Aerosols. A Review. *Review of Geophysics*, 38, 513–543.

Hopkins, B., 1965. Forest and Savannah, Ibadan: Heinneman Publ., p. 38

Hubbard, F.H., 1975. Precambrian Crustal Development in Western Nigeria. *Geological Society of America Bulletin*, 86, 548–554.

IARC, 1997. IARC (International Agency for Research on Cancer) Silica, some silicates, coal dust and paraaramid fibrils. IARC Mongraphs on the Evaluation of Carcinogenic Risks to Humans. Lyon. 68

Ideriah, T. J. K., Braide, S. A., y F.G. and O.I., 2001. Determination of Indoor and Outdoor Concentrations of Suspended Particulate Matter in Southeastern Nigeria. *Ghana Journal of Science*, 41, 23–27.

Ikotun, O.O., Olafusi., O. S. and Bolarinwa, O. A., 2012. Influence of Human Activities on the Water Quality of Ogun River in Nigeria. *Civil and Environmental Research*, 2(9),.36–48.

Jibiri, N.N. & Bankole, O.S., 2006. Soil radioactivity and radiation absorbed dose rates at roadsides in high-traffic density areas in Ibadan metropolis, southwestern Nigeria. *Radiation Protection Dosimetry*, 118(4), pp.453–458.

Jickells, T.D., An, Z.S., Andersen, K.K., Baker, A.R., Bergametti, G., Brooks, N., Cao, J.J., Mahowald, N., Prospero, J.M., Ridgwell, A.J., Tegen, I., Torres, R., 2005. Global iron connections between desert dust, ocean biogeochemistry, and climate. *Science*, 308, 67–71.

Jomova, K., Valko, M., 2011. Advances in metal-induced oxidative stress and human disease. *Toxicology*, 283, 65–87.

Jones H.A. and Hockey R.D., 1964. The Geology of part of Southwestern Nigeria. Bull. Geol. Surv. Nig. p.101.

Jones, P., Charlson, R., Rodhe, H., 1995. *Aerosols in Climate Change 1994* J. T. et al. Houghton, ed., Cambridge University Press, New York.

Juneng, L. et al., 2009. Spatio-temporal characteristics of PM10 concentration across Malaysia. *Atmospheric Environment*, 43, 4584–4594.

Kalderon-Asael, B., Sandler, A., and Dayan., U., 2009. Mineralogical and chemical characterization of suspended atmospheric particles over the east Mediterranean based on synoptic-scale circulation patterns. *Atmospheric Environment*, 43, 3963–3970.

Kim, I.S., Lee, J.Y. & Kim, Y.P., 2013. Impact of polycyclic aromatic hydrocarbon (PAH) emissions from North Korea to the air quality in the Seoul Metropolitan Area, South Korea. *Atmospheric Environment*, 70, 159–165.

De Kok, T.M.C.M., Driece, H.A.L., Hogervorst, J.G.F., Briede, J.J., 2005. Toxicological assessment of ambient and traffic-related particulate matter: a review of recent studies. *Mutation Research*, 613, 103–122.

Krueger, B. J., Grassian, V. H., Cowin, J. P. and Laskin, A.
Krueger, B. J., Grassian, V. H., Cowin, J. P. and Laskin, A.
Krueger, B. J., Grassian, V. H., Cowin, J. P. and Laskin, A.
Krueger, B. J., Grassian, V. H., Cowin, J. P. and Laskin, A., 2004. Heterogeneous chemistry of individual mineral dust particles from different dust source regions: the importance of particle mineralogy. *Atmospheric Environment*, 38(36), 6253–6261.

Lack, D. A., 2003. Modelling the Formation of Atmospheric Aerosol from Gaseous Organic Precursors. Ph.D Thesis (unpublished), School of Natural Resources Sciences, Queensland University of Technology. p. 277.

Larney, F. J., Leys, J. F., Muller, J. F., McTainsh, G. H., 1999. Dust and endosulfan deposition in cotton-growing area of Northern New South Wales, Australia. *Australia. J. Environ. Qual.*, 28, 692–701.

Larssen, T., Carmichael, G. R., 2000. Acid rain and acidification in China: the importance of base cation deposition. *Environmental Pollution*, 10, pp.89–102.

Lawrence, C. R., Neff, J. C., 2009. The contemporary physical and chemical flux of aeolian dust: a synthesis of direct measurements of dust deposition. *Chemical Geology*, 267, pp.46–63.

Li, X. Y., Gilmour, P. S., Donaldson, K., & MacNee, W., 1997. In vivo and in vitro proinflammatory effects of particulate air pollution (PM10). *Environmental Health Perspectives*, 105, pp.1279–1283.

Lioy, P. J., Freeman, N.C.G., Millette, J. R., 2002. Dust: a metric for use in residential and building exposure assessment and source characterization. *Environmental Health Perspective.*, 110, pp.969–983.

Liu, J., 2005. Comparison of surface radiative flux data sets over the Arctic Ocean. *Journal of Geophysical Research*, 110(C2), p.C02015.

Liu, X., Zhu, J., Espen, P. V., Adams, F. and Xiao, Rui., 2005. Single particle characterization of spring and summer aerosols in Beijing : Formation of composite sulfate of calcium and potassium. , 39, pp.6909–6918.

Lodovici, M., Bigagli, E., 2011. Oxidative stress and air pollution exposure. *Toxicology*. 38, 102- 114.

Lonkar, P., Dedon, P.C., 2011. Reactive species and DNA damage in chronic inflammation: reconciling chemical mechanisms and biological fates. *International Journal of Cancer*, 128, pp.1999–2009.

Lu, S., Luan, Q., Jiao, Z., Wu, M., Li, Z., Shao, L. and Wang, F., 2007. Mineralogy of Inhalable Particulate Matter (PM10) in the Atmosphere of Beijing, China. *Water, Air, and Soil Pollution*, 186(1-4), pp.129–137. Available at: http://link.springer.com/10.1007/s11270-007-9470-5 [Accessed September 19, 2013].

Lu, S., Luan, Q. & Jiao, Z., 2007. Mineralogy of Inhalable Particulate Matter (PM 10) in the Atmosphere of Beijing , China. , 10, pp.129–137.

Ma, J. Z., Wang, W., Chen, Y., Liu, H. J., Yan, P., Ding, G. A., Wang, M. L., Sun, J. and Lelieveld, J., 2012. The IPAC-NC field campaign: a pollution and oxidization pool in the lower atmosphere over Huabei, China. *Atmospheric Chemistry and Physics*, 12(9), pp.3883–3908.

Massey, D. D., Kulshrestha, A. and Taneja, A., 2013. Particulate matter concentrations and their related metal toxicity in rural residential environment of semi-arid region of India. *Atmospheric Environment*, 67, pp.278–286.

Mathias-Maser, S., 1998. Primary Biological Aerosol Particles: Their Significance, Sources, Sampling Methods and Size Distribution in the Atmosphere. *Atmospheric Environment*. 23, 349-365

McTainsh, G. H., 1980. Harmattan dust deposition in northern Nigeria. *Nature*, 286, pp.587–8.

McTainsh G. H., Nickling W. G., Lynch, A., 1997. Dust deposition and particle size in Mali, West Africa. *Catena*, 29, 307–22.

Mishra, S. K., Tripathi, S. N., 2008. Modeling optical properties of mineral dust over the Indian Desert. *Journal of Geophysical Research*, 113, p.D23201.

Muhs, D. R., Benedict, J. B., 2008. Eolian additions to late quaternary alpine soils, Indian Peaks Wilderness Area, Colorado Front Range. *Antarctic and Alpine Research*, 38, 120–130.

Nazaroff, W. W. and Cass, G.R., 1991. Protecting museum collections from soiling due to the deposition of airborne particles. *Atmospheric Environment*, 25A, pp.841–852.

Obaje, N. G., 2009. *Geology and Mineral Resources of Nigeria.* Edited by Bhattacharji et al., Springers London. p.219

Odewande, A.A. & Abimbola, A.F., 2008. Contamination indices and heavy metal concentrations in urban soil of Ibadan metropolis, southwestern Nigeria. *Environmental Geochemistry and Health*, 30(3), pp.243–54.

Okunlola, O.A., Adeigbe, O.C. & Oluwatoke, O.O., 2009. Compositional and petrogenetic features of schistose rocks of Ibadan Area , Southwestern Nigeria. *Earth Sciences Research Journal*, 13(2), pp.119–133.

Okuo, J. M. and Ndiokwere, C.L., 2006. Elemental Concentration of Total Suspended Particulate Matter in Relation to Air Pollution in the Niger Delta of Nigeria: A case Study of Warri. *Trends in Applied Sciences Research*, 1(1), pp.91–96.

Olade, M. A. and Elueze, A.A., 1979. Petrochemistry of the Ilesha amphibolites and Precambrian crustal evolution in the Pan-African domain of S.W. Nigeria. *Precambrian Research*, 8, p.303 318.

Olatunji S. O., Akinsoji, O., 2013. Assessment of Air Quality and Noise around some Telecommunication Base Transceiver Stations In Ibadan SW. International Journal of Engineering Research and Application, 3, 1041–1048.

Olatunji, A. S., Abimbola, A. F., Fadina, O and Kolawole, T., 2010. Evaluation of the Metal Content of Outdoor and Indoor Particulate Matter within the University of Ibadan, Nigeria. *Journal of Science Research*, 9, 52–61.

Olayinka, A.I., Abimbola, A. F. Isibor, R. A. and Rafiu A. R., 1999. A geoelectrical-hydrogeochemical investigation of shallow groundwater occurrence in Ibadan, southwestern Nigeria. *Environmental Geology*, 37(1-2), pp.31–39. Available at: http://link.springer.com/10.1007/s002540050357.

Olayinka, A.I., 1992. Geophysical siting of boreholes in crystalline basement areas of Africa. *Journal of African Earth Sciences*, 14, 197–207.

Oluwole, O., Otaniyi, O. O., Ana, G. A. Olopade, C. O., 2012. Indoor air pollution from biomass fuels: a major health hazard in developing countries. *Journal of Public Health*, 20(6), 565–575.

Oluyemi E. A.; Asubiojo, 2001. Ambient Air Particulate Matter in Lagos, Nigeria. *Chemical Society of Ethopia*, 15(2), 97–108.

Onianwa, P. C., 2001. Monitoring atmospheric metal pollution: a review of the use of mosses as indicators. *Environmental monitoring and assessment*, 71(1), pp.13–50.

Osibanjo, O., Daso, A. P. and Gbadebo, A. M., 2011. The impact of industries on surface water quality of River Ona and River Alaro in Oluyole Industrial Estate, Ibadan , Nigeria. *African Journal of Biotechnology,* 10(4), 696–702.

Osornio-Vargas, A. R., Serrano, J., Rojas-Bracho, L., Miranda, J., Garcı´a-Cuellar, C., Reyna, M. A., Flores, G., Zuk, M., Quintero, M., Vazquez, I., Sa´nchez-Pe´rez, Y., Lo´pez, T., Rosas, I., 2011. In vitro biological effects of airborne PM2.5 and PM10 from a semi-desert city on the Mexico–US border. *Chemosphere*, 83, 618–626.

Oversby, V.M., 1975. Lead Isotopic study of aplitic from the Precambrian Basement rocks near Ibadan southwest Nigeria, Earth Planet Sci, lett. , 177–180.

Owoade, O. K., Olise, F. S., Obioh, I. B., Olaniyi, H. B., Ferrero, L. and Bolzacchini, E., 2009. EDXRF elemental assay of airborne particulates : A case study of an iron and steel smelting industry , Lagos , Nigeria. *Scientific Research and Essay*, 4(11), 1342–1347.

Oyawoye, M. O. 1972. The Basement Complex of Nigeria. In: African geology, Dessauvagie T. F. J, Whiteman A. J. (eds). Ibadan University Press, 66–102

Pandis, S. N., Harley, R. A. and Seinfeld, J.H., 1992. Secondary Organic Aerosol Formation and Transport. *Atmospheric Environment*, 26, 2269–2282.

Peacock, J.L., Anderson, H.R., Bremner, S.A., Marston, L., Seemungal, T.A., Strachan, D.P., Wedzicha, J.A., 2011. Outdoor air pollution and respiratory health in patientswith COPD. *Thorax*, 66, 591–596.

Penner, J. E., Eddleman, H. and Novakov, T., 1993. Towards the Development of Global Inventory for Black Carbon Emission. *Atmospheric Environment*, 27, 1227–1295.

Pope III, C. A., Burnett, R. T., Thurston, G. D., Thun, M. J., Calle, E. E., Krewski, D., 2004. Cardiovascular mortality and long-term exposure to particulate air pollution: Epidemiological evidence of general pathophysiological pathways of disease. *Circulation*, 109, pp.71–77.

Pope III, C.A., Burnett, R.T., Krewski, D., Jerrett, M., Shi, Y., Calle, E.E., Thun, M.J., 2009. Cardiovascular mortality and exposure to airborne fine particulate matter and cigarette smoke: shape of the exposure response relationship. *Circulation*, 120, pp.941–948.

Pope, C., Dockery D., S.J. and R.M., 2009. Respiratory Health and PM10 Pollution. *American Review of Respiratory Disease*, 144, pp.668–674.

Pósfai, M., Axisa, D., Tompa, É., Freney, E., Bruintjes, R., and Buseck, P. R., 2013.

Interactions of mineral dust with pollution and clouds: An individual-particle TEM study of atmospheric aerosol from Saudi Arabia. *Atmospheric Research*, 122, pp.347–361.

Prospero, M., 1999. Long-term measurements of the transport of African mineral dust to the southeastern United States : Implications for regional air quality are also observed. *Journal of Geophysical Research*, 104, pp.15,917–15927.

Pye, K., 1987. Aeolian Dust and Dust Deposits. London Academic Press. p.334.

Quintana, R., Serrano, J., Go´mez, V., deFoy, B., Miranda, J., Garcia-Cuellar, C., Vega, E., 2011. The oxidative potential and biological effects induced by PM10 obtained in Mexico City and at a receptor site during the MILAGRO Campaign. *Environmental Pollution*, 159, pp.3446–3454.

Raaschou-Nielsen, O., Andersen, Z., Hvidberg, M., Jensen, S. S., Ketzel, M., Sørensen, M., Loft, S., Overvad, K., Tjønneland, A., 2011. Lung Cancer Incidence and Long- Term Exposure to Air Pollution from Traffic. Environ. *Environmental Health Perspectives*, 19, 860–865.

Rahaman, M. A., 1988. Recent Advances in the study of the Basement Complex of Nigeria in: Precambrian Geology of Nigeria, edited by P.O. Oluyole. A publication of the Geological survey of Nigeria., 11–44.

Rahaman, M. A., 1976. Review of the Basement Geology of Southwestern Nigeria. In C. A. Kogbe, ed. *Geology of Nigeria*. Elizabethan Publishing, Lagos, pp. 41–58.

Rahaman, M. A. and Ocan, O. O., 1978. On relationships in the Precambrian Migmatite-gneisses of Nigeria. *Nigerian Journal of Mining and Geology*, 15, pp.23–32.

Rahaman, M. A. and Lancelot, J. R., 1984. Continental Crust Evolution in SW Nigeria: Constraint from from U/Pb dating of pre-Pan-African Gneisses. In *Rapport d' activite 1980-1984*. Documents et Travaux du Centre Geologique et Geophysique de Montpellier, p. 41.

Rashki, A., Eriksson, P. G., Rautenbach, C. J., De W., Kaskaoutis, D. G., Grote, W. and Dykstra, J., 2013. Assessment of chemical and mineralogical characteristics of airborne dust in the Sistan region, Iran. *Chemosphere*, 90(2), pp.227–36.

Reid, E. A., 2003. Characterization of African dust transported to Puerto Rico by individual particle and size segregated bulk analysis. *Journal of Geophysical Research*, 108(D19), p.8591.

Reid, J. S., 2003. Comparison of size and morphological measurements of coarse mode dust particles from Africa. *Journal of Geophysical Research*, 108(D19), p.8593.

Resch F, Sunnu A, A., 2007. Saharan dust flux and deposition rate near the Gulf of Guinea. *Tellus*, 60, pp.98–105.

Richards, R., 2003. What effects do mineral particles have in the lung? *Mineralogical Magazine*, 67(2), pp.129–139.

Rizzo, M. and Scheff, P., 2007. Fine particulate source apportionment using data from the USEPA speciation trends network in Chicago, Illinois: Comparison of two source apportionment models. *Atmospheric Environment*, 41(29), pp.6276–6288. Available at: http://linkinghub.elsevier.com/retrieve/pii/S1352231007003287 [Accessed November 9, 2013].

Rosenfeld, D., Lohmann, U., Raga, G.B., O'Dowd, C.D., Kulmala, M., Fuzzi, S., R. & Andreae, M. O., 2008. Flood or drought: how do aerosols affect precipitation? *Science*, 321, p.1301.

Rosler I. J. and Lange H., 1976. Geochemische Tabellen, Stuttgart: Ferdinand Enke Verlag Stuttgart. p. 420-457

Rusconi, F., Catelan, D., Accetta, G., Peluso, M., Pistelli, R., Barbone, F., Di Felice, E., Munnia, A., Murgia, P., Paladini, L., Serci, A., Biggeri, A., 2011. Asthma symptoms, lung function, and markers of oxidative stress and inflammation in children exposed to oil refinery pollution. *Journal of Asthma*, 48, pp.84–90.

Samet, J. M., Dominici, F., Curriero, F. C., Coursac, I., Zeger, S. L., 2000. Fine particulate air pollution and mortality in 20 US Cities, 1987-1994. *New England Journal of Medicine*, 343(24), pp.1742–1749.

Saud, T. et al., 2013. Spatial variation of chemical constituents from the burning of commonly used biomass fuels in rural areas of the Indo-Gangetic Plain (IGP), India. *Atmospheric Environment*, 71, pp.158–169.

Seinfeld, J.H., Pandis, S.N., 2006. *Atmospheric Chemistry and Physics: from Air Pollution to Climate Change.* Second. John Wiley, ed., New York. p. 840

Serrano, E., Beceiro, E., López, P., & Prada, D., 1996. Heavy metals determination in atmospheric particulate matter of La Coruña. *Quimica Analitica*, 15, pp.38–44.

Sharma, P., Sharma, P., Jain, S. and Kumar, P., 2013. An integrated statistical approach for evaluating the exceedence of criteria pollutants in the ambient air of megacity Delhi. *Atmospheric Environment*, 70, pp.7–17.

Slinn, S.A. and S.W.G.N., 1981. Prediction for Particle Deposition on Natural Waters. *Atmospheric Environment*, 15, pp.2377–2393.

Smyth, A. M., Thompson, S. L., de Foy, B., Olson, M. R. Sager, N., McGinnis, J., Schauer, J. J. Gross, D. S., 2013. Sources of metals and bromine-containing particles in Milwaukee. *Atmospheric Environment*, 73, 124–130.

Smyth, A. J., Montgomerry, R.F., 1962. *Soils and Land use in Central Western Nigeria*, Ibadan: Government Printer.

Sokolik, I. N. and Toon, O. B., 1999. Incorporation of mineralogical composition into models of the radiative properties of mineral aerosol from UV to IR wavelengths. *Journal of Geophysical Research*, 104, 9423-9444.

Sonibare, J. A. and Jimoda, L.A., 2009. Critical Air Pollutants from some Anthropogenic Combustion Processes in Lagos. *Nigeria Energy Sources*, 31, pp.1–13.

Stern. A. C. Boubel, R. W. and Turner, D.B., 1984. Fundamental of Air Pollution, Second Edition Second.,

Sunnu, A. Afeti, G. and Resch, F., 2008. A Longtime of Experimental Studies of the Saharan Dust Presence in West Africa. *Atmospheric Research*, 87, 13–26.

Tijani, M. N., Okunlola, O. a. & Abimbola, A.F., 2006. Lithogenic concentrations of trace metals in soils and saprolites over crystalline basement rocks: A case study from SW Nigeria. *Journal of African Earth Sciences*, 46(5), 427–438.

Toledo, V. E., 2008. Evaluation of levels , sources and distribution of toxic elements in PM10 in a suburban industrial region , Rio de Janeiro , Brazil., 49–59.

Wang, X., Wang, W., Yang, L., Gao, X., 2012. The secondary formation of inorganic aerosols in the droplet mode through heterogeneous aqueous reactions under haze conditions. *Atmospheric Environment*, 63, 68–76.

Wang, Y., Zhuang, G., Sun, Y., An, Z., 2006. The variation of characteristics and formation mechanisms of aerosols in dust , haze , and clear days in Beijing. *Atmospheric Environment*, 40, 6579–6591.

Watt, J., Jarrett, D. and Hamilton, R., 2008. Dose-response functions for the soiling of heritage materials due to air pollution exposure. *The Science of the total environment*, 400(1-3), pp.415–24. Available at: http://www.ncbi.nlm.nih.gov/pubmed/18774161 [Accessed December 23, 2014].

Whitby, K. T., 1978. The physical characteristics of sulphur aerosols. *Atmospheric Environment*, 12, pp.135–308.

WHO, 2002. Quantifying Selected Major Risks to Health. In: The World Health Report 2002-Reducing Risks, Promoting Healthy Life,.

WHO, 2000. WHO air quality guidelines. Regional Office for Europe, Copenhagen, Denmark.

Wilke, B.M. & Duke, B.J., 1984. Mineralogy and chemistry of Harmattan Dust in Northern Nigeria. *Catena*, 11, pp.91–96.

Wolf, M. E. and Hidy, G.M., 1997. Aerosol and Climate: Anthropogenic Emissions and Trend for 50 years. *Journal of Geophysical Research*, 102, pp.11113–11121.

Wood, W.W., Sanford, W.E., 1995. Eolian transport, saline lake basins and groundwater solutes. *Water Resources Research*, 31, pp.3121–3129.

Wright, J.B., 1985. *Geology and mineral resources ofWest Africa.*, London: George Allen & Unwin.

Xi, X. & Sokolik, I.N., 2012. Impact of Asian Dust Aerosol and Surface Albedo on Photosynthetically Active Radiation and Surface Radiative Balance in Dryland Ecosystems. , ID 276207, p.15.

Xie, R.K. et al., 2009. Characterization of individual airborne particles in Taiyuan City, China. *Air quality, atmosphere, & health*, 2(3), pp.123–131.

Xie, R.K. et al., 2005. Chemical characterization of individual particles (PM10) from ambient air in Guiyang City, China. *The Science of the total environment*, 343(1-3), pp.261–72. Available at: http://www.ncbi.nlm.nih.gov/pubmed/15862850 [Accessed September 11, 2013].

Yang, X.P., Zhu, B.Q., White, P.D., 2007. Provenance of aeolian sediment in the Taklamakan Desert of western China, inferred from REE and major-elemental data. *quant. int.*, 175, pp.71–85.

Zhang, C., Qiao, Q. & Piper, J.D.A., 2011. Assessment of heavy metal pollution from a Fe-smelting plant in urban river sediments using environmental magnetic and geochemical methods. *Environmental Pollution*, 159(10), pp.3057–3070.

Zhang, D. D., Peart, M. & Jim, C. Y., 2003. Precipitation chemistry of Lhasa and other remote towns , Tibet. *Atmospheric Environment*, 37, pp.231–240.

Ziech, D., Franco, R., Pappa, A., Panayiotidis, M. I., 2011. Reactive Oxygen Species (ROS)-induced genetic and epigenetic alterations in human carcinogenesis. *Mutation Research*, 711, pp.167–177.

Zufall, M. J. and Davidson, C. I., 1997. Dry deposition of particles to water surfaces. *a*, 32, pp.1623–1630.

APPENDIX I
XRD RESULTS OF ROCKS, SOILS AND DEPOSITED DUST

APPENDIX 1A

Tes

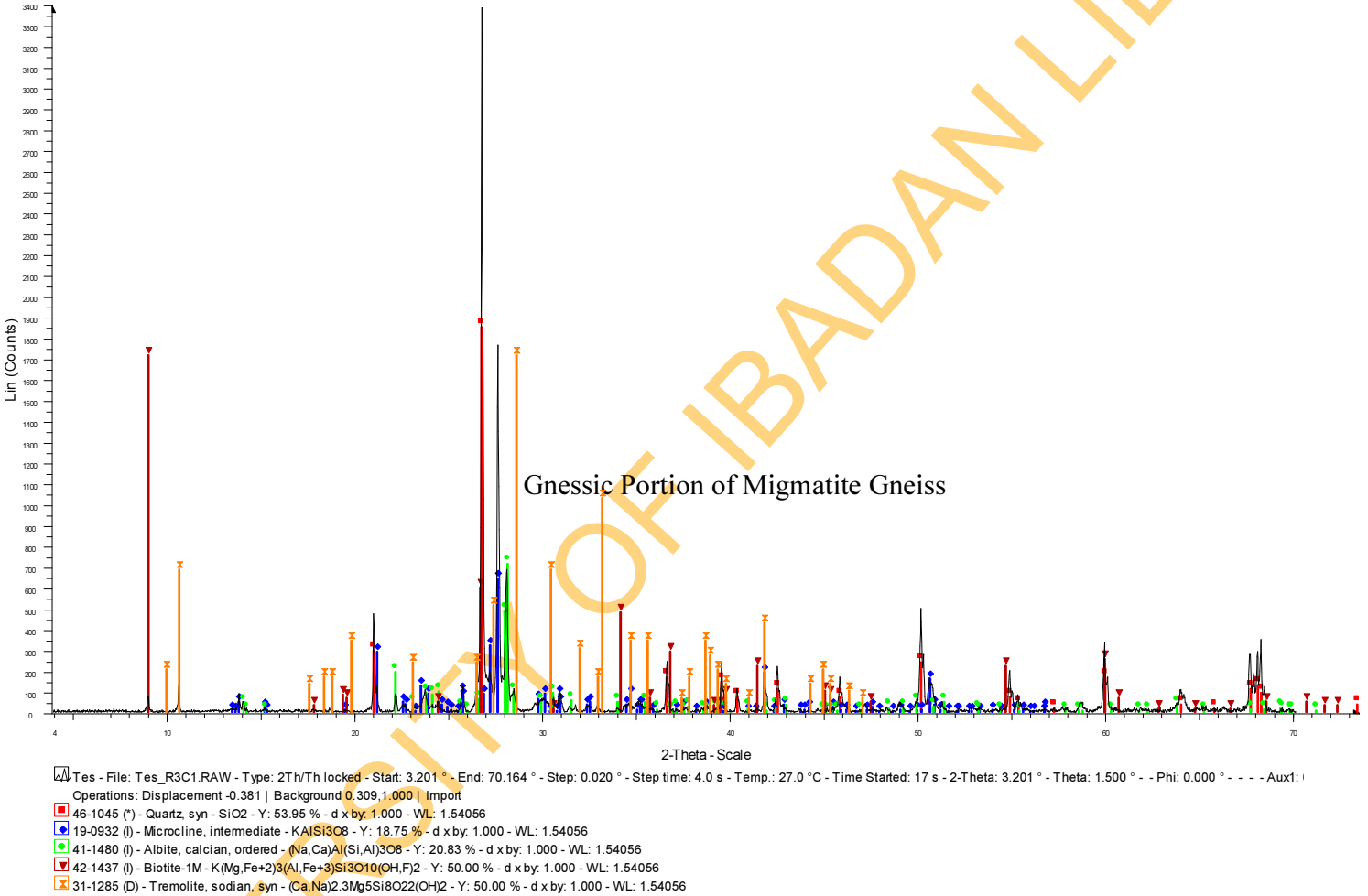

R1A

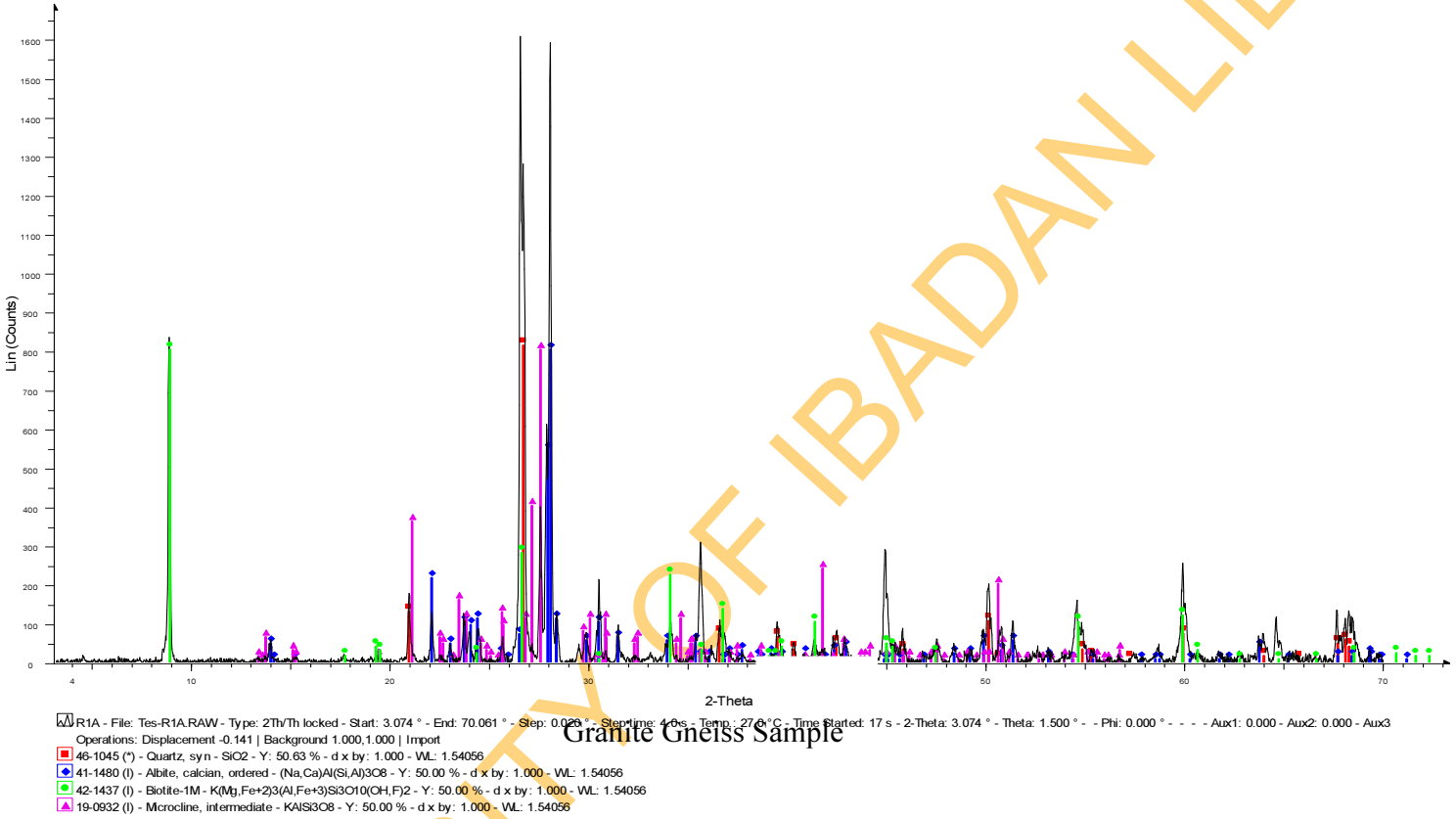

Granite Gneiss Sample

R2A

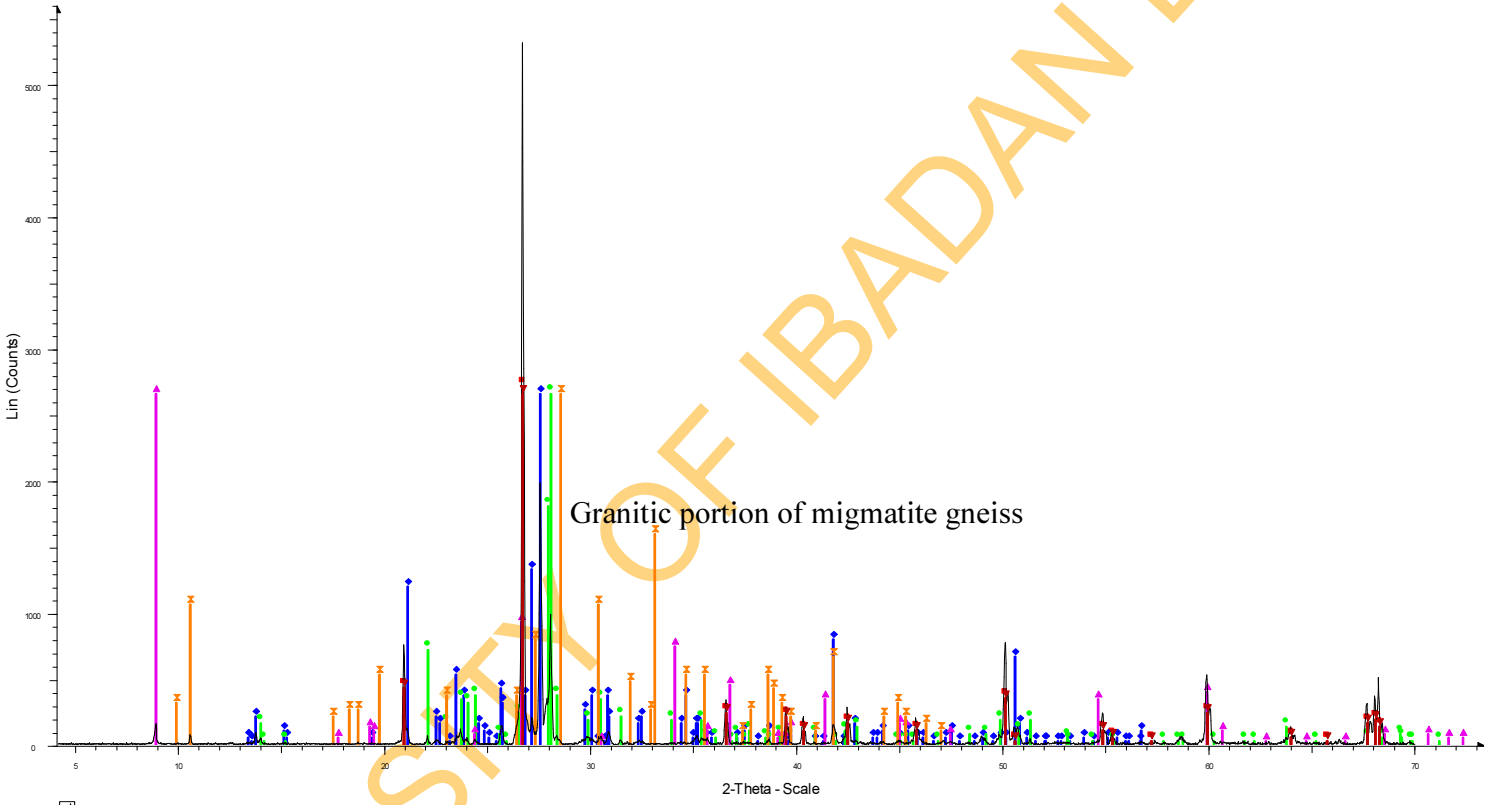

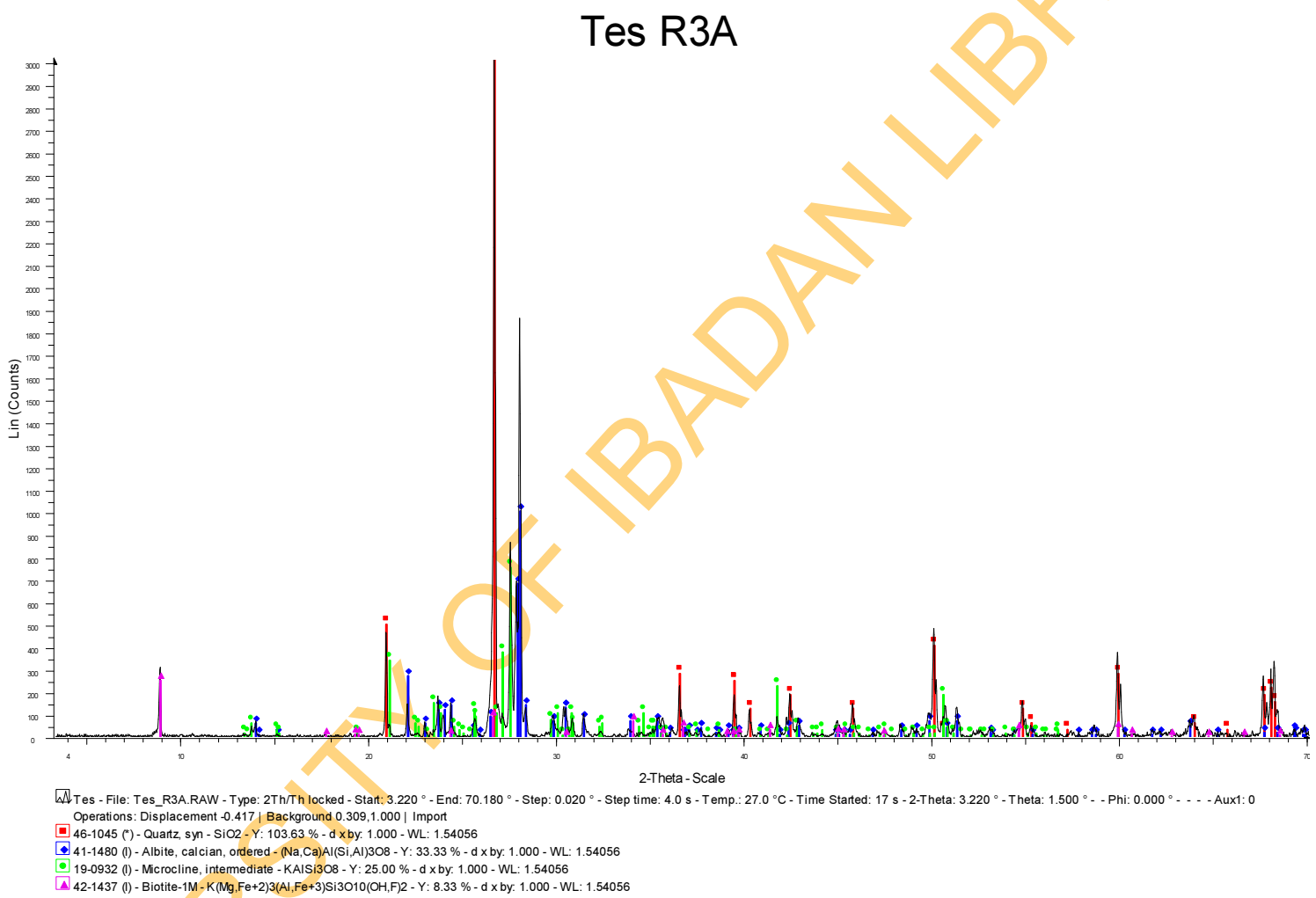

anite

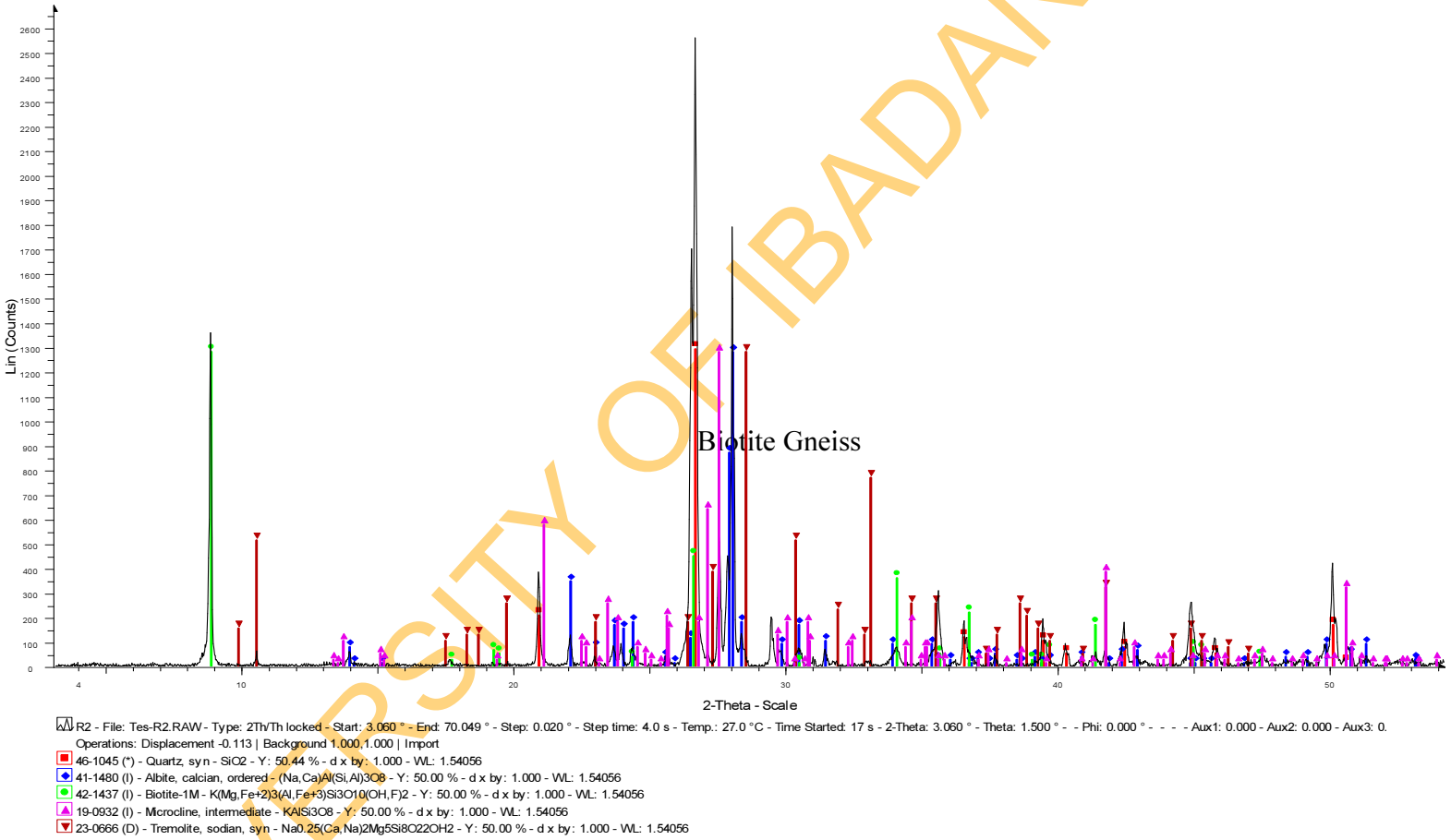

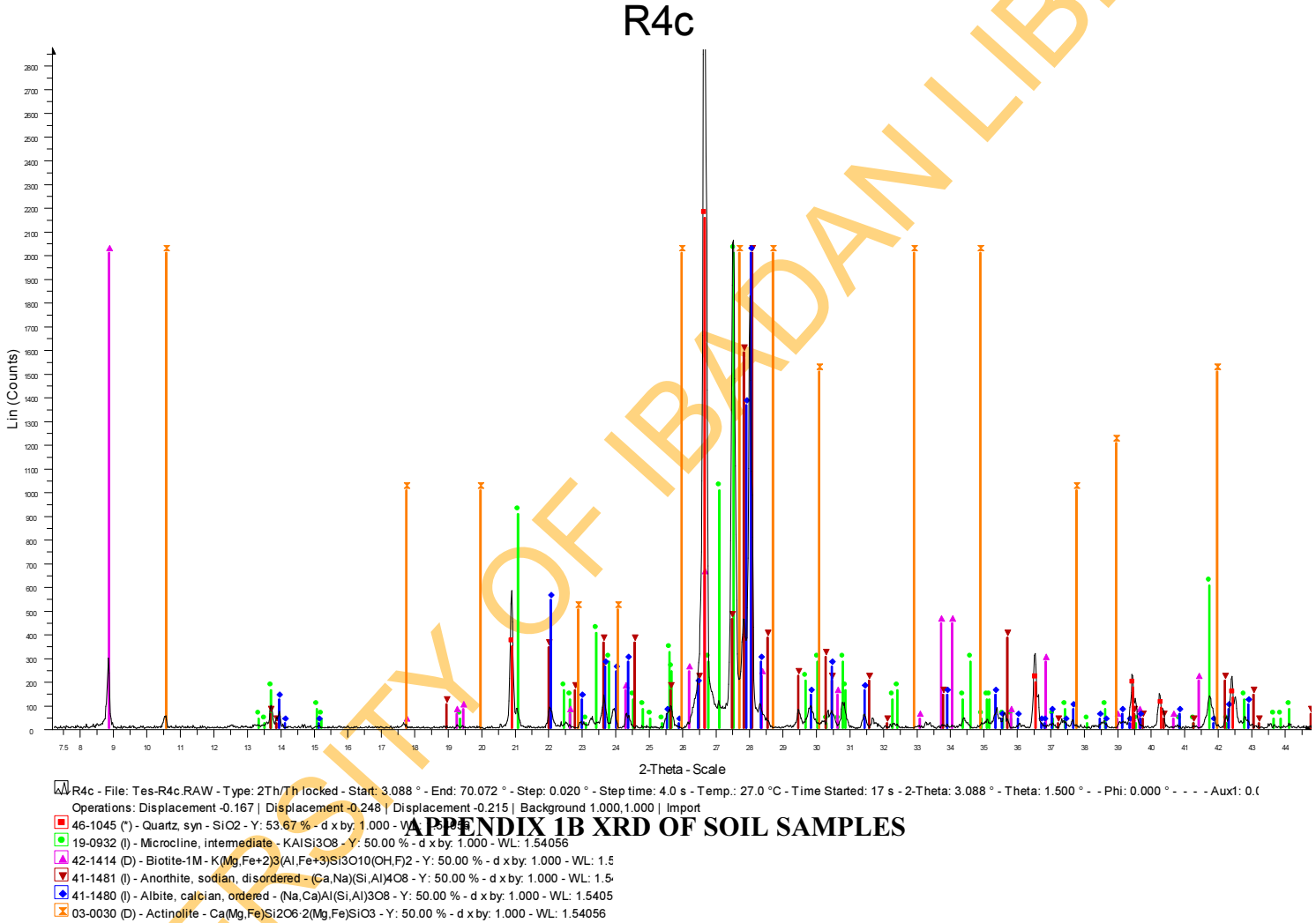

APPENDIX 1B XRD OF SOIL SAMPLES

S049

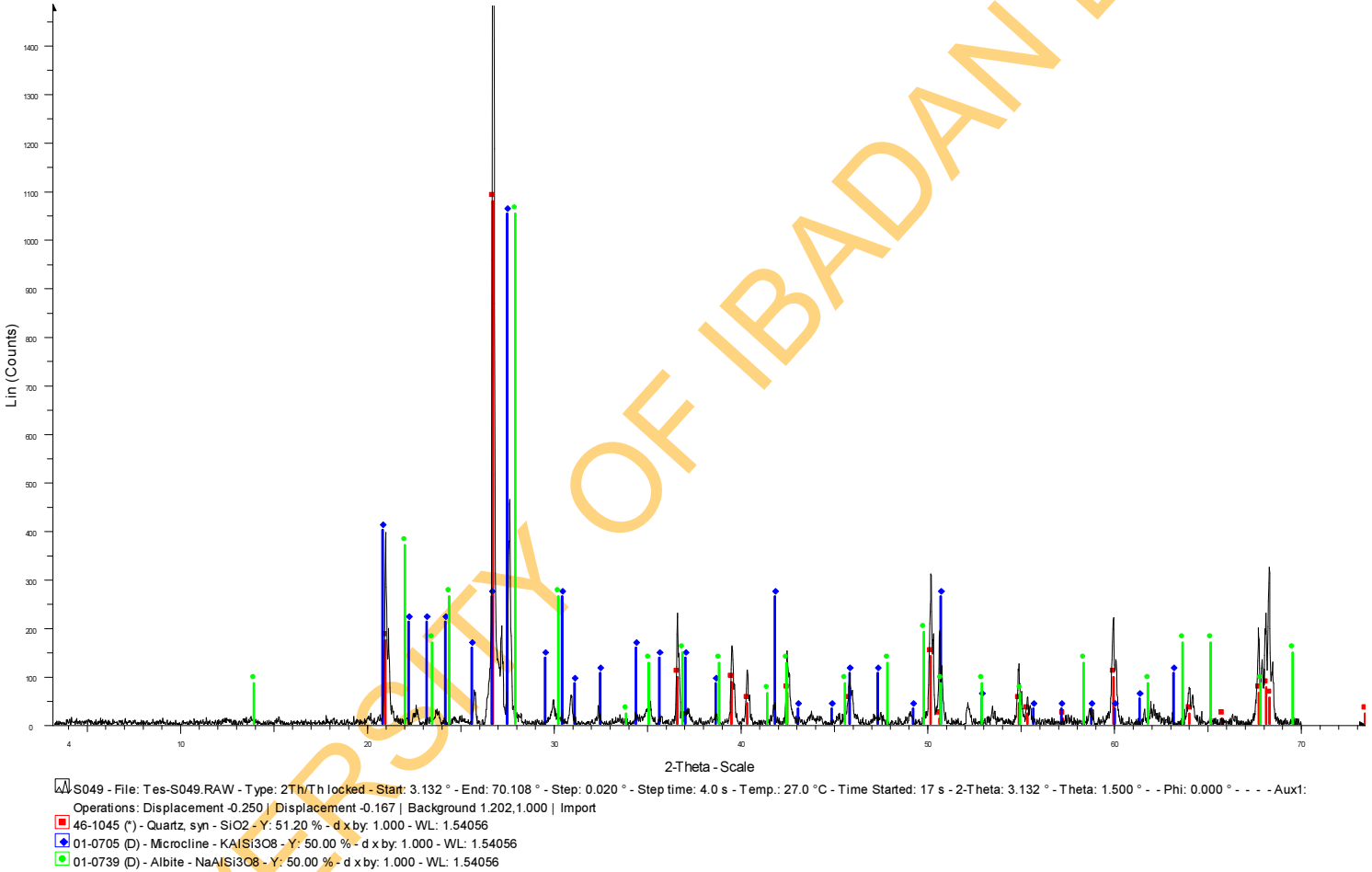

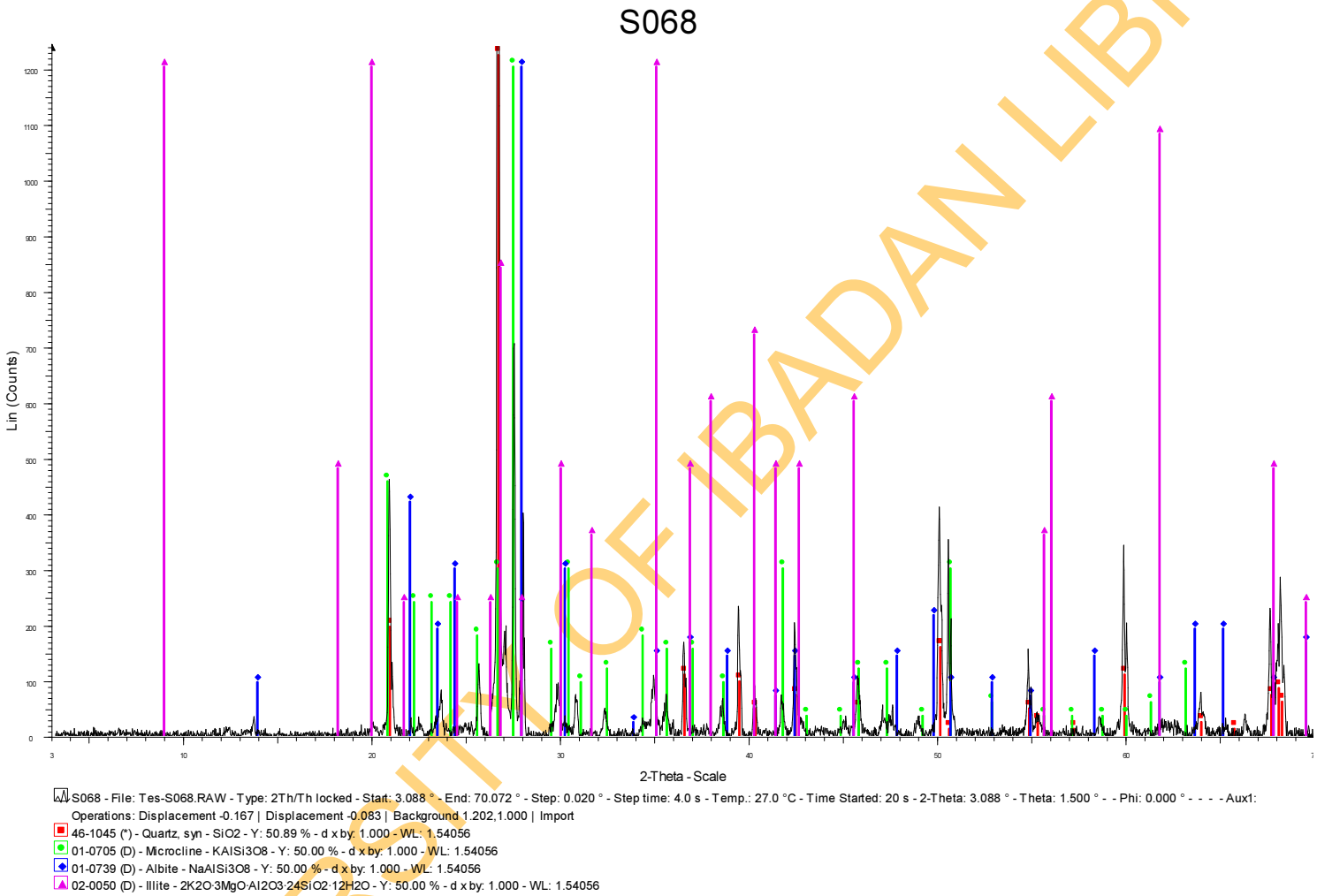

S095

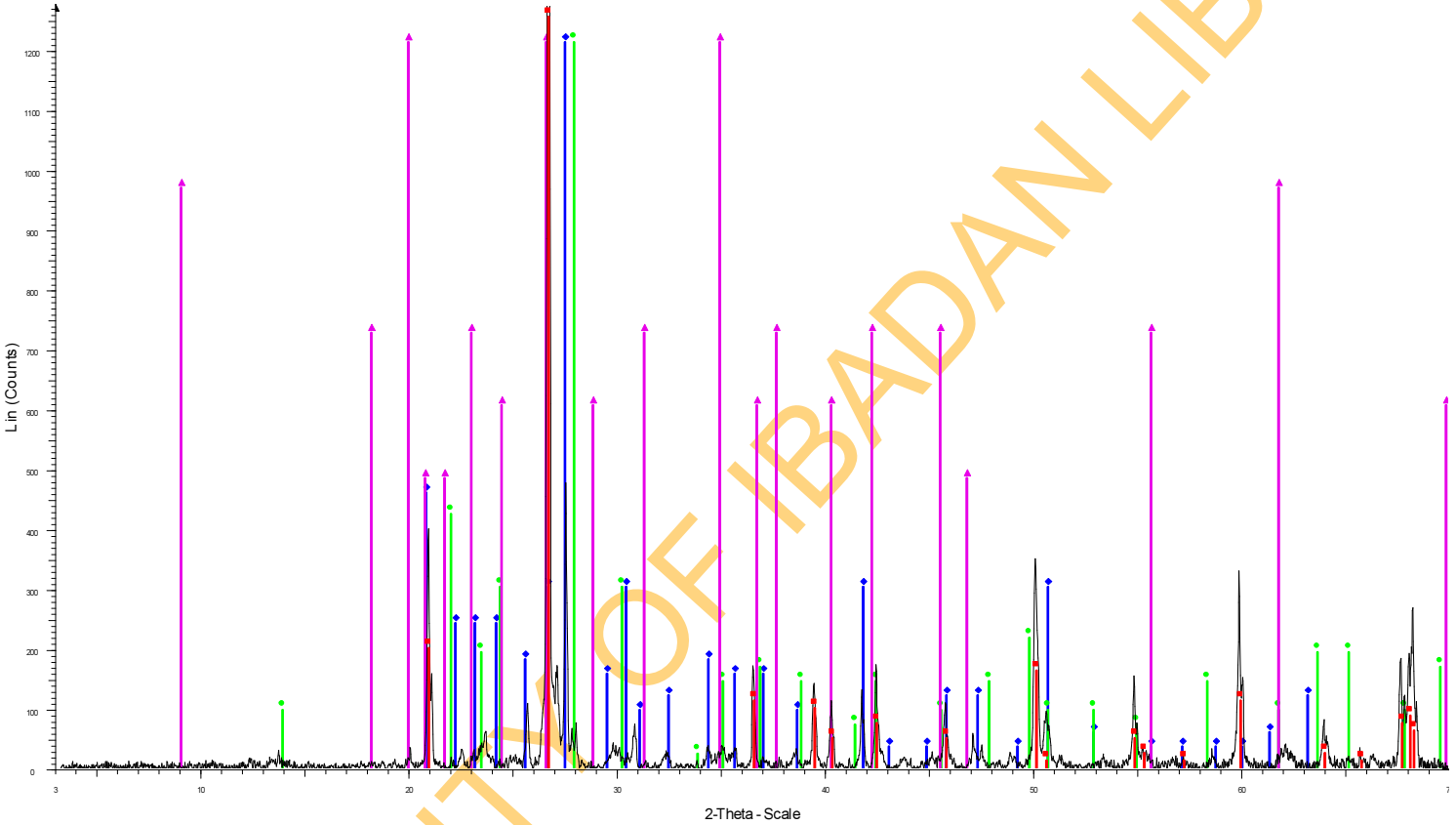

S118

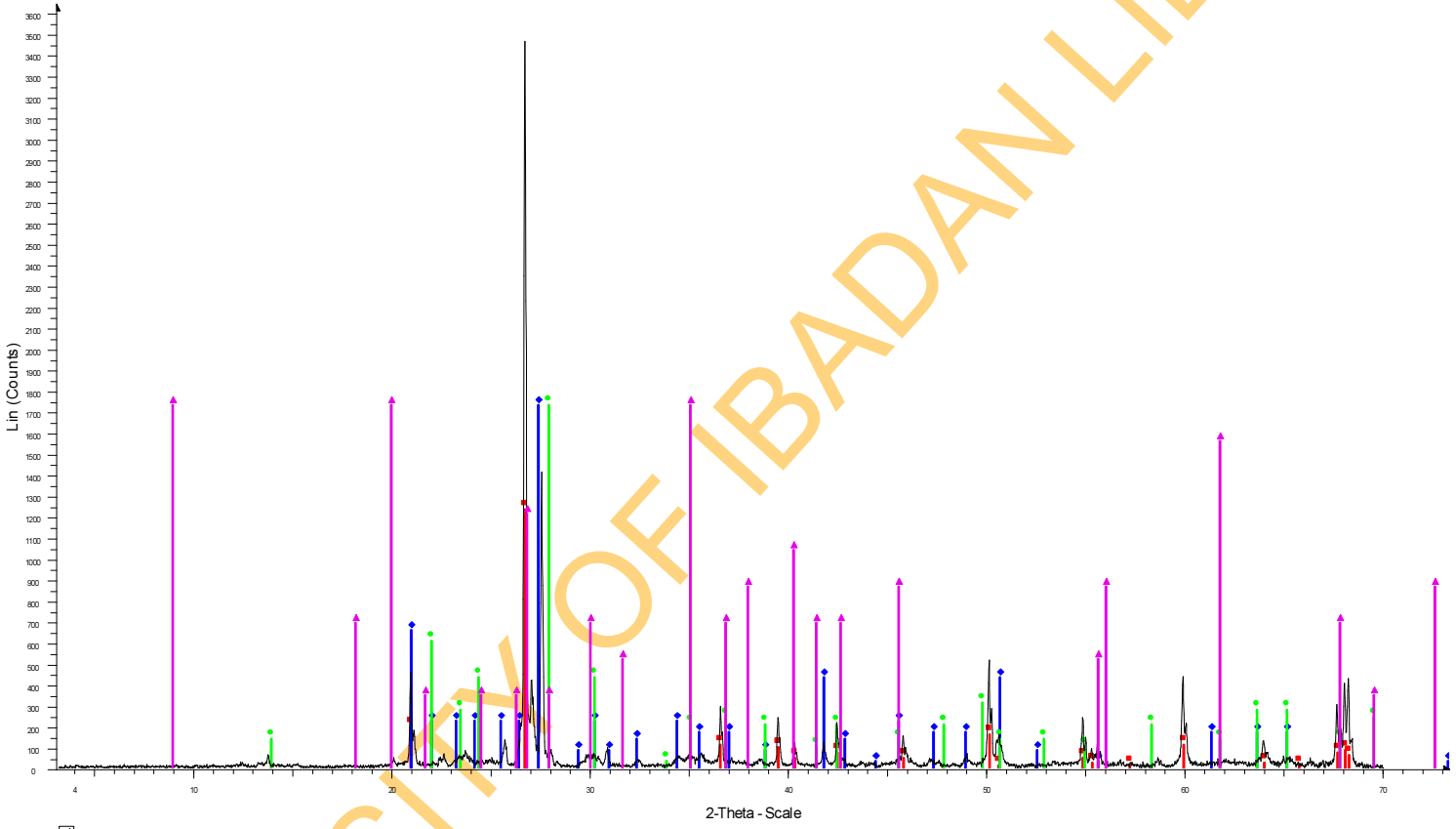

S129

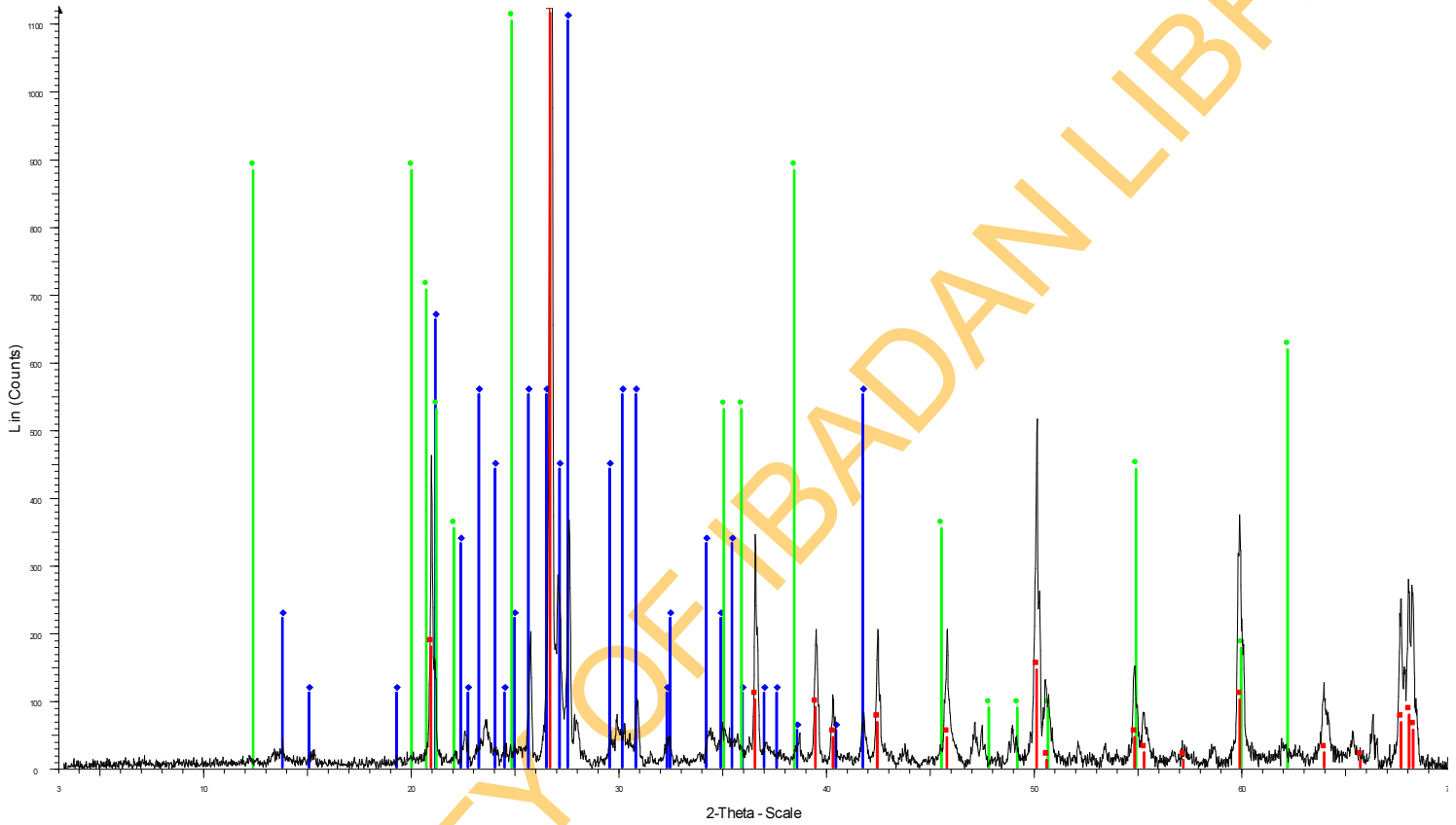

S132

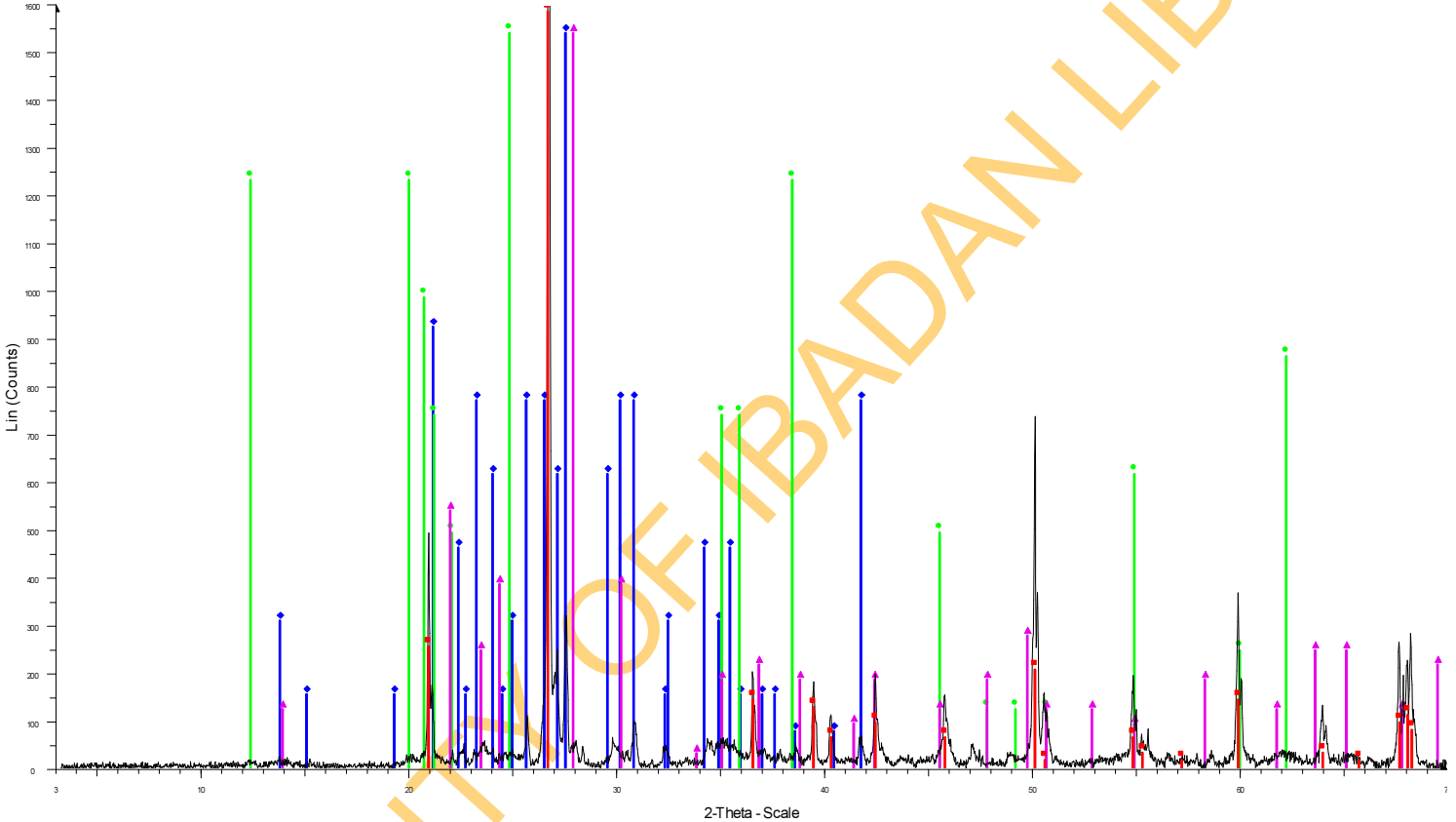

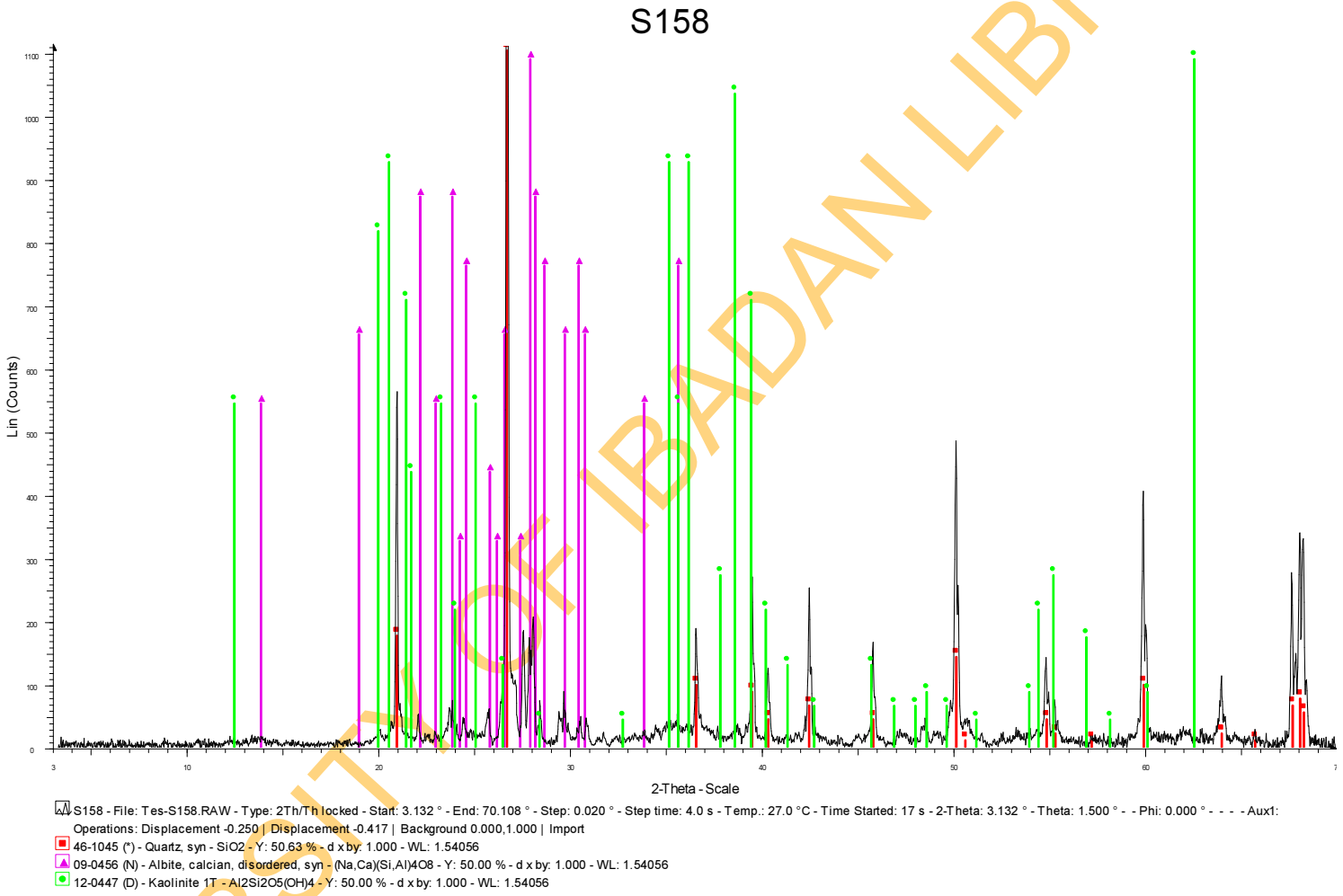

APPENDIX 1C XRD OF DEPOSITED DUST

XRD of Deposited Dust

PM10 olu.

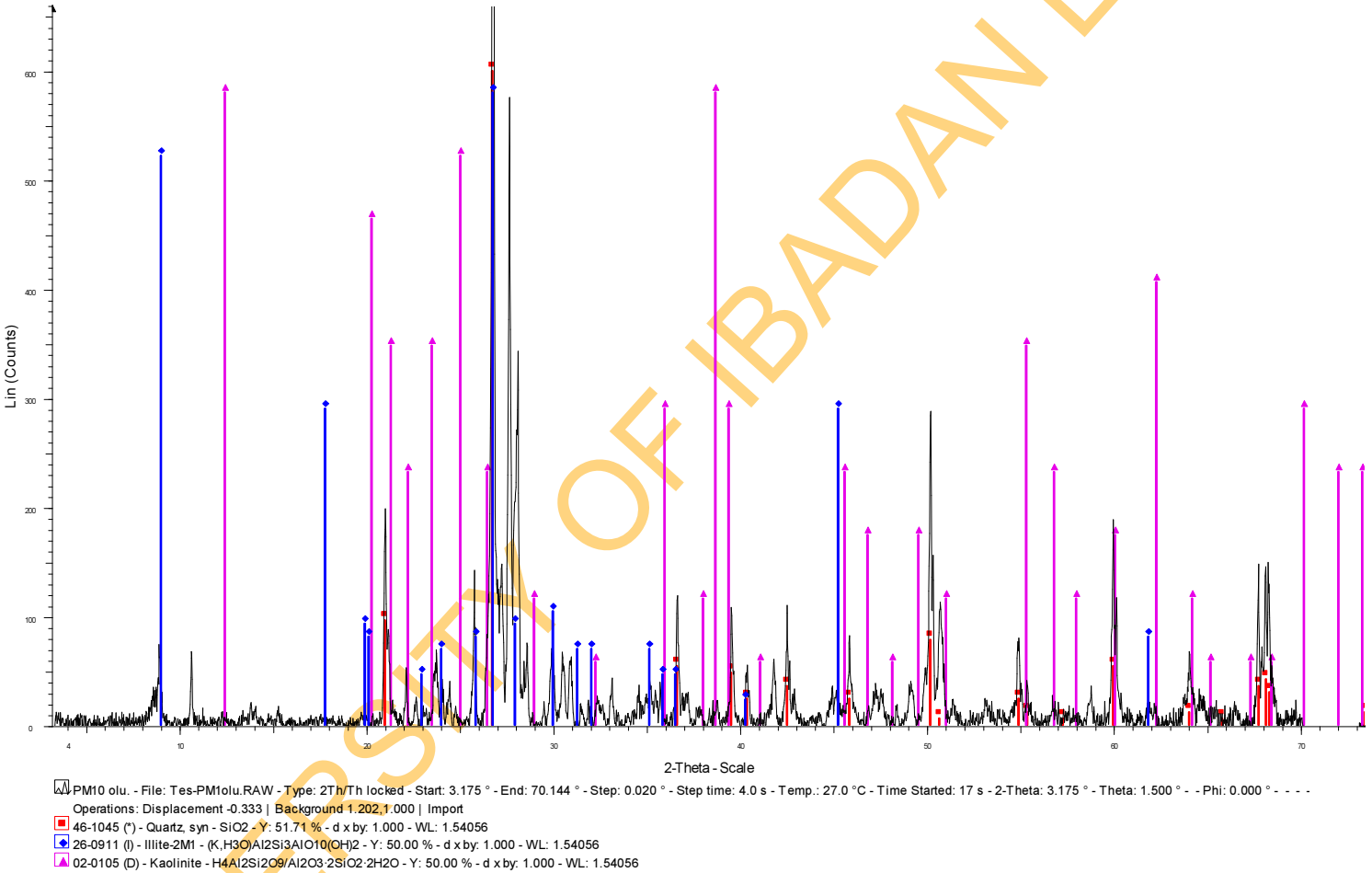

PM2

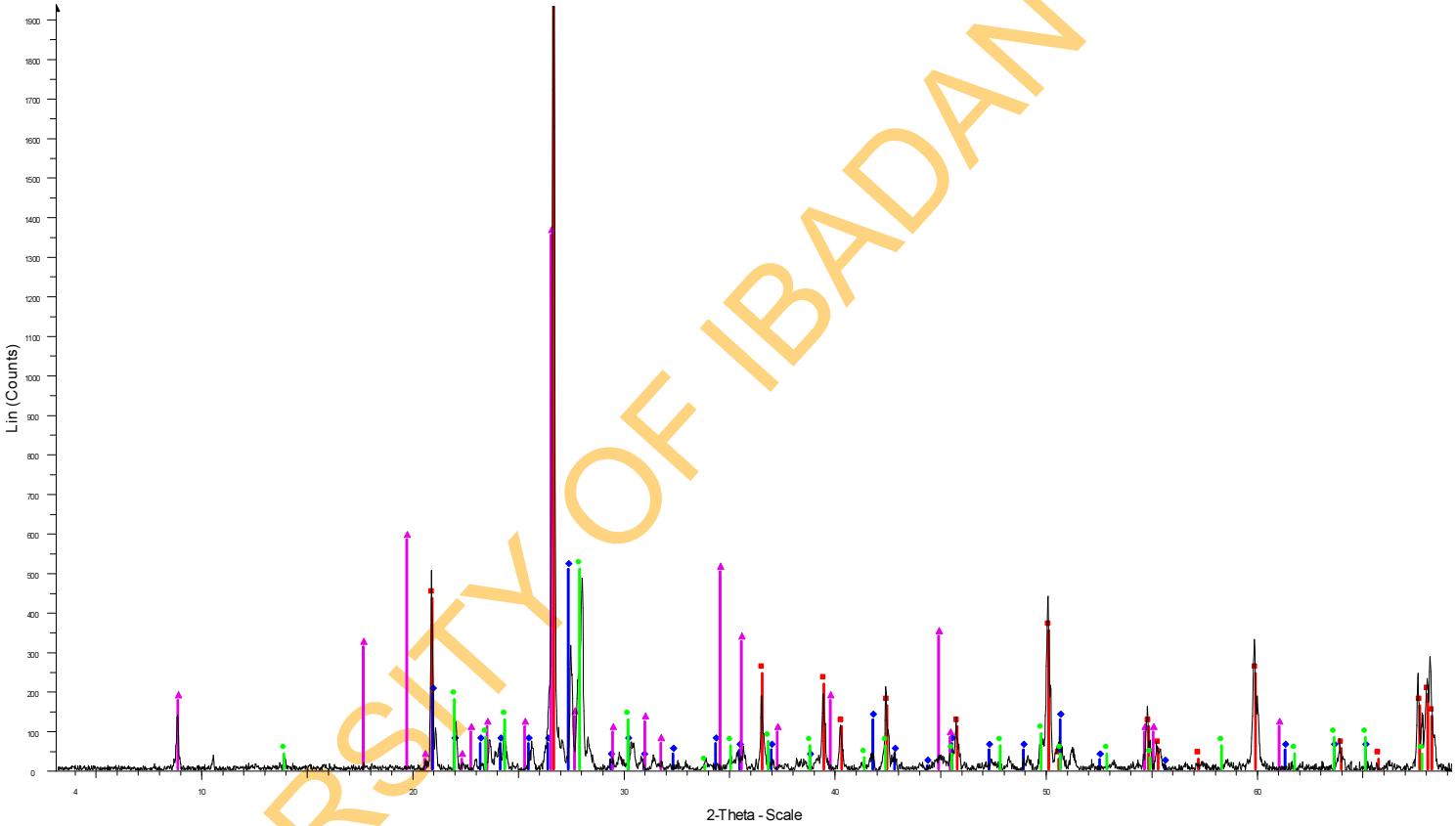

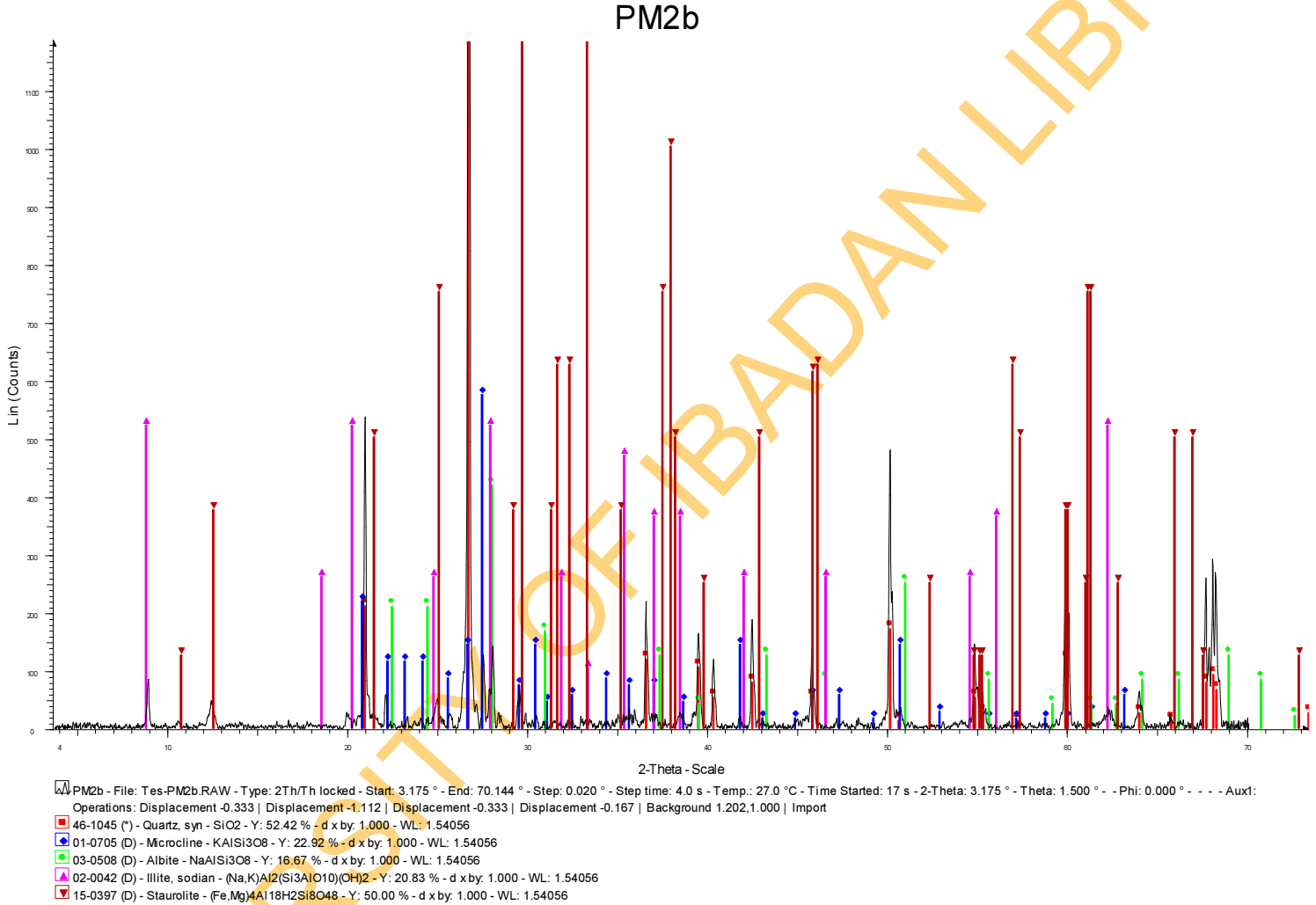

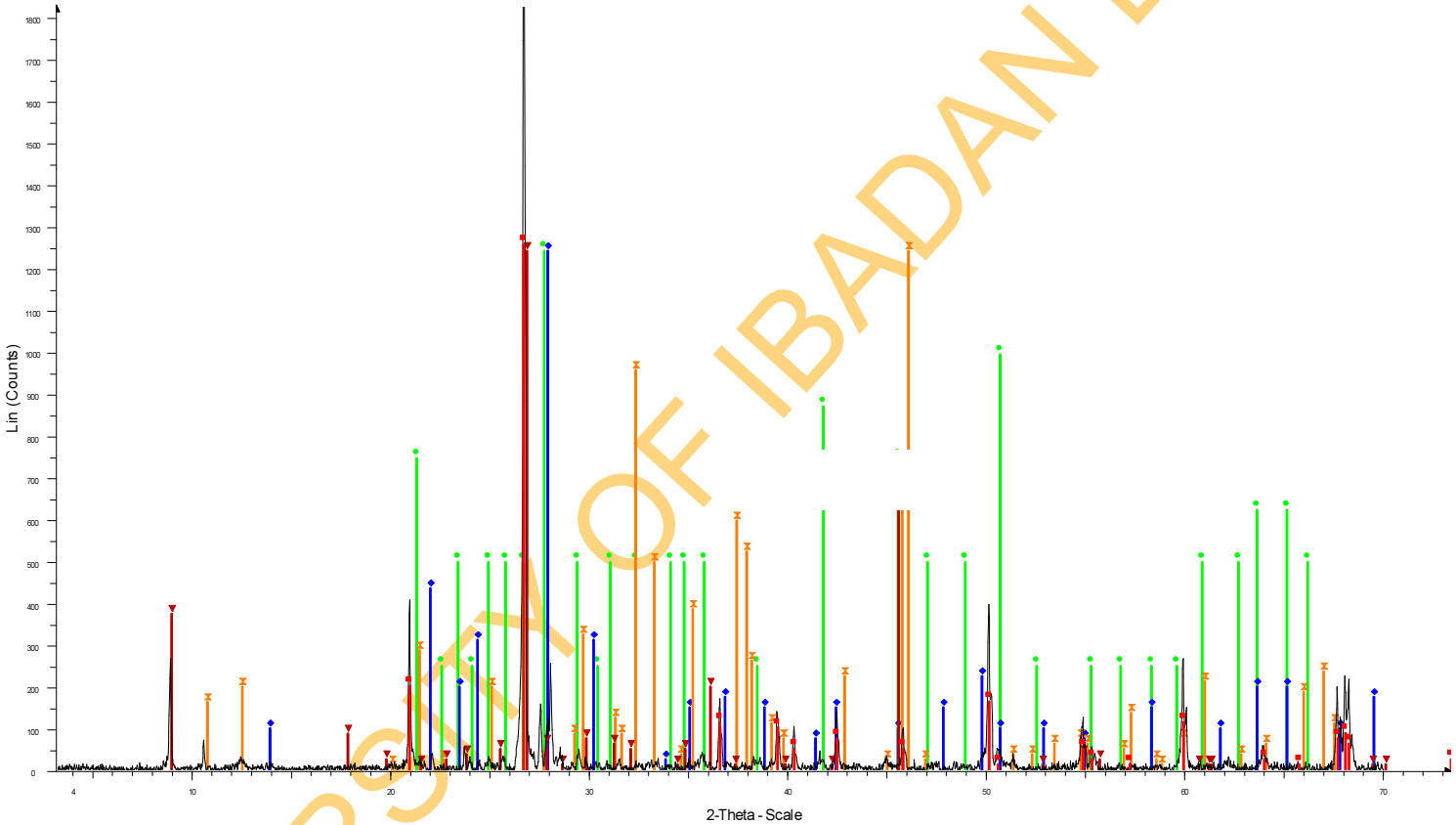

PM2c - File: Tes-PM2c.RAW - Type: 2Th/Th locked - Start: 3.132 ° - End: 70.108 ° - Step: 0.020 ° - Step time: 4.0 s - Temp.: 27.0 °C - Time Started: 17 s - 2-Theta: 3.132 ° - Theta: 1.500 ° - - Phi: 0.000 ° - - - - Aux1:
Operations: Displacement -0.250 | Background 1.202,1.000 | Import

46-1045 (*) - Quartz, syn - SiO2 - Y: 50.56 % - d x by: 1.000 - WL: 1.54056

02-0513 (D) - Microcline - Al2O3·K2O·6SiO2 - Y: 50.00 % - d x by: 1.000 - WL: 1.54056

01-0739 (D) - Albite - NaAlSi3O8 - Y: 50.00 % - d x by: 1.000 - WL: 1.54056

41-1484 (I) - Staurolite - Fe2Al9Si4O22(OH)2 - Y: 50.00 % - d x by: 1.000 - WL: 1.54056

46-1409 (I) - Muscovite, vanadian barian - (K,Ba,Na)0.75(Al,Mg,Cr,V)2(Si,Al,V)4O10(OH,O)2 - Y: 50.00 % - d x by: 1.000 - WL: 1.54056

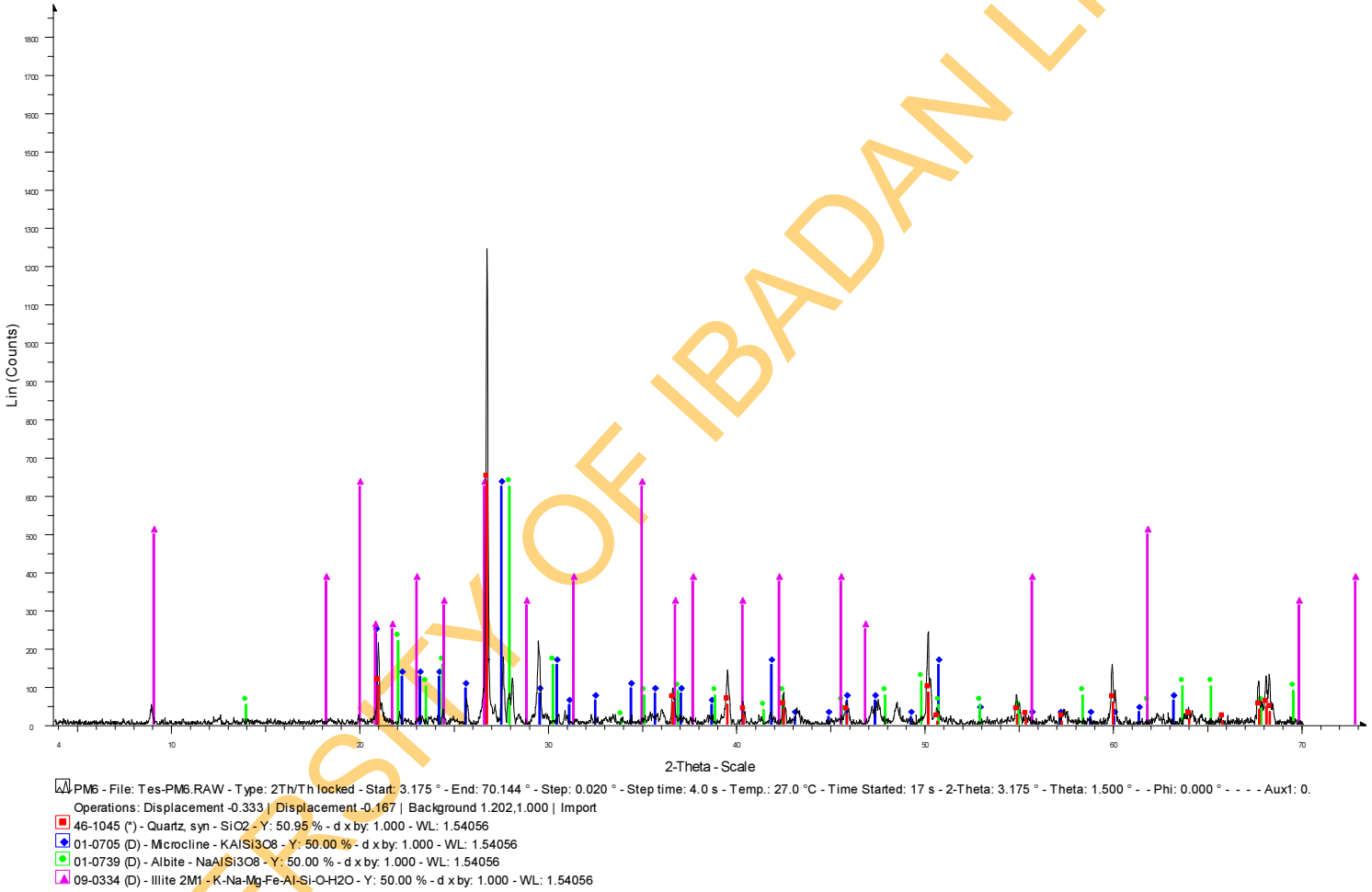

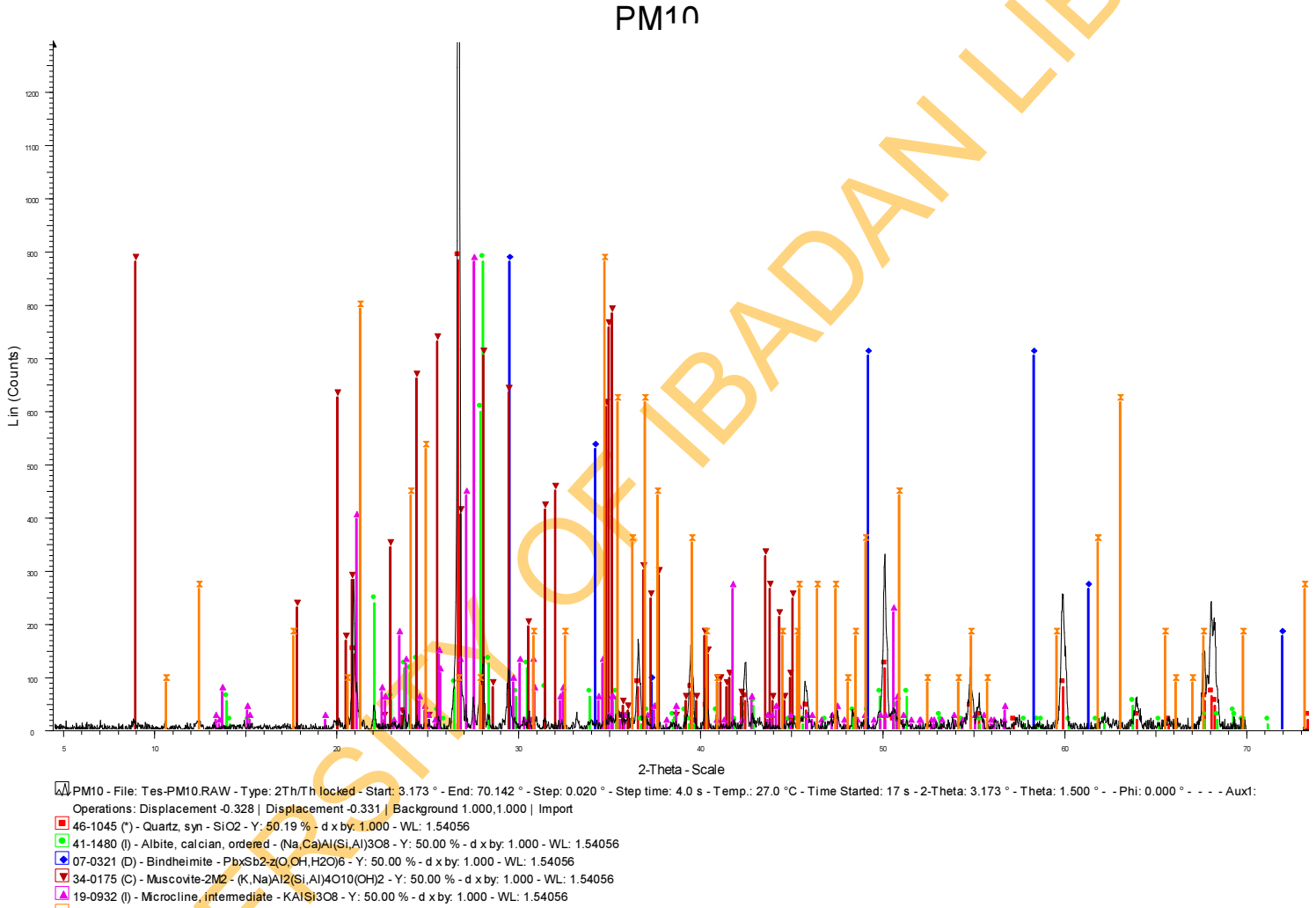

PM12

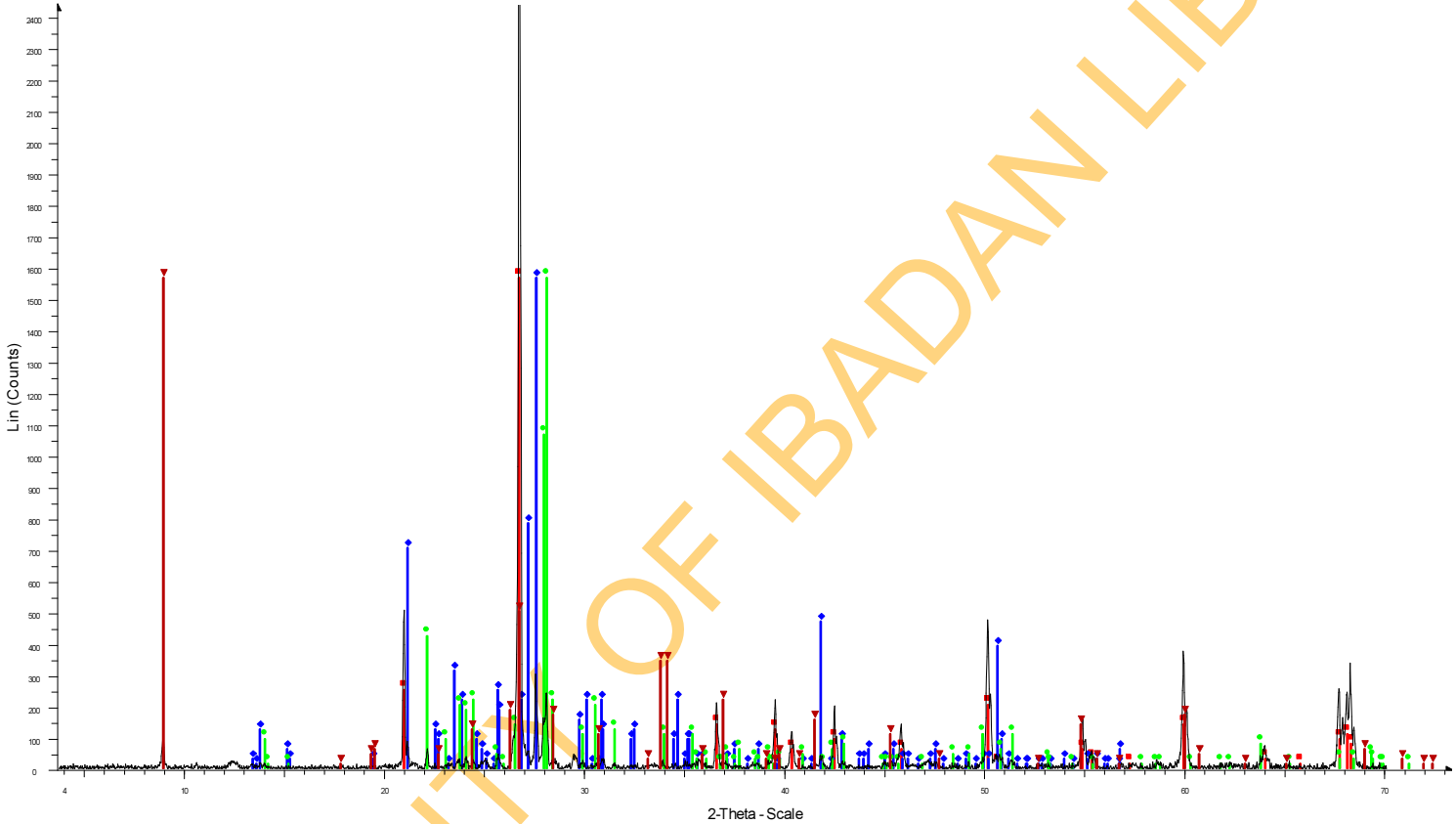

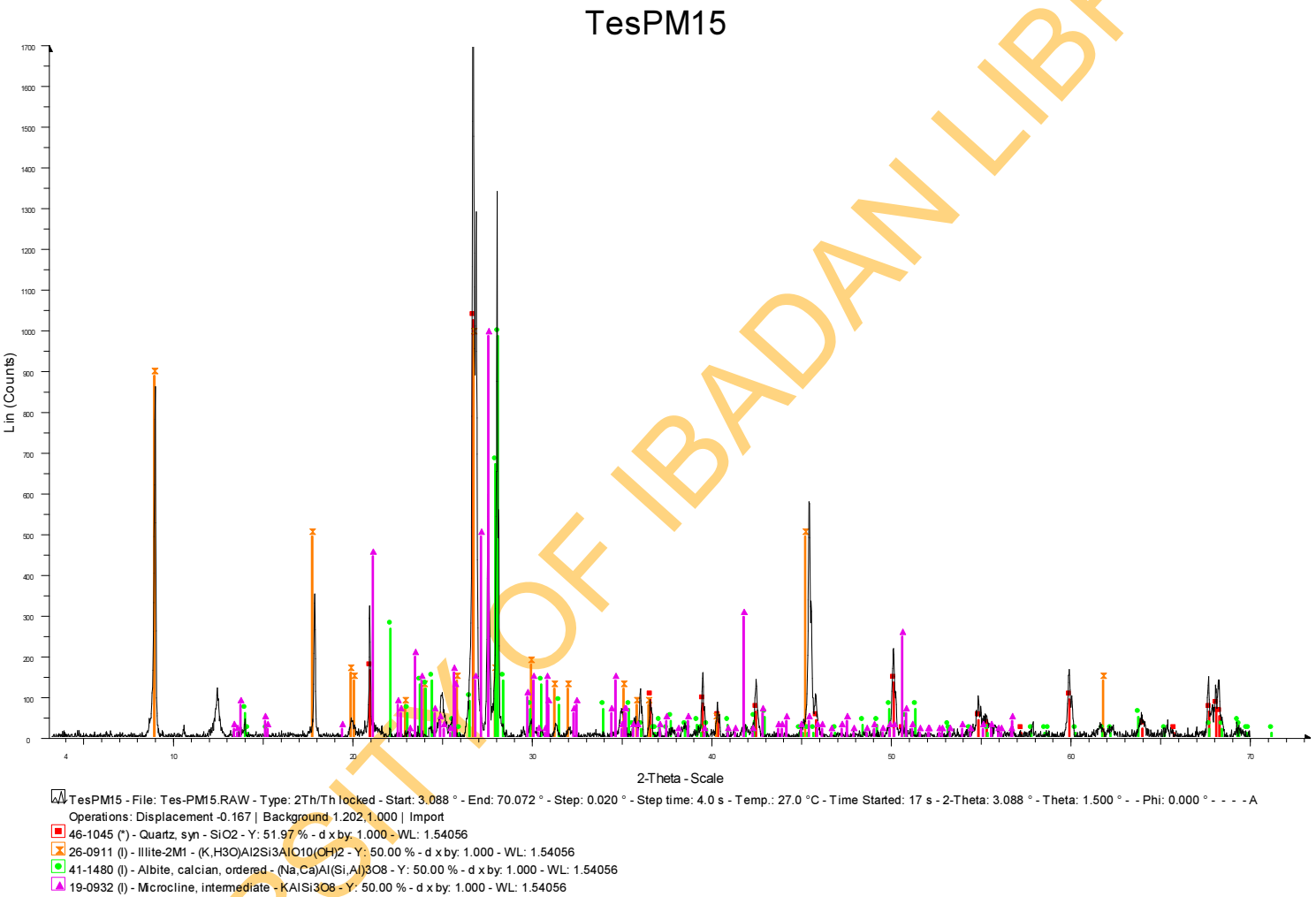

PM17

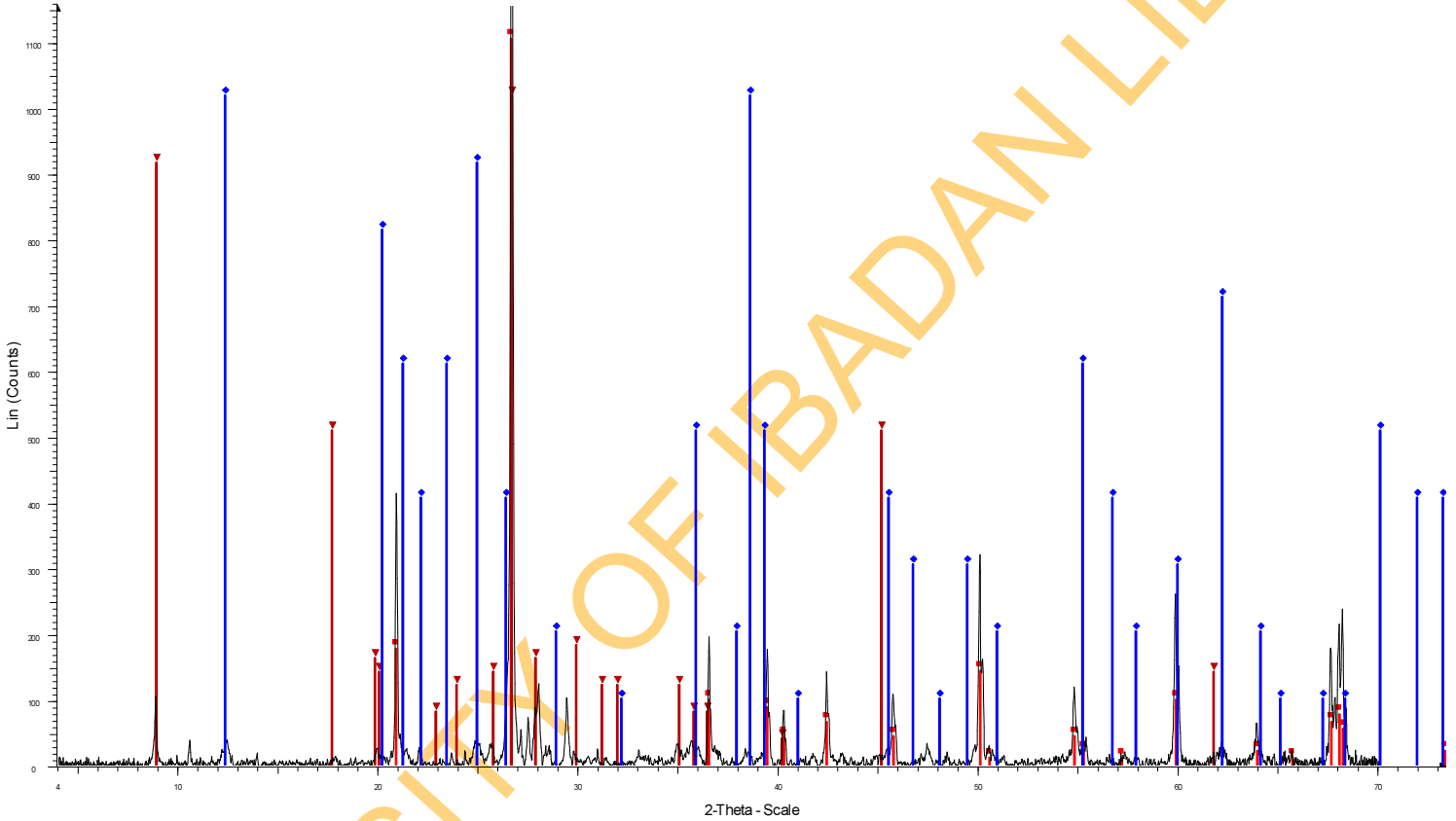

PM17 - File: Tes-PM17.RAW - Type: 2Th/Th locked - Start: 3.175 ° - End: 70.144 ° - Step: 0.020 ° - Step time: 4.0 s - Temp.: 27.0 °C - Time Started: 17 s - 2-Theta: 3.175 ° - Theta: 1.500 ° - - Phi: 0.000 ° - - - - Aux1: Operations: Displacement -0.333 | Displacement -0.250 | Displacement -0.333 | Displacement -0.417 | Displacement -0.500 | Background 1.202,1.000 | Import

46-1045 (*) - Quartz, syn - SiO2 - Y: 54.26 % - d x by: 1.000 - WL: 1.54056

26-0911 (I) - Illite-2M1 - (K,H3O)Al2Si3AlO10(OH)2 - Y: 50.00 % - d x by: 1.000 - WL: 1.54056

02-0105 (D) - Kaolinite - H4Al2Si2O9/Al2O3·2SiO2·2H2O - Y: 50.00 % - d x by: 1.000 - WL: 1.54056

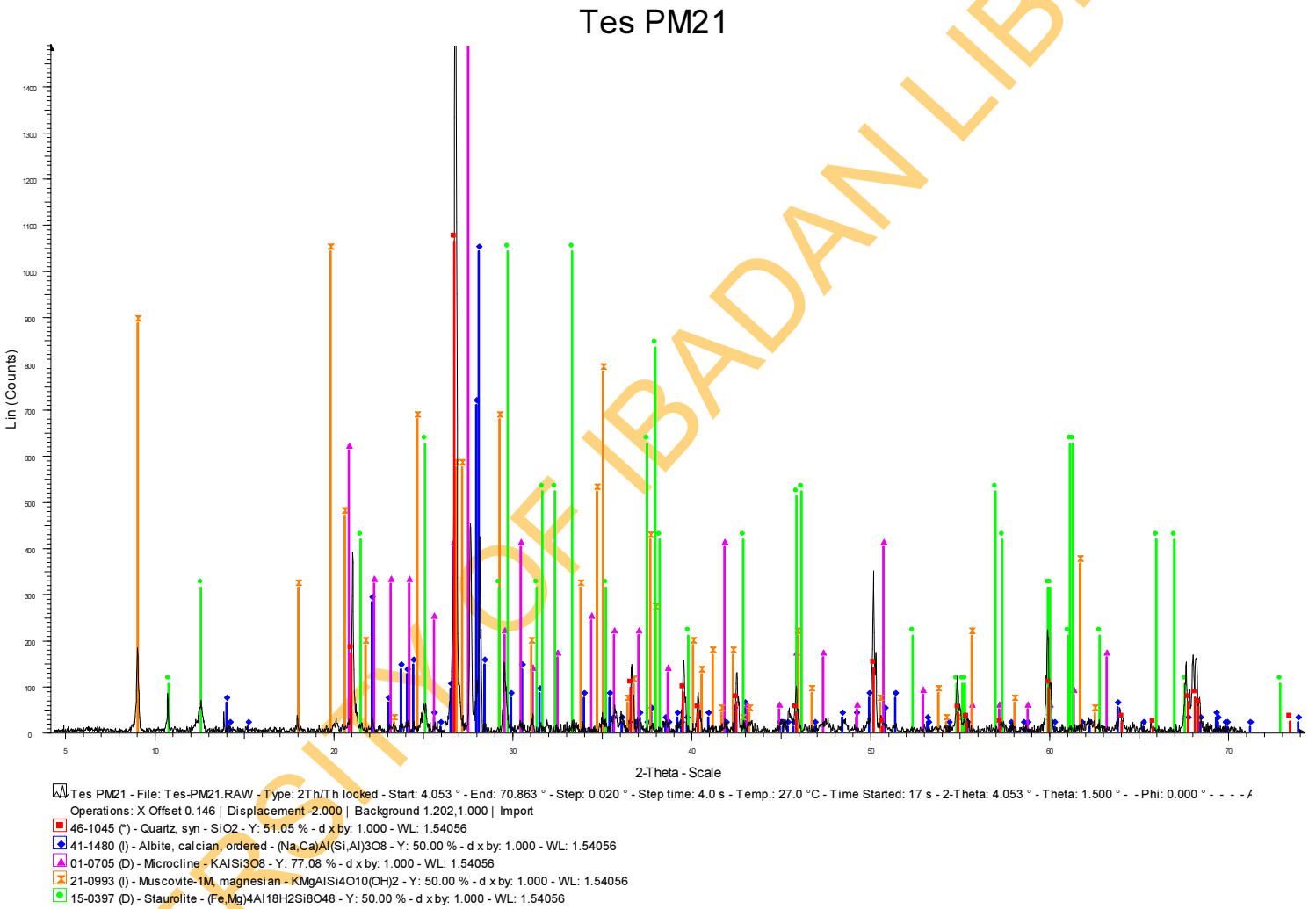

PM25

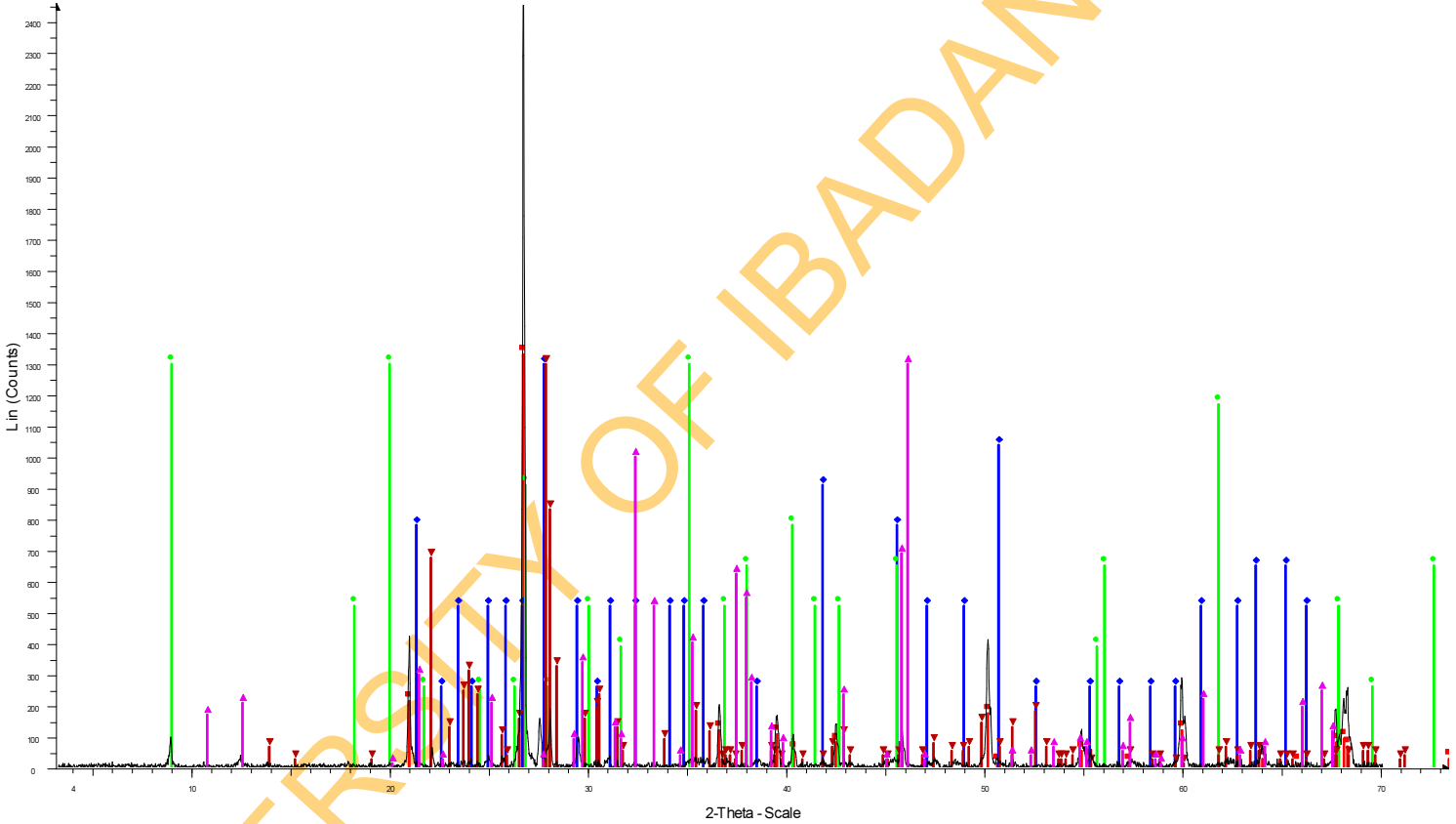

APPENDIX II
CHEMICAL ANALYSES RESULTS

Sample Location	Al µg/m^3	Ba µg/m^3	Ca µg/m^3	Cu µg/m^3	Fe µg/m^3	La µg/m^3		Mg µg/m^3	Mn µg/m^3	Mo µg/m^3	Na µg/m^3	Ni µg/m^3	Pb µg/m^3	Si µg/m^3	Ti µg/m^3	Zn µg/m^3	PM_{10} µg/m^3
P1	134.04	2.25	381.43	0.32	357.11	0.44	1113.13	112.84	3.89	7.46	174.39	<0.05	<0.05	128.77	5.56	2.6	917.28
P2	160.18	2.46	133.63	2.31	157.78	0.64	1186.67	79.56	0.82	4.91	100.53	<0.05	4.53	103.45	2.6	1.11	144.83
P3	108.6	1.52	273.8	0.12	293.25	<0.05	1550.09	97.02	2.66	4.53	160.91	1.46	<0.05	100.96	1.99	2.46	386.22
P4	97.08	1.87	323.8	0.58	173.39	0.15	842.69	104.91	1.29	<0.05	184.74	1.87	<0.05	100.44	1.61	1.67	185.06
P5	118.01	1.96	302.87	3.3	342.25	<0.05	904.30	101.32	3.65	<0.05	156.81	<0.05	10.38	109.53	2.57	3.04	466.69
P6	85.23	0.94	266.7	0.67	147.25	<0.05	30.99	93.68	0.7	<0.05	159.33	<0.05	<0.05	90.41	0.94	3.19	112.65
P7	97.75	1.14	252.22	<0.05	226.84	0.41	1180.23	92.22	1.4	<0.05	154.88	<0.05	<0.05	96.67	1.02	1.02	241.39
P8	75.94	0.91	268.3	11.32	91.52	<0.05	900.29	95.12	1.29	8.57	168.89	1.14	<0.05	69.42	1.7	5.41	321.85
P9	73.51	1.05	231.99	8.45	89.85	<0.05	1082.13	88.95	1.02	8.63	156.37	1.17	<0.05	74.82	1.67	3.39	48.28
P10	132.66	2.16	316.02	7.51	399.42	<0.05	680.94	106.05	5.7	6.75	168.54	0.7	4.06	123.48	4.97	7.95	547.15
P11	75.7	0.67	210.2	5.03	98.51	<0.05		86.75	1.35	6.9	139.65	0.96	<0.05	79.3	1.96	3.07	450.59
P12	100.64	1.32	281.43	7.69	241.14	0.38		98.22	3.42	7.13	174.39	2.51	<0.05	96.75	3.22	6.02	337.94
P13	71.55	0.56	183.36	8.1	87.6	0.44		82.69	0.88	5.5	129.15	0.85	<0.05	73.19	1.78	3.1	128.74
P14	75.15	0.99	291.32	7.49	109.18	<0.05	243.92	97.02	1.7	5.15	171.52	2.28	<0.05	66.26	1.81	5.99	96.56
P15	66.49	2.31	208.6	2.49	83.07	1.12	197.49	82.6	3.39	6.75	122.63	<0.05	0.85	64.74	0	0	128.74
P16	145.67	0.56	361.05	2.31	447.19	2.04	192.19	109.53	1.73	3.22	157.69	<0.05	<0.05	129.74	2.28	4.59	434.5
P17	125.82	1.17	292.98	1.96	332.66	1.69	384.71	99.36	0.03	3.39	142.02	<0.05	<0.05	125.7	1.02	1.55	321.85
P18	64.82	2.4	188.13	1.9	73.68	0.99	537.08	78.8	3.51	5.82	95.88	<0.05	<0.05	60.18	<0.05	<0.05	96.56
P19	75.88	2.11	206.52	3.36	107.63	1.11	297.95	82.49	2.89	5.88	91.87	<0.05	<0.05	79.53	<0.05	<0.05	531.06
P20	86.64	1.58	248.19	1.52	168.98	1.29	271.61	87.63	2.02	7.37	97.72	<0.05	<0.05	86.84	<0.05	0.12	595.43
P21	64.47	2.28	221.67	0	82.87	1.16	391.70	83.98	3.19	4.24	99.71	<0.05	<0.05	60.06	<0.05	0.15	321.85
P22	216.99	0.47	136.7	10.56	287.66	1.59	170.15	96.58	0.58	2.92	62.16	<0.05	<0.05	135.03	12.75	1.64	1094.3
P23	65.96	2.46	196.67	<0.05	74.68	1.04	318.33	80.41	3.48	5.38	83.42	<0.05	<0.05	61.52	<0.05	<0.05	209.2
P24	65.03	<0.05	228.27	2.4	75.94	<0.05		88.6	0.94	<0.05	59.65	<0.05	<0.05	64.04	0.41	4.09	418.41
P25	63.19	<0.05	257.6	2.16	72.22	<0.05		88.77	0.85	<0.05	60.53	<0.05	<0.05	66.11	0.38	4.09	289.67
P26	284.04	7.95	162.46	<0.05	425.67	1.52		120.76	4.44	<0.05	98.54	<0.05	<0.05	154.8	<0.05	<0.05	804.63
P27	119.71	1.52	315.67	<0.05	113.04	<0.05		91.17	0.94	<0.05	187.54	<0.05	<0.05	65.56	<0.05	8.07	595.43
P28	197.13	1.75	416.37	<0.05	294.91	<0.05	350.99	155.26	3.63	<0.05	180.41	<0.05	2.11	88.95	<0.05	54.04	321.85

P29	131.93	2.4	358.01	2.11	387.08	0.32	321.17	109.53	4.39	2.72	193.19	<0.05	8.33	120.09	3.25	6.11	563.24
P30	71.99	0.82	245.23	1.05	90	<0.05	266.46	90.64	0	3.48	174.39	<0.05	3.45	79.59	<0.05	<0.05	160.93
P31	121.84	1.73	346.81	3.42	321.67	0.38	359.74	106.93	2.92	1.14	198.07	<0.05	<0.05	118.86	2.05	3.86	354.04
P32	83.13	<0.05	264.04	2.72	105.44	0	269.88	91.46	1.67	1.02	59.82	<0.05	<0.05	77.57	0.85	3.57	337.94
P33	62.37	<0.05	301.61	1.81	72.43	0.15	387.95	96.23	0.94	<0.05	62.6	1.32	<0.05	62.98	0.29	2.05	466.69
P34	63.68	2.31	207.95	<0.05	90.15	1.01	378.42	79.59	3.48	5.82	88.98	<0.05	<0.05	63.65	<0.05	<0.05	337.94
P35	69.15	2.34	228.68	<0.05	93.57	1.23	283.39	85.96	2.6	5.76	95.82	<0.05	<0.05	64.59	<0.05	<0.05	482.78
P36	69.36	0.41	285.41	2.34	63.07	0	176.52	94.33	0	1.26	189.88	<0.05	4.94	65.56	<0.05	<0.05	128.74
P37	64.88	<0.05	176.73	1.73	80.18	0	383.63	79.71	0.94	0	57.78	<0.05	0.03	68.1	0.53	1.61	241.39
P38	67.05	<0.05	318.63	2.19	73.54	<0.05		93.74	1.02	<0.05	62.57	<0.05	<0.05	75.32	0.58	1.84	289.67
P39	69.36	<0.05	313.86	2.54	87.69	0.06		95.91	1.99	<0.05	63.25	0.26	<0.05	71.7	0.88	1.99	32.43
P40	75.15	<0.05	131.4	3.48	116.29	0.18		71.26	1.73	2.13	54.71	0.26	<0.05	74.91	1.11	2.02	756.35
P41	78.1	<0.05	249.91	1.4	109.27	0.03	325.18	91.29	1.78	<0.05	59.91	0	<0.05	78.6	0.99	3.01	386.22
P42	76.73	<0.05	319.88	2.22	87.95	0.03	319.09	99.36	1.75	<0.05	63.77	0.64	4.33	81.37	0.91	2.49	88.51
P43	59.82	<0.05	307.6	3.89	60.99	0.26	505.18	92.49	0.61	<0.05	63.25	<0.05	<0.05	65.99	0.18	2.05	241.39
P44	64.85	0.47	251.46	0	82.16	<0.05	269.09	91.4	0.12	<0.05	149.06	<0.05	<0.05	56.67	<0.05	<0.05	386.22
P45	73.98	0.7	186.67	0	108.25	<0.05	273.33	80.18	0.7	<0.05	108.25	<0.05	<0.05	64.27	<0.05	<0.05	547.15
P46	61.35	<0.05	298.1	2.6	65.76	0.15	383.54	95.67	0.67	<0.05	63.01	<0.05	<0.05	61.02	0.15	2.34	112.65
P47	152.13	<0.05	243.71	3.3	107.6	<0.05	157.95	90.7	1.67	<0.05	61.81	0.09	<0.05	107.46	0.94	4.62	193.11
P48	149.36	<0.05	240.32	2.31	90.15	<0.05	325.96	90.73	1.4	<0.05	60.5	<0.05	<0.05	97.46	0.73	4.77	358.63
P49	67.43	<0.05	263.51	1.81	89.74	<0.05	349.04	90.61	1.75	<0.05	61.17	<0.05	<0.05	66.43	0.7	2.98	160.93
P50	61.26	<0.05	316.37	2.25	62.22	0.06	384.04	95.96	0.58	<0.05	64.74	0.06	<0.05	68.13	0.12	2.37	128.74
P51	73.51	0.73	268.63	<0.05	113.36	<0.05	505.18	91.61	0.38	2.87	161.78	<0.05	<0.05	73.89	<0.05	4.12	209.2
P52	136.49	0.5	65.15	0.26	116.35	0.12		63.71	0.12	<0.05	74.24	3.8	<0.05	77.4	<0.05	<0.05	152.88
P53	162.75	0.76	88.27	<0.05	134.71	<0.05		68.71	0.67	<0.05	106.84	4.91	6.49	102.89	<0.05	<0.05	160.93
P54	140.99	0.85	134.44	6.52	129.27	<0.05		85.03	2.46	6.05	114.15	<0.05	<0.05	88.98	1.67	3.57	177.02
P55	88.25	2.05	261.96	10.12	148.89	1.3		87.95	2.43	9.01	140.32	<0.05	0.85	92.57	<0.05	0.73	321.85
P56	66.55	2.25	292.22	9.21	78.33	1.49		93.63	3.04	3.07	153.51	<0.05	<0.05	60.73	<0.05	<0.05	337.94
P57	135.09	2.34	122.98	2.72	94.5	1.1		82.22	2.72	4.82	64.12	<0.05	0.73	80.94	<0.05	<0.05	177.02

P58	148.95	2.34	72.84	0	108.42	0.48		63.98	2.57	4.77	68.22	<0.05	<0.05	76.52	<0.05	<0.05	185.06
P59	63.68	2.31	207.95	0	90.15	1.01		79.59	3.48	5.82	88.98	<0.05	<0.05	63.65	<0.05	<0.05	337.94
P60	142.69	2.08	135.76	0	136.96	1.1		82.08	1.9	2.75	55.99	<0.05	<0.05	94.94	<0.05	<0.05	152.88
P61	74.15	2.34	249.39	0	115.85	1.35		89.33	2.28	4.91	127.84	<0.05	<0.05	73.89	<0.05	<0.05	225.3
P62	104.47	2.69	103.27	0	58.68	0.72		71.08	3.98	3.65	78.6	<0.05	<0.05	64.12	<0.05	<0.05	263.11
P63	145.79	2.16	118.1	0	148.16	1		79.12	1.58	4.71	59.01	<0.05	<0.05	98.04	<0.05	<0.05	193.11
P64	69.85	<0.05	372.43	1.87	107.57	0.18		103.6	1.84	0.26	66.55	<0.05	<0.05	72.02	0.76	2.13	209.2
P65	138.48	<0.05	172.37	2.63	69.97	0.18		76.46	0.53	<0.05	58.68	<0.05	<0.05	76.87	0.29	2.72	177.02
P66	134.36	<0.05	160.5	1.35	109.85	0.2	197.49	73.77	2.19	<0.05	54.44	0.35	<0.05	86.78	0.88	2.87	80.46
P67	134.74	<0.05	144.09	2.31	112.16	0	192.19	86.4	1.75	<0.05	55.38	<0.05	<0.05	89.39	0.67	1.9	177.02
P68	141.55	<0.05	148.68	2.43	92.34	0.03	384.71	87.69	1.32	<0.05	56.32	0.94	2.75	90.88	0.73	3.22	160.93
P69	111.02	<0.05	156.05	1.43	66.84	0.09		81.02	0.61	<0.05	57.19	<0.05	1.43	75.09	0.23	2.22	169.98
P70	63.33	<0.05	283.65	1.46	84.09	0.03		91.02	1.11	1.43	62.51	<0.05	0	65.76	0.41	3.07	225.3
P71	67.34	<0.05	342.95	4.71	86.61	0.12		99.42	1.23	<0.05	65.35	<0.05	1.46	71.64	0.53	1.61	193.11
P72	68.42	<0.05	240.41	1.29	98.36	0		89.97	1.9	<0.05	60.18	<0.05	<0.05	69.01	0.76	2.84	273.57
P73	75.82	<0.05	288.95	2.13	110.73	0.18		99.21	2.11	<0.05	62.87	0.2	<0.05	79.44	0.99	2.54	273.57
P74	113.74	<0.05	1700	0.96	75.56	<0.05		74.59	0.85	<0.05	53.92	0.09	<0.05	77.81	0.47	5.73	466.69
P75	149.94	<0.05	96.81	3.01	83.74	<0.05		70.96	0.85	<0.05	55	0	1.4	82.22	0.47	5.44	206.09
P76	129.44	<0.05	211.87	1.61	62.6	<0.05		92.89	0.5	<0.05	59.39	0	1.9	79.94	0.18	3.54	160.93
P77	152.13	<0.05	243.71	3.3	107.6	<0.05		90.7	1.67	<0.05	61.81	0.09	0	107.46	0.94	4.62	193.11
P78	65.06	<0.05	297.95	2.69	67.22	<0.05		93.83	0.79	<0.05	63.83	1.55	0	62.92	0.23	2.49	159.01
P79	64.85	<0.05	368.8	1.46	96.32	<0.05		89.77	1.61	<0.05	62.95	0	0	66.46	0.53	1.7	225.3
P80	73.13	<0.05	337.87	3.25	110.76	0.12		99.53	1.99	<0.05	62.6	0.44	0	76.2	0.82	4.24	193.11
P81	118.77	<0.05	201.08	1.55	70.29	0.03		85.35	0.73	<0.05	56.67	0	0	77.11	0.32	4.21	170.12
P82	144.39	<0.05	162.22	1.17	93.57	0.09		86.61	2.4	<0.05	54.77	0	0	88.54	0.91	5.41	305.76
P83	73.22	<0.05	356.43	2.98	99.44	<0.05		101.93	1.96	<0.05	65.7	0.38	1.08	73.19	0.82	3.3	169.98
P84	131.9	<0.05	257.43	2.75	94.42	<0.05		89.15	1.49	<0.05	57.89	0.41	0	86.7	0.88	3.65	305.76
P85	90.53	<0.05	340.06	2.49	177.43	<0.05		102.69	4.91	<0.05	63.51	0.23	0	88.98	2.11	5.09	321.85
P86	122.95	<0.05	193.51	1.11	62.05	<0.05		88.25	0.53	<0.05	58.8	0.15	0	80.85	0.12	3.27	48.28

P87	149.36	<0.05	240.32	2.31	90.15	<0.05	90.73	1.4	<0.05	60.5	0	0	97.46	0.73	4.77	358.63
P88	73.74	<0.05	290.94	1.35	114.71	<0.05	96.55	2.4	0.99	62.34	0.79	0	73.71	1.02	4.12	289.67
P89	83.13	<0.05	264.04	2.72	105.44	<0.05	91.46	1.67	1.02	59.82	0	0	77.57	0.85	3.57	337.94
P90	67.43	<0.05	263.51	1.81	89.74	<0.05	90.61	1.75	0	61.17	0	0	66.43	0.7	2.98	289.67
P91	146.02	1.4	205.85	0	139.82	<0.05	84.27	1.99	0	79.47	0	0	80.53	0	0	128.74
P92	75.5	0.82	316.73	0	108.25	<0.05	101.81	1.17	0	175.03	0	0	64.15	0	0	225.3
P93	82.16	0.94	218.01	0	161.46	<0.05	85.91	3.16	0	125.79	0	0	65.79	0	0	354.04
P94	71.52	<0.05	291.87	1.58	106.67	0.23	100.91	2.31	<0.05	65.15	1.14	0	71.7	1.11	2.95	241.39
P95	56.78	<0.05	160.15	0.76	64.33	0.2	70.91	0.53	<0.05	55.73	15.38	0	50	0.15	1.26	257.48
P96	121.11	<0.05	133.07	1.9	82.16	0	72.49	0.85	<0.05	56.52	0.06	2.05	73.36	0.44	2.19	48.28
P97	140.67	<0.05	74.53	1.58	76.05	0.12	68.54	0.61	<0.05	54.44	0.23	0	70.53	0.23	2.89	152.88
P98	69.09	<0.05	420.15	1.67	94.24	0.26	104.39	1.29	<0.05	67.54	0.23	0	66.35	0.61	2.4	193.11
P99	119.36	<0.05	164.71	0.85	62.98	0	87.19	0.53	<0.05	57.19	0	1.32	74.62	0.09	2.31	168.97
P100	80.82	<0.05	256.32	1.26	158.3	0.09	94.18	4.36	<0.05	61.11	0.41	2.02	75.73	1.73	4.47	273.57
P101	127.98	<0.05	213.92	1.7	69.12	0.06	92.98	0.73	<0.05	59.59	<0.05	1.84	79.42	0.2	3.04	152.7
P102	65.96	<0.05	237.6	1.87	84.56	0.06	91.93	1.87	<0.05	505.88	0.15	<0.05	61.99	0.47	3.07	305.76
P103	136.84	<0.05	131.2	2.51	62.4	<0.05	72.89	0.38	<0.05	56.08	0.29	0.03	70.29	0.18	3.07	154.14
P104	132.19	<0.05	132.37	2.87	72.05	0.18	87.28	0.82	<0.05	57.11	<0.05	1.23	78.01	0.26	2.34	185.06
P105	69.65	<0.05	358.1	1.81	94.53	0.09	104.01	1.4	<0.05	172.63	0.79	4.3	68.3	0.53	3.1	177.02
P106	61.99	<0.05	201.11	1.29	79.77	<0.05	83.89	1.17	<0.05	58.16	0.67	<0.05	57.75	0.26	1.9	177.02
P107	67.25	<0.05	448.3	1.35	84.06	0.15	106.43	1.4	<0.05	68.19	<0.05	<0.05	66.99	0.38	3.45	321.85
P108	154.88	<0.05	249.56	2.87	112.95	0.06	85.53	1.26	<0.05	60.73	0.67	<0.05	94.18	0.76	2.54	201.16
P109	122.63	<0.05	188.71	2.78	64.8	<0.05	88.92	0.58	<0.05	58.19	0.09	<0.05	81.46	0.15	3.16	152.88
P110	135.41	<0.05	137.11	3.36	63.16	<0.05	73.54	0.38	<0.05	56.23	0.5	<0.05	70.03	0.12	3.92	144.83
P111	62.37	<0.05	301.61	1.81	72.43	0.15	96.23	0.94	<0.05	62.6	1.32	<0.05	62.98	0.29	2.05	466.69
P112	119.33	<0.05	176.58	2.63	61.2	0.03	88.63	0.44	<0.05	56.87	0.99	<0.05	76.05	0.06	2.89	177.02
P113	127.78	<0.05	217.75	3.3	75.32	0.06	92.49	0.73	<0.05	58.98	<0.05	<0.05	82.75	0.29	3.25	160.93
P114	135.61	<0.05	221.37	1.87	64.21	<0.05	95.56	0.7	<0.05	59.12	1.35	<0.05	78.95	0.03	2.92	160.93
P115	126.58	<0.05	226.58	1.78	66.84	<0.05	94.59	0.67	<0.05	59.33	0.18	<0.05	78.98	0.18	2.69	169.87

P116	111.96	<0.05	204.18	2.43	72.13	0.09	86.9	0.79	<0.05	414.62	0.96	<0.05	73.36	0.12	2.66	160.93
P117	158.86	<0.05	251.2	4.44	74.06	0.03	101.14	0.79	<0.05	60.32	0.73	<0.05	85.58	0.29	2.89	168.97
P118	127.49	<0.05	208.3	4.09	68.16	<0.05	93.68	0.67	<0.05	58.3	1.4	<0.05	80.09	0.23	4.33	206.09
P119	117.28	<0.05	198.51	3.6	69.15	<0.05	88.98	0.58	<0.05	57.31	0.79	1.61	76.05	0.15	2.54	185.06
P120	140.64	<0.05	145.47	1.75	74.33	<0.05	74.97	0.61	<0.05	54.04	1.43	<0.05	71.81	0.2	2.51	152.88
P121	184.59	<0.05	240.94	4.18	243.33	<0.05	90.99	3.33	<0.05	57.54	0.18	<0.05	136.7	3.1	5.2	402.31
P122	162.31	<0.05	262.63	2.66	127.84	0.29	96.08	2.6	<0.05	473.04	0.94	3.89	103.77	1.23	4.06	80.46
P123	134.36	0.76	135.29	3.24	92.75	0.96	85.09	<0.05	4.01	103.54	1.53	5.26	102.57	0	4.98	337.94
P124	171.23	1.08	180.2	2.22	146.23	0.35	97.28	0.99	2.46	106.93	0.4	13.16	119.12	2.63	3.38	466.69
P125	170.23	1.17	1250.85	3.46	125.85	1.47	317.49	3.22	4.59	135.47	0.96	1.41	80.06	0.5	5.2	482.78
P126	158.07	0.85	148.71	1.61	146.02	0.52	86.29	1.37	1.48	88.04	0.4	0.8	111.61	1.14	2.43	498.87
P127	135.35	1.84	325.26	1.35	240.53	0.59	118.86	3.42	0.95	266.52	0.4	1.02	141.29	5.79	2.14	659.8
P128	111.7	1.2	224.01	0.66	149.74	0.59	95.73	1.14	0.89	131.11	0.51	5.09	129.94	1.87	2.25	724.17
P129	106.29	1.05	217.54	0.88	156.93	0.41	95.12	1.23	1.54	134.94	0.51	2.31	120.96	2.72	2.55	627.61
P130	132.43	1.52	315.76	7.19	187.05	2.95	113.22	3.86	5.16	162.34	11.73	1.2	147.6	5.18	7.51	772.44
P131	120.99	1.55	406.99	6	177.75	0.47	121.87	3.86	3.44	228.63	1.46	0.77	149.04	4.91	4.77	708.07
P132	135.23	1.64	382.66	5.45	191.75	0.5	118.57	3.98	2.4	199.06	2.02	0.4	154.65	5.47	4.24	772.44
P133	125.32	1.17	342.54	10.46	155.64	4.86	108.74	2.81	9.43	212.34	3.77	2.25	141.08	4.18	11.99	627.61
P134	122.02	1.58	318.19	7.75	182.22	0.74	115.44	4.09	2.85	180.56	0.96	6.52	134.01	5.5	3.89	691.98
P135	95.5	<0.05	1062.84	2.51	98.07	0.52	358.83	3.51	1.84	57.81	0.64	0.64	108.36	1.05	3.27	370.13
P136	116.07	<0.05	906.84	2.46	98.74	0.8	313.07	3.36	1.84	55.61	0.89	0.89	99.74	0.91	3.19	466.69
P137	179.18	<0.05	178.27	2.08	157.31	1.55	93.71	4.33	2.19	56.78	1.34	0.9	141.17	2.34	3.42	627.61
P138	201.36	1.52	298.01	0.74	167.89	0.4	109.77	2.69	0.65	170.82	0.51	1.6	101.11	<0.05	1.42	643.7
P139	268.78	2.34	354.74	1.2	265.32	1.03	123.45	4.8	1.25	178.19	1.09	3.39	111.05	<0.05	2.67	949.46
P140	61.7	1.2	224.01	0	99.74	<0.05	45.73	1.14	<0.05	89.65	<0.05	5.09	79.94	1.87	<0.05	193.11
P141	31.35	0.91	166.08	2.25	154.91	<0.05	25.91	3.65	1.32	134.74	1.14	4.94	27.63	0.44	33.74	170.12
P142	68.01	1.96	302.87	3.3	292.25	<0.05	51.32	3.65	<0.05	216.52	<0.05	10.38	59.53	2.57	3.04	305.76
P143	35.23	0.94	266.7	0.67	97.25	<0.05	43.68	0.7	<0.05	93.71	<0.05	0	40.41	0.94	3.19	169.98
P144	112.75	0.76	88.27	<0.05	84.71	<0.05	18.71	0.67	<0.05	24.24	4.91	6.49	52.89	<0.05	<0.05	305.76

P145	56.29	1.05	217.54	<0.05	106.93	0.41	45.12	1.23	<0.05	130.56	<0.05	2.31	70.96	2.72	<0.05	321.85
P146	14.09	0.38	259.15	2.11	27.81	0.41	40.64	<0.05	2.13	79.15	<0.05	9.06	11.64	<0.05	19.06	48.28
P147	11.08	0.26	187.78	<0.05	9.47	0	29.09	<0.05	<0.05	106.37	<0.05	7.25	8.8	<0.05	0.44	358.63
P148	47.75	1.14	252.22	<0.05	176.84	0.41	42.22	1.4	<0.05	118.54	<0.05	<0.05	46.67	1.02	1.02	289.67
P149	25.94	0.91	268.3	11.32	41.52	0	45.12	1.29	8.57	121.52	1.14	<0.05	19.42	1.7	5.41	241.39
P150	82.43	1.52	315.76	7.19	137.05	0.61	63.22	3.86	9.04	103.51	11.73	<0.05	97.6	5.18	7.51	321.85
P151	85.09	2.34	122.98	2.72	44.5	1.1	32.22	2.72	4.82	14.12	<0.05	0.73	30.94	<0.05	<0.05	48.28
P152	75.82	1.17	292.98	1.96	282.66	1.69	49.36	0.03	3.39	92.02	0	0	75.7	1.02	1.55	547.15
P153	14.82	2.4	188.13	1.9	23.68	0.99	28.8	3.51	5.82	45.88	<0.05	<0.05	10.18	<0.05	<0.05	450.59
P154	25.88	2.11	206.52	3.36	57.63	1.11	32.49	2.89	5.88	41.87	<0.05	<0.05	29.53	<0.05	<0.05	337.94
P155	10.26	2.6	203.95	2.05	14.24	1.07	31.23	3.51	2.43	63.77	<0.05	<0.05	10.67	<0.05	1.52	128.74
P156	98.95	2.34	72.84	<0.05	58.42	0.48	13.98	2.57	4.77	18.22	<0.05	<0.05	26.52	<0.05	<0.05	96.56
P157	36.64	1.58	248.19	1.52	118.98	1.29	37.63	2.02	7.37	47.72	<0.05	<0.05	36.84	<0.05	0.12	128.74
P158	13.68	2.31	207.95	<0.05	40.15	1.01	29.59	3.48	5.82	38.98	<0.05	<0.05	13.65	<0.05	<0.05	434.5
P159	14.47	2.28	221.67	<0.05	32.87	1.16	33.98	3.19	4.24	49.71	<0.05	<0.05	10.06	<0.05	0.15	321.85
P160	92.69	2.08	135.76	<0.05	86.96	1.1	32.08	1.9	2.75	5.99	<0.05	<0.05	44.94	<0.05	<0.05	96.56
P161	24.15	2.34	249.39	<0.05	65.85	1.35	39.33	2.28	4.91	77.84	<0.05	<0.05	23.89	<0.05	<0.05	531.06
P162	166.99	0.47	136.7	10.56	237.66	1.59	46.58	0.58	2.92	12.16	<0.05	<0.05	85.03	12.75	1.64	595.43
P163	54.47	2.69	103.27	0	8.68	0.72	21.08	3.98	3.65	28.6	<0.05	<0.05	14.12	<0.05	<0.05	321.85
P164	155.56	2.46	306.67	<0.05	113.8	<0.005	83.63	3.63	<0.05	60.82	<0.05	<0.05	87.95	<0.05	<0.005	1094.3
P165	129.59	1.64	222.11	<0.05	83.86	<0.005	57.31	2.34	<0.05	74.85	<0.05	<0.05	70.41	<0.05	<0.005	248.19
P166	83.63	0.35	126.67	<0.05	32.05	<0.005	23.39	<0.005	<0.05	74.39	<0.05	<0.05	17.66	<0.05	<0.005	207.95
P167	2.57	0.12	12.16	<0.05	1.29	<0.005	1.17	<0.005	<0.05	18.01	<0.05	<0.05	3.04	<0.05	<0.005	221.67
P168	96.02	1.4	205.85	<0.05	89.82	<0.005	34.27	1.99	<0.05	29.47	<0.05	<0.05	30.53	<0.05	<0.005	135.76
P169	234.04	7.95	162.46	<0.05	375.67	<0.005	70.76	4.44	<0.05	48.54	<0.05	<0.05	104.8	<0.05	<0.005	249.39
P170	63.39	1.52	298.01	<0.05	117.89	<0.005	59.77	2.69	<0.05	120.82	<0.05	<0.05	51.11	<0.05	<0.005	136.7
P171	96.96	2.34	354.74	<0.05	215.32	<0.005	73.45	4.8	<0.05	128.19	<0.05	<0.05	61.05	<0.05	<0.005	103.27
P172	14.85	0.47	251.46	<0.05	32.16	<0.005	41.4	0.12	<0.05	99.06	<0.05	<0.05	6.67	<0.05	<0.005	306.67
P173	69.71	1.52	315.67	<0.05	63.04	<0.005	41.17	0.94	<0.05	137.54	<0.05	<0.05	15.56	<0.05	8.07	222.11

P174	42.22	1.75	188.89	<0.05	98.13	<0.005	53.22	1.52	<0.05	63.86	<0.05	<0.05	46.2	<0.05	<0.05	126.67
P175	23.98	0.7	186.67	<0.05	58.25	<0.005	30.18	0.7	<0.05	58.25	<0.05	<0.05	14.27	<0.05	<0.05	12.16
P176	147.13	1.75	416.37	<0.05	244.91	<0.005	105.26	3.63	<0.05	130.41	<0.05	2.11	38.95	<0.05	54.04	205.85
P177	25.5	0.82	316.73	<0.05	58.25	<0.005	51.81	1.17	<0.05	125.03	<0.05	<0.005	14.15	<0.05	<0.05	162.46
P178	32.16	0.94	218.01	<0.05	111.46	<0.005	35.91	3.16	<0.05	75.79	<0.05	<0.005	15.79	<0.05	<0.05	298.01
P179	13.57	0.47	196.14	<0.05	17.66	<0.005	31.58	<0.005	<0.05	74.97	<0.05	<0.005	1.64	<0.05	<0.05	354.74
P180	16.14	0.82	190.06	<0.05	114.5	<0.005	32.28	4.8	<0.05	76.26	<0.05	38.48	6.32	<0.05	318.36	251.46
P181	82.19	<0.05	132.37	2.87	22.05	0.18	37.28	0.82	<0.05	7.11	<0.05	1.23	28.01	0.26	2.34	128.74
P182	19.65	<0.05	358.1	1.81	44.53	0.09	54.01	1.4	<0.05	122.63	0.79	4.3	18.3	0.53	3.1	96.56
P183	11.99	<0.05	201.11	1.29	29.77	<0.05	33.89	1.17	<0.05	8.16	0.67	<0.05	7.75	0.26	1.9	128.74
P184	17.25	<0.05	448.3	1.35	34.06	0.15	56.43	1.4	<0.05	18.19	<0.05	<0.05	16.99	0.38	3.45	434.5
P185	104.88	<0.05	249.56	2.87	62.95	0.06	35.53	1.26	<0.05	10.73	0.67	<0.05	44.18	0.76	2.54	321.85
P186	72.63	<0.05	188.71	2.78	14.8	0	38.92	0.58	<0.05	8.19	0.09	<0.05	31.46	0.15	3.16	96.56
P187	85.41	<0.05	137.11	3.36	13.16	0	23.54	0.38	<0.05	6.23	0.5	<0.05	20.03	0.12	3.92	531.06
P188	12.37	<0.05	301.61	1.81	22.43	0.15	46.23	0.94	<0.05	12.6	1.32	<0.05	12.98	0.29	2.05	595.43
P189	69.33	<0.05	176.58	2.63	11.2	0.03	38.63	0.44	<0.05	6.87	0.99	<0.05	26.05	0.06	2.89	321.85
P190	11.35	<0.05	298.1	2.6	15.76	0.15	45.67	0.67	<0.05	13.01	<0.05	<0.05	11.02	0.15	2.34	1094.3
P191	77.78	<0.05	217.75	3.3	25.32	0.06	42.49	0.73	<0.05	8.98	<0.05	<0.05	32.75	0.29	3.25	209.2
P192	85.61	<0.05	221.37	1.87	14.21	<0.05	45.56	0.7	<0.05	9.12	1.35	<0.05	28.95	0.03	2.92	251.2
P193	76.58	<0.05	226.58	1.78	16.84	<0.05	44.59	0.67	<0.05	9.33	0.18	<0.05	28.98	0.18	2.69	208.3
P194	61.96	<0.05	204.18	2.43	22.13	0.09	36.9	0.79	<0.05	364.62	0.96	<0.05	23.36	0.12	2.66	193.11
P195	108.86	<0.05	251.2	4.44	24.06	0.03	51.14	0.79	<0.05	10.32	0.73	<0.05	35.58	0.29	2.89	170.12
P196	77.49	<0.05	208.3	4.09	18.16	<0.05	43.68	0.67	<0.05	8.3	1.4	<0.05	30.09	0.23	4.33	305.76
P197	67.28	<0.05	198.51	3.6	19.15	<0.05	38.98	0.58	<0.05	7.31	0.79	1.61	26.05	0.15	2.54	169.98
P198	90.64	<0.05	145.47	1.75	24.33	<0.05	24.97	0.61	<0.05	4.04	1.43	<0.05	21.81	0.2	2.51	305.76
P199	17.05	<0.05	318.63	2.19	23.54	0	43.74	1.02	<0.05	12.57	<0.05	<0.05	25.32	0.58	1.84	321.85
P200	13.33	<0.05	283.65	1.46	34.09	0.03	41.02	1.11	1.43	12.51	<0.05	<0.05	15.76	0.41	3.07	48.28
P201	19.36	<0.05	313.86	2.54	37.69	0.06	45.91	1.99	<0.05	13.25	0.26	<0.05	21.7	0.88	1.99	358.63
P202	134.59	<0.05	240.94	4.18	193.33	0	40.99	3.33	<0.05	7.54	0.18	<0.05	86.7	3.1	5.2	289.67

P203	17.34	<0.05	342.95	4.71	36.61	0.12	49.42	1.23	<0.05	15.35	0	1.46	21.64	0.53	1.61	221.37
P204	18.42	<0.05	240.41	1.29	48.36	0	39.97	1.9	<0.05	10.18	0	0	19.01	0.76	2.84	226.58
P205	25.15	<0.05	131.4	3.48	66.29	0.18	21.26	1.73	2.13	4.71	0.26	0	24.91	1.11	2.02	204.18

Dumpsite Factor Analysis

	Factor 1	Factor 2	Factor 3	Communalities
Al	.32	**.87**	.34	.973
Ca	**-.96**	-.24	.10	.982
Cu	.28	-.30	**-.88**	.951
Fe	**.62**	**.75**	.18	.988
Mg	**-.94**	-.14	.28	.979
Mn	.13	**.97**	.05	.967
Na	**-.94**	-.32	.09	.989
Si	.12	**.86**	.32	.846
Ti	.36	**.93**	.07	.995
Zn	.01	.09	**.97**	.942
PM10	**.98**	.15	-.06	.984
La	.40	**-.54**	**-.66**	.885
Eigen Value	4.512	4.455	2.512	
% Variance	37.597	37.124	20.934	
Cumulative %	37.597	74.722	95.656	

Factor 1: Fe, PM- (Ca, Mg, Na,)
Factor 2: Al, Fe, Mn, Ti, (La)
Factor 3: Zn (La, Cu)

Traffic Factor Analysis

	Factor 1	Factor 2	Factor 3	Factor 4	Factor 5	Communalities
Al	**0.84**	0.23	-0.20	0.21	-0.11	**0.95**
Ba	0.25	-0.09	-0.22	**0.83**	-0.08	**0.90**
Ca	0.08	**0.85**	-0.03	0.03	0.20	**0.96**
Cu	0.20	-0.09	**0.79**	-0.33	0.05	**0.93**
Fe	**0.79**	0.38	-0.07	0.27	0.21	**0.92**
La	0.38	-0.49	-0.20	0.29	-0.44	**0.82**
Mg	0.49	**0.81**	-0.14	0.17	-0.06	**0.97**
Mn	0.14	0.14	0.08	**0.85**	0.21	**0.93**
Mo	-0.19	-0.32	**0.74**	0.27	-0.10	**0.91**
Na	0.01	0.76	0.26	0.02	0.33	**0.97**
Ni	-0.17	0.30	**0.77**	-0.07	-0.08	**0.96**
Pb	0.16	0.10	-0.14	0.14	**0.89**	**0.94**
Si	**0.89**	0.18	-0.04	0.15	0.14	**0.97**
Ti	0.76	-0.10	0.41	-0.31	0.17	**0.97**
Zn	0.05	**0.78**	-0.13	-0.02	-0.15	**0.89**
PM10	**0.79**	-0.11	-0.06	0.12	-0.04	**0.86**
Eigen Value	5.06	3.87	2.71	1.30	1.05	
% Variance	33.71	25.81	18.05	8.69	7.02	
Cumulative %	33.71	59.51	77.57	86.26	93.28	

Factor 1: Al, Fe, Si, PM
Factor 2: Ca, Mg, Zn
Factor 3: Cu, Mo, Ni
Factor 4: Ba, Mn
Factor 5: Pb

Industrial Factor

	Factor 1	Factor 2	Factor 3	Factor 4	Factor 5	Communalities
Al	.487	-.128	**-.805**	.116	.165	.942
Ba	**.985**	-.095	-.019	.058	-.002	.984
Ca	.065	.117	-.090	**.966**	-.116	.973
Cu	.097	**.819**	.451	.101	.100	.903
Fe	**.952**	-.136	.050	-.118	-.054	.944
La	.035	**.951**	-.014	.036	-.088	.914
Mg	.011	.071	-.148	**.964**	-.076	.963
Mn	**.875**	.194	.154	.322	-.118	.945
Mo	-.176	**.936**	.141	.201	.061	.971
Na	**.684**	.114	**.535**	.146	-.122	.803
Ni	.159	**.722**	.048	-.204	-.315	.689
Pb	-.232	-.082	-.110	-.210	**.906**	.938
Si	.385	.243	**.753**	-.421	-.071	.956
Ti	.322	.227	**.884**	-.095	.015	.946
Zn	-.082	**.962**	.175	.104	.012	.973
PM10	**.885**	.032	.053	-.168	-.192	.852
Eigen Value	**4.514**	**4.128**	**2.609**	**2.382**	**1.062**	
% Variance	**28.211**	**25.800**	**16.309**	**14.884**	**6.638**	
Cumulative %	**28.211**	**54.012**	**70.321**	**85.205**	**91.844**	

Factor 1: Ba, Fe, Mn, Na, PM
Factor 2: Cu, La, Mn, Mo, Ni, Zn
Factor 3: Na, Si, Ti,
Factor 4: Ca, Mg,

Residential Factor Analysis

	Factor 1	Factor 2	Factor 3	Factor 4	Communalities
Al	.01	**.54**	**-.78**	.06	.90
Ca	.25	.20	**.83**	.25	.86
Cu	-.17	**.91**	-.01	.04	.85
Fe	**.98**	.07	.03	.04	.96
La	.33	-.44	.19	**.58**	.67
Mg	.26	.47	**.78**	.22	.94
Mn	**.95**	-.05	.15	.07	.94
Na	-.02	.12	-.03	**.82**	.69
Ni	-.33	**-.70**	-.04	.06	.60
Si	.44	**.64**	-.47	.16	.86
Ti	**.98**	.01	.06	.03	.97
Zn	**.72**	.46	.00	.10	.74
PM10	-.08	-.26	**.74**	-.19	.66
Eigen Value	3.92	2.77	2.74	1.20	
% Variance	30.17	21.34	21.09	9.24	
Cumulative %	30.17	51.51	72.60	81.84	

Factor 1: Fe, Mn, Ti, Zn,
Factor 2: Al, Cu, Si, (Ni)
Factor 3: Ca, Mg, PM10, (Al)
Factor 4: La, Na

All factor analysis

	Factor 1	Factor 2	Factor 3	Factor 4	Factor 5	Communalities
Al	**.63**	-.48	.20	-.07	-.29	0.96
Ba	.27	-.36	**.58**	**.53**	.12	0.90
Ca	**.50**	.09	**-.66**	.46	-.12	0.94
Cu	.36	**.76**	.01	-.14	.19	0.70
Fe	**.73**	-.35	.11	-.08	.25	0.92
La	.39	.40	.41	.28	**-.45**	0.87
Mg	**.59**	-.03	**-.57**	.43	-.23	0.94
Mn	**.54**	-.05	.27	**.53**	.30	0.71
Mo	.05	**.73**	.30	.34	.21	0.89
Na	**.53**	.14	-.46	-.09	.36	0.83
Ni	.32	.42	.05	-.24	**-.51**	0.93
Pb	.29	-.23	-.10	-.40	.04	0.94
Si	**.84**	-.08	.22	-.33	-.05	0.81
Ti	**.68**	.30	.10	-.44	.19	0.90
Zn	.35	-.06	-.41	.07	.05	0.95
PM10	**.75**	-.08	.16	-.12	-.05	0.93
Eigen Value	**3.48**	**2.50**	**2.11**	**2.10**	**2.06**	
% Variance	**24.89**	**17.87**	**15.06**	**14.97**	**14.69**	
Cumulative %	**24.89**	**42.76**	**57.82**	**72.79**	**87.48**	

Factor 1: Al, Ca, Fe, Mg, Mn, PM10
Factor 2: Ca, Mg, Na
Factor 3: Zn, Pb
Factor: Cu, La, Mo
Factor 5: Ba, Mn

Industrial Area Correlation Coefficients

	Al	Ba	Ca	Cu	Fe	La	Mg	Mn	Mo	Na	Ni	Pb	Si	Ti	Zn	PM
Al	1.00															
Ba	**.50**	1.00														
Ca	.16	.11	1.00													
Cu	-.37	.01	.13	1.00												
Fe	.42	**.94**	-.07	-.06	1.00											
La	-.12	-.06	.15	**.72**	-.06	1.00										
Mg	.19	.06	**.99**	.05	-.11	.10	1.00									
Mn	.31	**.85**	.39	.40	**.76**	.19	.31	1.00								
Mo	-.27	-.25	.25	**.84**	-.31	**.90**	.21	.09	1.00							
Na	-.08	**.68**	.12	.36	**.67**	.21	.03	**.71**	.14	1.00						
Ni	-.16	.09	-.01	.54	.08	**.63**	-.04	.29	.52	.10	1.00					
Pb	.07	-.23	-.29	-.10	-.24	-.18	-.22	-.42	-.07	-.42	-.23	1.00				
Si	**-.50**	.31	-.39	**.51**	.41	.21	-.47	.37	.17	**.60**	.40	-.16	1.00			
Ti	**-.59**	.26	-.11	**.59**	.35	.20	-.18	.44	.24	**.65**	.36	-.13	**.89**	1.00		
Zn	-.28	-.17	.18	**.86**	-.21	**.93**	.12	.15	**.99**	.20	.59	-.12	.30	.31	1.00	
PM	.27	**.85**	-.05	.10	**.84**	.07	-.12	**.76**	-.18	.55	.26	-.31	.50	.33	-.05	1.00

Residential Area Correlation Coefficients

	Al	Ca	Cu	Fe	La	Mg	Mn	Na	Ni	Si	Ti	Zn	PM10
Al	1.00												
Ca	**-0.50**	1.00											
Cu	**0.53**	0.15	1.00										
Fe	0.03	0.33	-0.09	1.00									
La	-0.25	0.38	-0.38	0.30	1.00								
Mg	-0.32	**0.88**	0.39	0.30	0.19	1.00							
Mn	-0.16	0.31	-0.20	**0.93**	0.30	0.34	1.00						
Na	0.05	0.06	0.08	0.02	0.12	0.14	0.13	1.00					
Ni	-0.30	-0.21	-0.38	-0.32	0.23	-0.37	-0.27	-0.12	1.00				
Si	**0.80**	-0.07	**0.55**	0.48	-0.02	0.11	0.29	0.10	-0.49	1.00			
Ti	-0.02	0.31	-0.14	**0.97**	0.35	0.33	**0.95**	-0.01	-0.28	0.45	1.00		
Zn	0.19	0.20	0.29	**0.70**	-0.02	0.39	**0.71**	0.24	**-0.53**	**0.50**	**0.66**	1.00	
PM10	**-0.65**	0.35	-0.21	-0.08	0.07	0.34	0.08	-0.07	0.18	**-0.52**	-0.03	-0.20	1.00

Dumpsite Correlation Coefficient

	Al	Ca	Cu	Fe	La	Mg	Mn	Mo	Na	Ni	Si	Ti	Zn	PM
Al	1.00													
Ca	-.17	1.00												
Cu	.23	.17	1.00											
Fe	.41	**-.66**	-.15	1.00										
La	-.27	-.02	**.63**	-.12	1.00									
Mg	.01	**.95**	.05	**-.55**	-.20	1.00								
Mn	.34	-.09	.32	.63	.03	-.06	1.00							
Mo	-.10	-.47	.35	.21	.35	**-.54**	-.04	1.00						
Na	-.20	.05	-.43	-.30	-.28	.12	-.74	.25	1.00					
Ni	-.02	.17	.25	.20	.14	.18	.49	.16	-.25	1.00				
Si	**.91**	-.03	.44	.41	-.17	.09	**.56**	-.09	-.44	.20	1.00			
Ti	.39	-.17	.43	**.61**	.06	-.12	**.94**	.15	**-.69**	**.49**	**.63**	1.00		
Zn	**.73**	.07	**.51**	.28	.00	.16	**.68**	-.23	**-.71**	.12	**.85**	**.68**	1.00	
PM	.05	**-.79**	-.18	**.60**	.24	**-.82**	-.01	.51	-.03	-.18	-.05	.08	-.16	1.00

Traffic Area Correlation Coefficients

	Al	Ba	Ca	Cu	Fe	La	Mg	Mn	Mo	Na	Ni	Pb	Si	Ti	Zn	PM
Al	1.00															
Ba	**.54**	1.00														
Ca	.09	-.18	1.00													
Cu	-.02	-.35	-.16	1.00												
Fe	**.75**	.33	.50	-.04	1.00											
La	.27	.34	-.33	-.16	.21	1.00										
Mg	**.68**	.24	**.69**	-.09	**.70**	-.12	1.00									
Mn	.22	**.60**	.23	-.16	.41	.09	.32	1.00								
Mo	-.36	-.06	-.23	.44	-.25	.14	-.39	.17	1.00							
Na	.09	-.09	.75	.08	.39	-.48	.50	.09	-.06	1.00						
Ni	-.18	-.18	.11	**.50**	-.09	-.40	.02	-.06	.31	.39	1.00					
Pb	.18	.11	.22	-.01	.36	-.26	.20	.31	-.18	.26	-.18	1.00				
Si	**.81**	.36	.26	.04	**.92**	.27	**.57**	.21	-.24	.27	-.09	.26	1.00			
Ti	.43	-.19	-.01	**.54**	.44	.07	.17	.00	.10	.04	.12	.15	**.56**	1.00		
Zn	.33	-.08	**.53**	-.04	.21	-.30	**.76**	.17	-.25	.32	.01	.13	.02	-.05	1.00	
PM	**.60**	.27	.07	.03	**.53**	.31	.32	.27	-.07	-.14	-.28	.05	**.58**	**.58**	-.02	1.00

APPENDIX III
SEM/EDS RESULTS

Spectrum processing :
Peak possibly omitted : 2.310 keV
Processing option : Oxygen by stoichiometry (Normalised)
Number of iter

Element	Weight%	Atomic%	Compound %	Formula
Si K	46.74	33.33	100.00	SiO_2
O	53.26	66.67		
Totals	100.00			

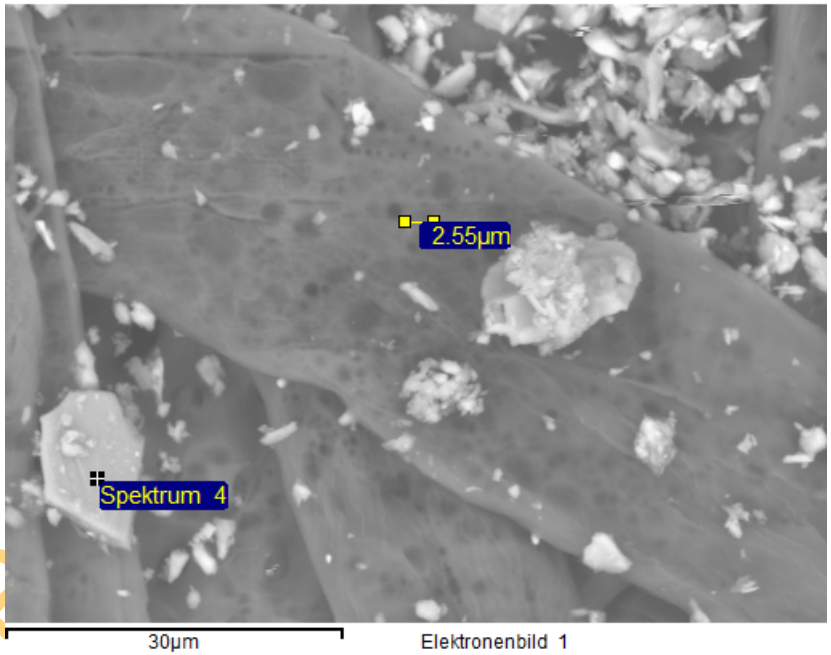

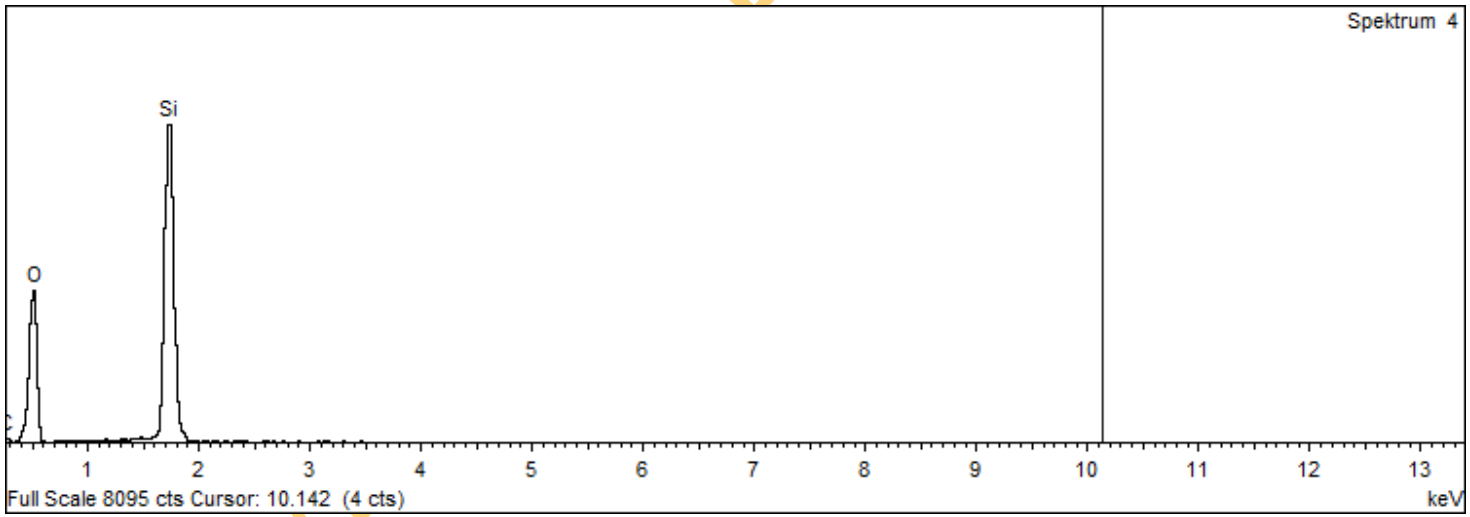

Spectrum processing :
Peak possibly omitted : 2.310 keV
Processing option : Oxygen by stoichiometry (Normalised)
Number of iterations = 2

Element	Weight%	Atomic%	Compound %	Formula
Na K	0.75	0.71	1.01	Na_2O
Mg K	0.36	0.33	0.60	MgO
Al K	8.87	7.23	16.75	Al_2O_3
Si K	27.96	21.89	59.81	SiO_2
K K	5.53	3.11	6.66	K_2O
Ca K	1.60	0.88	2.24	CaO
Ti K	0.63	0.29	1.06	TiO_2
Fe K	9.23	3.63	11.88	FeO
O	45.07	61.94		
Totals	100.00			

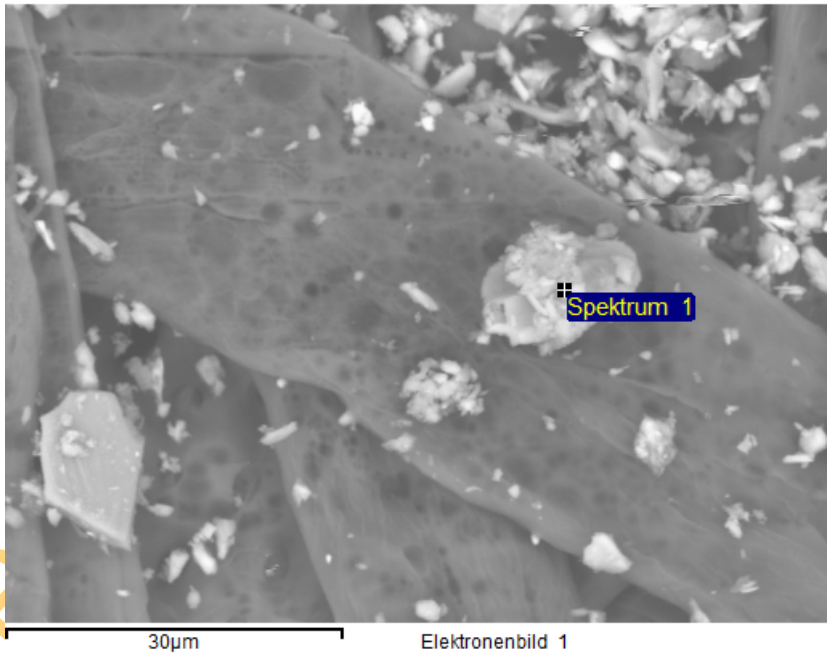

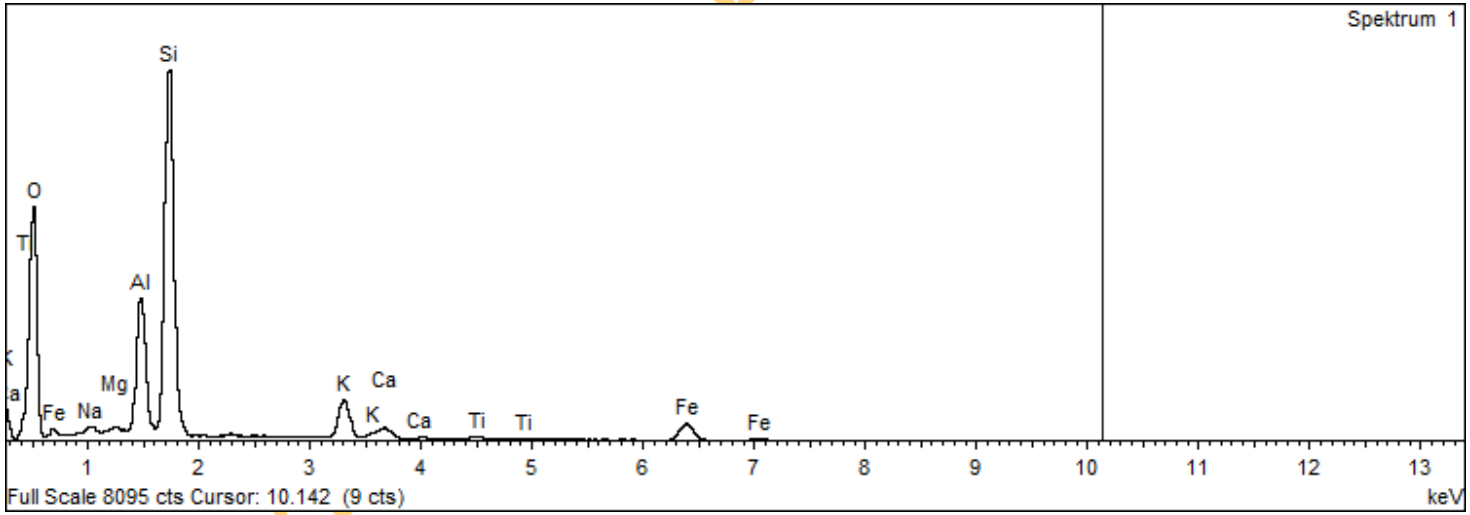

Spectrum processing :
Peak possibly omitted : 4.466 keV
Processing option : Oxygen by stoichiometry (Normalised)
Number of iterations = 2

Element	Weight%	Atomic%	Compound %	Formula
Na K	1.48	1.35	1.99	Na_2O
Al K	9.18	7.17	17.35	Al_2O_3
Si K	31.91	23.91	68.26	SiO_2
K K	10.29	5.54	12.39	K_2O
O	47.14	62.03		
Totals	100.00			

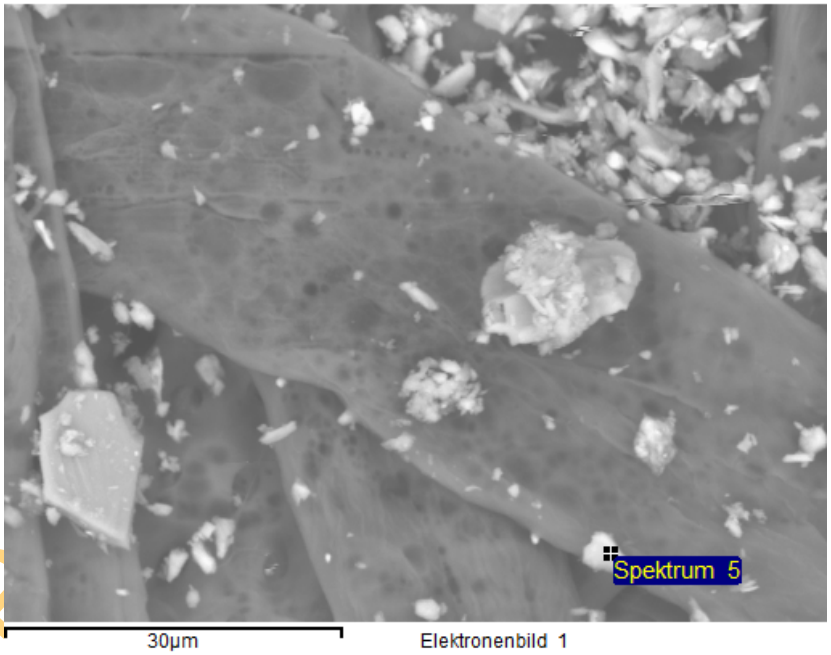

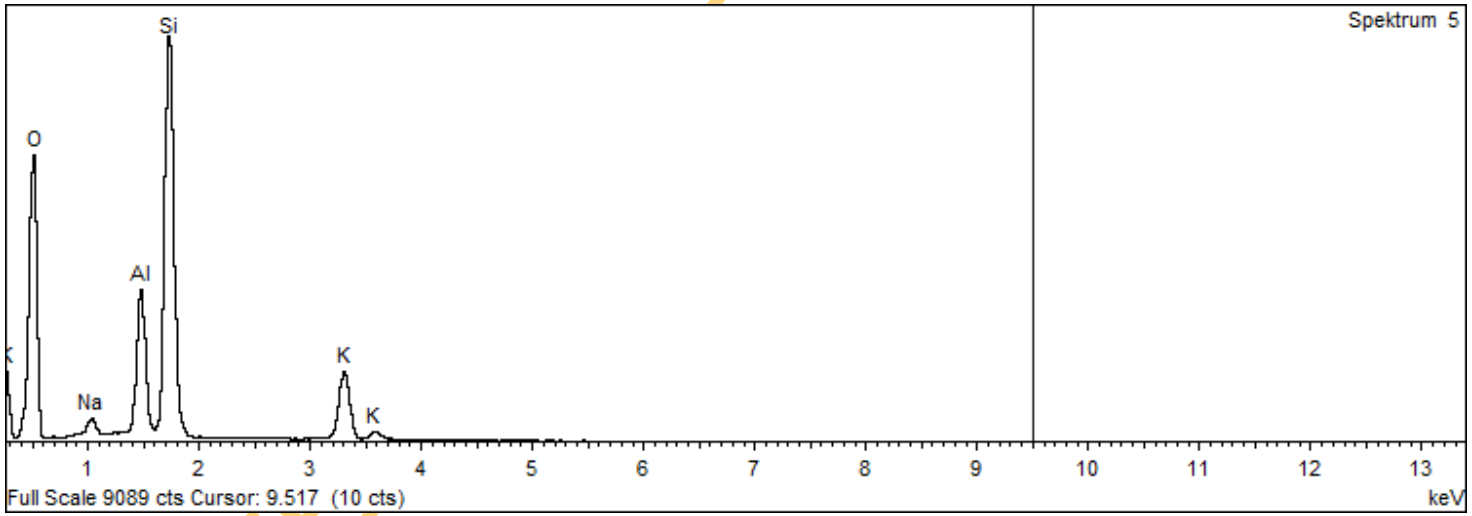

Spectrum processing :
No peaks omitted

Processing option : Oxygen by stoichiometry (Normalised)
Number of iterations = 2

Element	Weight%	Atomic%	Compound %	Formula
Na K	0.30	0.33	0.40	Na_2O
Mg K	1.56	1.62	2.59	MgO
Al K	6.40	5.97	12.10	Al_2O_3
Si K	16.68	14.94	35.68	SiO_2
K K	8.98	5.78	10.81	K_2O
Ti K	2.37	1.24	3.95	TiO_2
Fe K	26.79	12.07	34.46	FeO
O	36.92	58.06		
Totals	100.00			

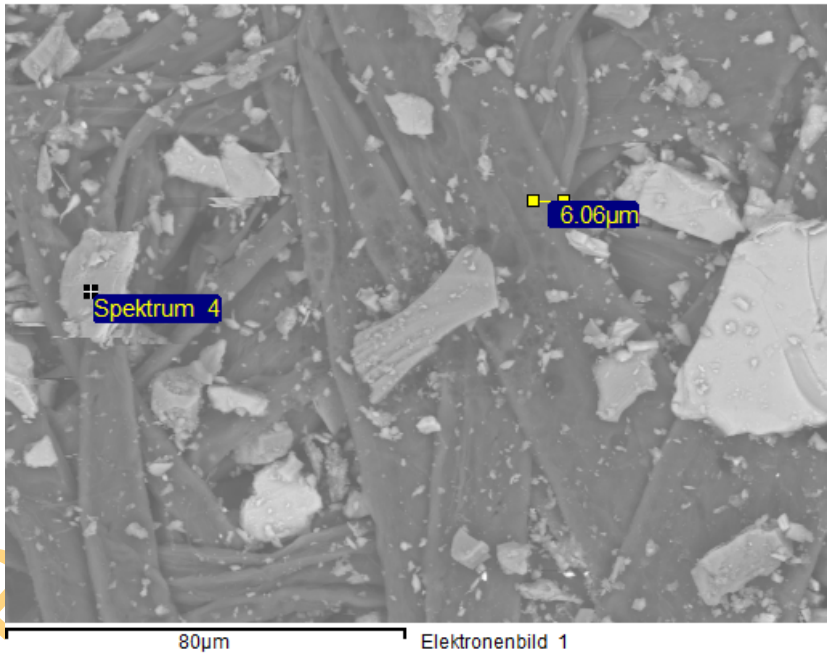

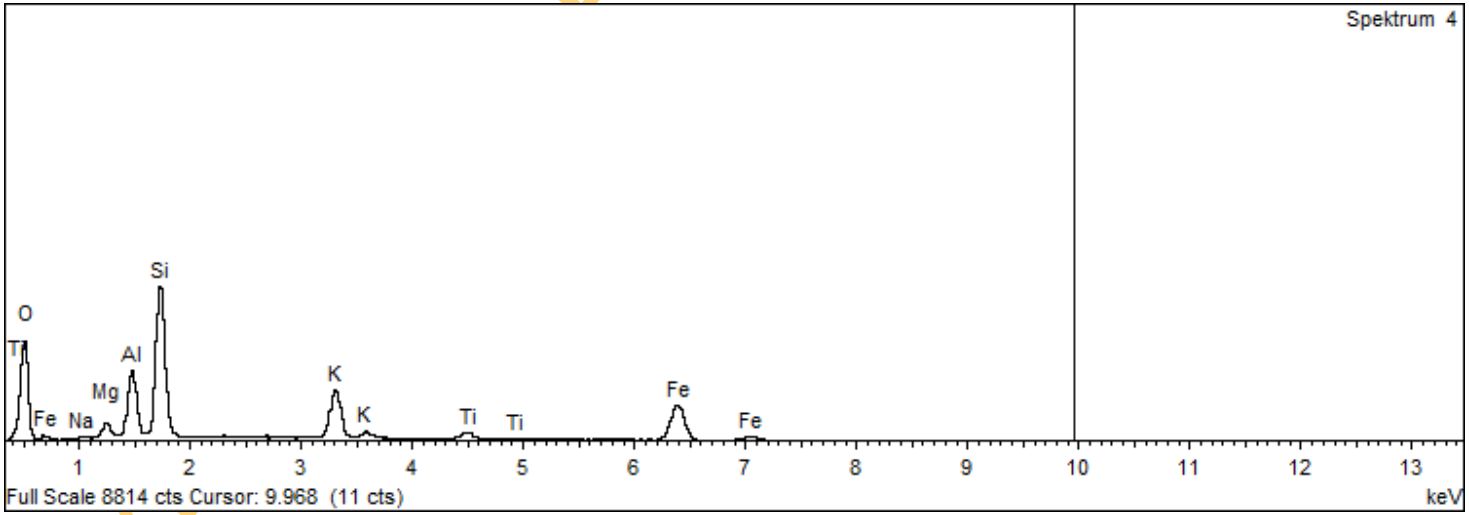

Spectrum processing :
Peak possibly omitted : 8.050 keV

Processing option : Oxygen by stoichiometry (Normalised)
Number of iterations = 2

Element	Weight%	Atomic%	Compound %	Formula
Mg K	2.19	2.19	3.64	MgO
Al K	7.47	6.71	14.11	Al_2O_3
Si K	18.99	16.39	40.62	SiO_2
K K	7.40	4.59	8.91	K_2O
Ti K	1.90	0.96	3.18	TiO_2
Fe K	22.97	9.97	29.55	FeO
O	39.08	59.21		
Totals	100.00			

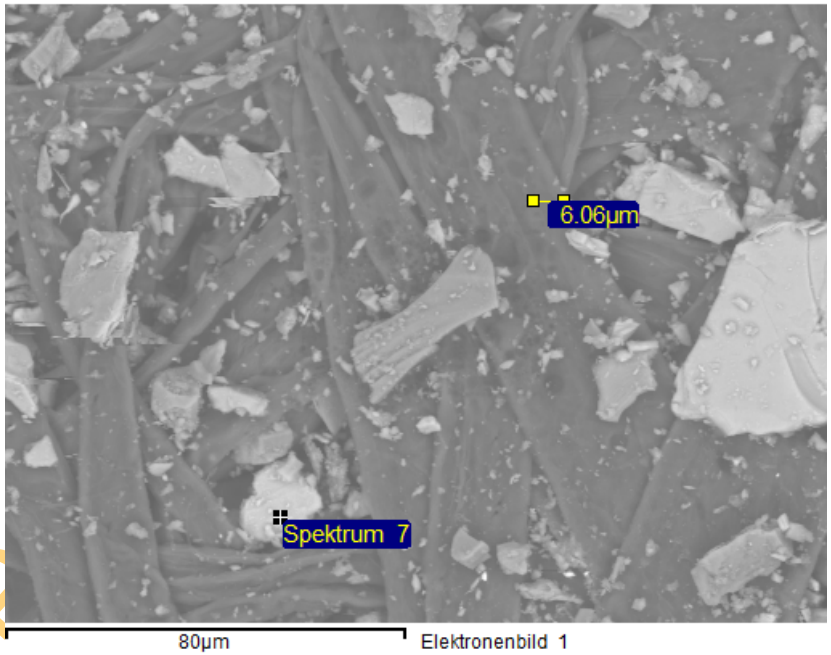

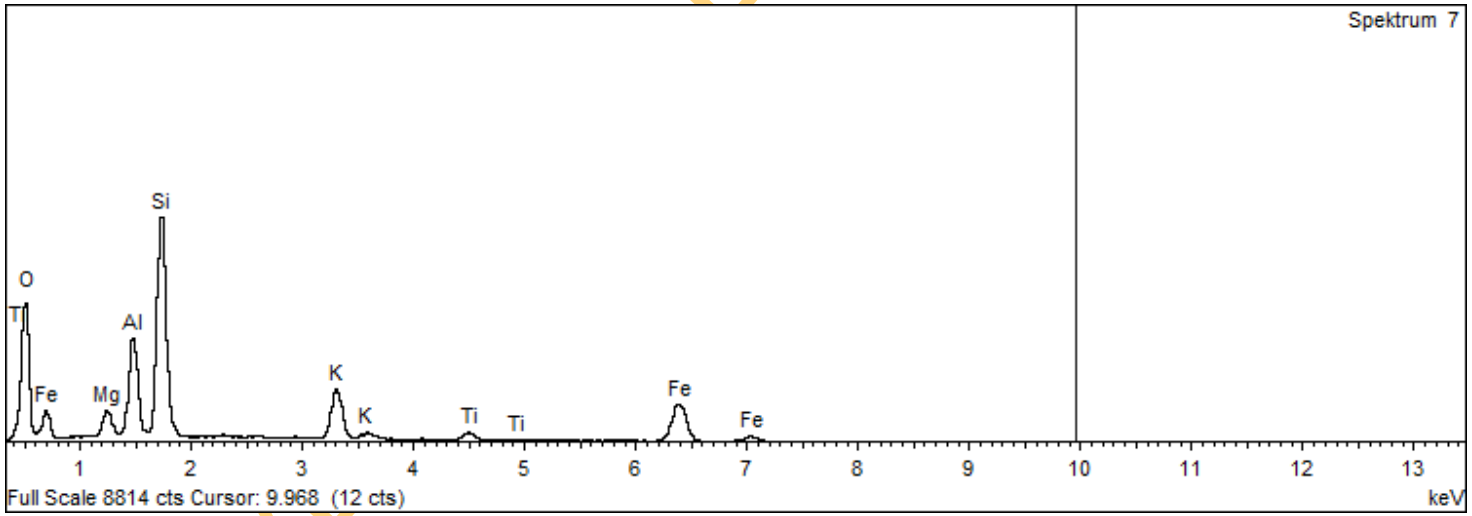

Spectrum processing :
No peaks omitted

Processing option : Oxygen by stoichiometry (Normalised)
Number of iterations = 2

Element	Weight%	Atomic%	Compound %	Formula
Na K	0.59	0.54	0.79	Na_2O
Al K	9.77	7.69	18.46	Al_2O_3
Si K	31.10	23.50	66.53	SiO_2
K K	10.59	5.75	12.76	K_2O
Fe K	1.13	0.43	1.45	FeO
O	46.82	62.10		
Totals	100.00			

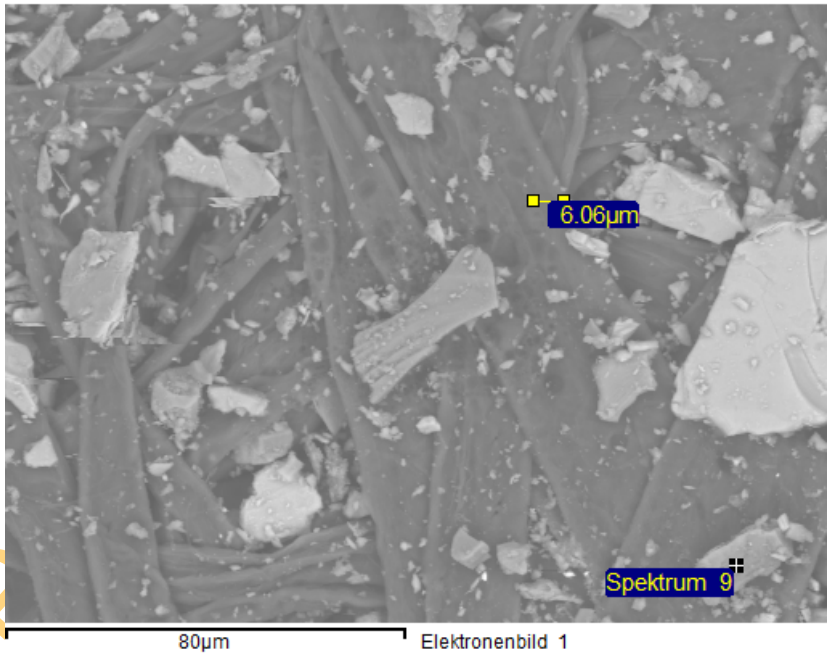

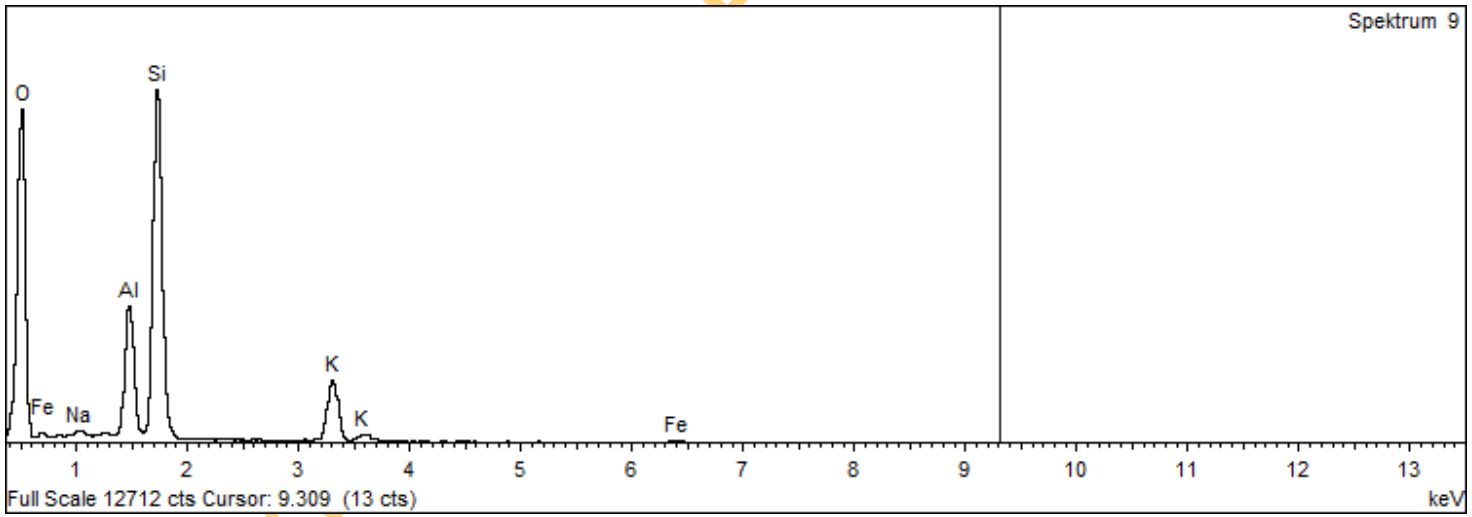

Spectrum processing :
No peaks omitted

Processing option : Oxygen by stoichiometry (Normalised)
Number of iterations = 2

Element	Weight%	Atomic%	Compound %	Formula
Mg K	1.34	1.25	2.23	MgO
Al K	13.14	10.99	24.84	Al_2O_3
Si K	17.37	13.96	37.17	SiO_2
P K	0.65	0.48	1.49	P_2O_5
S K	0.72	0.50	1.79	SO_3
Cl K	0.51	0.33	0.00	
K K	1.33	0.77	1.61	K_2O
Ca K	14.77	8.32	20.67	CaO
Ti K	0.67	0.31	1.11	TiO_2
Fe K	6.67	2.70	8.58	FeO
O	42.81	60.39		
Totals	100.00			

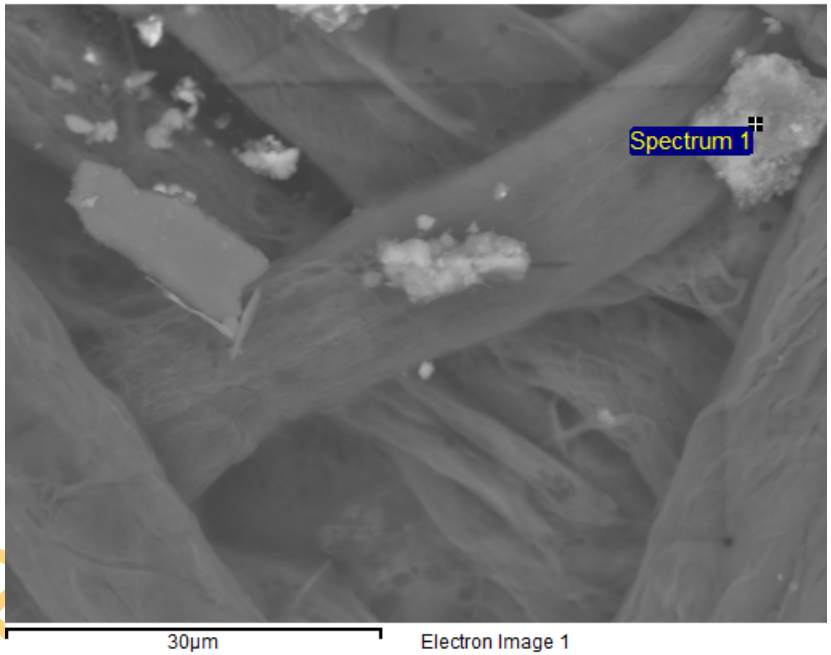

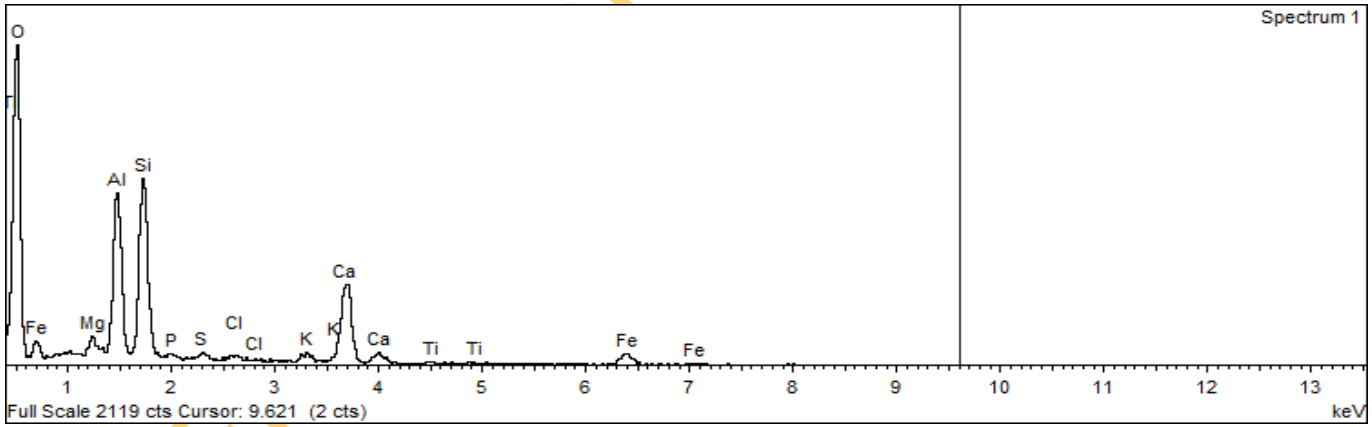

Spectrum processing :
No peaks omitted

Processing option : Oxygen by stoichiometry (Normalised)
Number of iterations = 2

Standard :
Al Al_2O_3 1-Jun-1999 12:00 AM
Si SiO_2 1-Jun-1999 12:00 AM
Fe Fe 1-Jun-1999 12:00 AM

Element	Weight%	Atomic%	Compound %	Formula
Al K	21.79	16.55	41.16	Al_2O_3
Si K	25.88	18.88	55.37	SiO_2
Fe K	2.70	0.99	3.47	FeO
O	49.64	63.58		
Totals	100.00			

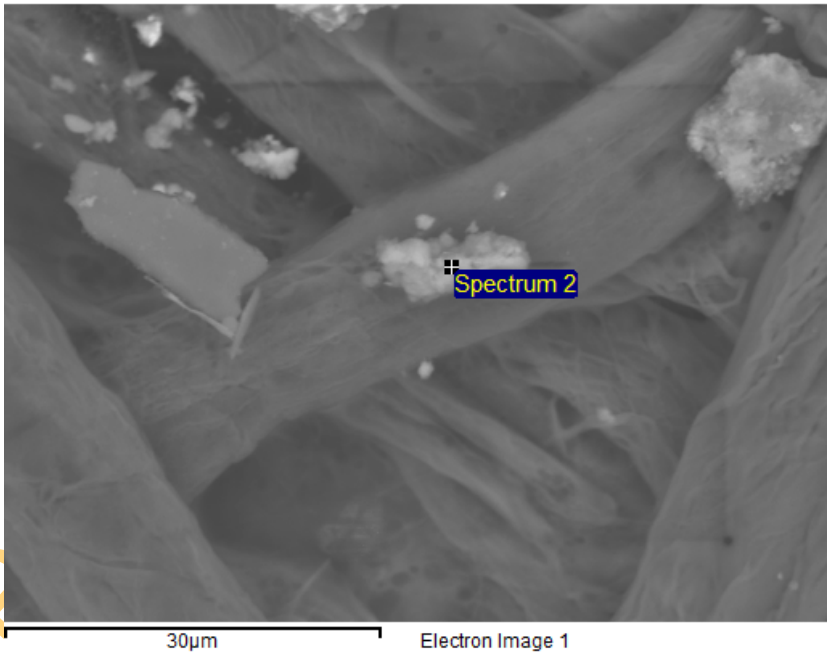

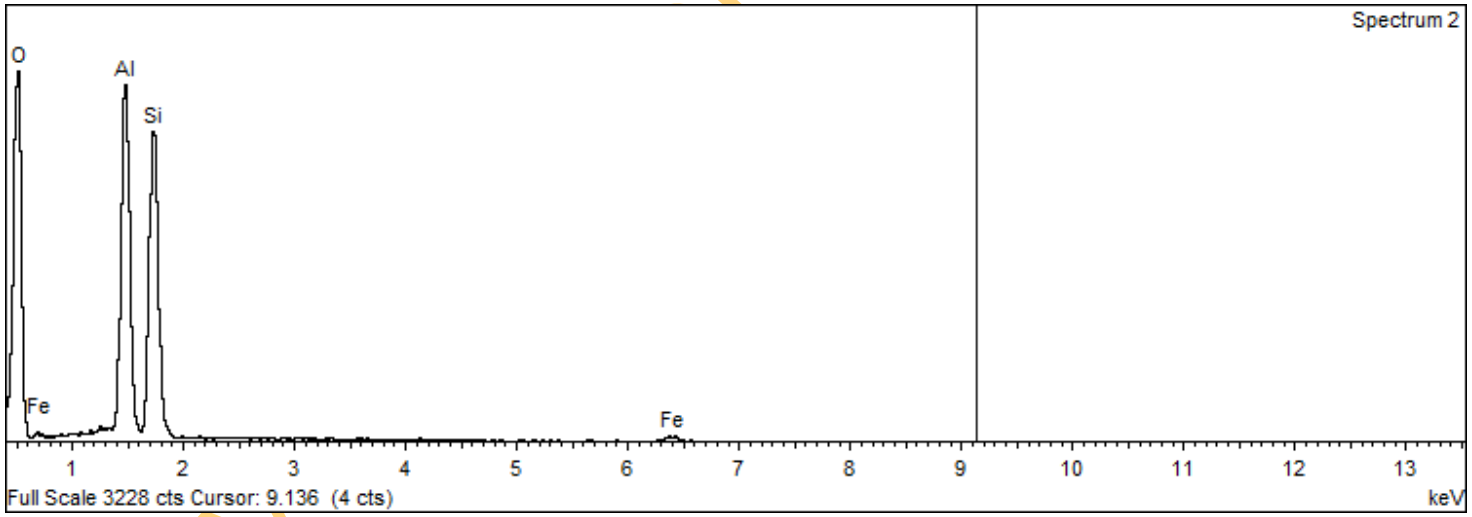

Spectrum processing :
No peaks omitted

Processing option : Oxygen by stoichiometry (Normalised)
Number of iterations = 2
Standard :
Mg MgO 1-Jun-1999 12:00 AM
Al Al_2O_3 1-Jun-1999 12:00 AM
Si SiO_2 1-Jun-1999 12:00 AM
P GaP 1-Jun-1999 12:00 AM
S FeS_2 1-Jun-1999 12:00 AM
Ca Wollastonite 1-Jun-1999 12:00 AM
Ti Ti 1-Jun-1999 12:00 AM
Fe Fe 1-Jun-1999 12:00 AM

Element	Weight%	Atomic%	Compound %	Formula
Mg K	2.26	2.00	3.74	MgO
Al K	13.80	11.01	26.06	Al_2O_3
Si K	20.89	16.01	44.69	SiO_2
P K	1.61	1.12	3.68	P_2O_5
S K	1.72	1.15	4.29	SO_3
Ca K	3.87	2.08	5.42	CaO
Ti K	1.40	0.63	2.34	TiO_2
Fe K	7.60	2.93	9.78	FeO
O	46.86	63.07		
Totals	100.00			

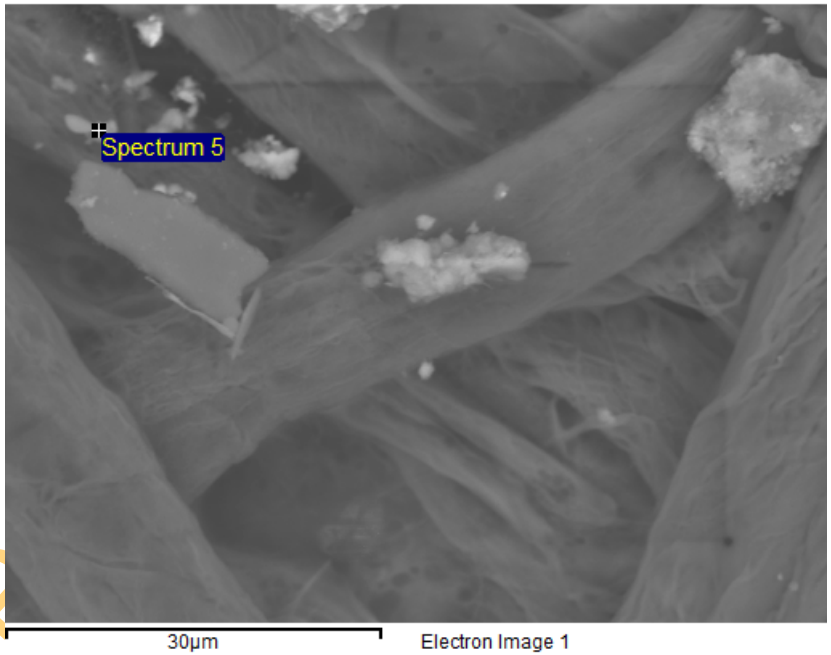

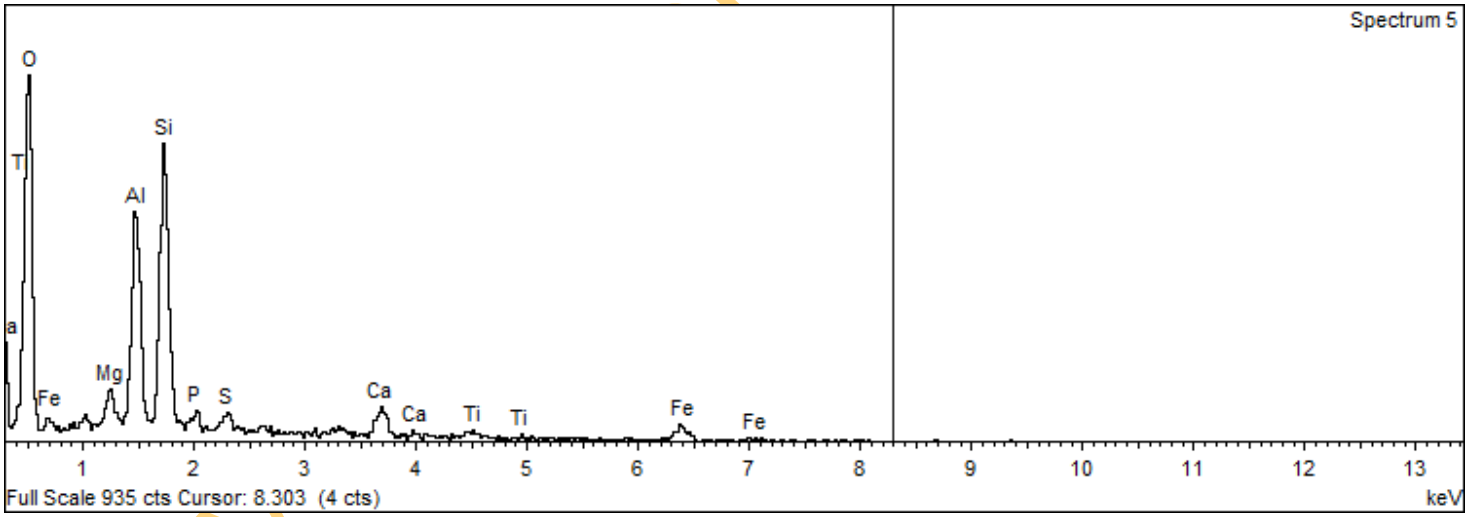

Spectrum processing :
Peak possibly omitted : 4.519 keV

Processing option : Oxygen by stoichiometry (Normalised)
Number of iterations = 2

Standard :
Al Al_2O_3 1-Jun-1999 12:00 AM
Si SiO_2 1-Jun-1999 12:00 AM
K MAD-10 Feldspar 1-Jun-1999 12:00 AM
Ca Wollastonite 1-Jun-1999 12:00 AM
Fe Fe 1-Jun-1999 12:00 AM

Element	Weight%	Atomic%	Compound %	Formula
Al K	15.86	13.58	29.96	Al_2O_3
Si K	18.51	15.22	39.59	SiO_2
K K	2.14	1.27	2.58	K_2O
Ca K	2.21	1.28	3.10	CaO
Fe K	19.25	7.96	24.77	FeO
O	42.03	60.69		
Totals	100.00			

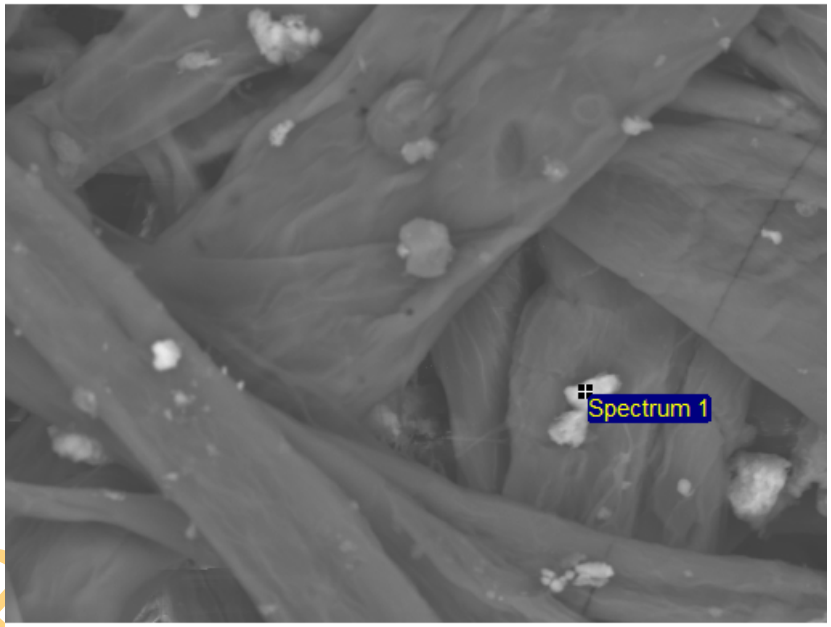

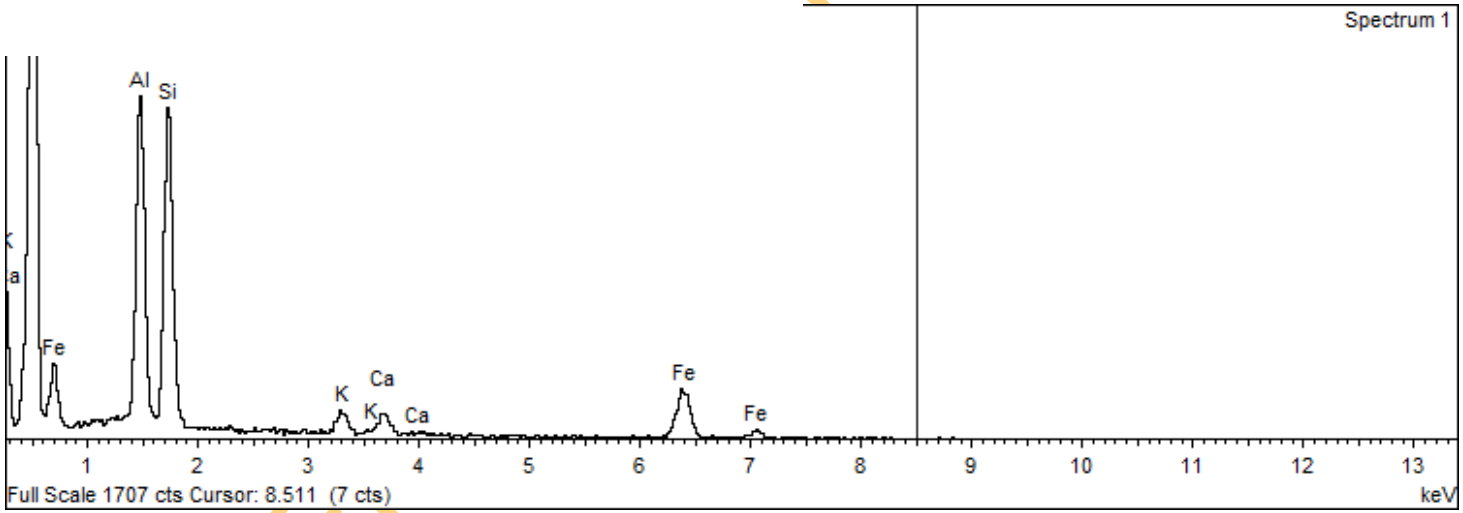

Spectrum processing :
Peak possibly omitted : 4.515 keV

Processing option : Oxygen by stoichiometry (Normalised)
Number of iterations = 2

Standard :
Mg MgO 1-Jun-1999 12:00 AM
Al Al_2O_3 1-Jun-1999 12:00 AM
Si SiO_2 1-Jun-1999 12:00 AM
S FeS_2 1-Jun-1999 12:00 AM
K MAD-10 Feldspar 1-Jun-1999 12:00 AM
Ca Wollastonite 1-Jun-1999 12:00 AM
Fe Fe 1-Jun-1999 12:00 AM

Element	Weight%	Atomic%	Compound%	Formula
Mg K	1.06	1.08	1.76	MgO
Al K	7.06	6.46	13.34	Al_2O_3
Si K	11.03	9.69	23.59	SiO_2
S K	0.95	0.73	2.37	SO_3
K K	0.68	0.43	0.82	K_2O
Ca K	33.77	20.79	47.25	CaO
Fe K	8.45	3.73	10.87	FeO
O	37.00	57.08		
Totals	100.00			

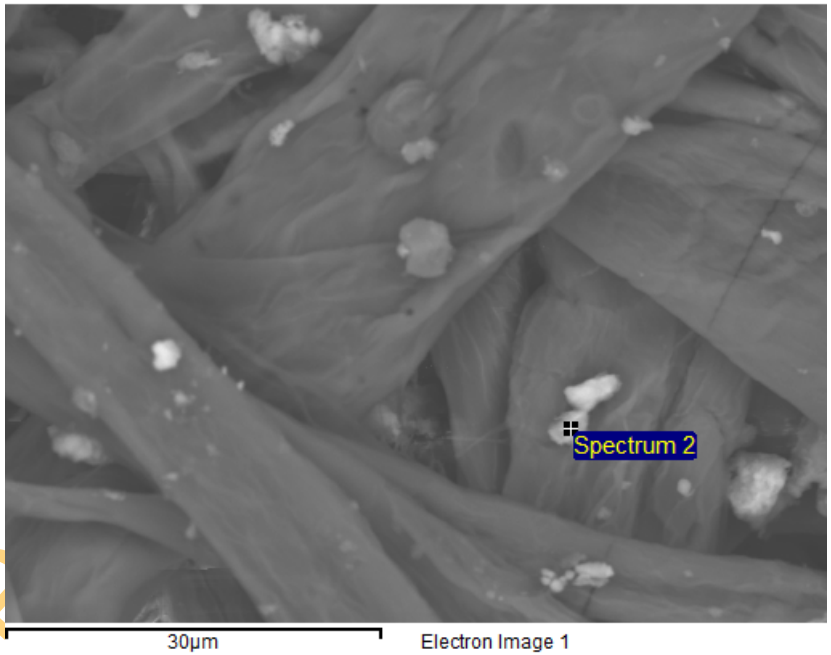

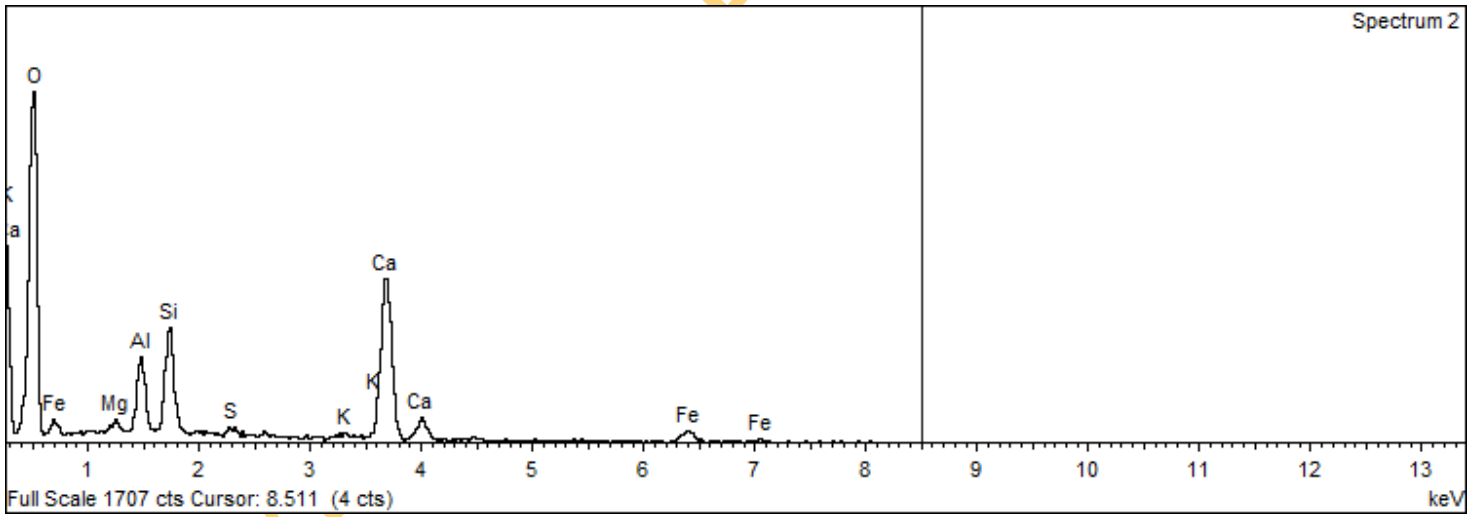

Spectrum processing :
No peaks omitted

Processing option : Oxygen by stoichiometry (Normalised)
Number of iterations = 2

Standard :
Al Al_2O_3 1-Jun-1999 12:00 AM
Si SiO_2 1-Jun-1999 12:00 AM
P GaP 1-Jun-1999 12:00 AM
Ca Wollastonite 1-Jun-1999 12:00 AM
Ti Ti 1-Jun-1999 12:00 AM
Fe Fe 1-Jun-1999 12:00 AM

Element	Weight%	Atomic%	Compound%	Formula
Al K	11.71	10.93	22.12	Al_2O_3
Si K	13.85	12.42	29.63	SiO_2
P K	0.81	0.66	1.85	P_2O_5
Ca K	0.60	0.38	0.84	CaO
Ti K	1.03	0.54	1.72	TiO_2
Fe K	34.08	15.37	43.84	FeO
O	37.93	59.71		
Totals	100.00			

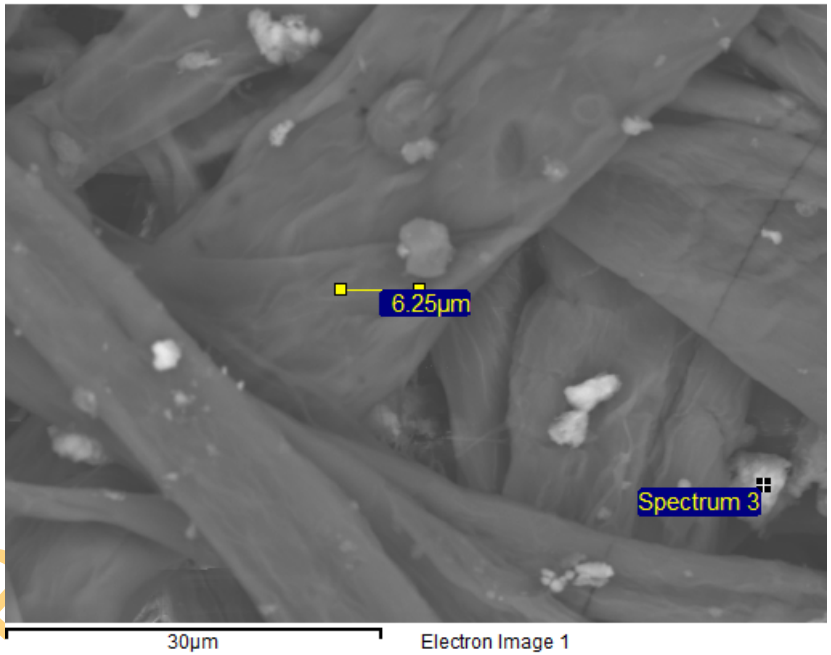

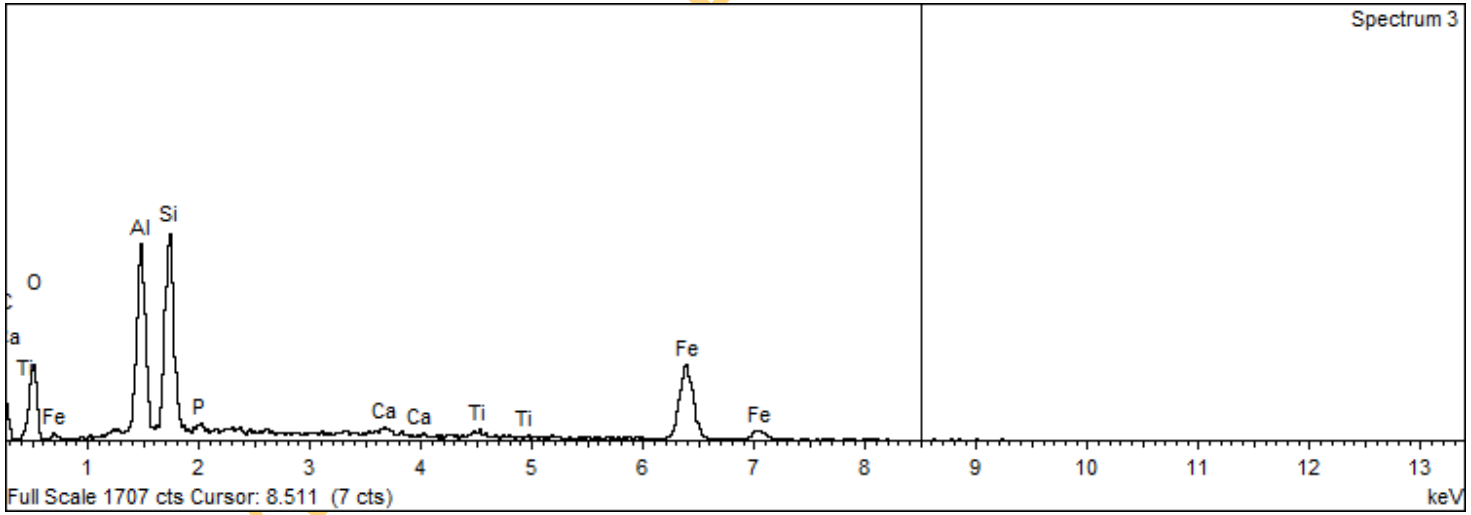

Spectrum processing :
Peak possibly omitted : 3.690 keV

Processing option : Oxygen by stoichiometry (Normalised)
Number of iterations = 2

Standard :
Al Al_2O_3 1-Jun-1999 12:00 AM
Si SiO_2 1-Jun-1999 12:00 AM
Ti Ti 1-Jun-1999 12:00 AM
Fe Fe 1-Jun-1999 12:00 AM

Element	Weight%	Atomic%	Compd%	Formula
Al K	2.13	2.06	4.02	Al_2O_3
Si K	1.52	1.42	3.25	SiO_2
Ti K	54.53	29.77	90.95	TiO_2
Fe K	1.38	0.65	1.78	FeO
O	40.44	66.11		
Totals	100.00			

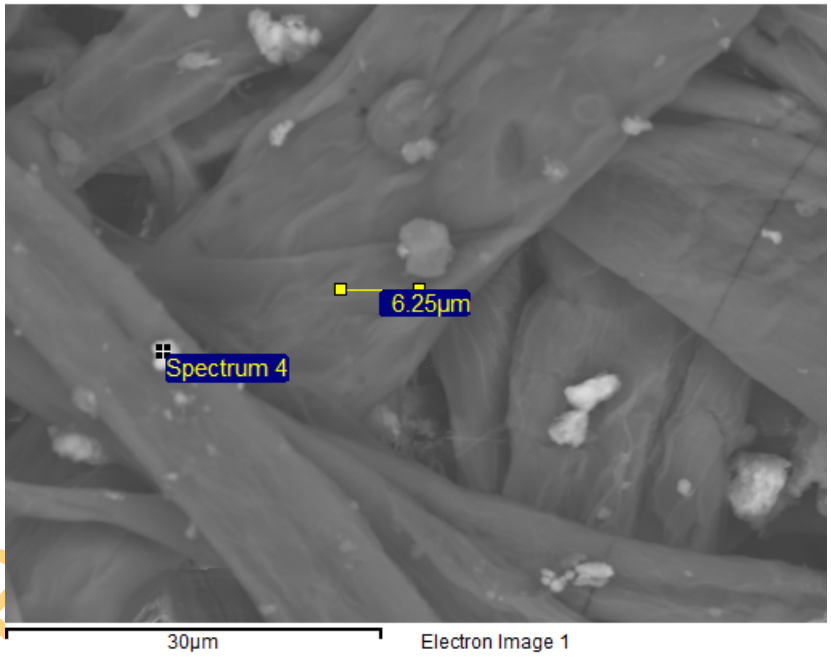

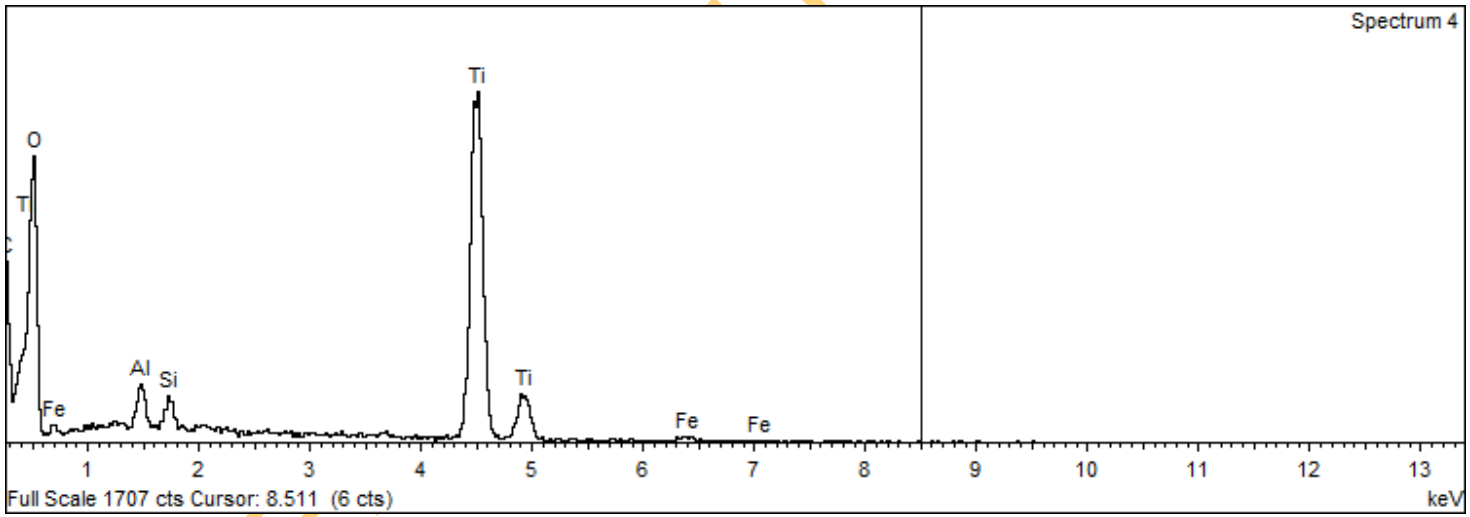

Spectrum processing :
Peak possibly omitted : 4.555 keV

Processing option : Oxygen by stoichiometry (Normalised)
Number of iterations = 2

Standard :
Mg MgO 1-Jun-1999 12:00 AM
Al Al_2O_3 1-Jun-1999 12:00 AM
Si SiO_2 1-Jun-1999 12:00 AM
K MAD-10 Feldspar 1-Jun-1999 12:00 AM
Ca Wollastonite 1-Jun-1999 12:00 AM
Fe Fe 1-Jun-1999 12:00 AM

Element	Weight%	Atomic%	Compd%	Formula
Mg K	0.85	0.74	1.41	MgO
Al K	13.94	10.95	26.34	Al_2O_3
Si K	28.03	21.14	59.96	SiO_2
K K	2.18	1.18	2.62	K_2O
Ca K	1.08	0.57	1.51	CaO
Fe K	6.34	2.41	8.16	FeO
O	47.58	63.01		
Totals	100.00			

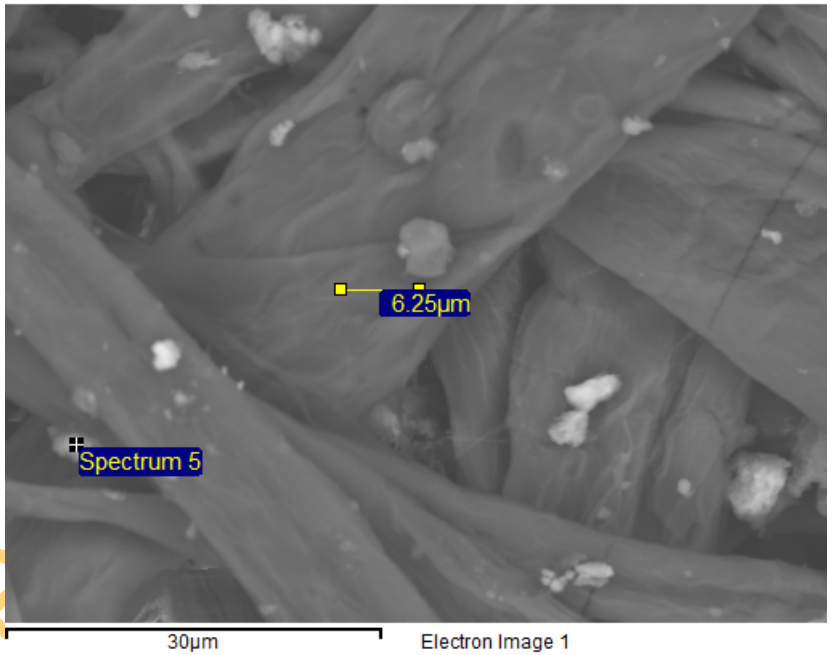

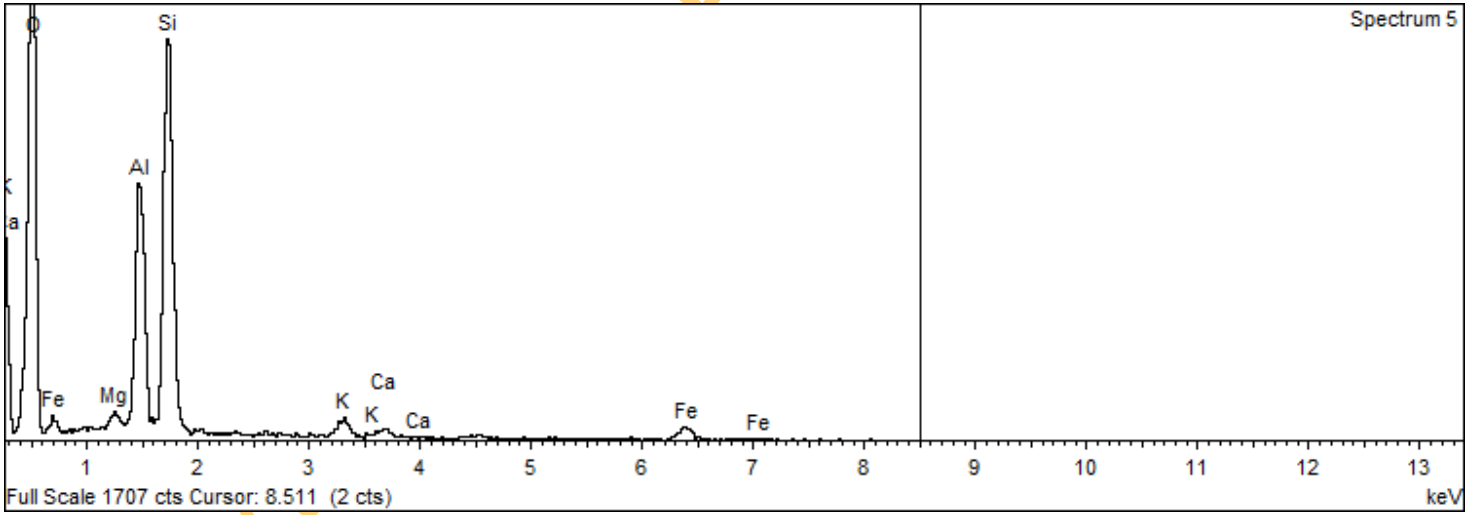

Spectrum processing :
Peak possibly omitted : 2.625 keV

Processing option : Oxygen by stoichiometry (Normalised)
Number of iterations = 2

Standard :
Al Al_2O_3 1-Jun-1999 12:00 AM
Si SiO_2 1-Jun-1999 12:00 AM
P GaP 1-Jun-1999 12:00 AM
K MAD-10 Feldspar 1-Jun-1999 12:00 AM
Ca Wollastonite 1-Jun-1999 12:00 AM
Fe Fe 1-Jun-1999 12:00 AM

Element	Weight%	Atomic%	Compd%	Formula
Al K	17.85	14.33	33.73	Al_2O_3
Si K	22.50	17.35	48.13	SiO_2
P K	0.61	0.42	1.39	P_2O_5
K K	0.46	0.26	0.56	K_2O
Ca K	2.15	1.16	3.01	CaO
Fe K	10.25	3.98	13.19	FeO
O	46.18	62.51		
Totals	100.00			

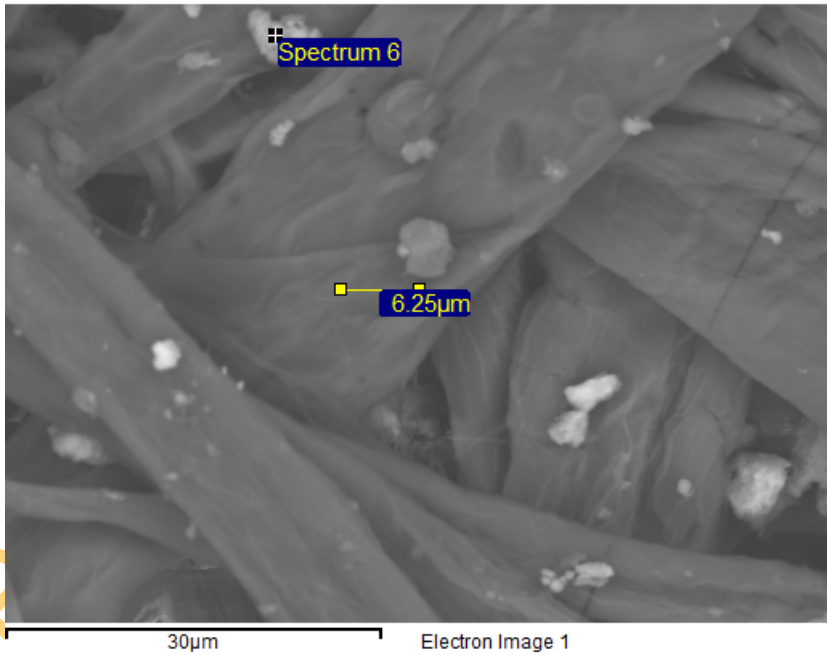

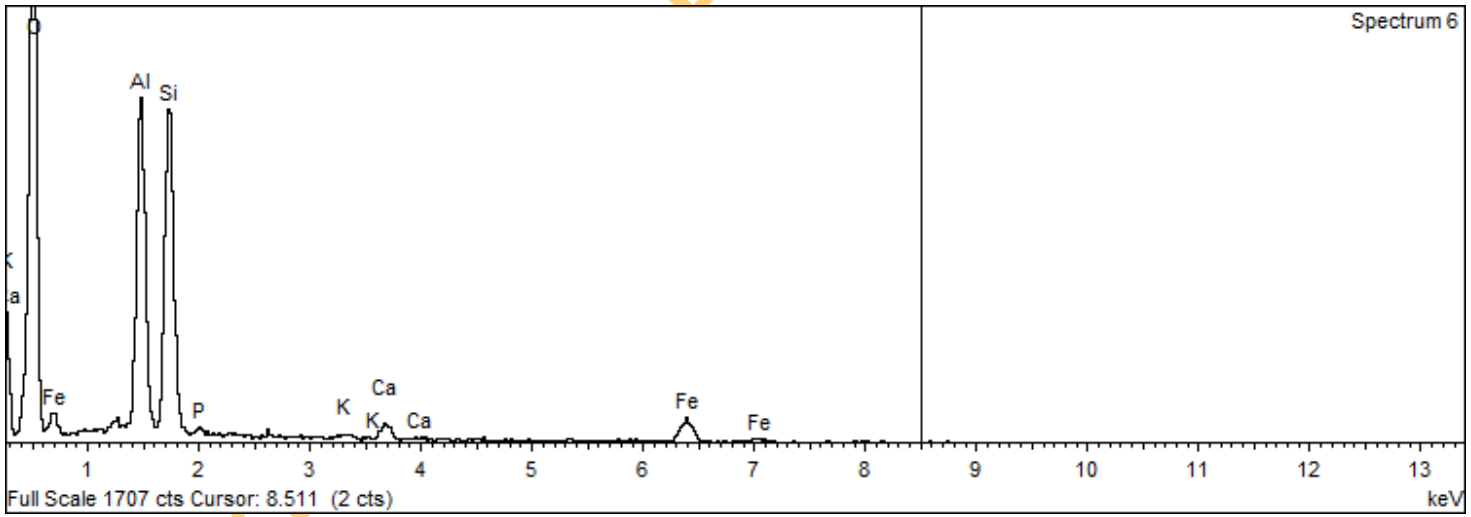

Spectrum processing :
No peaks omitted

Processing option : Oxygen by stoichiometry (Normalised)
Number of iterations = 2

Standard :
Mg MgO 1-Jun-1999 12:00 AM
Al Al_2O_3 1-Jun-1999 12:00 AM
Si SiO_2 1-Jun-1999 12:00 AM
K MAD-10 Feldspar 1-Jun-1999 12:00 AM
Ca Wollastonite 1-Jun-1999 12:00 AM
Ti Ti 1-Jun-1999 12:00 AM
Fe Fe 1-Jun-1999 12:00 AM

Element	Weight%	Atomic%	Compound%	Formula
Mg K	2.27	2.09	3.77	MgO
Al K	13.39	11.08	25.30	Al_2O_3
Si K	19.26	15.31	41.20	SiO_2
K K	2.56	1.46	3.08	K_2O
Ca K	2.11	1.17	2.95	CaO
Ti K	8.10	3.78	13.51	TiO_2
Fe K	7.92	3.17	10.19	FeO
O	44.39	61.95		
Totals	100.00			

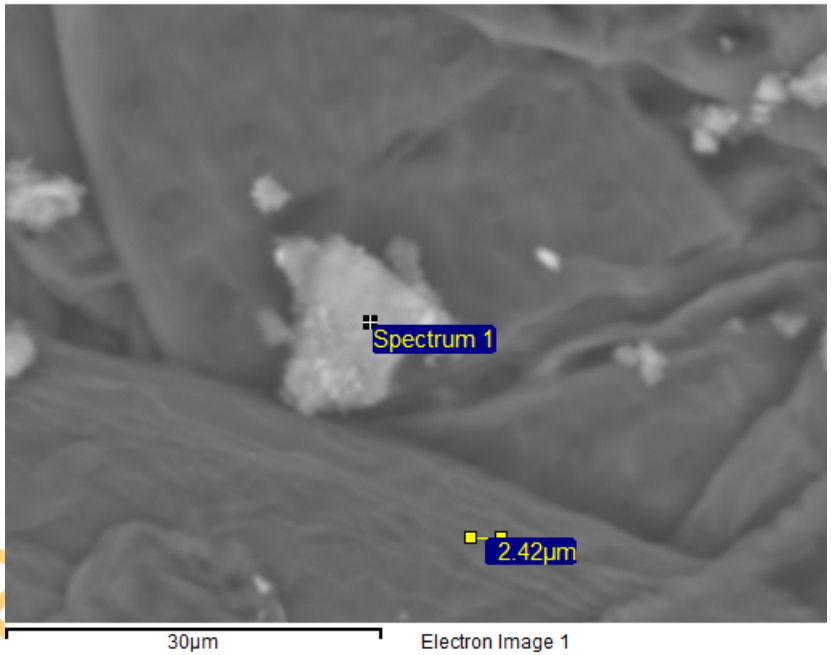

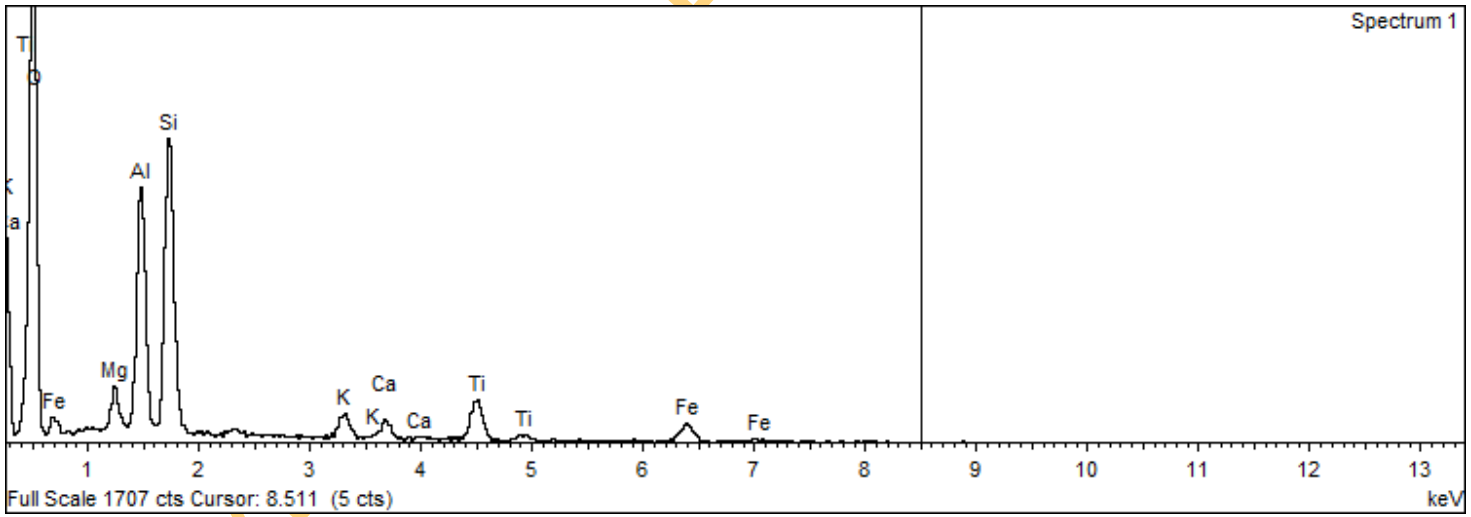

Spectrum processing :
No peaks omitted

Processing option : Oxygen by stoichiometry (Normalised)
Number of iterations = 2

Standard :
Na Albite 1-Jun-1999 12:00 AM
Al Al_2O_3 1-Jun-1999 12:00 AM
Si SiO_2 1-Jun-1999 12:00 AM
S FeS_2 1-Jun-1999 12:00 AM
Ca Wollastonite 1-Jun-1999 12:00 AM

Element	Weight%	Atomic%	Compd%	Formula
Na K	0.00	0.00	0.00	Na_2O
Al K	0.49	0.41	0.93	Al_2O_3
Si K	1.06	0.85	2.26	SiO_2
S K	22.75	16.04	56.81	SO_3
Ca K	28.59	16.13	40.00	CaO
O	47.11	66.57		
Totals	100.00			

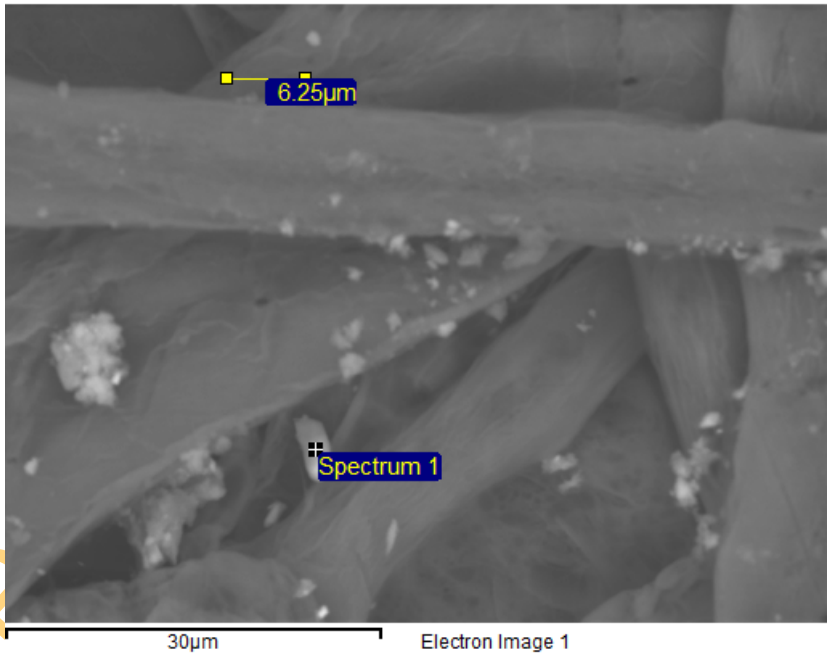

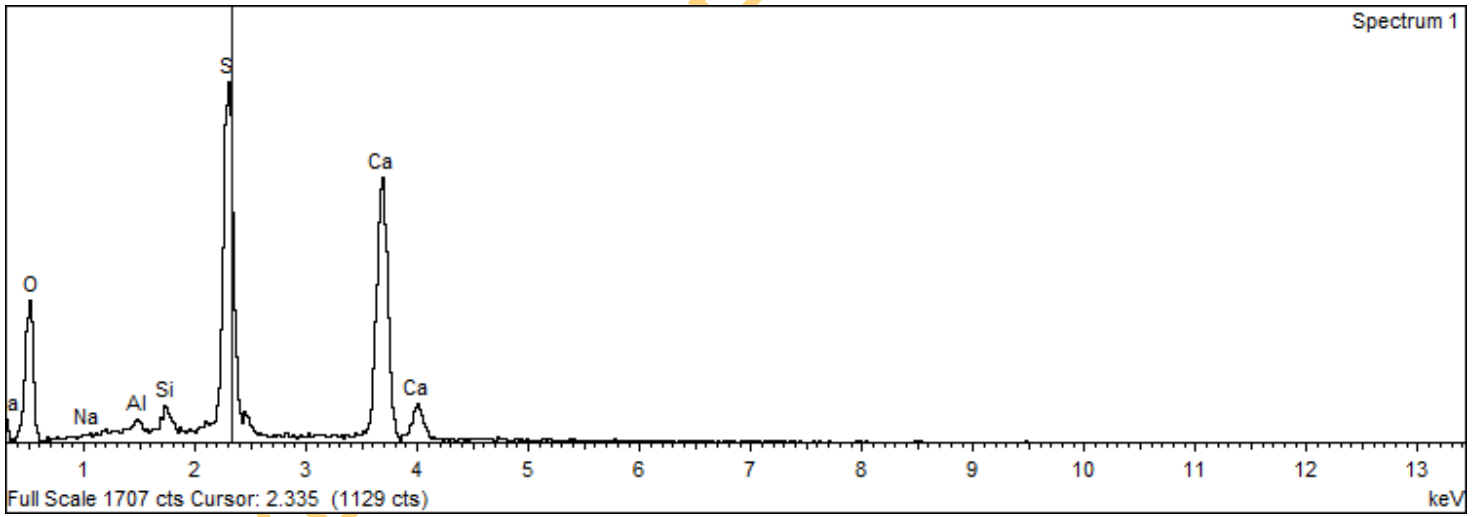

Spectrum processing :
Peak possibly omitted : 4.495 keV
Processing option : Oxygen by stoichiometry (Normalised)
Number of iterations = 2
Standard :
Na Albite 1-Jun-1999 12:00 AM
Mg MgO 1-Jun-1999 12:00 AM
Al Al_2O_3 1-Jun-1999 12:00 AM
Si SiO_2 1-Jun-1999 12:00 AM
P GaP 1-Jun-1999 12:00 AM
S FeS_2 1-Jun-1999 12:00 AM
K MAD-10 Feldspar 1-Jun-1999 12:00 AM
Ca Wollastonite 1-Jun-1999 12:00 AM
Fe Fe 1-Jun-1999 12:00 AM

Element	Weight%	Atomic%	Compd%	Formula
Na K	0.00	0.00	0.00	Na_2O
Mg K	1.41	1.29	2.33	MgO
Al K	12.97	10.74	24.51	Al_2O_3
Si K	19.04	15.14	40.73	SiO_2
P K	1.66	1.20	3.81	P_2O_5
S K	0.62	0.43	1.55	SO_3
K K	0.54	0.31	0.65	K_2O
Ca K	9.44	5.26	13.20	CaO
Fe K	10.27	4.11	13.21	FeO
O	44.05	61.51		
Totals	100.00			

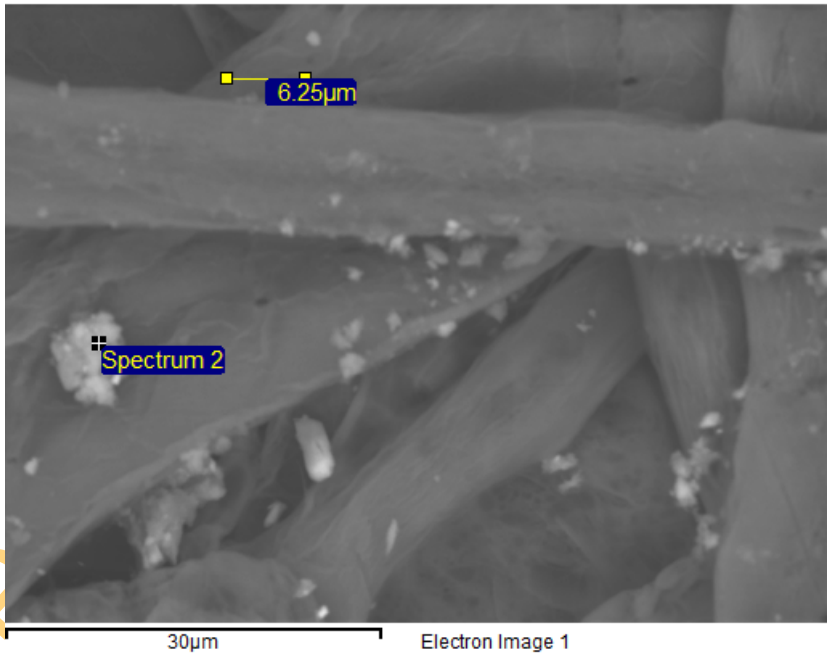

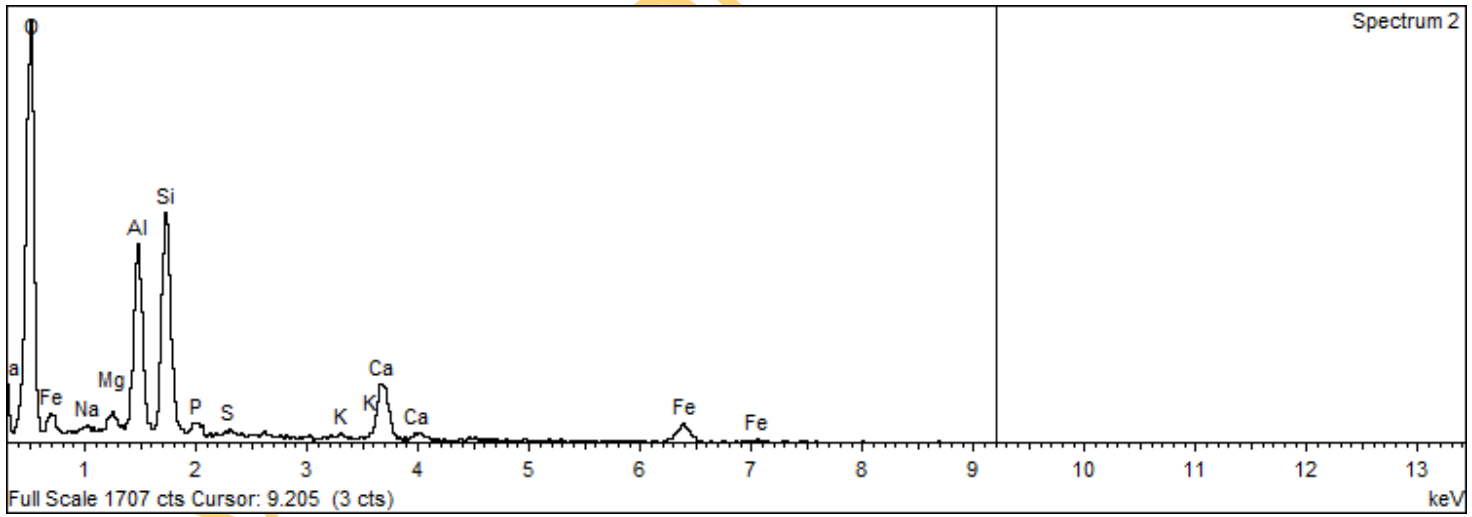

Spectrum processing :
No peaks omitted
Processing option : Oxygen by stoichiometry (Normalised)
Number of iterations = 2
Standard :
Mg MgO 1-Jun-1999 12:00 AM
Al Al_2O_3 1-Jun-1999 12:00 AM
Si SiO_2 1-Jun-1999 12:00 AM
P GaP 1-Jun-1999 12:00 AM
K MAD-10 Feldspar 1-Jun-1999 12:00 AM
Ca Wollastonite 1-Jun-1999 12:00 AM
Ti Ti 1-Jun-1999 12:00 AM
Fe Fe 1-Jun-1999 12:00 AM

Element	Weight%	Atomic%	Compound%	Formula
Mg K	0.80	0.70	1.33	MgO
Al K	15.82	12.51	29.89	Al_2O_3
Si K	23.37	17.75	50.00	SiO_2
P K	1.36	0.94	3.11	P_2O_5
K K	0.47	0.26	0.57	K_2O
Ca K	4.13	2.20	5.78	CaO
Ti K	1.33	0.59	2.22	TiO_2
Fe K	5.52	2.11	7.10	FeO
O	47.19	62.94		
Totals	100.00			

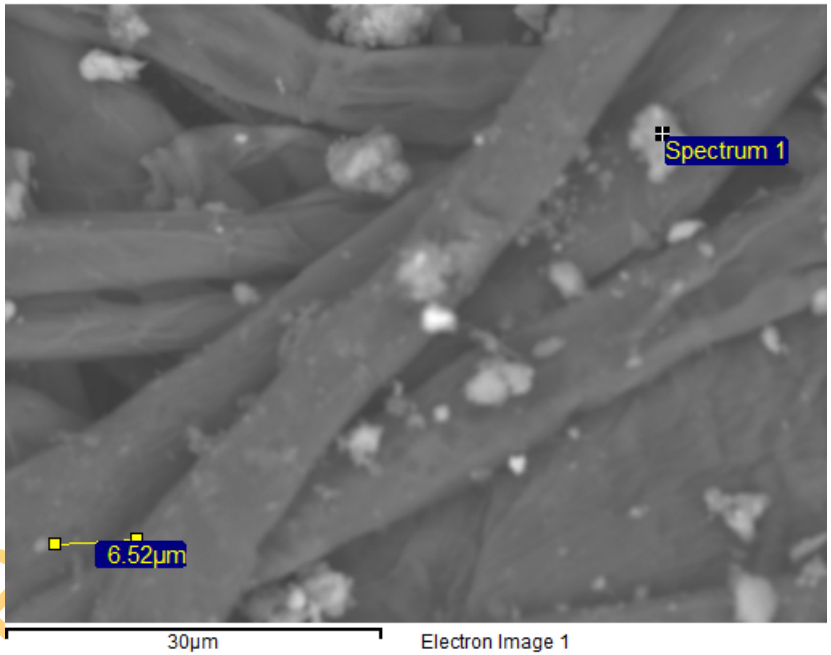

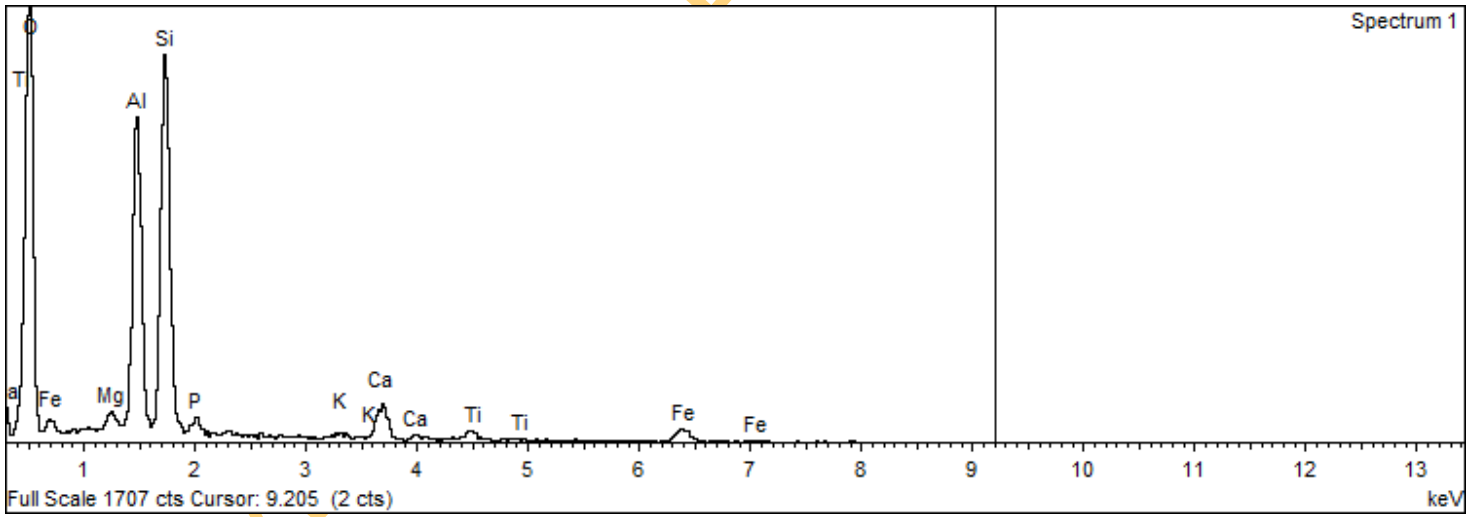

Spectrum processing :
Peaks possibly omitted : 1.040, 2.310 keV

Processing option : Oxygen by stoichiometry (Normalised)
Number of iterations = 2

Standard :
Al Al_2O_3 1-Jun-1999 12:00 AM
Si SiO_2 1-Jun-1999 12:00 AM
K MAD-10 Feldspar 1-Jun-1999 12:00 AM
Ca Wollastonite 1-Jun-1999 12:00 AM
Ti Ti 1-Jun-1999 12:00 AM
Fe Fe 1-Jun-1999 12:00 AM

Element	Weight%	Atomic%	Compd%	Formula
Al K	16.20	12.31	30.60	Al_2O_3
Si K	29.87	21.81	63.90	SiO_2
K K	0.64	0.34	0.77	K_2O
Ca K	1.33	0.68	1.86	CaO
Ti K	0.84	0.36	1.40	TiO_2
Fe K	1.14	0.42	1.47	FeO
O	49.99	64.08		
Totals	100.00			

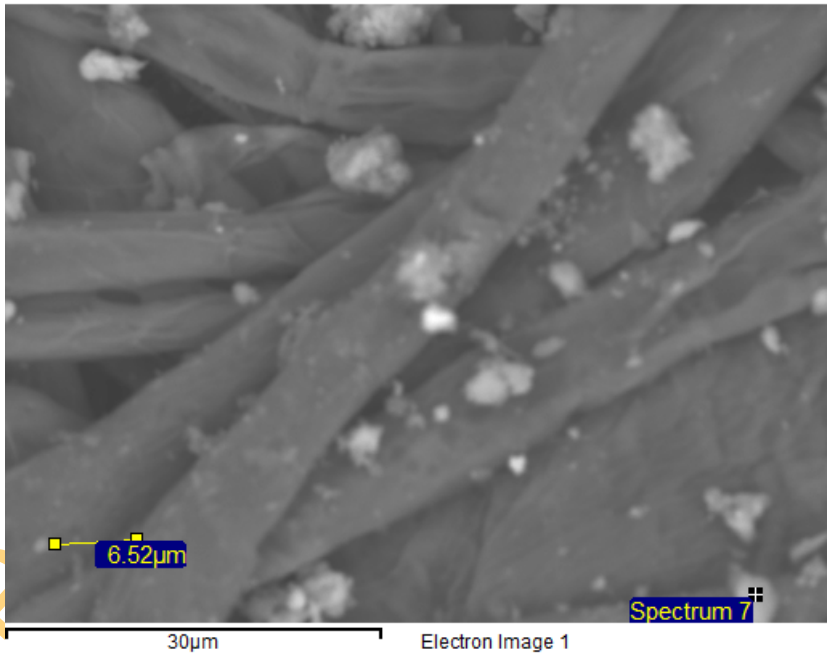

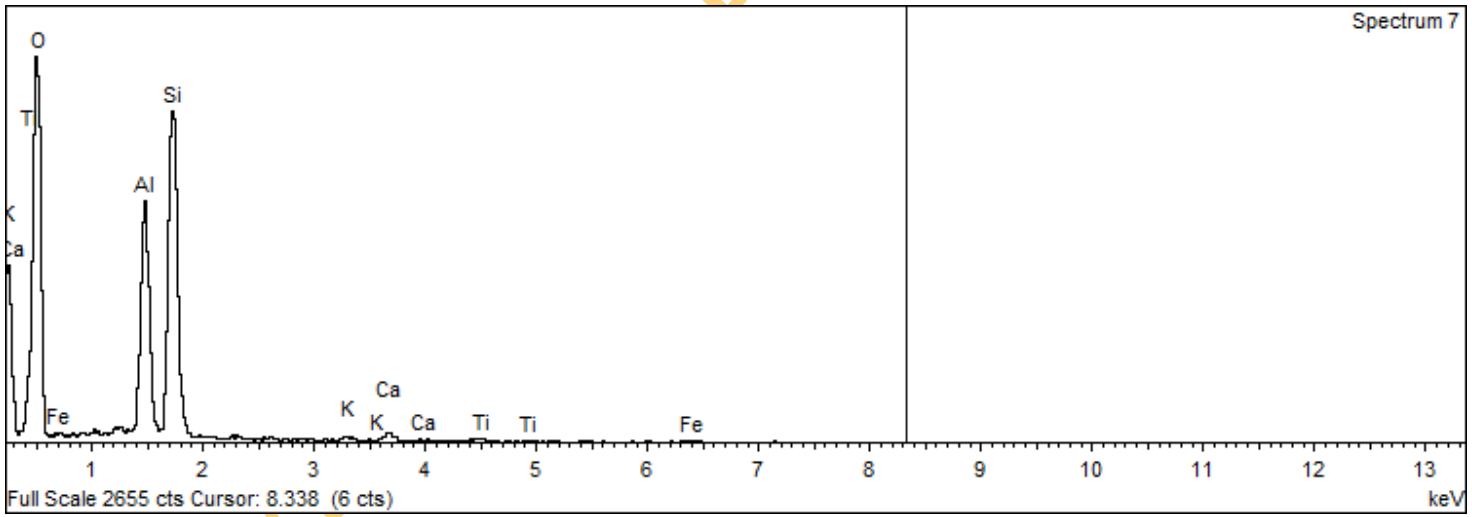

Spectrum processing :
Peaks possibly omitted : 2.325, 4.505 keV

Processing option : Oxygen by stoichiometry (Normalised)
Number of iterations = 2

Standard :
Mg MgO 1-Jun-1999 12:00 AM
Al Al_2O_3 1-Jun-1999 12:00 AM
Si SiO_2 1-Jun-1999 12:00 AM
K MAD-10 Feldspar 1-Jun-1999 12:00 AM
Ca Wollastonite 1-Jun-1999 12:00 AM
Fe Fe 1-Jun-1999 12:00 AM

Element	Weight%	Atomic%	Compd%	Formula
Mg K	0.71	0.60	1.17	MgO
Al K	13.74	10.49	25.96	$Al2O_3$
Si K	31.22	22.90	66.79	SiO_2
K K	2.15	1.14	2.59	K2O
Ca K	0.73	0.37	1.02	CaO
Fe K	1.91	0.71	2.46	FeO
O	49.54	63.79		
Totals	100.00			

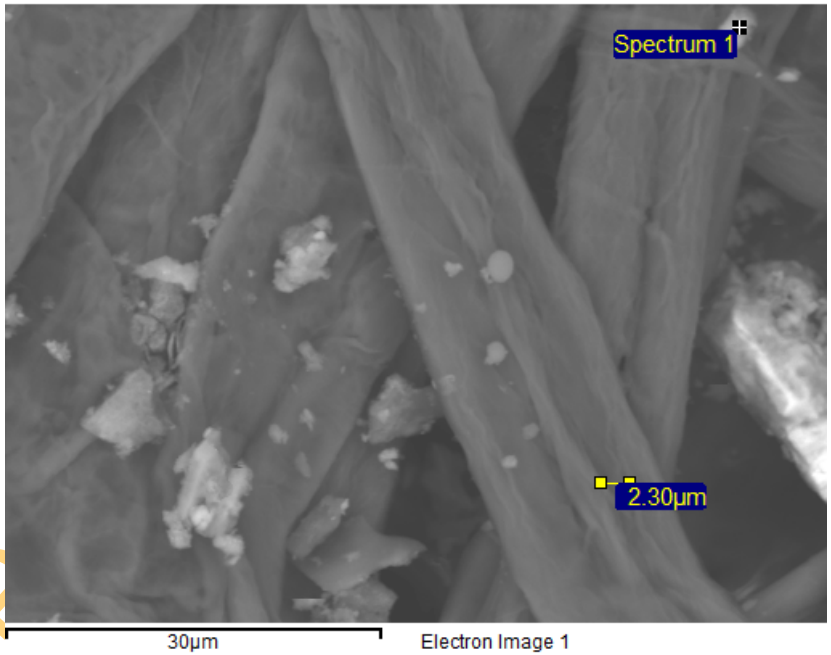

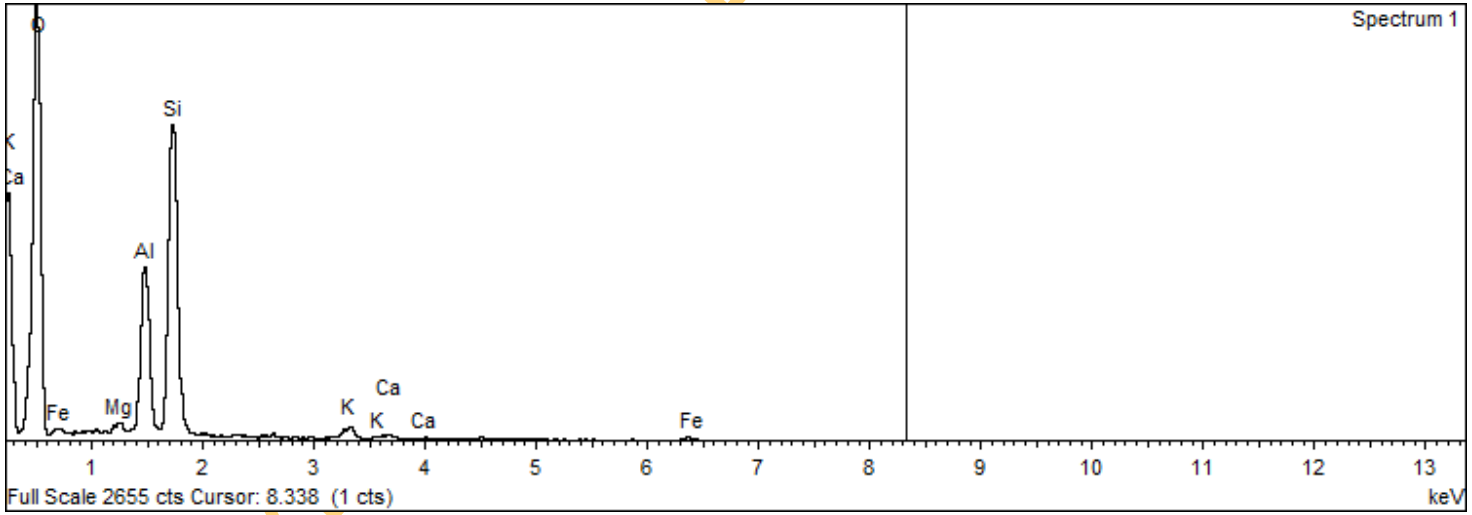

Spectrum processing :
No peaks omitted

Processing option : Oxygen by stoichiometry (Normalised)
Number of iterations = 2

Standard :
Mg MgO 1-Jun-1999 12:00 AM
Al Al2O3 1-Jun-1999 12:00 AM
Si SiO2 1-Jun-1999 12:00 AM
P GaP 1-Jun-1999 12:00 AM
K MAD-10 Feldspar 1-Jun-1999 12:00 AM
Ca Wollastonite 1-Jun-1999 12:00 AM
Fe Fe 1-Jun-1999 12:00 AM

Element	Weight%	Atomic%	Compound%	Formula
Mg K	0.76	0.66	1.26	MgO
Al K	13.67	10.67	25.84	Al_2O_3
Si K	27.42	20.56	58.66	SiO_2
P K	1.16	0.79	2.67	P_2O_5
K K	1.02	0.55	1.23	K_2O
Ca K	2.81	1.47	3.93	CaO
Fe K	4.99	1.88	6.42	FeO
O	48.16	63.41		
Totals	100.00			

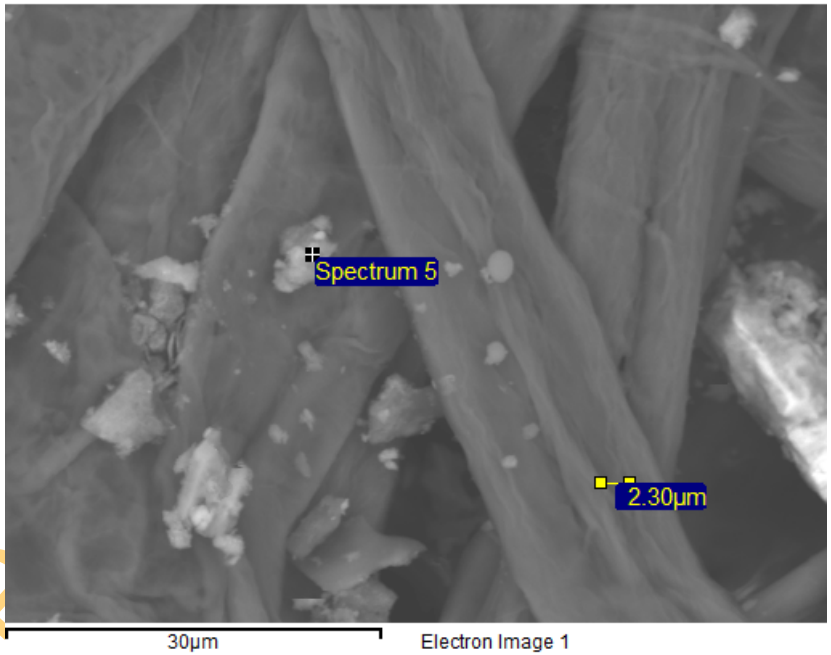

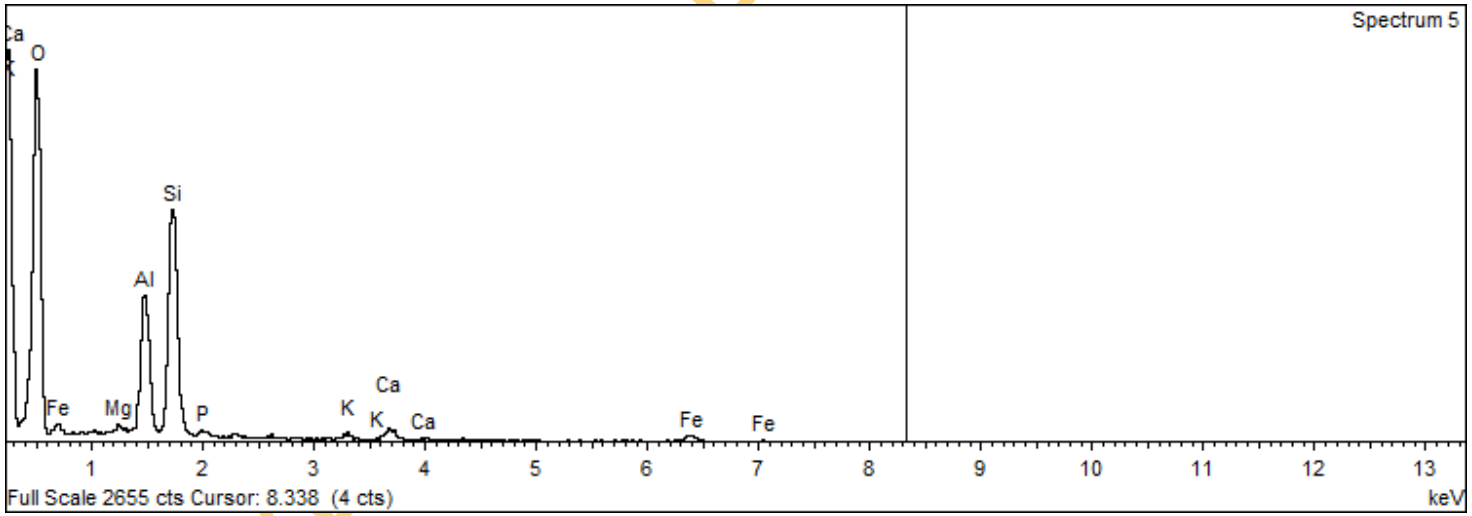

Spectrum processing :
Peak possibly omitted: 4.525 keV

Processing option : Oxygen by stoichiometry (Normalised)
Number of iterations = 2

Standard :
Al Al_2O_3 1-Jun-1999 12:00 AM
Si SiO_2 1-Jun-1999 12:00 AM
K MAD-10 Feldspar 1-Jun-1999 12:00 AM
Fe Fe 1-Jun-1999 12:00 AM

Element	Weight%	Atomic%	Compound%	Formula
Al K	20.15	15.30	38.08	Al_2O_3
Si K	27.26	19.88	58.32	SiO_2
K K	0.56	0.30	0.68	K_2O
Fe K	2.27	0.83	2.92	FeO
O	49.75	63.69		
Totals	100.00			

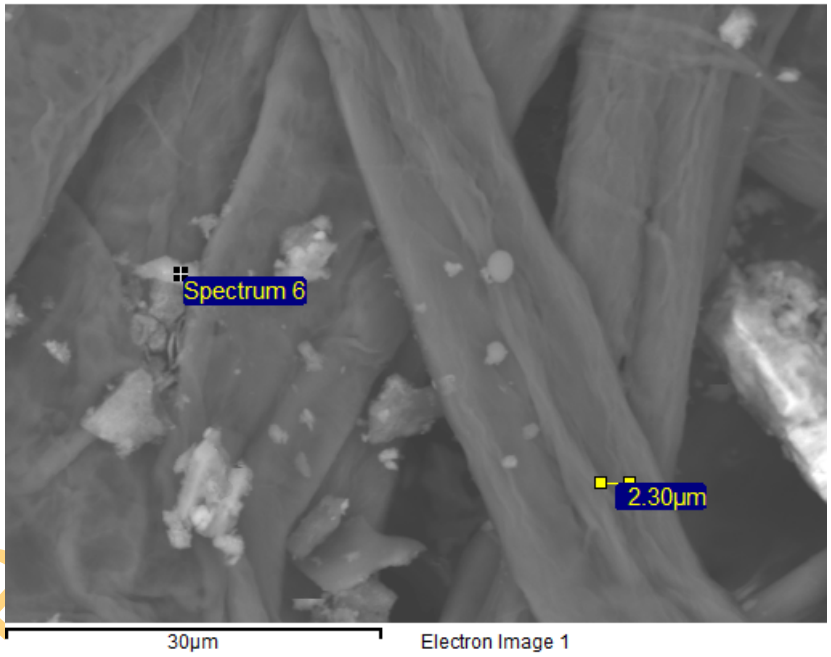

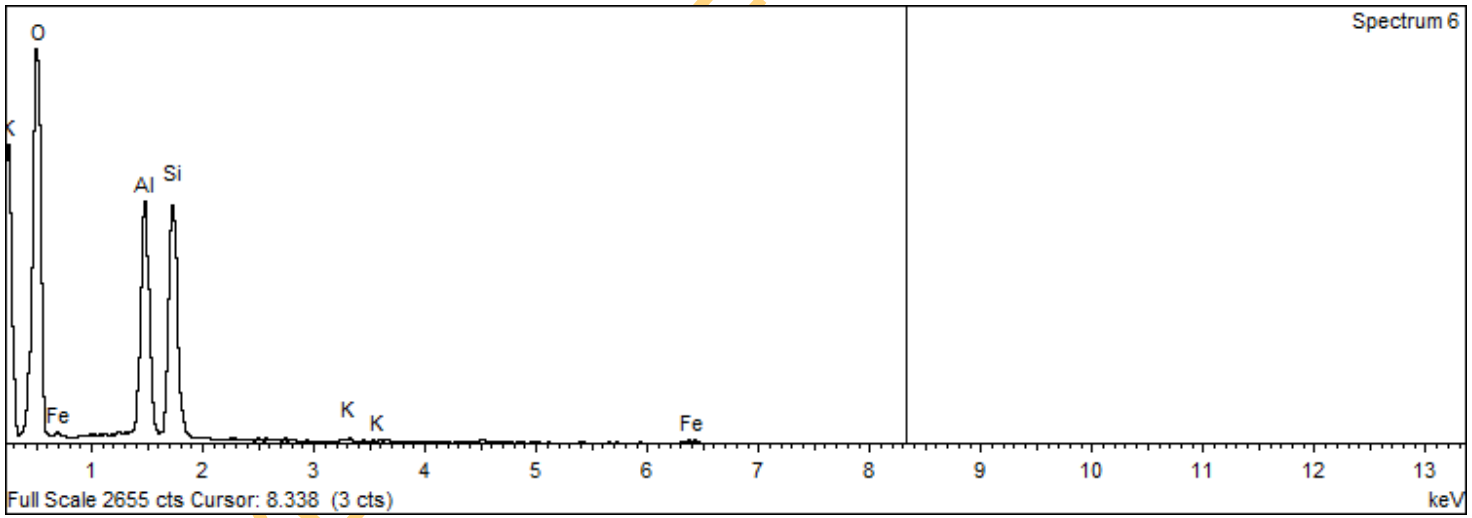

Spectrum processing :
No peaks omitted
Processing option : Oxygen by stoichiometry (Normalised)
Number of iterations = 3

Standard :
Na Albite 1-Jun-1999 12:00 AM
Mg MgO 1-Jun-1999 12:00 AM
Al Al_2O_3 1-Jun-1999 12:00 AM
Si SiO_2 1-Jun-1999 12:00 AM
K MAD-10 Feldspar 1-Jun-1999 12:00 AM
Ca Wollastonite 1-Jun-1999 12:00 AM
Ti Ti 1-Jun-1999 12:00 AM
Fe Fe 1-Jun-1999 12:00 AM

Element	Weight%	Atomic%	Compound%	Formula
Na K	0.67	0.66	0.90	Na_2O
Mg K	5.25	4.86	8.70	MgO
Al K	8.03	6.71	15.17	Al_2O_3
Si K	21.91	17.58	46.87	SiO_2
K K	0.66	0.38	0.80	K_2O
Ca K	7.27	4.09	10.17	CaO
Ti K	0.41	0.19	0.68	TiO_2
Fe K	12.99	5.24	16.71	FeO
O	42.82	60.30		
Totals	100.00			

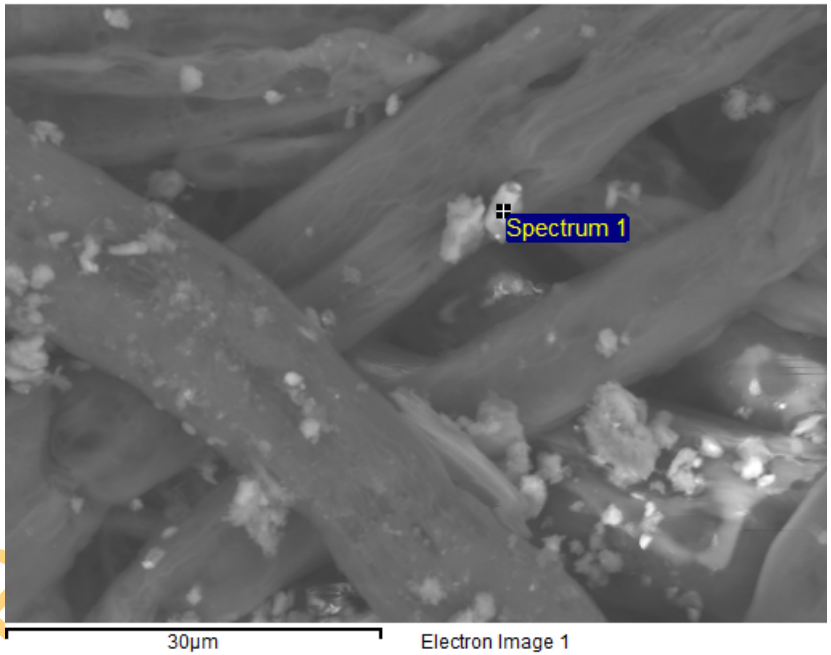

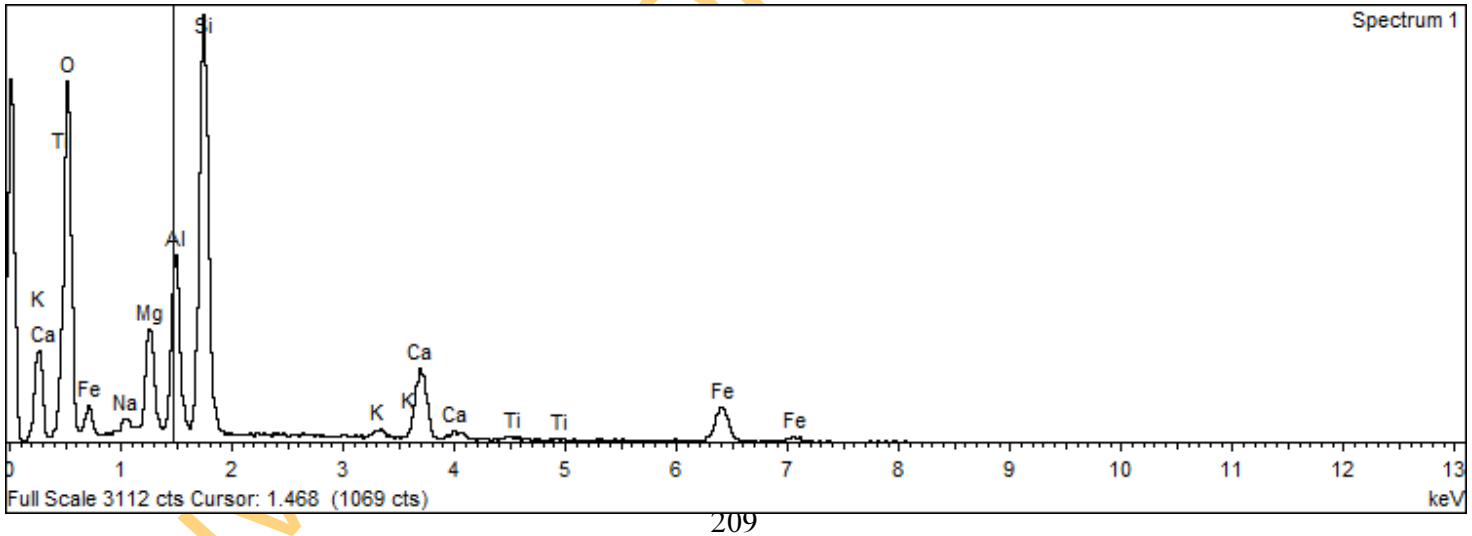

Spectrum processing :
Peak possibly omitted : 4.455 keV

Processing option : Oxygen by stoichiometry (Normalised)
Number of iterations = 3

Standard :
Na Albite 1-Jun-1999 12:00 AM
Al Al_2O_3 1-Jun-1999 12:00 AM
Si SiO2 1-Jun-1999 12:00 AM
K MAD-10 Feldspar 1-Jun-1999 12:00 AM
Ca Wollastonite 1-Jun-1999 12:00 AM
Fe Fe 1-Jun-1999 12:00 AM

Element	Weight%	Atomic%	Compd%	Formula
Na K	0.18	0.17	0.25	Na2O
Al K	10.66	8.40	20.15	Al2O3
Si K	30.31	22.95	64.84	SiO2
K K	11.12	6.05	13.40	K2O
Ca K	0.00	0.00	0.00	CaO
Fe K	1.07	0.41	1.37	FeO
O	46.66	62.02		
Totals	100.00			

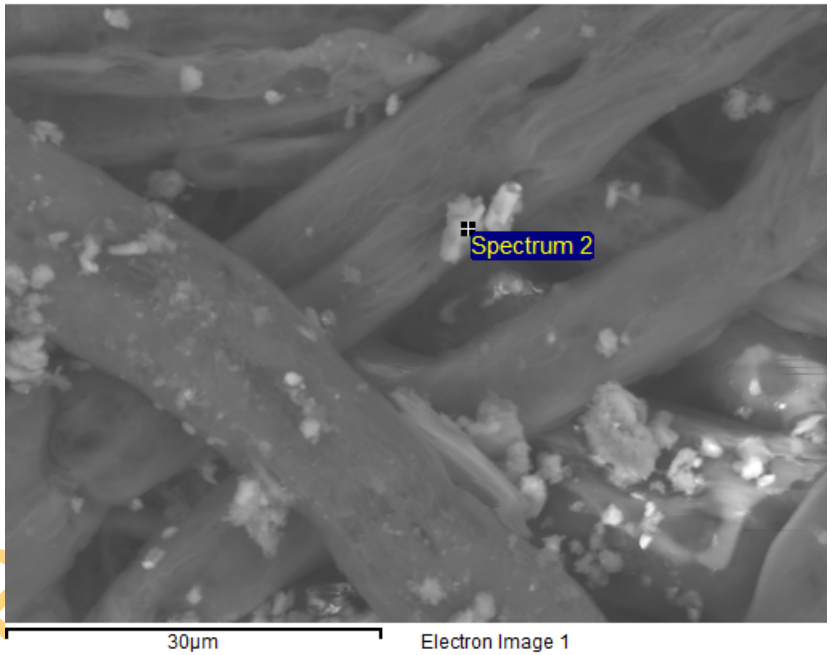

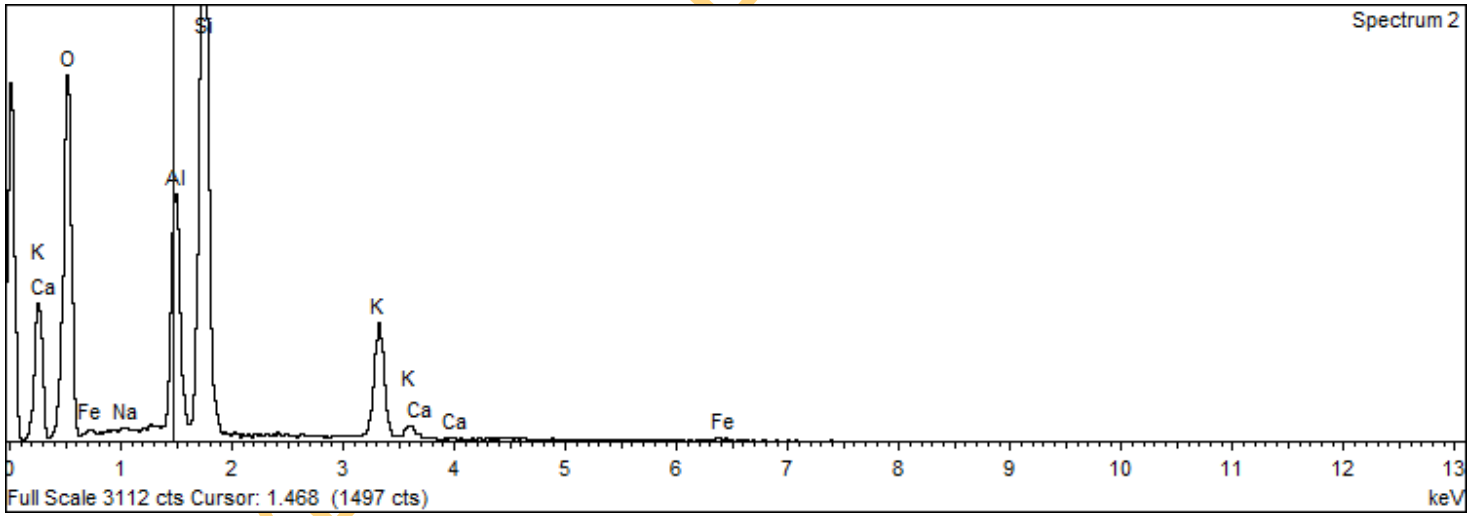

Spectrum processing :
No peaks omitted

Processing option : Oxygen by stoichiometry (Normalised)
Number of iterations = 2

Standard :
Al Al_2O_3 1-Jun-1999 12:00 AM
Si SiO_2 1-Jun-1999 12:00 AM
S FeS_2 1-Jun-1999 12:00 AM
K MAD-10 Feldspar 1-Jun-1999 12:00 AM
Ca Wollastonite 1-Jun-1999 12:00 AM
Ti Ti 1-Jun-1999 12:00 AM
Fe Fe 1-Jun-1999 12:00 AM

Element	Weight%	Atomic%	Compound%	Formula
Al K	12.23	9.43	23.10	Al_2O_3
Si K	31.58	23.38	67.55	SiO_2
S K	0.49	0.31	1.21	SO_3
K K	0.41	0.22	0.49	K_2O
Ca K	0.66	0.34	0.92	CaO
Ti K	0.40	0.17	0.66	TiO_2
Fe K	4.71	1.75	6.06	FeO
O	49.54	64.39		
Totals	100.00			

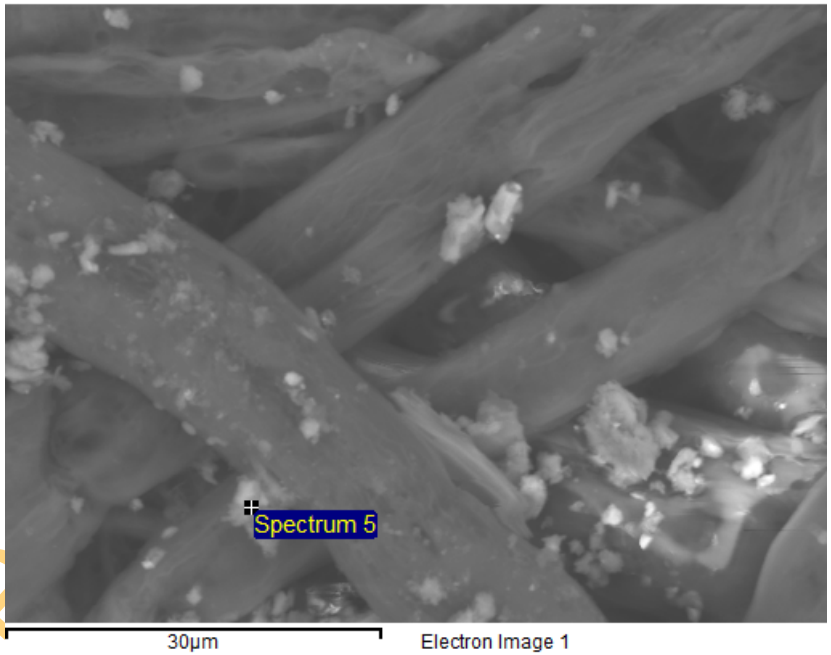

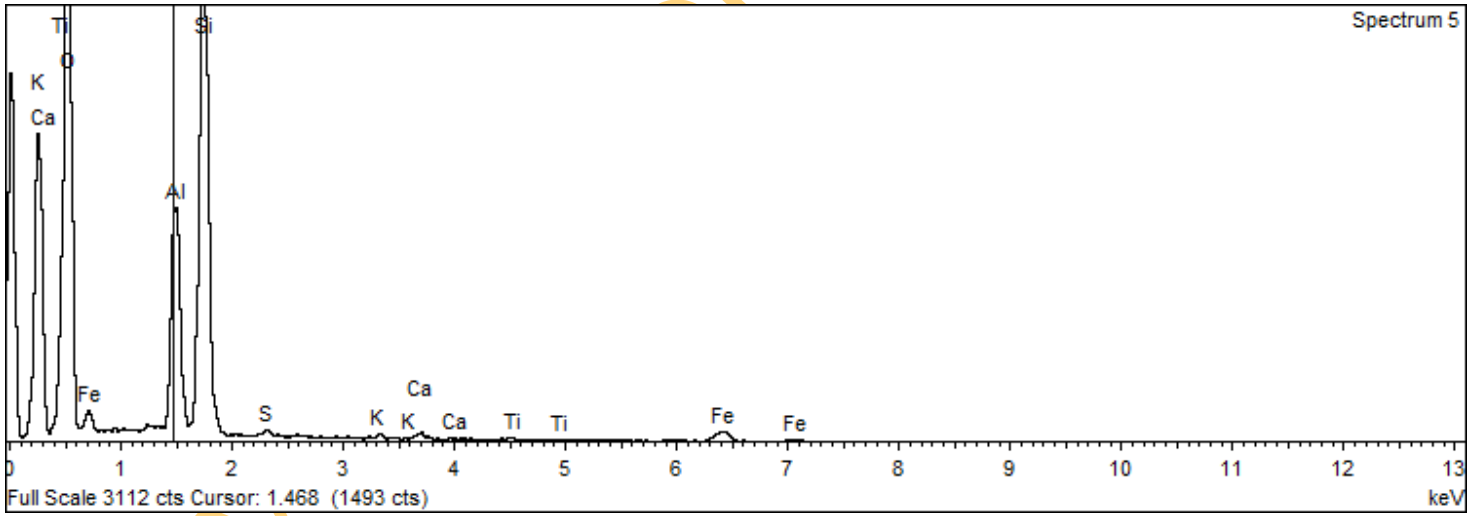

Spectrum processing :
Peak possibly omitted : 3.684 keV

Processing option : Oxygen by stoichiometry (Normalised)
Number of iterations = 3

Standard :
Al Al_2O_3 1-Jun-1999 12:00 AM
Si SiO_2 1-Jun-1999 12:00 AM
Fe Fe 1-Jun-1999 12:00 AM

Element	Weight%	Atomic%	Compd%	Formula
Al K	15.77	14.26	29.79	Al_2O_3
Si K	14.43	12.54	30.87	SiO_2
Fe K	30.58	13.36	39.34	FeO
O	39.22	59.83		
Totals	100.00			

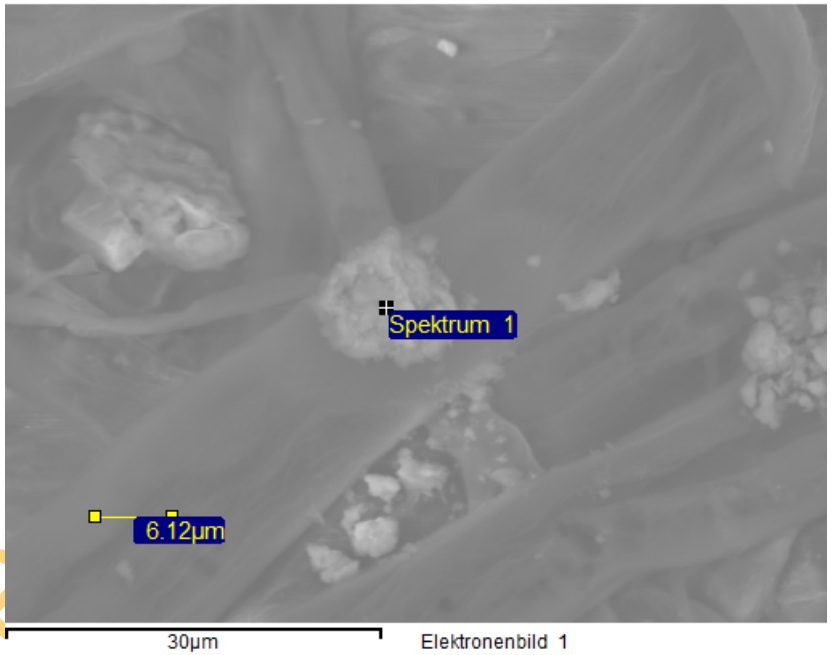

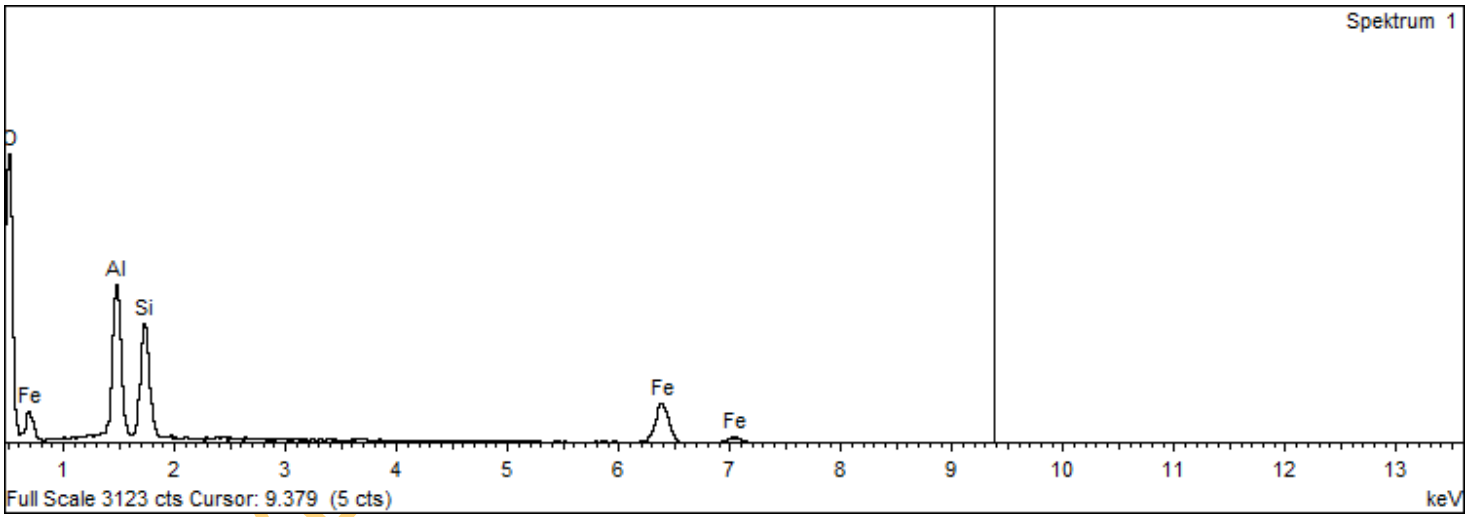

Spectrum processing :
No peaks omitted

Processing option : Oxygen by stoichiometry (Normalised)
Number of iterations = 2

Standard :
Al Al2O3 1-Jun-1999 12:00 AM
Si SiO2 1-Jun-1999 12:00 AM
K MAD-10 Feldspar 1-Jun-1999 12:00 AM
Ti Ti 1-Jun-1999 12:00 AM
Fe Fe 1-Jun-1999 12:00 AM

Element	Weight%	Atomic%	Compound%	Formula
Al K	5.32	4.90	10.04	Al_2O_3
Si K	20.52	18.17	43.91	SiO_2
K K	2.53	1.61	3.05	K_2O
Ti K	2.69	1.39	4.48	TiO_2
Fe K	29.94	13.33	38.51	FeO
O	39.00	60.60		
Totals	100.00			

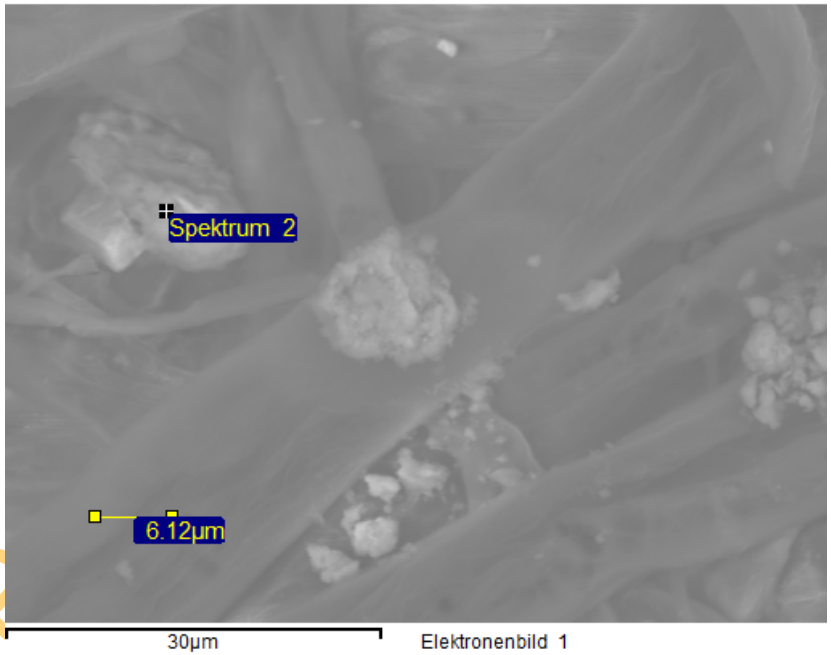

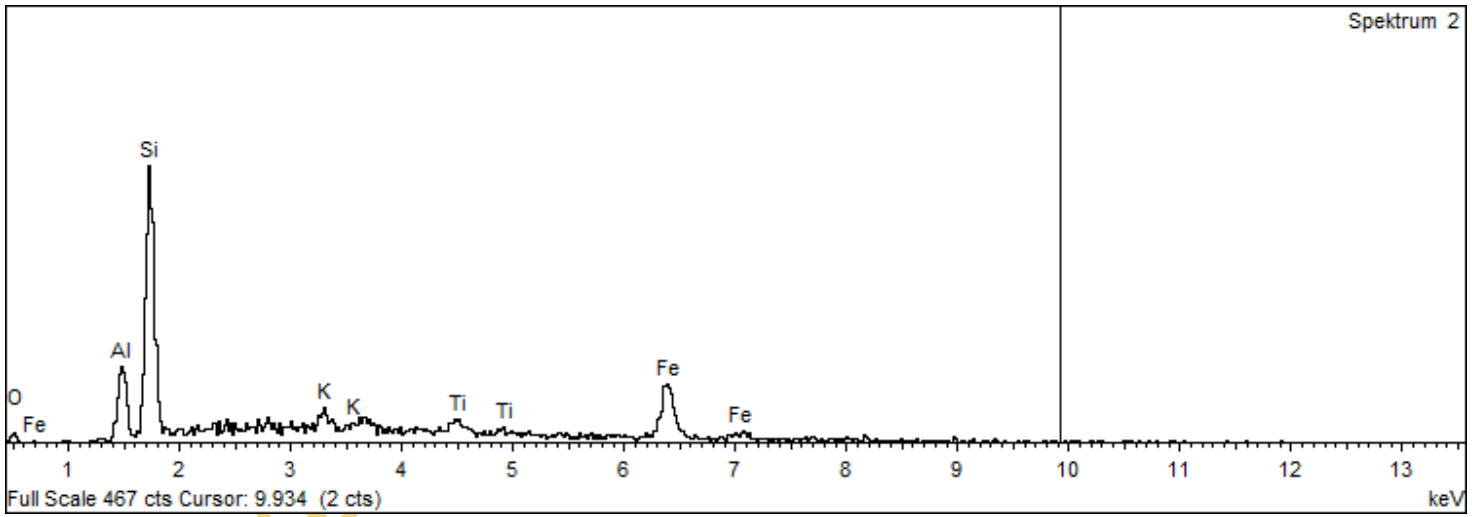

Spectrum processing :
No peaks omitted

Processing option : Oxygen by stoichiometry (Normalised)
Number of iterations = 2

Standard :
Al Al2O3 1-Jun-1999 12:00 AM
Si SiO2 1-Jun-1999 12:00 AM
K MAD-10 Feldspar 1-Jun-1999 12:00 AM
Ca Wollastonite 1-Jun-1999 12:00 AM
Fe Fe 1-Jun-1999 12:00 AM

Element	Weight%	Atomic%	Compound%	Formula
Al K	8.32	7.53	15.72	Al2O3
Si K	11.75	10.22	25.14	SiO2
K K	2.00	1.25	2.41	K2O
Ca K	37.82	23.04	52.92	CaO
Fe K	2.96	1.29	3.81	FeO
O	37.14	56.68		
Totals	100.00			

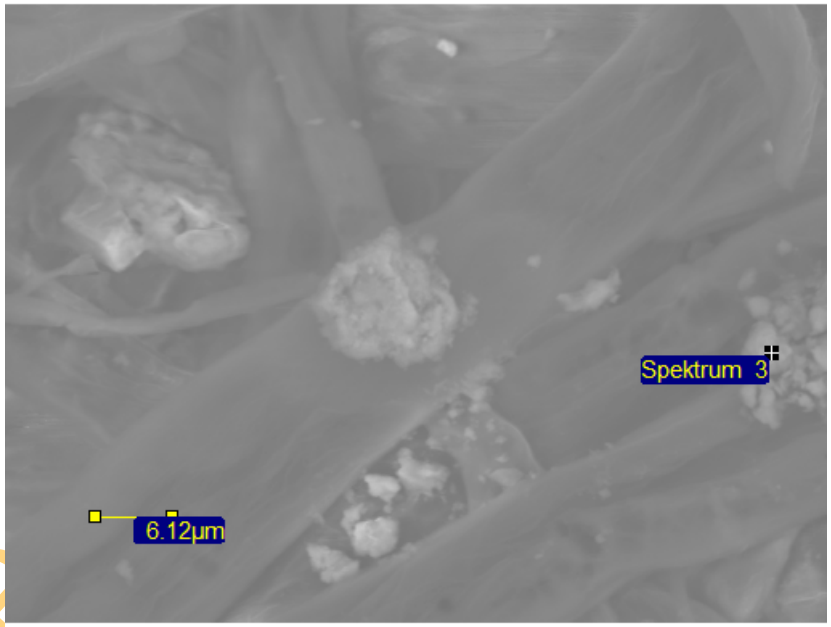

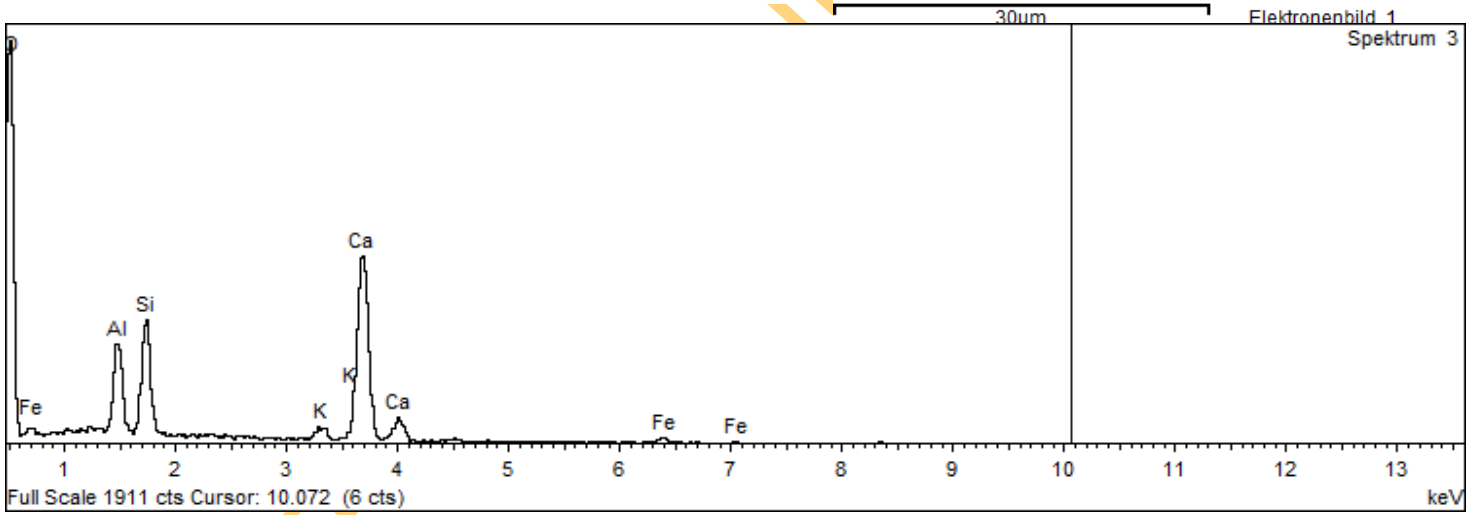

Spectrum processing :
No peaks omitted

Processing option : Oxygen by stoichiometry (Normalised)
Number of iterations = 3

Standard :
Al Al_2O_3 1-Jun-1999 12:00 AM
Si SiO_2 1-Jun-1999 12:00 AM
Fe Fe 1-Jun-1999 12:00 AM

Element	Weight%	Atomic%	Compound%	Formula
Al K	22.83	17.16	43.14	Al_2O_3
Si K	26.09	18.83	55.81	SiO_2
Fe K	0.82	0.30	1.05	FeO
O	50.26	63.71		
Totals	100.00			

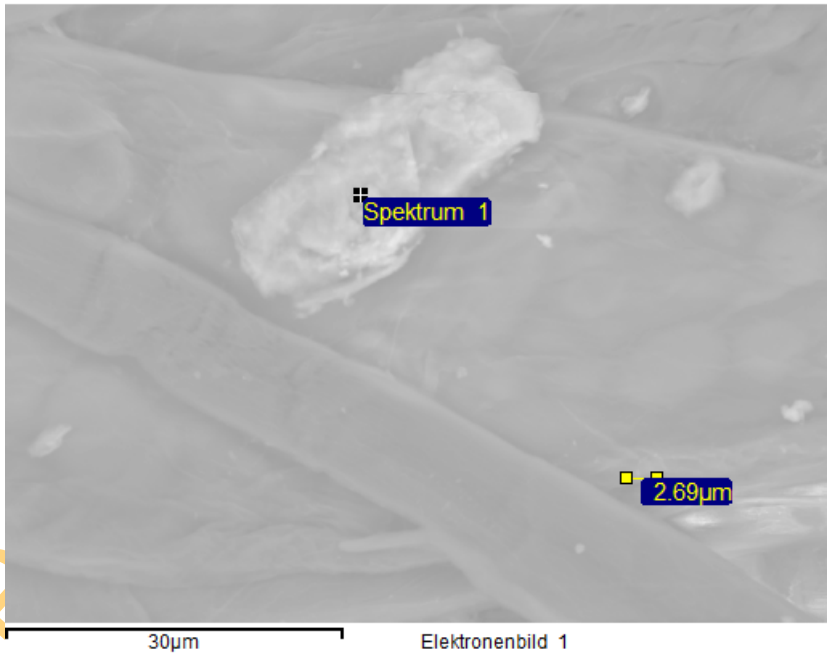

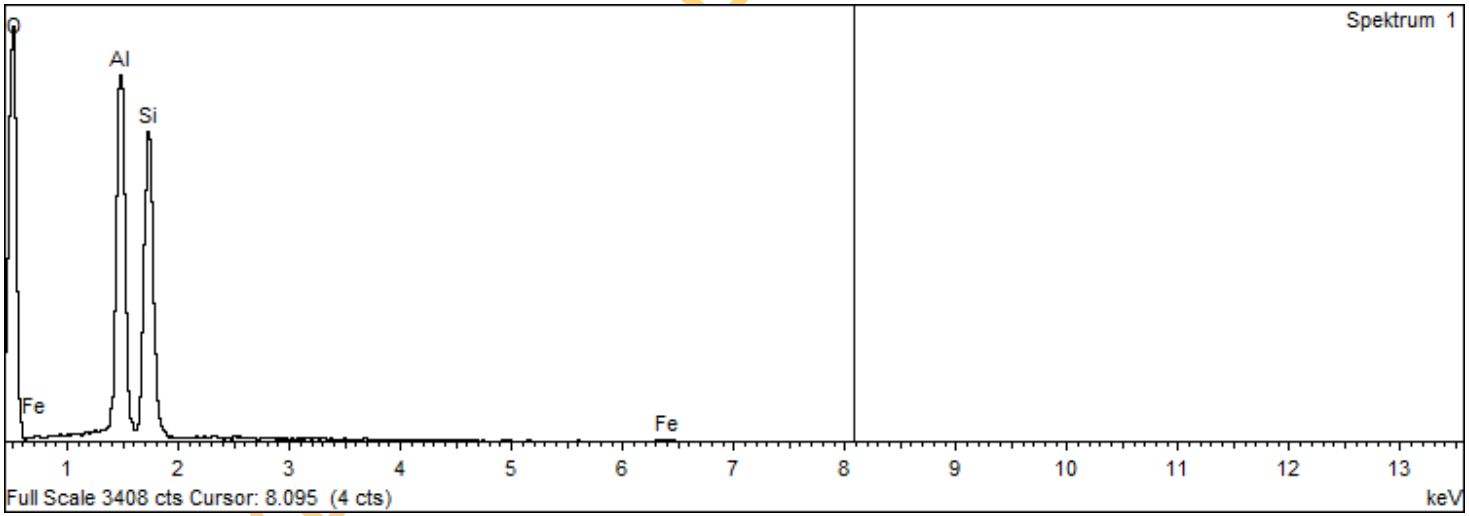

Spectrum processing :
No peaks omitted

Processing option : Oxygen by stoichiometry (Normalised)
Number of iterations = 2

Standard :
Mg MgO 1-Jun-1999 12:00 AM
Si SiO_2 1-Jun-1999 12:00 AM
Fe Fe 1-Jun-1999 12:00 AM

Element	Weight%	Atomic%	Compd%	Formula
Mg K	19.42	16.12	32.20	MgO
Si K	31.10	22.35	66.52	SiO_2
Fe K	0.99	0.36	1.27	FeO
O	48.49	61.17		
Totals	100.00			

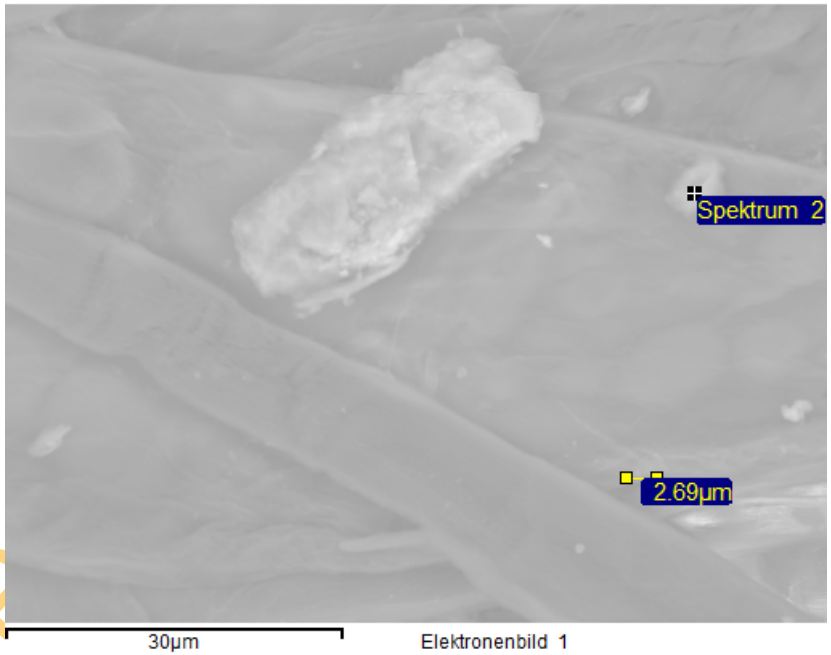

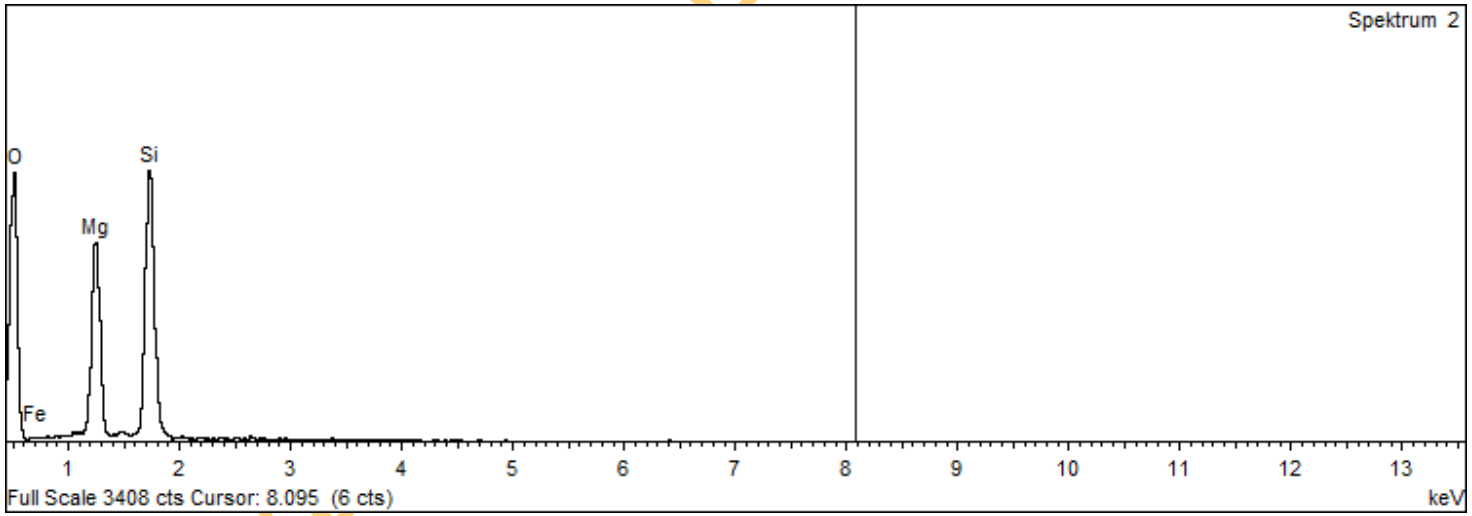

Spectrum processing :
No peaks omitted

Processing option : Oxygen by stoichiometry (Normalised)
Number of iterations = 3

Standard :
Mg MgO 1-Jun-1999 12:00 AM
Al Al_2O_3 1-Jun-1999 12:00 AM
Si SiO2 1-Jun-1999 12:00 AM
K MAD-10 Feldspar 1-Jun-1999 12:00 AM
Ti Ti 1-Jun-1999 12:00 AM
Fe Fe 1-Jun-1999 12:00 AM

Element	Weight%	Atomic%	Compound%	Formula
Mg K	4.32	3.98	7.17	MgO
Al K	12.39	10.27	23.41	Al_2O_3
Si K	20.57	16.38	44.00	SiO_2
K K	5.73	3.28	6.90	K_2O
Ti K	2.06	0.96	3.44	TiO_2
Fe K	11.73	4.70	15.08	FeO
O	43.20	60.42		
Totals	100.00			

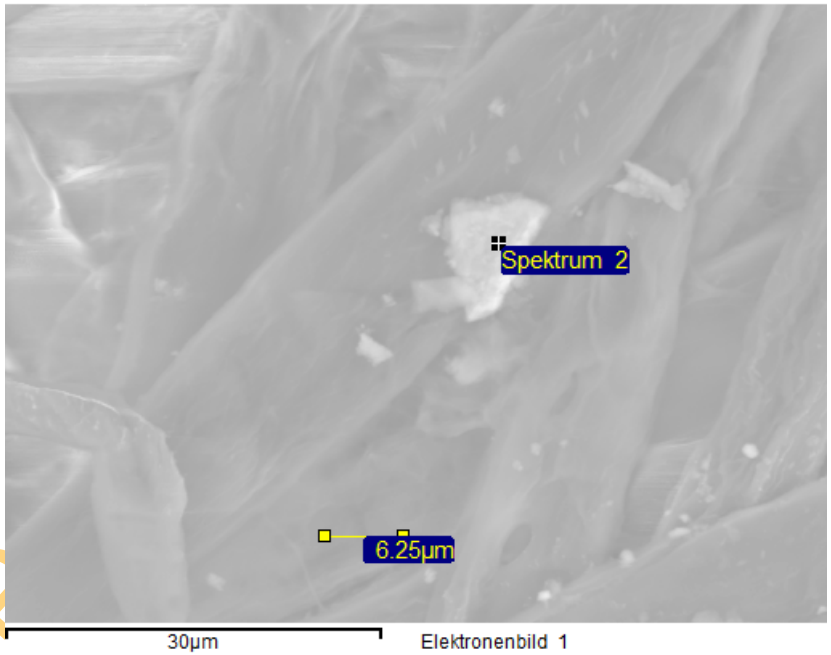

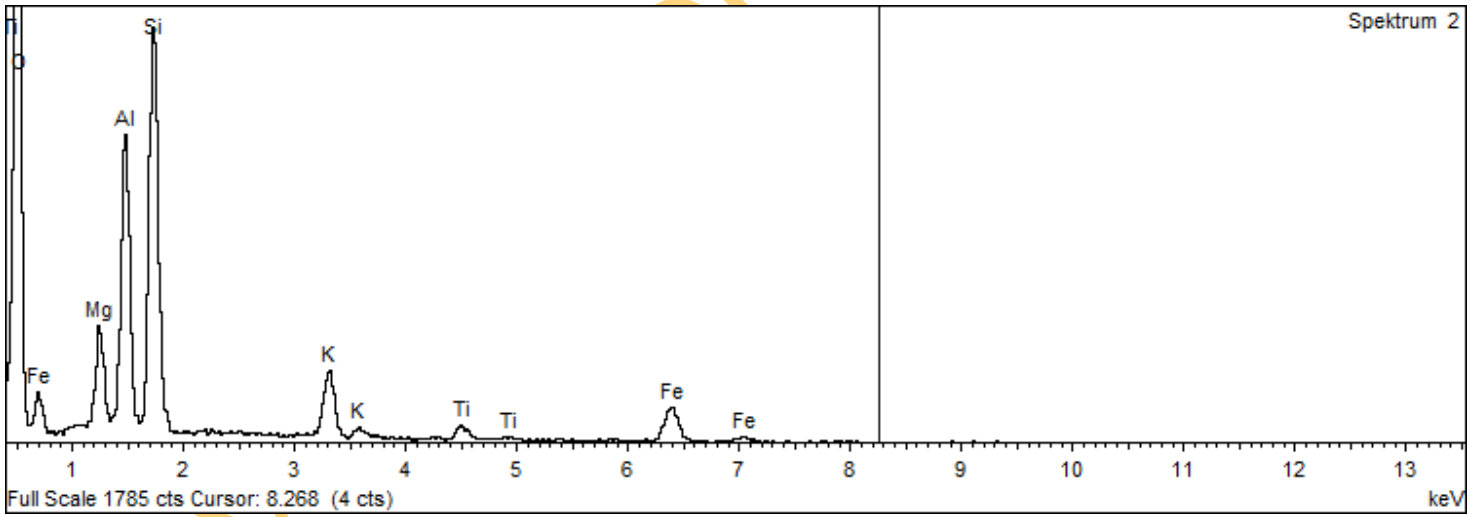

Spectrum processing :
No peaks omitted

Processing option : Oxygen by stoichiometry (Normalised)
Number of iterations = 2

Standard :
Na Albite 1-Jun-1999 12:00 AM
Al Al_2O_3 1-Jun-1999 12:00 AM
Si SiO_2 1-Jun-1999 12:00 AM
Ca Wollastonite 1-Jun-1999 12:00 AM
Fe Fe 1-Jun-1999 12:00 AM

Element	Weight%	Atomic%	Compound%	Formula
Na K	4.73	4.25	6.38	Na_2O
Al K	11.38	8.70	21.50	Al_2O_3
Si K	30.63	22.50	65.52	SiO_2
Ca K	2.66	1.37	3.73	CaO
Fe K	2.23	0.82	2.87	FeO
O	48.37	62.36		
Totals	100.00			

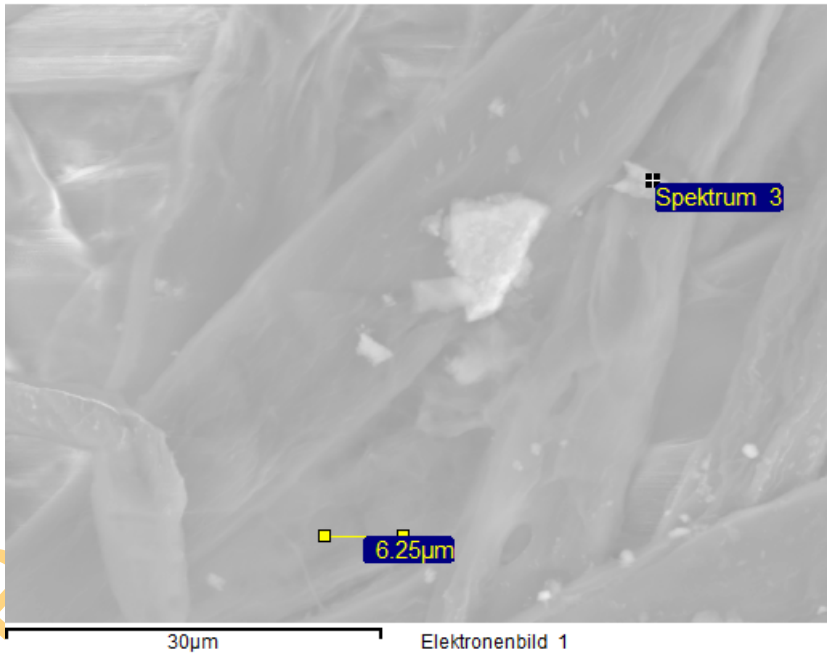

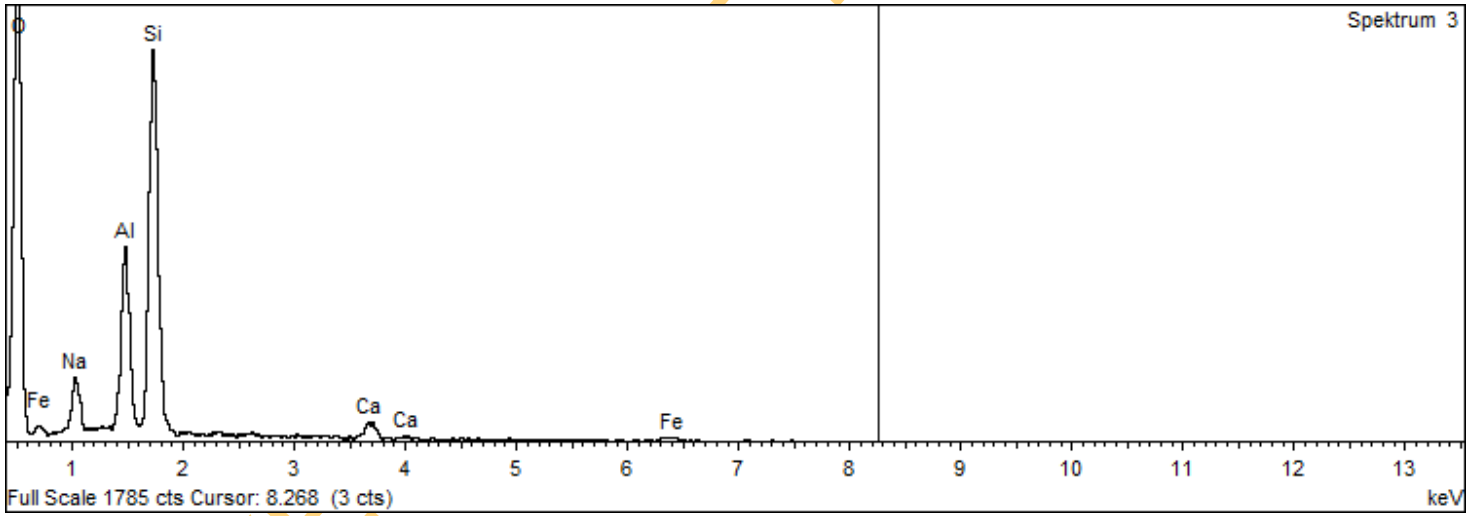

Spectrum processing :
Peaks possibly omitted : 2.616, 3.330, 3.700 keV

Processing option : Oxygen by stoichiometry (Normalised)
Number of iterations = 2

Standard :
Al Al_2O_3 1-Jun-1999 12:00 AM
Si SiO_2 1-Jun-1999 12:00 AM
Ti Ti 1-Jun-1999 12:00 AM
Fe Fe 1-Jun-1999 12:00 AM

Element	Weight%	Atomic%	Compd%	Formula
Al K	6.56	7.65	12.40	Al_2O_3
Si K	2.22	2.49	4.75	SiO_2
Ti K	1.82	1.19	3.03	TiO_2
Fe K	62.04	34.93	79.82	FeO
O	27.36	53.75		
Totals	100.00